THERMODYNAMICS OF THE Fe-V-O SYSTEM

THERMODYNAMICS OF THE Fe-V-O SYSTEM

By

ANTONY KONTOPOULOS, DIPL. ENG.

A Thesis

Submitted to the School of Graduate Studies

in Partial Fulfilment of the Requirements

for the Degree

Doctor of Philosophy

McMaster University

January 1971

DOCTOR OF PHILOSOPHY (1971)   McMASTER UNIVERSITY
(Metallurgy)   Hamilton, Ontario

TITLE: Thermodynamics of the Fe-V-O System

AUTHOR: Antony Kontopoulos, Dipl. Eng. (National Technical
                University of Athens)

SUPERVISOR: Professor D.A.R. Kay

NUMBER OF PAGES: (xviii); 220

SCOPE AND CONTENTS:

This thesis is concerned with the determination of the thermodynamics of the Fe-V-O system.

In the first part the thermodynamics of liquid Fe-V-O alloys were studied in the temperature range $1550\text{-}1700^{\circ}C$ using H_2O/H_2 equilibration and/or an oxygen probe. 1st and 2nd order interaction parameters between V and O were determined, and the deoxidation reactions occurring when V is used as a deoxidizer were studied. Deoxidation diagrams are presented for V concentrations up to 12 wt.%.

In the second part the thermodynamic equilibria between the lower oxides of vanadium $(V - VO_{0.2-x}, \ VO_{0.2+x} - VO_{1-y}, \ VO_{1+y} - VO_{1.5})$ were determined in the range $800\text{-}1400^{\circ}C$ using a solid state EMF technique, and the free energy of formation of the oxides $VO_{0.2\pm x}, \ VO_{1\pm y}, \ VO_{1.5}$ was estimated.

ACKNOWLEDGMENTS

TABLE OF CONTENTS

LIST OF FIGURES

LIST OF TABLES

LIST OF SYMBOLS

a_i Raoultian activity of i

$e_i^{(j)}$ First order free energy interaction parameter, wt. % scale

f_i Henrian activity coefficient of i, wt. % scale

h_i Henrian activity of i, wt. % scale

k Equilibrium constant

k' Apparent equilibrium constant

$l_i^{(j)}$ Second order enthalpy interaction parameter, wt. % scale

N_i Mole (atom) fraction of i

$p_i^{(j)}$ Second order entropy interaction parameter, wt. % scale

$r_i^{(j)}$ Second order free energy interaction parameter, wt. % scale

R Gas constant

$s_i^{(j)}$ First order entropy interaction parameter, wt. % scale

$\%i$ wt. % of i

γ_i Raoultian activity coefficient of i

γ_i^o Raoultian activity coefficient of i at infinite dilution

$\sigma_i^{(j)}$ First order entropy interaction parameter, MF scale

$\epsilon_i^{(j)}$ First order free energy interaction parameter, MF scale

$\eta_i^{(j)}$ First order enthalpy interaction parameter, MF scale

$\lambda_i^{(j)}$ Second order enthalpy interaction parameter, MF scale

$\pi_i^{(j)}$ Second order entropy interaction parameter, MF scale

$\rho_i^{(j)}$ Second order free energy interaction coefficient, MF scale

$\underline{X}$ Element X dissolved in liquid iron. Unless otherwise stated, the standard state for the Henrian activity of $\underline{X}$ is the 1 wt. % solution in liquid iron, and the reference state the infinitely dilute solution.

(g) Gas

(l) Liquid

(s) Solid

Reaction 1 $\quad H_2(g) + \underline{O} = H_2O(g)$

Reaction 2 $\quad \dfrac{1}{2} \ O_2(g) = \underline{O}$

Reaction 3 $\quad Fe(l) + 2 \ \underline{V} + 4 \ \underline{O} = FeV_2O_4(s)$

Reaction 4 $\quad 2 \ \underline{V} + 3 \ \underline{O} = V_2O_3(s)$
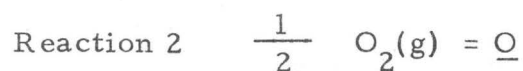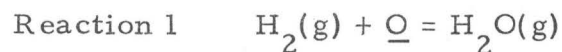
CHAPTER 1

INTRODUCTION

This thesis is divided into two parts.

In the first part the thermodynamics of liquid Fe-V-O alloys were studied in the temperature range 1550-1700°C. The effect of vanadium on the activity coefficient of oxygen was determined and expressed in terms of 1st and 2nd order free energy, enthalpy and entropy interaction parameters, and the thermodynamics of the deoxidation reactions occurring when vanadium is used as a deoxidizer in liquid iron were established.

In the second part the thermodynamic equilibria involving vanadium and its lower oxides (V - $VO_{0.2}$, $VO_{0.2}$ - VO, VO - V_2O_3) were determined in the temperature range 800 - 1400°C, and the free energies of formation of $VO_{0.2}$, VO and V_2O_3 were estimated.

The necessity of accurate knowledge of the interaction parameters between alloying elements and oxygen in liquid iron has always been important, and is more so today since the oxygen probe is finding extensive use in the steelmaking industry. The probe measures the activity of oxygen, and only by accurate knowledge of the interaction parameters between oxygen and alloying elements is it possible to convert the activity of oxygen to concentration.

The interaction parameter between vanadium and oxygen has been determined before by several investigators, but their results are in poor agreement. Values of $e_o^{(v)}$ from the literature range from -0.11 to -0.36 at 1600°C.

Vanadium is also a mild deoxidizer, and has been used as such in the place of Al in continuously cast rimmed steels with significant

improvement in cleanliness. It also has a potential use as a predeoxidizer to reduce the oxygen content of the melt before the final deoxidation with aluminum; formation of aluminates, which are less likely to be absorbed into the slag, can be avoided in this way.

The deoxidation of iron with vanadium has been studied before, but again differences exist in the free energy changes of the deoxidation reactions as well as in the products of these reactions; two investigations have reported FeV_2O_4 and V_2O_3 as the deoxidation products, while a third reported V_2O_2 in addition to the other two.

In view of the existing discrepancies in the literature, it was decided to undertake a thermodynamic study of the liquid Fe-V-O system.

The technique chosen was to equilibrate Fe-V melts with H_2O/H_2 gas mixtures of known composition. This technique was applied for V contents up to 2%. During this time many papers appeared in the literature describing successful applications of the oxygen probe in this type of study, and we decided to construct a probe and use it to extend the investigation up to 12%V. The probe used had a stabilized zirconia electrolyte and a Cr, Cr_2O_3 mixture as reference electrode. The Cr, Cr_2O_3 electrode has been reported to exhibit nonreversible behaviour when used at lower temperatures. The only reasonable alternative choices as solid reference electrodes are mixtures of lower oxides of vanadium or niobium. We decided to study the thermodynamic equilibria involving vanadium and its lower oxides, hoping that an oxide mixture from this system could be used as reference electrode for the oxygen probe. A solid state EMF technique was used, and the study was successfully completed. We were not able to check the performance of these mixtures as a reference electrode however, as our attempts to construct an oxygen probe with ThO_2 (Y_2O_3) electrolytes were not successful, and these mixtures are not compatible with ZrO_2-based electrolytes.

PART I

A THERMODYNAMIC STUDY OF THE LIQUID Fe-V-O SYSTEM

INTRODUCTION

This part is dealing with the thermodynamics of the liquid Fe-V-O system.

The thermodynamic treatment of liquid metallic solutions is briefly reviewed, and a literature survey on the thermodynamics of Fe-O and Fe-V-O melts is presented. The experimental apparatus and techniques are described, and the experimental results are presented and discussed.

CHAPTER 2

THERMODYNAMIC DESCRIPTION OF LIQUID METALLIC SOLUTIONS

2.1   INTRODUCTION

The thermodynamic description of liquid metallic solutions consists essentially in obtaining a suitable analytical representation of the activities of the various components of the mixture.

This representation has to be:

(a)   thermodynamically consistent;

(b)   in agreement with the limiting laws for the solutes and the solvent (Henry's and Raoult's laws).

For convenience, it should also be as simple as possible and compatible with the precision of the experimental data.

For the time being, none of the existing formalisms for the thermodynamic description of the liquid metallic solutions is satisfactory over the entire range of concentrations.

In the following, we shall briefly present the interaction coefficient formalism, introduced by Wagner and extended by Lupis and Elliott, and the quadratic formalism, introduced by Darken. Finally, some mathematical models of solutions will be presented, and the attempts to predict the solution behaviour using these models.

2.2   INTERACTION COEFFICIENT FORMALISM

This formalism was introduced by Wagner[1] and generalized by Lupis and Elliott[2, 3, 4].

Consider a solution consisting of the solutes $j = 2, 3, .., m$ in the solvent 1. The general excess partial molar property Θ_i^E (Θ_i may refer

5

to any thermodynamic potential, as the free energy, entropy or enthalpy) can be expanded through a Taylor series around the position $N_1 = 1$:

$$\Theta_i^E = (\Theta_i^E)^\circ + \sum_{j=2}^{m} \left(\frac{\partial \Theta_i^E}{\partial N_j}\right)_{N_1 \to 1} N_j + \frac{1}{2!} \sum_{j=2}^{m} \sum_{k=2}^{m} \left(\frac{\partial^2 \Theta_i^E}{\partial N_j \partial N_k}\right)_{N_1 \to 1} N_j N_k + O(N^3)$$

$$= (\Theta_i^E)^\circ + \sum_{j=2}^{m} \left(\frac{\partial \Theta_i^E}{\partial N_j}\right)_{N_1 \to 1} N_j + \sum_{j=2}^{m} \left(\frac{\partial^2 \Theta_i^E}{\partial N_j^2}\right)_{N_1 \to 1} N_j^2 +$$

$$+ \frac{1}{2} \sum_{j=2}^{m} \sum_{\substack{k=2 \\ k \neq j}}^{m} \left(\frac{\partial^2 \Theta_i^E}{\partial N_j \partial N_k}\right)_{N_1 \to 1} N_j N_k + O(N^3) \qquad (2.1)$$

Following the terminology of Lupis and Elliott[4] we define:

First Order Interaction coefficients: $\delta_i^{(j)} = \left(\dfrac{\partial \Theta_i^E}{\partial N_j}\right)_{N_1 \to 1}$ (2.2)

Second Order Interaction Coefficients:

$$\left.\begin{aligned} \kappa_i^{(j)} &= \left(\frac{\partial^2 \Theta_i^E}{\partial N_j^2}\right)_{N_1 \to 1} \\[2em] \kappa_i^{(j,k)} &= \frac{1}{2}\left(\frac{\partial^2 \Theta_i^E}{\partial N_j \partial N_k}\right)_{N_1 \to 1} \end{aligned}\right\} \qquad (2.3)$$

In the same way third and higher order interaction coefficients can be defined.

With the definition of eqns. (2.2) and (2.3), eqn. (2.1) becomes:

$$\Theta_i^E = (\Theta_i^E)^\circ + \sum_{j=2}^{m} \delta_i^{(j)} N_j + \sum_{j=2}^{m} \kappa_i^{(j)} N_j^2 +$$

$$+ \sum_{j=2}^{m} \sum_{\substack{k=2 \\ k \neq j}}^{m} \kappa_i^{(j,k)} \, N_j \, N_k \; + \; O(N^3) \tag{2.4}$$

Because of the convenient usage of the activity coefficient, it is usual to refer to Θ_i^E as $\dfrac{G_i^E}{RT}$ ($= \ln \gamma_i$) in the case of free energy, and to S_i^E and H_i^E in the case of entropy and enthalpy respectively. The so defined interaction coefficients are called first (second, etc.) order free energy, entropy or enthalpy interaction coefficients.

Table 2-1 gives the definition of interaction coefficients with the symbols currently used. The definitions of interaction coefficients based on the composition in wt. % are also included.

From the relationship

$$G_i^E = H_i^M - T \, S_i^E \tag{2.5}$$

it follows directly that[2]:

$$\epsilon_i^{(j)} = \frac{\eta_i^{(j)}}{RT} - \frac{\sigma_i^{(j)}}{R} \tag{2.6}$$

and similarly

$$\rho_i^{(j)} = \frac{\lambda_i^{(j)}}{RT} - \frac{\pi_i^{(j)}}{R} \tag{2.7}$$

Similar relations hold between (e, h, s) and (r, p, l).

There are a number of interrelationships between like interaction coefficients, which have been derived by Wagner[1], Schenck, Frohberg and Steinmets[5], and Lupis and Elliott[4]. These relationships are shown in Table 2-2.

Some useful relationships between interaction coefficients based on mole fraction and on wt. % scale are given in Table 2-3.

TABLE 2-1. DEFINITIONS OF INTERACTION COEFFICIENTS

(at $N_1 \to 1$, or (wt. % 1) $\to 100$)

Order	Free Energy*		Entropy		Enthalpy		System for Obtaining Property
	N	%	N	%	N	%	
Zero	$\ln \gamma_i^o$ or $\log f_i = 0$ $\ln \phi_i = 0^+$		$(S_i^{E})^o$	$(\mathscr{S}_i^{E})^o = 0$	$(H_i^{E})^o$	$(\mathscr{H}_i^{E})^o = 0$	1-i binary
First	$\epsilon_i^{(i)}$	$e_i^{(i)}$	$\sigma_i^{(i)}$	$s_i^{(i)}$	$\eta_i^{(i)}$	$h_i^{(i)}$	1-i binary
	$\epsilon_i^{(j)}$	$e_i^{(j)}$	$\sigma_i^{(j)}$	$s_i^{(j)}$	$\eta_i^{(j)}$	$h_i^{(j)}$	1-i-j ternary
Second	$\rho_i^{(i)}$	$r_i^{(i)}$	$\pi_i^{(i)}$	$p_i^{(i)}$	$\lambda_i^{(i)}$	$l_i^{(i)}$	1-i binary
	$\rho_i^{(j)}$	$r_i^{(j)}$	$\pi_i^{(j)}$	$p_i^{(j)}$	$\lambda_i^{(j)}$	$l_i^{(j)}$	1-i-j ternary
	$\rho_i^{(j,k)}$	$r_i^{(j,k)}$	$\pi_i^{(j,k)}$	$p_i^{(j,k)}$	$\lambda_i^{(j,k)}$	$l_i^{(j,k)}$	1-i-j-k quartemary

*
$$\frac{G_i^E}{RT} = \ln \gamma_i + \ln \phi_i = \ln (\gamma_i / \gamma_i^o)$$

Representative equations:
$$\ln \gamma_i = \ln \gamma_i^o + \sum_{j=2}^{m} \epsilon_i^{(j)} N_j + \sum_{j=2}^{m} \rho_i^{(j)} N_j^2 + \sum_{j=2}^{m} \sum_{\substack{k=2 \\ k \neq j}}^{m} \rho_i^{(j,k)} N_j N_k + O(N^3)$$

$$\log f_i = \sum_{j=2}^{m} e_i^{(j)} (\%j) + \sum_{j=2}^{m} r_i^{(j)} (\%j)^2 + \sum_{j=2}^{m} \sum_{\substack{k=2 \\ k \neq j}}^{m} r_i^{(j,k)} (\%j)(\%k) + O(\%^3)$$

TABLE 2-2

RECIPROCAL RELATIONSHIPS AMONG INTERACTION COEFFICIENTS

Free energy (G_i^E/RT)	Entropy (S_i^E)	Enthalpy (H_i^M)
$\epsilon_i^{(j)} = \epsilon_j^{(i)}$	$\sigma_i^{(j)} = \sigma_j^{(i)}$	$\eta_i^{(j)} = \eta_j^{(i)}$
$\rho_i^{(i,j)} + \epsilon_i^{(j)} = 2\,\rho_j^{(i)} + \epsilon_i^{(i)}$	$\pi_i^{(i,j)} + \sigma_i^{(j)} = 2\pi_j^{(i)} + \sigma_i^{(i)}$	$\lambda_i^{(i,j)} + \eta_i^{(j)} = 2\lambda_j^{(i)} + \eta_i^{(i)}$
$\rho_i^{(j,k)} + \epsilon_j^{(k)} = \rho_j^{(i,k)} + \epsilon_i^{(k)}$	$\pi_i^{(j,k)} + \sigma_j^{(k)} = \pi_j^{(i,k)} + \sigma_i^{(k)}$	$\lambda_i^{(j,k)} + \eta_j^{(k)} = \lambda_j^{(i,k)} + \eta_i^{(k)}$
$= \rho_k^{(i,j)} + \epsilon_i^{(j)}$	$= \pi_k^{(i,j)} + \sigma_i^{(j)}$	$= \lambda_k^{(i,j)} + \eta_i^{(j)}$

TABLE 2-3

RELATIONSHIPS BETWEEN 1st ORDER INTERACTION COEFFICIENTS

BASED ON M F AND ON WT. % SCALE

$$\epsilon_i^{(j)} = 230 \frac{M_j}{M_1} e_i^{(j)} + \frac{M_1 - M_j}{M_1}$$

$$\sigma_i^{(j)} = 100 \frac{M_j}{M_1} s_i^{(j)} - R \frac{M_1 - M_j}{M_1}$$

$$\eta_i^{(j)} = 100 \frac{M_j}{M_1} h_i^{(j)}$$

Figure 2-1 is a graphical representation of the first and second order interaction coefficients in the 1-i-j system.

2.3   THE QUADRATIC FORMALISM

Darken[7] applied the first order interaction coefficient formalism to a ternary system, and showed that it is thermodynamically inconsistent, as it satisfies the Gibbs-Duhem relationship only in the very special case where all the interaction coefficients are equal. So he developed the quadratic formalism, which he presented in two papers[6, 7].

For a binary system, he divided the entire concentration range into three regions, two terminal and one central. He pointed out two apparently general features of binary metallic solutions.

(a) In each terminal region, the second derivative of the molal (gram-atomic) excess free energy with respect to atom fraction, which he calls "excess stability", is substantially constant.

(b) In the central region, the stability may vary strongly and even dramatically with composition, sometimes exhibiting a pronounced maximum; the maximum often occurs at compositions corresponding to small whole number ratios of N_2/N_1 and in accord with classical valences.

In the terminal regions, the activity coefficient of the solvent may be adequately represented up to surprisingly high solute concentrations by an expression of the type

$$\log \gamma_1 = \alpha_{12} \ N_2^2 \qquad\qquad (2.8)$$

By applying the Gibbs-Duhem equation, the activity coefficient of the solute is

$$\log \gamma_2 = \alpha_{12} \ N_1^2 + I \qquad\qquad (2.9)$$

I being an integration constant not necessarily equal to zero.
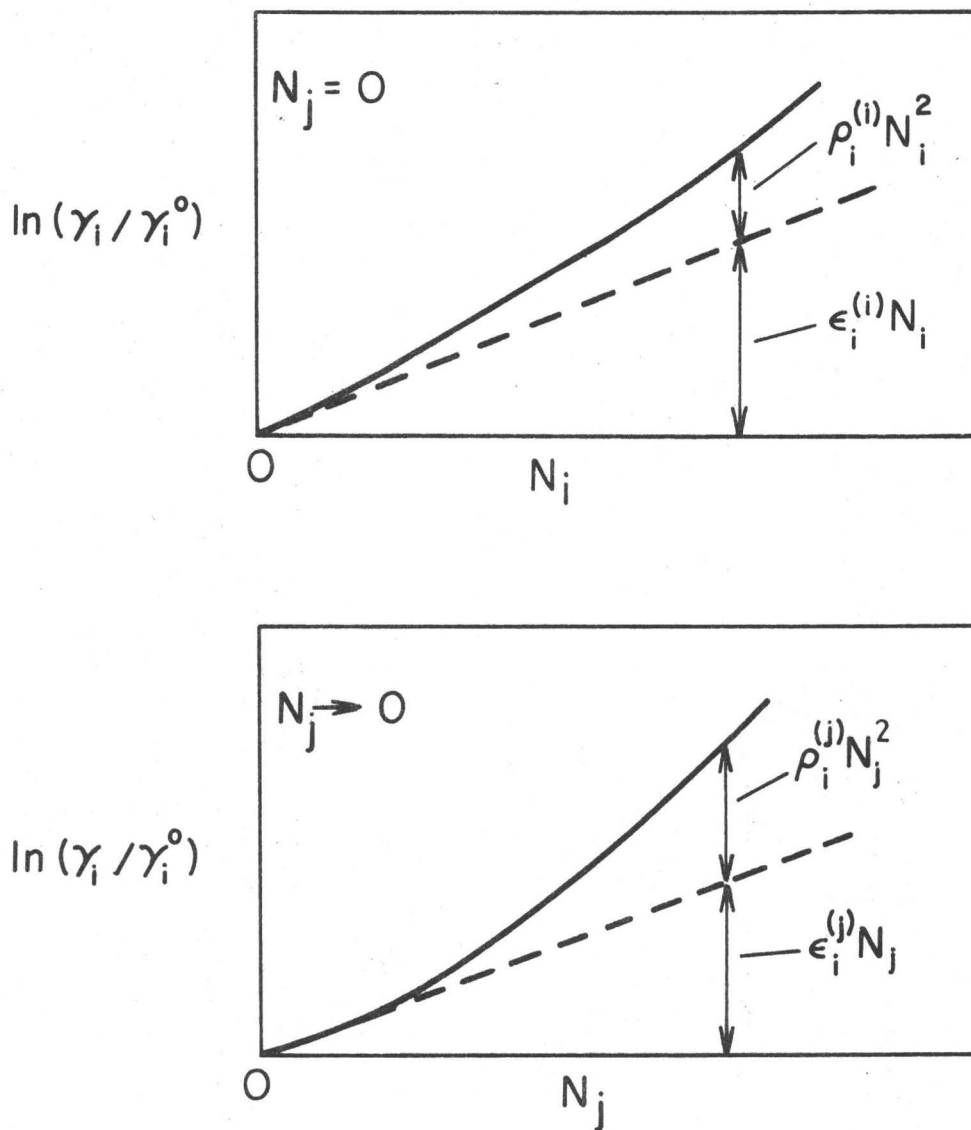
Fig. 2.1 Illustration of the first and second order interaction coefficients in the ternary l-i-j system.

Equations (2.8) and (2.9) are the analytical representations of the activity coefficients of the constituents of a binary solution in the two terminal regions.

For a ternary system 1-2-3, where 1 is the solvent, Darken[7] derived the following analytical expressions for the activity coefficients:

$$\log \gamma_1 = a_{12} N_2^2 + a_{13} N_3^2 + (a_{12} + a_{13} - a_{23}) N_2 N_3 \tag{2.10}$$

$$\log (\gamma_2/\gamma_2^{\,o}) = -2 a_{12} N_2 + (a_{23} - a_{12} - a_{13}) N_3 + a_{12} N_2^2 + a_{13} N_3^2 +$$

$$+ (a_{12} + a_{13} - a_{23}) N_2 N_3 \tag{2.11}$$

$$\log (\gamma_3/\gamma_3^{\,o}) = -2 a_{13} N_3 + (a_{23} - a_{12} - a_{13}) N_2 + a_{12} N_2^2 + a_{13} N_3^2$$

$$+ (a_{12} + a_{13} - a_{23}) N_2 N_3 \tag{2.12}$$

Darken[7] also derived the relations between the coefficients a of the quadratic formalism and the first order free energy interaction coefficients:

$$\epsilon_2^{(2)} = - 2 \times 2.303 \times a_{12} \tag{2.13}$$

$$\epsilon_3^{(3)} = - 2 \times 2.303 \; a_{13} \tag{2.14}$$

$$\epsilon_2^{(3)} = \epsilon_3^{(2)} = 2.303 (a_{23} - a_{12} - a_{13}) \tag{2.15}$$

2.4   PHYSICAL MODELS OF SOLUTIONS

Many attempts have been made to describe the thermodynamic

behaviour of solutions on the basis of a physical model, and many models have been presented. However, none can be satisfactorily applied to every solution.

The simplest model is the ideal solution one. The assumptions of this model are:

(a) The liquid solution of atoms A, B, etc. can be approximated by a quasicrystalline lattice.

(b) The constituent kinds of atoms are of approximately the same size and shape, so that they can be interchanged between the lattice sites without change of the lattice structure, lattice vibrations or the internal states of the atoms.

(c) There are no preferential interaction energies between atoms.

Under these assumptions the enthalpy of mixing is zero and the entropy of mixing is the configurational entropy of mixing. For a binary solution consisting of n_A moles of A and n_B moles of B this entropy is[8]

$$\Delta S = - R (n_A \ln N_A + n_B \ln N_B) \tag{2.16}$$

N_A and N_B being the mole fractions of A and B.

The isothermal free energy of mixing then is

$$\Delta G = RT (n_A \ln N_A + n_B \ln N_B) \tag{2.17}$$

This equation totally describes the system.

A more complicated physical model is the "regular solution" one, proposed by Hildebrand[9, 10, 11]. The assumptions (a) and (b) of the ideal solution model are retained, but assumption (c) is removed, thus allowing for preferential interactions between otherwise similar atoms in a quasicrystalline lattice. Under these assumptions the entropy

of mixing is the same as for an ideal solution, eqn. (2.16), but the enthalpy
of mixing is non-zero, and can be shown[12] to be

$$\Delta H = zwN_{Av} \; \frac{n_A \, n_B}{n_A + n_B} \tag{2.18}$$

where z is the average number of nearest neighbours of a given atom,
N_{Av} is the Avogadro number and

$$w = w_{AB} - (w_{AA}/2) - (w_{BB}/2) \tag{2.19}$$

w_{ij} being the increase in potential energy when a pair of atoms i and j are
brought together from infinite distance to their equilibrium separation
in the lattice.

The free energy of mixing then for a regular solution is

$$\Delta G = zwN_{Av} \; \frac{n_A \, n_B}{n_A + n_B} \; + RT \left[n_A \ln N_A + n_B \ln N_B \right] \tag{2.20}$$

The excess free energy of mixing for a regular solution is
therefore:

$$G^E = \Delta H = zwN_{Av} \; \frac{n_A \, n_B}{n_A + n_B} \tag{2.21}$$

But

$$\frac{\partial G^E}{\partial n_i} = RT \ln \gamma_i \tag{2.22}$$

From (2.21) it follows directly that

$$\ln \gamma_A = \frac{1}{RT} \left(\frac{\partial (\Delta H)}{\partial n_A} \right) = \frac{\Delta \overline{H}_A}{RT} = \frac{z N_{Av} w}{RT} \; N_B^2 \tag{2.23}$$

$$\ln \gamma_B = \frac{\Delta \overline{H}_B}{RT} = \frac{z N_{Av} w}{RT} \; N_A^2 \tag{2.24}$$

$\Delta \overline{H}_i$ being the partial molar heat of solution of i.

The simple regular solution model is incorrect, because it neglects thermal entropy factors and it assumes random atomic arrangement. Both of these factors are important, but is is difficult to devise a model which will include them together in a satisfactory manner. In the "quasichemical solution" model, developed by Guggenheim[13], the random atomic arrangement assumption is removed, so preferential interactions are allowed between the solute atoms. Formulae derived using this model are involved and will not be presented here.

Alcock and Richardson[14] applied the regular solution model to derive an equation for the activity coefficient of a dilute solute s in an alloy of two metals, x and y. Assuming that the distribution of atoms in the solution is random, that the coordination number of all three types of atoms is equal, and that the energy of interaction between atom pairs is independent of concentration, they showed that

$$\ln \gamma_{s(x+y)} = N_x \ln \gamma_{s(x)} + N_y \ln \gamma_{s(y)} - N_x \ln \gamma_{x(x+y)} - N_y \ln \gamma_{y(x+y)}$$

(2.25)

From this,

$$\left[\frac{\partial \ln \gamma_{s\ (x+y)}}{\partial N_y} \right]_{N_y \to 0} \equiv \epsilon_s^{(y)} = \ln \gamma_{s(y)} - \ln \gamma_{s(x)} - \ln \gamma_{y(x)}$$

(2.26)

where $\gamma_{i(j)}$, $\gamma_{i(j+k)}$: activity coefficients of i in the binary i-j and in the ternary i-j-k respectively.

By applying the above equations to simple systems they demonstrated that is is possible to predict with useful accuracy the behaviour of dilute solutions in ternary solutions from data of the three binary systems concerned. Eqn. (2-26) gave values of the interaction parameter $\epsilon_s^{(y)}$

which were correct in sign, but between two and three times smaller than the experimental values, except with $\epsilon_o^{(Al)}$, which is predicted 10 times smaller. It was suggested that these differences might be partly or entirely caused by clustering about the solute atoms of that component of the alloy which interacts more strongly with the solute.

Alcock and Richardson[15] later improved the calculations by using a quasichemical approach, where they took into account the clustering around the solute atoms. According to this model, the predicted interaction parameter is

$$\left[\frac{\partial \ln \gamma_{s(x+y)}}{\partial N_y} \right]_{N_y \to o} \equiv \epsilon_s^{(y)} = \frac{-z(K-1)}{N_x + KN_y} \tag{2.27}$$

where

$$K = \left[\frac{\gamma_{s(x)} \; \gamma_{y(x+y)}}{\gamma_{s(y)} \; \gamma_{x(x+y)}} \right]^{\frac{1}{z}} \tag{2.28}$$

where z is the number of nearest neighbours of each atom. This model predicts somewhat higher values of ϵ than the first one, but still lower than the experimental values, especially when the solute is oxygen or sulfur.

Belton and Tankins[16] pointed out that all the above models assume that the strongly electronegative ions, such as oxygen and sulfur, have the same environment as metallic solutes; this, they argue, is unlikely, as the heats of solution of these elements are large, being more typical of molecule formation rather than alloying. For example, the heats of solution of monatomic oxygen and sulfur in liquid iron are -90 and -74 kcal respectively, as compared with maximum heats of solution of metallic elements in liquid iron of about -13 kcal. They proposed a model in which a dilute solute o in a liquid binary mixture of x and y is considered to form the distinct molecular species xo and yo. They further assumed

that the average energy of interaction of these molecular species with the surrounding metal atoms is small and such that, to a first approximation, the partial molar properties of the species may be considered ideal. According to this model the standard free energy of solution of o in a mixture of x and y is, assuming random distribution of the molecular species,

$$G^M_{o(x+y)} = N_y (G^M_{o(y)} - H^M_y + RT \ln N_y)$$

$$+ N_x (G^M_{o(x)} - H^M_x + RT \ln N_x) \qquad (2.29)$$

where $G^M_{o(y)}$, $G^M_{o(x)}$ are the standard free energies of solution of oxygen in the metals x and y respectively.

CHAPTER 3

LITERATURE REVIEW

3.1   THE BINARY Fe-O SYSTEM

The role of oxygen as a principal reagent in the refining of liquid iron and the necessity for its removal in the finished product have simulated numerous studies of its chemical behaviour in liquid iron.

The usual method employed is to equilibrate the molten metal with a gaseous atmosphere of fixed and known oxygen potential. The partial pressure of oxygen in equilibrium with iron and iron oxide at $1600^{\circ}C$ is extremely low (10^{-8} at). Because of the difficulties involved in controlling such a low pressure, the oxygen potential of the atmosphere is usually fixed by a gas mixture of H_2-H_2O or CO-CO_2 of known composition. The reaction between these atmospheres and molten iron can be written as

$$H_2(g) + \underline{O} = H_2O(g) \tag{3.1}$$

$$CO(g) + \underline{O} = CO_2(g) \tag{3.2}$$

the underlined symbols referring to elements dissolved in liquid iron; unless otherwise stated, the standard state for the activity of underlined elements is the 1 wt.% solution in liquid iron, and the reference state for the activity coefficient the infinitely dilute solution in liquid iron.

The equilibrium constant for the reaction (3.1) is:

$$k_1 = \frac{P_{H_2O}}{P_{H_2}} \cdot \frac{1}{h_o} \tag{3.3}$$

19

where

$$h_o = f_o \; [\%O] \tag{3.4}$$

$$\log f_o = \log f_o^{(o)} = e_o^{(o)} \; \left[\%O \right] \tag{3.5}$$

Equation (3.3) can be rewritten as

$$\log k_1 = \log k_1' - e_o^{(o)} \; [\%O] \tag{3.6}$$

where k_1' is the apparent equilibrium constant,

$$k_1' = \frac{P_{H_2O}}{P_{H_2}} \; \frac{1}{[\%O]} \tag{3.7}$$

It is readily seen from (3.6) that the plot of $\log k_1'$ vs $[\%O]$ should yield a straight line of slope $e_o^{(o)}$ and intercept at zero $\log k_1$. It is to be noted that if the behaviour of oxygen in iron is Henrian, $e_o^{(o)}$ is zero and k_1 is the same as k_1'.

Table 3.1 presents the results of the most important investigations of the reaction (3.1), together with brief information on the experimental technique used.

Figure 6-1 presents the graphs of $\log k_1$ vs $1/T$ for some of the investigations presented in Table 3-1.

The two main points of disagreement between the various investigators concern the Henrian behaviour of oxygen in liquid iron and the temperature dependence of the equilibrium constant of the reaction (3.1).

It is rather difficult, in view of the experimental difficulties involved at high temperatures, to point out specifically the causes of the discrepancies. However, they can be attributed to three main sources:

TABLE 3.1

RESULTS OF SOME INVESTIGATORS FOR THE REACTION 1:

$$H_2(g) + \underline{O} = H_2O(g)$$

Investigator(s)	Year	Ref	Method	Furnace	Temp. Range $^\circ$C	Results	$e_o^{(o)}$
Chipman	1933	17	Equil. melt with H_2O/H_2 mixtures	IND	1550-1700	$\log k_1 = (6200/T) - 3.28$	-
Fontana and Chipman	1936	18	Equil. melt with preheated H_2O/H_2 mix.	IND	1600	$k_1 = 3.95$ at 1600°C	0
Chipman and Samarin	1937	19	as above	IND	1600-1700	$\log k_1 = (10200/T) - 5.5$	-
Dastur and Chipman	1949	20	Equil. melt with preheated $H_2O/H_2/Ar$ mix.	IND	1550-1700	$\log k_1 = (7050/T) - 3.17$	
Averin	1955	21	as above	IND		$\log k_1' = (9440/T) - 4.536$	Neg.
Gokcen	1956	22	as above	RES	1550-1700	$\log k_1 = \log k_1' =$ $= (6670/T) - 3.05$	0
Floridis and Chipman	1958	23	Equil. melt with preh. and non-preh. $H_2O/H_2/Ar$ mix.	IND and RES	1600	$\log k_1 = (7050/T) - 3.20$	-0.20 at 1600°C
Tankins et al	1964	24	Equil. melt with $H_2O/H_2/Ar$ mix	RES	1550-1700	$\log k_1 = \log k_1' =$ $= (6817/T) - 3.13$	0
Matoba and Kuwana	1965	25	Equil. melt with preh. $H_2O/H_2/Ar$ mix	IND	1550-1660	$\log k_1 = (7480/T) - 3.421$	-0.47 at 1600
Schenck and Steinmets	1967	26	Equil. melt with $H_2O/H_2/Ar$ mix	TAM-MAN	1550-1700	$\log k_1 = (6730/T) - 3.05$	Neg.
Present Work	1970		Equil. melt with $H_2O/H_2/Ar$ mix	RES	1550-1700	$\log k_1 = \log k_1' =$ $= (7460/T) - 3.43$	0

(a) Oxygen analysis

(b) Thermal diffusion in the gas phase

(c) Temperature measurement

(a) Nearly all of the oxygen analyses in the investigations were performed on vacuum fusion units. Gokcen[22] pointed out the possibilities of low and erratic values for samples containing over 200 ppm oxygen due to spatter upon melting when the samples are dropped in a graphite crucible not equipped with a baffle or lid. In addition, the ingots were generally sectioned and small samples were cut and analyzed. Thus, if segregation occurred within the ingot during solidification, erroneous results could be obtained.

(b) When a mixture of gases encounters a hot surface with a thermal gradient, the heavier molecules tend to concentrate away from the hot surface. This phenomenon is called thermal diffusion and has been discussed adequately by Dastur and Chipman[37]. The thermal gradient above the melt is particularly sharp in inductively heated melts. If thermal diffusion occurs, the P_{H_2O}/P_{H_2} ratio prevailing over the surface of the melt will be lower than the inlet ratio, thus giving high values for the apparent equilibrium constant. The addition of a gas of high molecular weight, such as Ar, and/or preheating of the incoming gas, will reduce or neutralize this effect. Much of the earlier work was subject to uncertainty of this nature, particularly when an induction furnace was used without special precautions.

(c) Optical temperature measurements may be subject to several sources of error: excessive extrapolation of the calibration curve, fume formation and emissivity effects. D'Entremont[27] showed that unexpected errors may arise due to variation of the emissivity of the melt with the oxygen content.

3.2   EFFECT OF V ON THE ACTIVITY COEFFICIENT OF O IN LIQUID IRON

The effect of V on the activity coefficient of O in liquid iron can be determined by equilibrating Fe-V melts with an atmosphere of known oxygen potential, i.e. H_2O/H_2. The equilibrium constant can be written as

$$k_1 = \frac{P_{H_2O}}{P_{H_2}} \cdot \frac{1}{h_o} \qquad (3.8)$$

where

$$h_o = f_o \cdot [\%O] \qquad (3.9)$$

and

$$f_o = f_o^{(o)} \cdot f_o^{(v)} \qquad (3.10)$$

or, in terms of first order free energy interaction parameters,

$$\log f_o = e_o^{(o)} \cdot [\%O] + e_o^{(v)} \cdot [\%V] \qquad (3.11)$$

so

$$\log k_1 = \log \left(\frac{P_{H_2O}}{P_{H_2}} \right) - \log h_o$$

$$= \log \left(\frac{P_{H_2O}}{P_{H_2}} \right) - e_o^{(o)} \cdot [\%O] - e_o^{(v)} \cdot [\%V] - \log [\%O] \qquad (3.12)$$

Since $\log k_1$ and $e_o^{(o)}$ are known from the binary Fe-O, and $[\%O]$, $[\% V]$ can be determined by chemical analysis and P_{H_2O}/P_{H_2} is known, $e_o^{(v)}$ can be determined from the above equation.

The first investigation in the Fe-V-O system was made by Chipman and Dastur[28] in 1951, using the method outlined above.

Experiments were conducted in an induction furnace. The incoming H_2O/H_2 gas was preheated and mixed with 4 parts of Ar to avoid thermal diffusion errors. All runs were made at 1600°C. Using the value of k_1 from their previous investigation[20] and assuming Henrian behaviour of oxygen in the melt, they found that for a particular oxygen potential in the gas phase vanadium additions increased the solubility of oxygen. Their data give a value of $e_O^{(v)}$ = -0.27 at 1600°C.

Narita[29, 30] in 1958, using a similar technique, determined the $e_O^{(v)}$ at 1600, 1650 and 1700°C as -0.365, -0.287 and -0.196 respectively.

In 1967 Schenck and Steinmets[32] determined the $e_O^{(v)}$ as -0.11 at 1600°C by equilibrating Fe-V melts with H_2/H_2O in a Tamman resistance furnace.

Pargeter[33] determined the $e_O^{(v)}$ as -0.290 at 1600°C by equilibrating Fe-V melts with H_2/H_2O atmospheres in a Pt resistance furnace.

Kershaw[34] using a levitation melting technique determined the $e_O^{(v)}$ between 1550 - 1750°C.

Fischer and Haussmann[31], employing an oxygen probe of the type

$$\text{Pt} | \text{air} \mid ZrO_2 (CaO) \mid [O] \quad \text{in liq. Fe-V} | \text{Pt}$$

determined the $e_O^{(v)}$ as -0.13 at 1600°C.

Fruehan[35] also employed oxygen probes of the type

$$\text{Mo} \mid \text{Cr, } Cr_2O_3 \mid ZrO_2 (CaO) \mid \text{Fe-V-O (1, sat. with } V_2O_3(s)) \mid \text{Mo}$$

or

$$\text{Mo} \mid \text{Cr, } Cr_2O_3 \mid ThO_2(Y_2O_3) \mid \text{Fe-V-O (1, sat. with } V_2O_3(s)) \mid \text{Mo}$$

to measure the activities of V and O in liquid Fe-V-O alloys of up to 36%V at 1600°C. He reported a value of $e_O^{(v)}$ = -0.14. He found the activity of V to show a negative deviation from Raoult's law and estimated the γ_V^o as 0.10.

The results of the above investigation are summarized in Table 3.2.

Once more, it is difficult to discuss why these big differences in the value of $e_o^{(v)}$ exist. The same reasons as those given in §3.1 may be blamed, with one addition: Vanadium oxides may have been present in the samples analyzed for oxygen in those investigations where equilibration of the melt with an oxide was sought[28, 29, 30]. This would lead to a higher oxygen content and consequently a more negative value of $e_o^{(v)}$.

3.3   EQUILIBRIA IN THE Fe-V-O SYSTEM

Chipman and Dastur[28] were again the first to study the equilibria in the Fe-V-O system. They equilibrated Fe-V melts with H_2O/H_2 atmospheres and gradually increased the $H_2O:H_2$ ratio until some of the dissolved V was oxidized and appeared as an oxide film on the surface of the melt. The H_2O/H_2 gas was mixed with 4 parts of Ar and preheated to avoid thermal diffusion error. All runs were conducted at $1600^{\circ}C$. At the end of the run the ingot was quenched, sectioned and sampled for O and V analysis. The oxide product was identified by X-ray diffraction techniques as the spinel FeV_2O_4 for two ingots containing 0.1%V and V_2O_3 for ingots of more than 0.17%V. Based on the identification of the oxide products, the corresponding reactions were written as

$$FeV_2O_4(s) + 4H_2(g) = 2\underline{V} + Fe(1) + 4H_2O(g) \qquad (3.13)$$
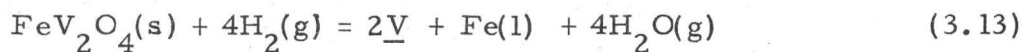
$$k_{3.13} = h_v^2 \left(\frac{P_{H_2O}}{P_{H_2}} \right)^4 \qquad (3.14)$$

for V concentrations for which FeV_2O_4 is the product, and

$$V_2O_3(s) + 3H_2(g) = 2\underline{V} + 3H_2O(g) \qquad (3.15)$$
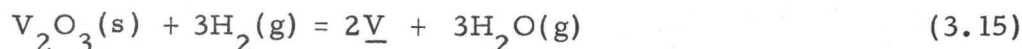
TABLE 3.2

VALUES OF e_o^V FROM VARIOUS INVESTIGATORS

T, °C	Chipman and Dastur[28]	Narita (29)	Schenck and Steinmetz[32]	Pargeter (33)	Kershaw (34)	Fischer and Haussmann[31]	Fruehan (35)	Present Work
1550					-0.268			-0.208
1600	-0.27	-0.365	-0.11	0.29	-0.244	-0.13	-0.14	-0.185
1650		-0.287			-0.208			-0.166
1700		-0.196			-0.189			-0.134
1750					-0.179			
Range investigated, %V	0-1.58	0-0.79	0-0.7	0-1.2	0-1.0	0-2.5	0-36	0-2.0

$$k_{3.15} = h_v^2 \left(\frac{P_{H_2O}}{P_{H_2}} \right)^3 \qquad (3.16)$$

for V concentrations for which V_2O_3 is the product.

A plot of log (P_{H_2O}/P_{H_2}) vs log h_v yields a straight line of slope 1/2 corresponding to reaction (3.13) and 2/3 corresponding to the reaction (3.15).

Karasev, Polyakov and Samarin[36] studied the same system at 1595 and 1695°C using a similar technique. They identified the spinel as the oxide phase for up to 0.2%V and the V_2O_3 at higher V concentration. But on plotting the log (P_{H_2O}/P_{H_2}) vs. log h_v they observed that the slope of the line for V concentrations greater than 0.3% was very close to 1, so they report that above 0.3%V the stable oxide is the vanadium monoxide, VO or V_2O_2. They argue that they did not identify the V_2O_2 by X-ray diffraction because it decomposes during quenching:

$$3V_2O_2(s) = 2V_2O_3(s) + 2V(s) \qquad (3.17)$$

and the resulting V was oxidized to V_2O_3:

$$2V(s) + 3/2 \ O_2(g) = V_2O_3(s) \qquad (3.18)$$

Narita[29, 30] studied the system with a similar method at 1600, 1650 and 1700°C. He identified as reaction products the spinel FeV_2O_4 and the oxide V_2O_3.

Table 3.3 summarizes the results of the above investigations.

TABLE 3.3

COMPARISON OF THE RESULTS FOR THE REACTIONS (3) and (4)

	Present Work 0 - 12%V	Chipman and Dastur[28] 0-1.30%V	Karasev et al[36] 0 - 2%V	Narita[29] 0 - 0.8%V
ΔG_3 at 1600°C	-220900 + 85.55T -60700 cal	-61200 cal	-232020 + 100.24T -44300 cal	-204519 + 75.524T -63070 cal
ΔG_4 at 1600°C	-198550 + 80.57T -47650	-195900 + 78.2T -49300 cal	-191700 + 82.92T -36400 cal	-193532 + 76.014T -51150 cal

Reaction (3): $2\underline{V} + 4\underline{O} + Fe(1) = FeV_2O_4(s)$

Reaction (4) $2\underline{V} + 3\underline{O} = V_2O_3(s)$

3.4   THE OXYGEN PROBE

The principle of the oxygen probe is discussed in more detail in § 9.2.

The oxygen probe is essentially an oxygen concentration electro-chemical cell, which measures the difference in the activities of oxygen between the two electrodes. It consists of two electrodes of fixed oxygen chemical potential separated by a solid electrolyte which conducts essentially via oxygen anions. In steelmaking applications one electrode is the liquid Fe-O-i alloy whose oxygen activity is being determined and the second (reference electrode) is one of fixed and known oxygen activity.

During the past decade a number of papers[45-56] describing the development of oxygen probes appeared in the literature.

3.4.1   Electrolytes

A more detailed discussion on the solid electrolytes is given in § 9.2. The most commonly used solid electrolyte in oxygen probes is the calcia stabilized zirconia (ZrO_2 + 15 mole pct CaO).

This material has been exhaustively studied at lower temperatures (around $1000^{\circ}C$), and the lowest oxygen pressure, above which the anionic conductivity is 99% of the total or higher, has been estimated at about 10^{-17} atm (Steele and Alcock[57]), i.e. just below the Fe-FeO equilibria. Other invesigators however (Tretjakow and Schmalzried[58] and recently Pugliese and Fitterer[59]) have reported successful experiments using this material down to the Cr, Cr_2O_3 equilibrium ($P_{O_2} \simeq 10^{-22}$ at $1000^{\circ}C$).

Meaningful extrapolation of these data to steelmaking temperatures is not possible. Baker and West[48] have tested ZrO_2 (CaO) electrolytes up to steelmaking temperatures, and report that they cannot be used below a $P_{O_2} \simeq 10^{-8.4}$ atm at $1600^{\circ}C$, which renders them useless for steelmaking purposes.

Fischer and Janke[60] also tested ZrO_2 (CaO) electrolytes at

steelmaking temperatures by measuring the equilibrium oxygen partial pressures of H_2O-H_2 gas mixtures using a ZrO_2 (CaO) tube and air as reference electrode. They find the EMF readings lower than those expected for a reversible galvanic cell, the deviation increasing with decreasing oxygen partial pressure and increasing temperature. At $1600^{\circ}C$ they set the critical P_{O_2} at about 2.8×10^{-10} atm.

Despite these rather disappointing figures, satisfactory performance of ZrO_2 (CaO) electrolytes in liquid steel has been demonstrated by Fischer and Ackermann[46] at oxygen contents down to 250 ppm ($\simeq 10^{-10}$ atm. O_2), by Schwerdtfeger[49] down to about 100 ppm ($\simeq 2.9 \times 10^{-11}$ atm O_2), and by Faurschou and co-workers[51, 52, 53] at all oxygen levels of interest in steelmaking. Gattelier et al.[56] of IRSID tested oxygen probes with ZrO_2(CaO) as electrolyte down to 80 ppm oxygen in binary Fe-O melts and also studied deoxidation kinetics by adding Si, Ti or Al; they reported satisfactory performance down to about 20 ppm oxygen. All the above investigators used air as reference electrode.

Fruehan and Turkdogan[54, 55] used oxygen probes with ZrO_2(CaO) or $ThO_2(Y_2O_3)$ as electrolytes and Cr, Cr_2O_3 as the reference electrode. The equilibrium oxygen partial pressure for Cr, Cr_2O_3 at $1600^{\circ}C$ is about 8.4×10^{-13} atm; this value is lower than the activity of oxygen in steel for most practical applications. They found that the $ThO_2(Y_2O_3)$ electrolytes were predominantly anionic conductors at $1600^{\circ}C$ down to oxygen partial pressures at least as low as those in equilibrium with Si-SiO_2 (2×10^{-16} atm) [55, 61]. They tested ZrO_2 (CaO) against $ThO_2(Y_2O_3)$ probes in liquid steel, and the results agreed to $\pm$ 2 mV, which is within the usual experimental scatter. They deduced from this fact that ZrO_2(CaO) exhibits insignificant electronic conductivity at $1600^{\circ}C$ down to oxygen partial pressure at least as low as that for the Cr, Cr_2O_3 equilibrium (8×10^{-13} atm). They estimate that the critical P_{O_2} below which the ZrO_2 (CaO) electrolyte exhibits appreciable electronic conductivity is less than 3×10^{-13} atm at

$1600^{\circ}C$. Below this value appreciable drift was observed in the EMF readings. No satisfactory explanation was offered for this drift; they stated as a possibility the polarization of the Cr, Cr_2O_3 electrode by mass transfer due to the partial electronic conductivity of the electrolyte.

3.4.2 Probe Designs

An early probe design[46, 47, 49] is shown on Fig. 3.1. It consists of a ZrO_2(CaO) tube closed at one end with a Pt wire fixed inside the closed end. The tube was flushed with a gas of known oxygen potential, most commonly air, which acted as the reference electrode. The tube was immersed in liquid iron and contact with the melt was made with a Pt or Mo wire.

The disadvantages of using the electrolyte in the form of a tube are: the very high cost, the poor thermal shock resistance, and the fact that fine pores and microcracks, which are invariably present in the tubes, are detrimental to the satisfactory operation of the cell, particularly with air as the reference electrode.

The high cost of zirconia tubes and their poor thermal shock resistance were resolved by Fitterer[50] who used a silica tube with a small pellet of ZrO_2(CaO) electrolyte fused at one end. Such probes are relatively inexpensive, and because they only employ a small electrolyte pellet they show better thermal shock resistance. Fitterer employed these electrolytes with air or CO_2 as the reference electrode.

The same type of probe with air as the reference electrode was developed and tested on a laboratory and industrial scale by the Mines Branch of the Department of Energy, Mines and Resources of Canada, and became commercially available through LEIGH INSTRUMENTS LTD. of Carleton Place, Ont.

The advantages of using air as the reference electrode are:

(a) the activity of oxygen in air is fixed and accurately known.
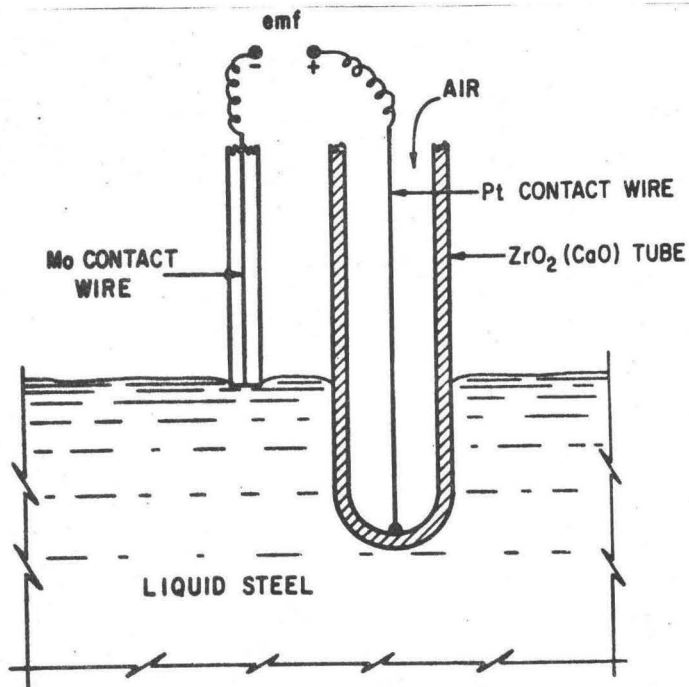
Fig. 3.1 ZrO_2 (CaO) tube used as oxygen probe with air as reference electrode. (From[54])
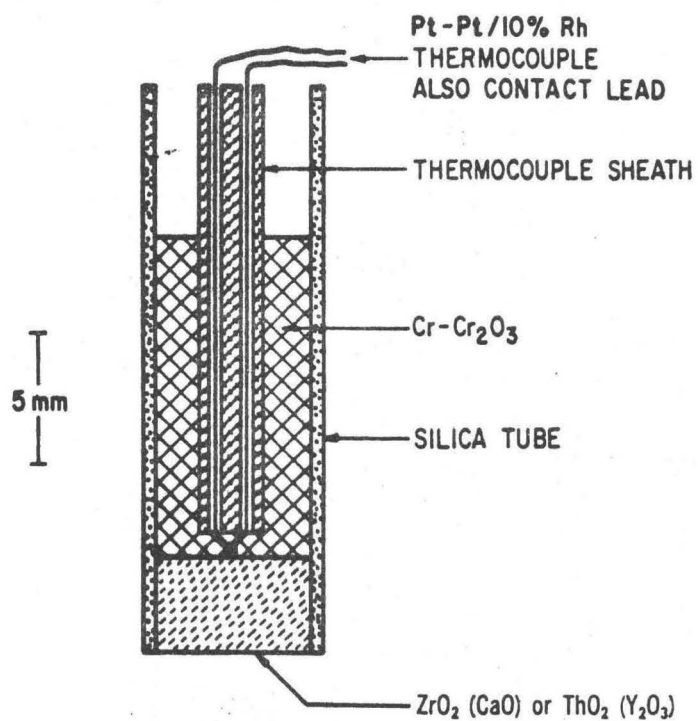
Fig. 3.2 The U.S.S. oxygen probe (From[54]).

(b)   It is ambient to the probe system, and this simplifies the continuous supply and delivery of the reference electrode.

(c) It is compatible with the use of zirconia electrolytes.

Its disadvantages are:

(a) There is always the possibility of air leaking through microcracks from the reference electrode to the metal, thus affecting the operation of the cell.

(b) It gives rise to a high EMF reading; as a result the determination of oxygen in steel becomes less accurate. Higher accuracy can be obtained when the activity of oxygen in the reference electrode is in a range similar to that of the oxygen in the melt.

(c) It is not compatible with the use of ThO_2-Y_2O_3 electrolytes (§ 9.2).

These disadvantages made Turkdogan and Fruehan[54, 55] of the United States Steel Corp. look for a solid reference electrode. The choice is severely limited, a mixture of Cr and Cr_2O_3 appearing to be the only choice compatible with ZrO_2(CaO) electrolytes. Using this as reference electrode they developed the U.S. Steel probe which is shown schematically in Fig. 3.2. This probe has been used extensively in a number of laboratory investigations[61], [35].

Table 3.4 summarizes the different probe designs which have been successfully employed in the measurement of oxygen activities in steel.

3.4.3   Calculation of the Activity of Oxygen from the Measured EMF

When air is used as reference electrode the oxygen probe is represented by the following cell:

$$\oplus \text{ air } \left| ZrO_2(CaO) \right| [O] \text{ in liq. Fe } \ominus \qquad (3.19)$$
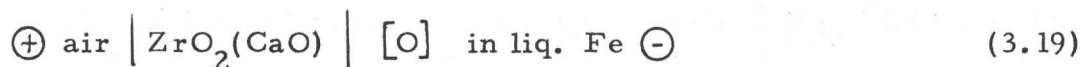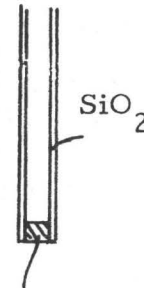
and the cell reaction is:

$$1/2 \ O_2(g) \longrightarrow \underline{O} \quad , \ \Delta G_2 \qquad (3.20)$$

TABLE 3.4   OXYGEN PROBE DESIGNS

Ref. / Cell	Gas			Solid		
	Ref.	Electrolyte	Organization	Ref.	Electrolyte	Organization
SiO_2 electrolyte pellet	air	ZrO_2(CaO)	U. of Pittsburg[50] Dept. of Energy, Mines and Resources and Leigh Instr. (51, 52, 53) IRSID[56]	Cr+ Cr_2O_3 Cr+ Cr_2O_3	ZrO_2(CaO) $ThO_2(Y_2O_3)$	U.S. Steel Corp.[54, 55] U.S. Steel Corp.[54, 55]
electrolyte tube	air or CO+ CO_2	ZrO_2(CaO) or (MgO) $ThO_2(Y_2O_3)$	M.P.I., Dusseldorf[46, 47] U.S. Steel Corp.[49] IRSID[56] U.S. Steel Corp.[49]	Cr+ Cr_2O_3 Gra- phite	ZrO_2(CaO) or (MgO) ZrO_2(CaO)	IRSID[56] U. of Tokyo[45]

for which

$$\Delta G_2 = \Delta G_2^o + RT \ln k_2 = \Delta G_2^o + RT \ln \frac{h_o}{\sqrt{P_{O_2}}} \qquad (3.21)$$

ΔG_2^o being the standard free energy change for the reaction (3.20) and P_{O_2} the partial pressure of oxygen in air (0.2095).

ΔG_2 is related to the measured EMF E(V) by the relation

$$\Delta G_2 = -2EF \qquad (3.22)$$

From (3.21) and (3.22) it follows that

$$\log h_o = \frac{1}{2} \log P_{O_2} - \frac{2EF}{4.574T} - \frac{\Delta G_2^o}{4.574T} \qquad (3.23)$$

Substituting the value for ΔG_2^o as calculated from the data of Floridis and Chipman[23] and 0.2095 for P_{O_2} in air, eqn. (3.23) yields

$$\log h_o = -0.19 + (6122 - 10.08E)/T \qquad (3.24)$$

where E is expressed in mV and T in ^oK.

When Cr, Cr_2O_3 is used as the reference electrode the oxygen probe is represented by the following cell:

$$\oplus \quad [O] \quad \text{in liq. Fe} \ \Big| \ ZrO_2(CaO) \ \Big| \ Cr, Cr_2O_3 \ \ominus \qquad (3.25)$$
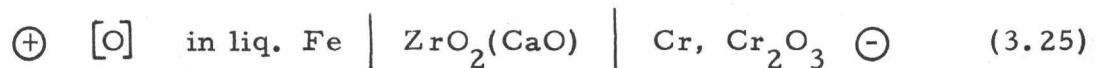
the cell reaction being

$$\underline{O} + \frac{2}{3} Cr(s) \longrightarrow \frac{1}{3} Cr_2O_3(s) \qquad (3.26)$$
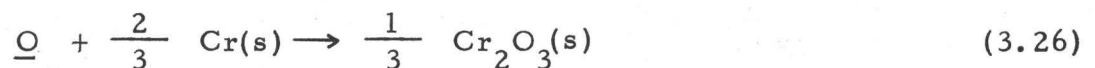
For this reaction

$$\Delta G_{3.26} = \Delta G_{3.26}^o - RT \ln h_o = -2EF \qquad (3.27)$$

$\Delta G^o_{3.26}$ being the standard free energy change for the reaction (3.26), equal to the difference of the free energy changes for the following reactions:

$$\frac{1}{2} \ O_2(g) + \frac{2}{3} \ Cr(s) \longrightarrow \frac{1}{3} \ Cr_2O_3(s) \tag{3.28}$$

$$\frac{1}{2} \ O_2(g) \longrightarrow \underline{O} \tag{3.29}$$
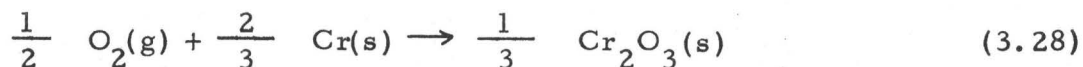
$$\Delta G^o_{3.26} = \Delta G^o_{3.28} - \Delta G^o_{3.29}$$

$$= RT\ln \sqrt{P_{O_2}} + RT\ln k_2$$

$$= RT\ln k_2 \ \sqrt{P_{O_2}} \tag{3.30}$$

k_2 is the equilibrium constant for the reaction (3.20) and P_{O_2} the oxygen pressure in equilibrium with Cr, Cr_2O_3.

From eqns. (3.27) and (3.30) we have

$$\log h_o = \frac{2EF}{4.574T} + \log k_2 \ \sqrt{P_{O_2}} \tag{3.31}$$

For the temperature dependence of P_{O_2} the data for the free energy of formation of Cr_2O_3 as given by Jeannin, Mannerskantz and Richardson[62] are used, extrapolated to steelmaking temperatures. Values from straight extrapolation differ by 330 cal per mole O_2 from values extrapolated using high temperature calorimetric data[63, 64]. With this value for P_{O_2} and Floridis and Chipman's[23] value for k_2, eqn. (3.31) yields

$$\log h_o = 4.52 - (13300 - 10.08E)/T \tag{3.32}$$

where E is expressed in mV and T in $^{\circ}$K.

This equation gives activities of oxygen 12% higher than the one derived by Fruehan et al[55], based on values of the free energy of formation of Cr_2O_3 compiled by Elliott et al[65].

CHAPTER 4

APPARATUS AND EXPERIMENTAL TECHNIQUE

4.1   INTRODUCTION

Two experimental methods were used in this study. The first consisted of equilibrating the Fe or Fe-V melts with H_2O/H_2 atmospheres diluted with Ar. This technique was used with alloys of up to 2%V. At higher V concentrations the H_2O/H_2 ratio required to achieve saturation of the melt with oxygen was relatively low, requiring operation of the water bath at temperatures near or lower than ambient. One alternative was to use solid oxalic acid dihydrate or a saturated lithium chloride solution instead of water to produce the H_2O/H_2 gas mixtures.

The second alternative was to use an oxygen probe to measure the activity of oxygen in the melt. This method was chosen because it also enabled the activity of V in the melts to be determined.

4.2   APPARATUS AND EXPERIMENTAL TECHNIQUE - H_2O/H_2 EQUILIBRIA

4.2.1   The Gas Train

The gas train is shown schematically in Fig. 4.1. The H_2O/H_2 mixtures were produced in a constant temperature water bath. Commercial purity H_2 was passed at room temperature through a palladium catalyst to convert traces of O_2 to H_2O, ascarite to remove CO_2, and a calibrated flow meter. It was then bubbled through the presaturator and the saturator. The presaturator consisted of a conical flask filled with distilled water and held at a temperature $20^{\circ}C$ higher than the saturator. The saturator consisted of eight conical flasks connected in series and immersed into a
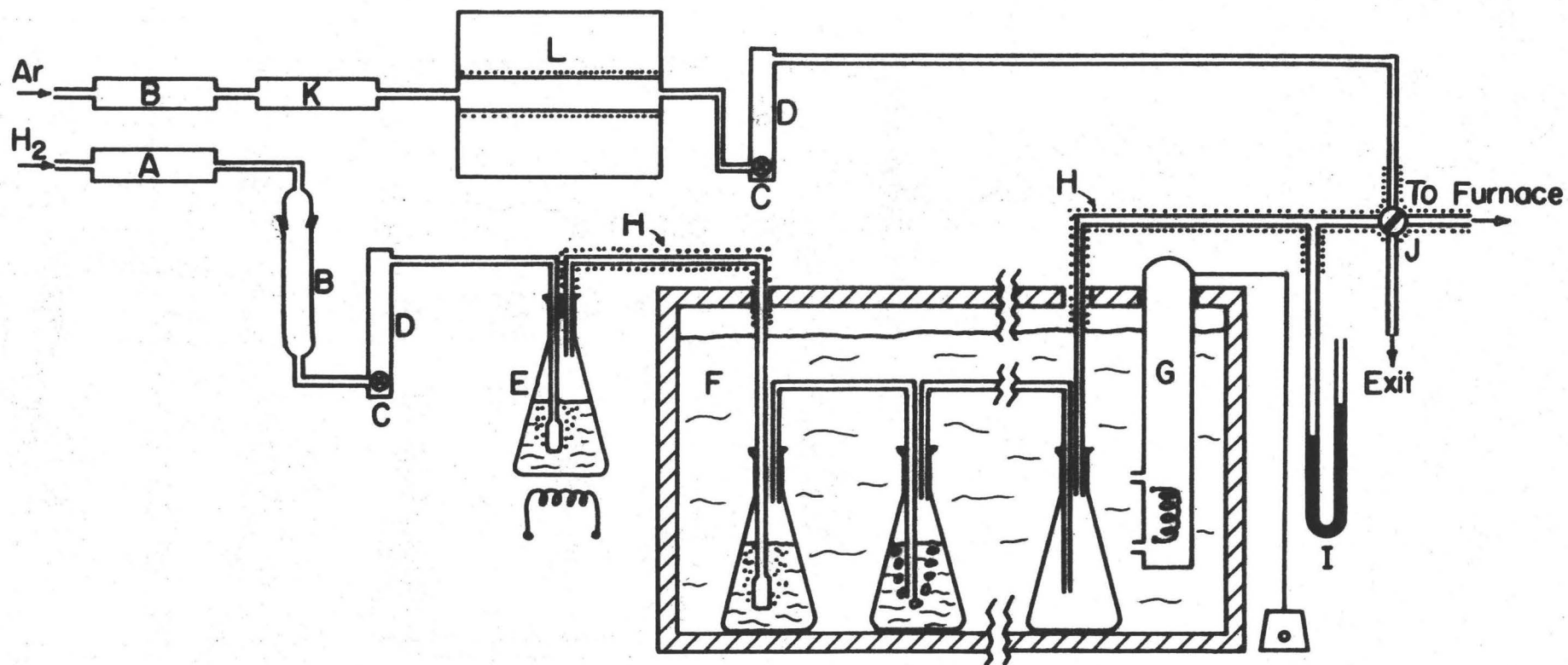
A	PALLADIUM CATALYST	G	WATER BATH HEATER AND CONTROLLER
B	ASCARITE	H	HEATING TAPE
C	NEEDLE VALVE	I	DIBUTYL-PHTALATE MANOMETER
D	FLOW METER	J	STOPCOCK
E	PRESATURATOR	K	MAGNESIUM PERCHLORATE
F	WATER BATH	L	ARGON DEOXIDIZING FURNACE

FIG. 4.1 The Gas Train.

water bath; the first seven flasks were filled with distilled water and the last one was empty. The temperature of the water bath was controlled by an immersion resistance heater, which also maintained a constant circulation of the water. The temperature control was better than $\pm 0.05^{\circ}C$. The line pressure was measured by a dibutyl phthalate manometer placed just after the saturator.

The efficiency of the saturator was checked over a wide range of operating conditions. The checks consisted of absorbing the water vapour in four tubes filled with magnesium perchlorate and finding the difference in weight before and after the check. The fourth tube was used to ensure that all the water vapour was eliminated from the gas; its weight did not change during the experiments. The total volume of the H_2 passed through the bath was measured with a laboratory wet test meter, previously calibrated for hydrogen by the soap bubble method. For flow rates of 0.2 - 1 1/min. H_2 and bath temperatures between 30 and $40^{\circ}C$ the measured values of the P_{H_2O}/P_{H_2} were within 2% of the tabulated values in the literature.

Argon was passed through tubes containing ascarite to remove CO_2, magnesium perchlorate to remove H_2O, and either Mg chips held at $600^{\circ}C$ or Zr sponge held at $750^{\circ}C$ to remove O_2. It was then passed through a calibrated flow meter and into the H_2/H_2O gas line.

The gas lines from the presaturator to the saturator and from the saturator to the furnace were made of 1/4 in. copper tubing and were heated to $80^{\circ}C$ to avoid condensation.

4.2.2   The Furnace

A vertically mounted, molybdenum wound, tubular resistance furnace was used for this investigation. The furnace and temperature control assembly are shown schematically in Fig. 4.2.

The furnace tube, of high purity recrystallized alumina, was
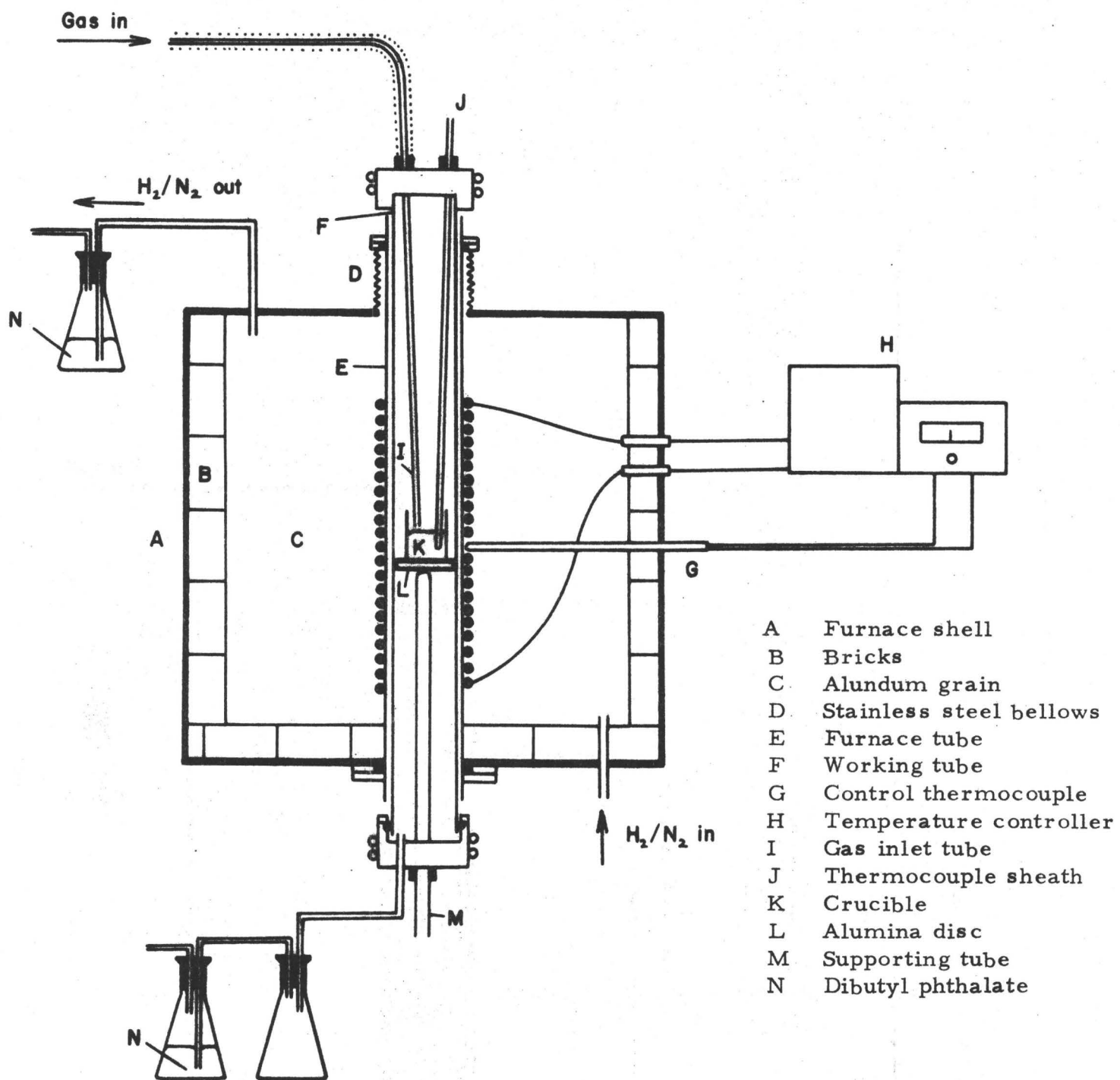
Fig. 4.2 The furnace and crucible assembly (not to scale).

A   Furnace shell
B   Bricks
C   Alundum grain
D   Stainless steel bellows
E   Furnace tube
F   Working tube
G   Control thermocouple
H   Temperature controller
I   Gas inlet tube
J   Thermocouple sheath
K   Crucible
L   Alumina disc
M   Supporting tube
N   Dibutyl phthalate

differentially wound with 0. 050 in. Mo wire over 10 in. with 10, 9, 8, 9 and 10 turns/in. for 1 1/2, 1 1/2, 4, 1 1/2 and 1 1/2 in. respectively. This differential winding gave a longer furnace hot zone.

The furnace tube was centrally located in a brick-lined cylindrical steel shell of 16 in. diameter and 20 in. height. The shell was fitted with a removable top to which a 5 in. long extension of 3 in. diameter stainless steel flexible bellows was welded. The purpose of the bellows was to allow for thermal expansion of the furnace tube. The tube was secured by means of water-cooled glands and "O" rings, located at the base of the shell and at the upper end of the bellows. In this way the shell was gas tight. The space inside the shell around the tube was filled with -8 + 72 mesh alundum grain. A protective 5% H_2 - 95% N_2 gas mixture was passed through the shell to prevent the Mo wire from oxidizing.

A Pt5%Rh-Pt20%Rh control thermocouple was placed inside a thin recrystallized alumina sheath located at the side of the shell and extending up to the hot zone of the furnace tube.

Power to the furnace was supplied through a proportional power controller (Barber-Coleman series 621) driven by a null balance millivoltmeter controller (Barber-Coleman model 377D) which received the output from the control thermocouple. A current limiting feature was incorporated in the power controller to limit the output current to a predetermined value. This is essential under load conditions where transformer coupled heating elements have a very low resistance when cold, and a very high resistance when hot, as is the case with Mo elements.

An alumina working tube was placed concentrically inside the furnace tube.

A typical temperature profile of the furnace is shown in Fig. 4. 3. The temperature variation at the hot zone of the furnace was $\pm 2^{\circ}C$ over 1 in. and $\pm 7^{\circ}C$ over 2 in.
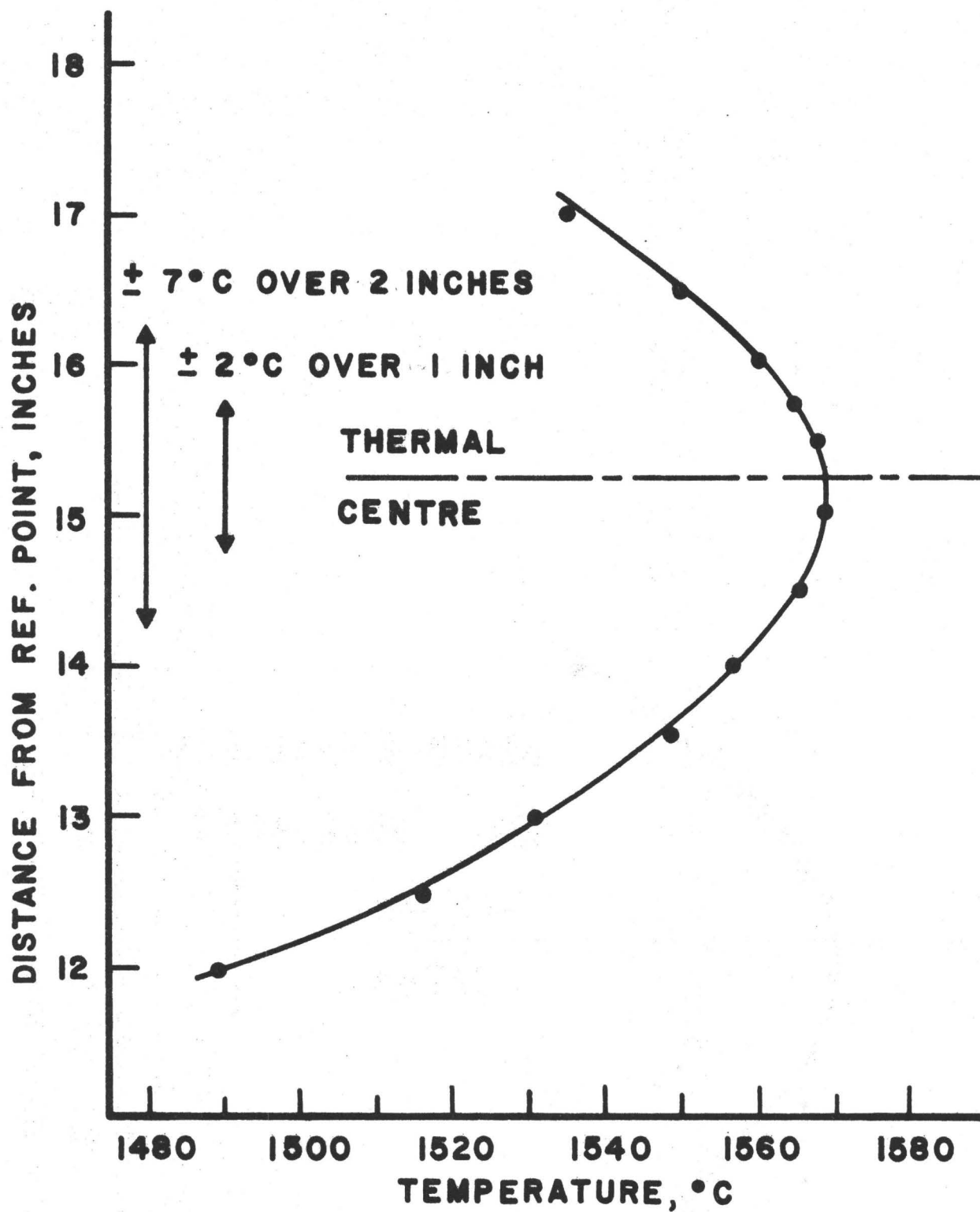
Fig. 4.3 Temperature profile of the resistance furnace.

The power controller limited variation in the furnace temperature to $\pm 2^{\circ}C$.

4.2.3   The Working Tube and Crucible Assembly

The working tube and crucible assembly are shown on Fig. 4.2. The working tube was of high purity recrystallized alumina and was fitted at the top and bottom with water-cooled brass heads that sealed through "O", ring seals onto the tube. The head at the top had an opening for insertion of a thermocouple sheath which was immersed into the melt; a second opening through which an alumina tube could be inserted to lead the incoming gas just above the surface of the melt. Sometimes this tube was immersed just below the surface, so that the gas was bubbled through the melt. A third opening was fitted with an optical flat so that the melt could be observed visually, and a fourth opening served for sampling and for making additions. The head at the bottom was fitted with a gas outlet and with a central opening through which a closed end alumina tube was inserted to support the crucible. All the openings in the heads were sealed with either swagelock fittings with teflon ferrules or with 'O' ring fittings to ensure gas tightness.

4.2.4   Materials

Armco iron, supplied from Corey Steel Co. in the form of 1 in. diameter rods, was used for most of the experiments. Typical analyses of two batches of this material are given in Table 4.1. The vanadium used was supplied in powdered form by Alfa Inorganics. A typical analysis is given in Table 4.2.

All the refractories used were of high purity recrystallized alumina (McDanel 997 for the furnace, working and gas inlet tubes, Morganite Triangle RR for the crucibles and thermocouple sheaths).

TABLE 4.1

ANALYSIS OF ARMCO IRON

in wt. %

Element	C	Mn	P	S	Si	Cu	O
Batch 1	0.027	0.045	0.006	0.013	0.000	0.010	0.06
Batch 2	0.024	0.033	0.005	0.015	0.001	0.018	0.07

TABLE 4.2

ANALYSIS OF VANADIUM

in ppm

Fe	Si	Al	C	Cr	Others
1000	800	200	900	600	100

4.2.5   Experimental Procedure

It was found that a much longer life could be obtained from the alumina furnace tube if it was held at 1300°C between experiments.

At the beginning of an experiment the crucible, containing about 130-140 g of metal, was placed into the bottom furnace head, the head was sealed into position and the crucible pushed with the supporting tube into the hot zone of the furnace at the rate of about 1 in. every 10 min., to avoid thermal shock. At the same time, the thermocouple sheath and gas inlet tube were inserted through the top head and lowered at the same rate into the hot zone. The furnace was continuously flushed with purified Ar.

After the crucible was into position the temperature of the furnace was raised to the desired experimental temperature.

When the temperature reached 1500°C the H_2O/H_2 gas mixture, which until this time was directed to the atmosphere, was admitted into the working tube. The flow rates of H_2 and Ar were adjusted to 300 and 1500 ml/min respectively for most of the experiments; lower and higher flow rates were tried together with varying H_2 to Ar ratios (2:1 to 5:1), giving results in agreement within the experimental error. The main reason for diluting the H_2O/H_2 mixtures with Ar was to avoid thermal diffusion errors[37], although this is less likely to happen in a resistance furnace. The addition of Ar also lowered the partial pressure of hydrogen, resulting in lower hydrogen content of the melt.

After the desired experimental temperature was reached the thermocouple sheath was immersed into the melt and the gas inlet tube was adjusted so as to blow gas just above or just below the surface of the melt.

In the case of runs in the binary Fe-O system sufficient time was allowed for equilibrium to be reached, usually 1 1/2 - 2 h, and then one or two suction samples were taken from the melt with a transparent

quartz tube (3mm ID). They were removed quickly from the furnace, quenched in liquid nitrogen and stored in a dessicator for analysis. The temperature was then changed and the same procedure followed. After equilibration at 3 or 4 experimental temperatures, the furnace temperature was reduced slowly to 1300°C and the crucible, gas inlet tube and thermocouple sheath were slowly removed.

The same procedure was followed for runs in the ternary Fe-V-O system when saturation with oxygen was not desired.

When saturation was sought, the V content of the melt was gradually increased by adding small pellets of V until, for the particular P_{H_2O}/P_{H_2} ratio used, an oxide layer appeared permanently on the surface. After each addition, the gas inlet tube was immersed into the melt and the gas bubbled through to enhance mixing. When an addition resulted in an excessive amount of oxide forming at a certain temperature, a higher experimental temperature was sought. This generally resulted in partial dissolution of the oxide layer, so that the surface of the melt was only partially covered.

After equilibrium was reached, the melt was sampled as previously described and new experimental conditions established.

At the end of the experiment the crucible was removed from the furnace and the oxide layer on top of the ingot was examined by X-ray diffraction techniques.

The ingots were also examined microscopically, and the non-metallic inclusions studied with an electron microprobe.

The oxide layer on the surface of some ingots was also studied under a scanning electron microscope.

4.3   EXPERIMENTS WITH THE OXYGEN PROBE

The experiments with the oxygen probe were performed in the same furnace as the H_2O/H_2 equilibria, and with similar furnace tube

and crucible assemblies. The materials used were again Armco iron from Corey Steel Co.; V and V_2O_3 in powdered form, from Alfa Inorganics.

4.3.1   Description of the Oxygen Probe

In view of the disadvantages of electrolytes in the form of tubes (§ 3.4.2) it was decided to use Fitterer type probes, i.e. electrolytes in form of small cylindrical pellets sealed at the end of a silica tube.

In view of the low oxygen activities expected in the system Fe-V-O it was decided to try both $ZrO_2(CaO)$ and ThO_2 (Y_2O_3) as electrolytes.

Small cylindrical pellets of ThO_2 (Y_2O_3), 4mm dia. by 6mm high, were prepared as outlined in §10.2. Unfortunately we were not able to achieve a satisfactory seal between these pellets and quartz or vycor glass. In all the attempts made either the electrolyte cracked due to thermal shock or the seal was not gas tight.

$ZrO_2(CaO)$ electrolytes were therefore used throughout this work. They measured 3 mm diameter by 6mm in height, and were supplied presealed into a 1 in. long by 6mm OD vycor tube by LEIGH INSTRUMENTS LTD. The vycor tube was extended to 24 in. in length, and packed with a powdered mixture of Cr and Cr_2O_3 (90/10 by weight) which acted as reference electrode. Contact was made through a Mo wire of 0.050 in. diameter. After the Mo wire was placed into position, the vycor tube was sealed under vacuum.

Fig. 4.4 shows an oxygen probe before and after use.

Contact with the melt was also made through a Mo wire in order to avoid a thermal EMF correction. This Mo wire was positioned through an alumina tube.
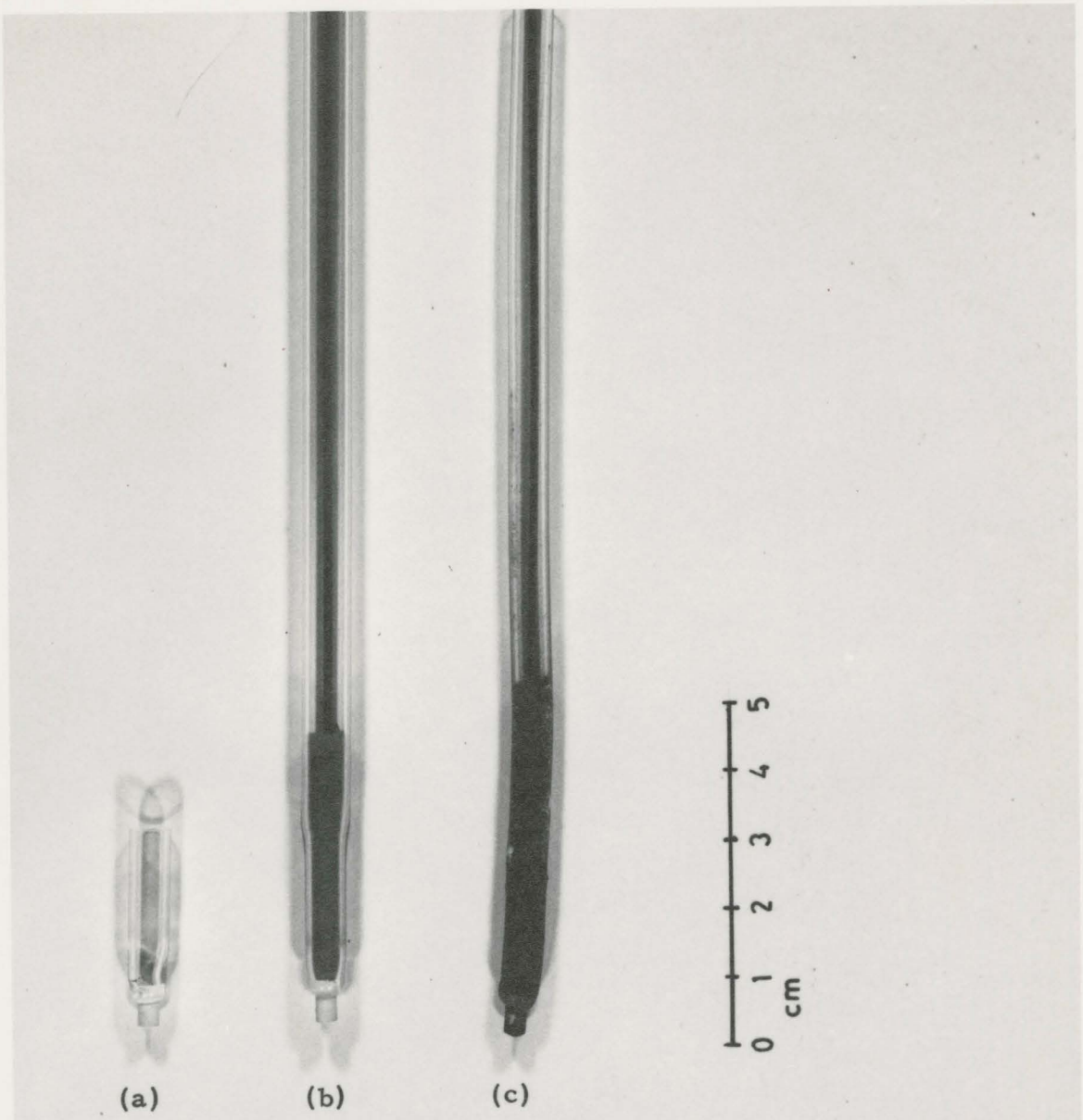
Fig. 4.4   Photograph of the Oxygen Probe

(a) Probe tip as supplied by LEIGH INSTR.

(b) Probe before use

(c) Probe after use

4.3.2   Experimental Procedure with the Oxygen Probe

The procedure adopted for H_2O/H_2 equilibration was also followed here.

The charge, consisting of a weighted amount of Fe and V totalling approximately 170g, and one pellet of V_2O_3, were placed in a high purity recrystallized alumina crucible and slowly raised into the hot zone of the furnace. The furnace tube was continuously flushed with purified Ar at a rate of 1 l/min.

After the crucible had been positioned in the hot zone, the furnace was raised to the desired experimental temperature. The melt was held at this temperature for 2 h to ensure equilibration with the V_2O_3 phase, although kinetic runs indicated that equilibration was reached within 45 min. The melt was then sampled, and an oxygen probe was slowly lowered into the melt. Simultaneously the tube containing the Mo contact wire was dipped into the melt, and the EMF between the probe and the contact wire was measured with a Croydon potentiometer. The probe was left in the melt for approximately 1 min, during which the EMF remained constant to $\pm$ 2 mV. Several probes were kept in the melt for up to 20 min at $1600^{\circ}C$, and their output was constant, within $\pm$ 3 mV, for this period. The probe was then withdrawn from the furnace, and the tube with the contact wire was raised out of the melt.

More V was added to the melt, and a V_2O_3 pellet when necessary, and the same procedure followed.

In one run at $1600^{\circ}C$ the oxygen was added to the melt in the form of Fe_2O_3 rather than V_2O_3, in order to establish the oxide in equilibrium with the melt.

When the addition of V_2O_3 or Fe_2O_3 resulted in an excessive amount of oxide covering the surface it was possible to reduce it with purified H_2, until a reasonable amount of oxide remained on the surface, so as to ensure saturation with oxygen, without interfering with sampling.

The temperature was measured with a Pt5%Rh-Pt20%Rh thermocouple placed into the crucible supporting tube. From time to time a check was made by dipping a quartz thermocouple sheath into the melt from the top of the furnace tube. The two temperatures always agreed within $\pm 2^{\circ}$C.

In Fe-V-O melts saturated with oxygen, a layer of oxide was formed at the end of the alumina tube containing the Mo wire, and contact was established through this oxide layer, resulting in an insignificant amount of Mo dissolving into the melt (less than 0.3%, as judged from the length of the Mo wire dissolved). This amount has a negligible effect on the activity of oxygen[23]. The Mo contact wire dissolved at a greater rate in Fe-O melts.

EMF readings were taken both with the furnace "on" and "off". No difference was observed between the two readings, indicating that the furnace current had no effect on the cell.

No probe failures were encountered at 1550 and 1600°C. Approximately 1 out of 5 probes failed at 1650°C and 1 out of 2 at 1700°C. The probe failures consisted of either the seal around the electrolyte pellet cracking just before dipping the probe into the melt, resulting in the electrolyte dropping onto the melt, or the vycor tube cracking after the probe had been dipped into the melt; contact was then established betwen the melt and the reference electrode, resulting in a zero EMF.

Reversibility of the probes (§ 9.5) was checked several times by setting the potentiometer dials to a reading 200 mV higher or lower than the equilibrium EMF, and closing the circuit for 5 sec. The probe EMF always returned to the equilibrium value within seconds.

4.4 CHEMICAL ANALYSIS

4.4.1 Oxygen Analysis

Oxygen analysis of the iron samples was performed on a LECO inert gas fusion apparatus. A flow sheet of the unit is shown on Fig. 4.5.

With the analyzer in the 'collect' position (Fig. 4.5) the sample is dropped into an inductively heated graphite crucible, held at $2100^{o}C$. The oxygen in the sample is converted to CO, which is swept by a current of purified He into a catalytic furnace filled with CuO, where it is oxidized to CO_2, and is further transported into a trap where it is absorbed. After a preset time ("collection time") the analyzer switches to the "analyze" position. (Fig. 4.5). The trap is heated to evolve the CO_2 which is swept by He into a chromatographic column and then through a thermal conductivity cell with pure He as reference. The output of the cell is amplified, integrated over time and the integral value, converted into μg of oxygen, appears on a digital voltmeter.

The whole operation is automatic, total time for a complete cycle being 2 1/2 - 4 min, depending on the chosen collection time.

Before each batch of analysis the analyzer is calibrated against standards provided by the manufacturers. These standards are tin capsules containing known amounts of potassium hydrogen phthalate ($C_6H_4(COOH)COOK$).

The accuracy of the analysis depends on the standards. It is very difficult to discuss the absolute accuracy of the standards; their reproducibility was found to be about $\pm$ 5% of their nominal value or 5 μg of O_2, whichever is bigger. Thus the reproducibility was of the order of $\pm$ 15 and $\pm$ 5 μg O_2 for the 300 and 30 μg O_2 standards respectively.

A series of checks was done by analyzing standard ferrous materials of the U.S. National Bureau of Standards. The certified values are shown in Table 4.3. These materials have been analyzed at

(a) COLLECT

FURNACE

PURIFYING TRAIN

FURNACE FLOW METER

TO ATM.

STEM OUT

2　　7

TRANSFER VALVE

3　6　4　5　COLUMN

TRAP

FURNACE He TANK

TO ATM.

CELL

ANALYZER FLOW METER

ANALYZER He TANK

(b) ANALYZE

FURNACE

PURIFYING TRAIN

FURNACE FLOW METER

STEM IN

2

TRANSFER VALVE

1　3　6　4　5　COLUMN

TO ATM.

TRAP

FURNACE He TANK

TO ATM.

CELL

ANALYZER He TANK
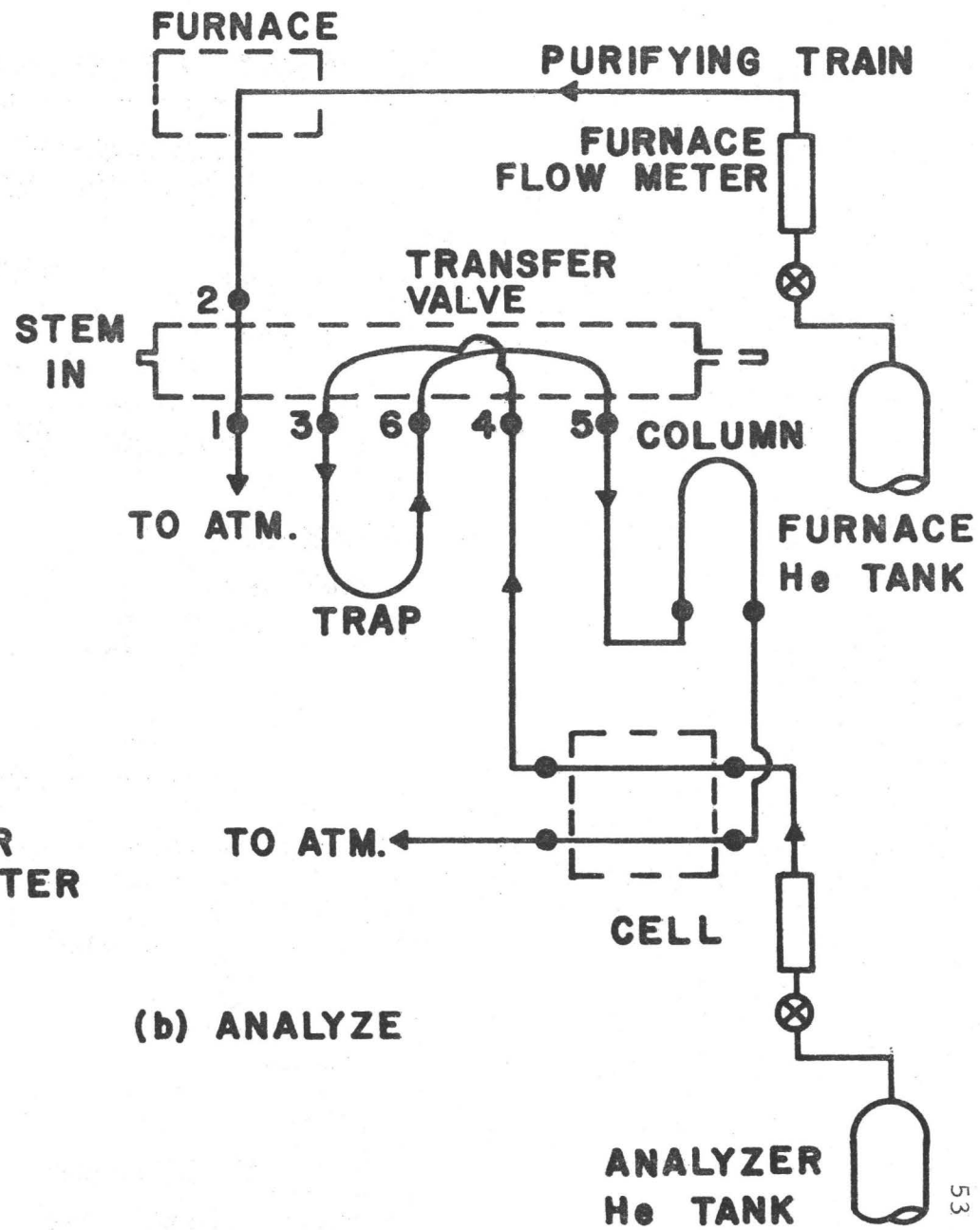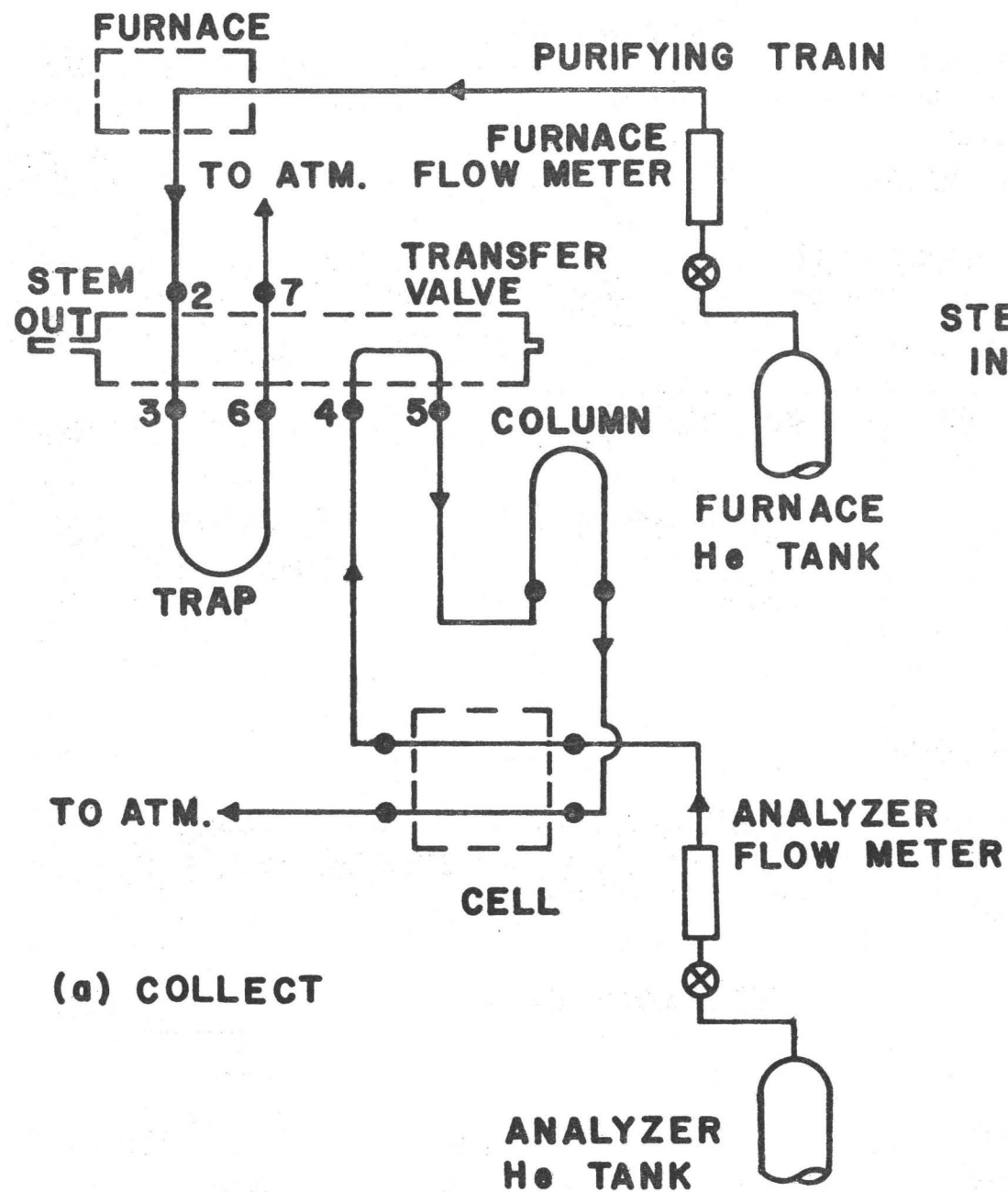
Fig. 4.5 Flow sheet of the LECCO oxygen analyzer.

TABLE 4.3

CERTIFICATE OF ANALYSIS

Standard Reference Materials 1090, 1091, 1092

Oxygen in Ferrous Materials

(By Vacuum and Inert Gas Fusion Methods)

No.	Type	Oxygen, ppm	Uncertainty, ppm[d]
1090	Ingot Iron[a]	484[e]	14
1091	Stainless Steel (AISI 431)[b]	131[f]	8
1092	Vacuum Melted Steel[c]	28[g]	2

Size: 1090, rods ¼ in. in diameter and 4 in. long; 1091, rods ⁵⁄₁₆ in. in diameter and 4 in. long; 1092, rods ¼ in. in diameter and 4 in. long.

[a] Determination on 0.5g sample.
[b] Determination on 0.75g sample.
[c] Determination on 2g sample.
[d] Standard deviation (1-sigma). These values include variations in the precision of the method, as well as differences which may be due to any inhomogeneity of the material.

[e] This value, obtained at NBS, is the average of 216 determinations on 54 rods. An average value of 487 parts per million was obtained by 18 cooperating laboratories. Of the 18 laboratories reporting, 7 were within the 2-sigma limit, 15 within the 3-sigma limit and 3 were outside the 3-sigma limit.
[f] This value, obtained at NBS, is the average of 286 determinations on 167 rods. An average value of 126 parts per million was obtained by 10 cooperating laboratories. Of the 10 laboratories reporting, 9 were within the 2-sigma limit and all were within the 3-sigma limit.
[g] This value, obtained at NBS, is the average of 105 determinations on 105 rods. An average value of 29 parts per million was obtained by 13 cooperating laboratories. Of the 13 laboratories reporting, 12 were within the 2-sigma limit and all were within the 3-sigma limit.

the request of NBS by 17 cooperating laboratories and the results are included in an NBS Publication[38]. A comparison of the mean and precision of these laboratories is presented in Table 4.4 and Fig. 4.6 for the SRM 1090.

These standards were analyzed in this laboratory at an estimated temperature of $2100^{o}C$ and with a collection time of 2 1/2 min. (4 min. overall time for each analysis). The results for the SRM 1090 are presented in Table 4.5. It is seen that the relative standard deviation rates among the best reported on Table 4.4; the mean value, 457 ppm oxygen, is 27 ppm lower than the NBS certified value. The average of the values reported from all laboratories with relative standard deviation less than 10% is 467.6 ppm, which compares very well with the value obtained from this laboratory.

Samples for oxygen analysis from the experimental runs were prepared as recommended by NBS[38]: the surfaces were carefully abraded with a clean sharp file, degreased with CP acetone and dried in warm air. After this step they were handled only with clean grease free forceps. They were stored in a dessicator until analyzed. The analysis was performed within a few hours of preparation.

4.4.2   Vanadium Analysis

Vanadium analysis was performed with a potentiometric titration method[39]. The sample was dissolved in a mixture of H_2SO_4-H_3PO_4 with some HNO_3 added. The vanadium was oxidized to V^{5+} with $KMnO_4$, the excess of the latter was destroyed with KNO_2 and urea was added to destroy any excess of KNO_2. The solution was then titrated with a ferrous ammonium sulphate solution of known strength. V^{5+} was reduced to V^{4+} and the course of the titration was followed potentiometrically using a Corning pH meter with platinum and calomel electrodes.

Table 4.4 Comparison of the mean and precision
of cooperating laboratories.

SRM 1090 - Ingot Iron

Oxygen, ppm

Lab.	Mean	Std. Dev.	Relative Std. Dev. %	Number of Determ.
1	466.3	29.5	6.3	30
2	699.2	348.4	49.8	12
3	455.8	20.2	4.4	12
4	410.8	33.7	8.2	12
5	504.4	13.4	2.7	9
6	459.2	17.8	3.9	12
7	497.7	9.7	1.8	11
8	509.1	12.3	2.4	9
9	459.9	31.4	6.8	12
10	456.0	9.1	2.0	15
11	449.2	27.4	6.1	12
12	454.9	16.7	3.7	15
13	465.5	9.0	1.9	9
14	458.9	19.6	4.3	9
15	446.7	6.9	1.5	12
16	443.5	7.1	1.6	12
17	532.3	23.8	4.5	6
NBS-A	462.9	11.2	2.4	88
NBS-B	484	14	2.9	216
Present Work	457	13.8	3.0	15
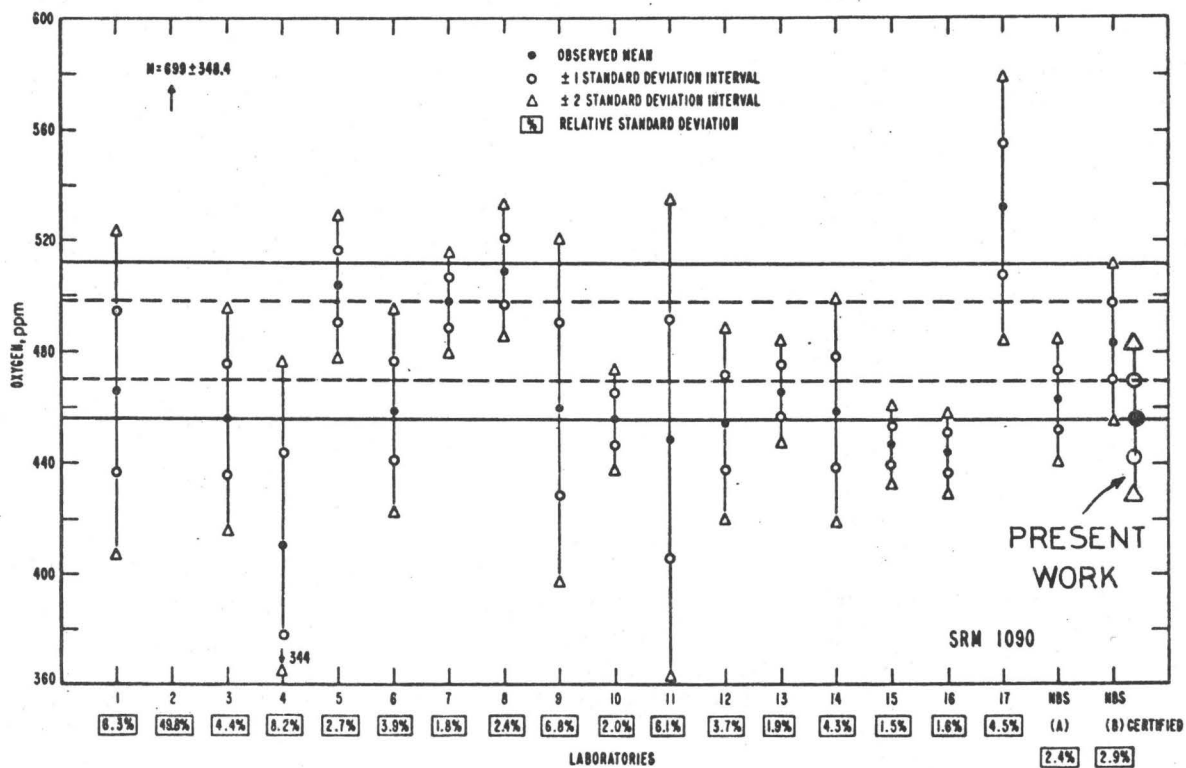
Fig. 4.6 Comparison of the mean and precision of cooperating laboratories for the SRM 1090.

TABLE 4.5

ANALYSIS RESULTS OF NBS SRM 1090

Determination No	Oxygen, ppm
1	464
2	451
3	434
4	448
5	467
6	466
7	445
8	442
9	460
10	482
11	451
12	463
13	448
14	450
15	481

Ave:	456.8
Standard dev:	13.8
Relative standard dev:	3.0%

The accuracy of the V analysis is estimated at $\pm\,0.01$ wt. % for the experiments with H_2O/H_2 equilibration and $\pm\,0.02$ wt. % for the ones with the oxygen probe. Taking into account the reproducibility of the analysis on different samples from the same melt, the reported values are considered accurate to $\pm\,0.02$ and $\pm\,0.04$ wt. %V for the two sets of experiments.

CHAPTER 5

EXPERIMENTAL RESULTS

5.1 INTRODUCTION

The first series of experiments consisted of studying the thermodynamics of the systems Fe-O and Fe-V-O, containing up to 2%V, in the temperature range 1550-1700°C, by equilibrating with $H_2O/H_2/Ar$ atmospheres.

In the second series, an oxygen probe, utilizing a stabilized zirconia electrolyte and a Cr, Cr_2O_3 reference electrode, was constructed and tested in the binary Fe-O system. Using this probe, the thermodynamic study of the Fe-V-O system was extended to 12%V and the activities of V were measured in the same composition range.

5.2 EQUILIBRATION WITH H_2O/H_2
5.2.1 The Binary Fe-O System
5.2.1.1 Kinetic Runs

A series of kinetic runs was carried out to determine the time required for equilibrium to be reached between the H_2O-H_2-Ar atmospheres and the melt.

It is desirable that equilibrium be reached from both a higher and a lower oxygen content than the equilibrium content. The results of a typical kinetic run, done at 1550°C, are presented in Table 5.1 and Fig. 5.1. The melt was deoxidized with H_2 down to 114 ppm oxygen and then an atmosphere of $(P_{H_2O}/P_{H_2}) = 0.2595$ was introduced. Within about 45 min. the equilibrium concentration of 630 ppm oxygen was reached. Then the (P_{H_2O}/P_{H_2}) ratio was changed to 0.0501 and the new equilibrium

60

TABLE 5.1

KINETIC RUNS

BINARY Fe-O SYSTEM

$$T = 1550^{\circ}C$$

RUN	TIME, h	P_{H_2O}/P_{H_2}	[O], ppm	$k_1' = \dfrac{P_{H_2O}}{P_{H_2}} \cdot \dfrac{1}{[\%O]}$
1	0	-	114	-
2	1/2	0.2593	541	4.793
3	1	0.2595	626	4.145
4	1 1/2	0.2595	622	4.172
5	2	0.2596	639	4.063
6	2 1/4	0.0497	211	2.357
7	2 1/2	0.0501	123	4.077
8	3	0.0501	121	4.144
9	4	0.0501	127	3.949

T = 1550° C

▲ P_{H_2O}/P_{H_2} = 0.2595

■ P_{H_2O}/P_{H_2} = 0.0501
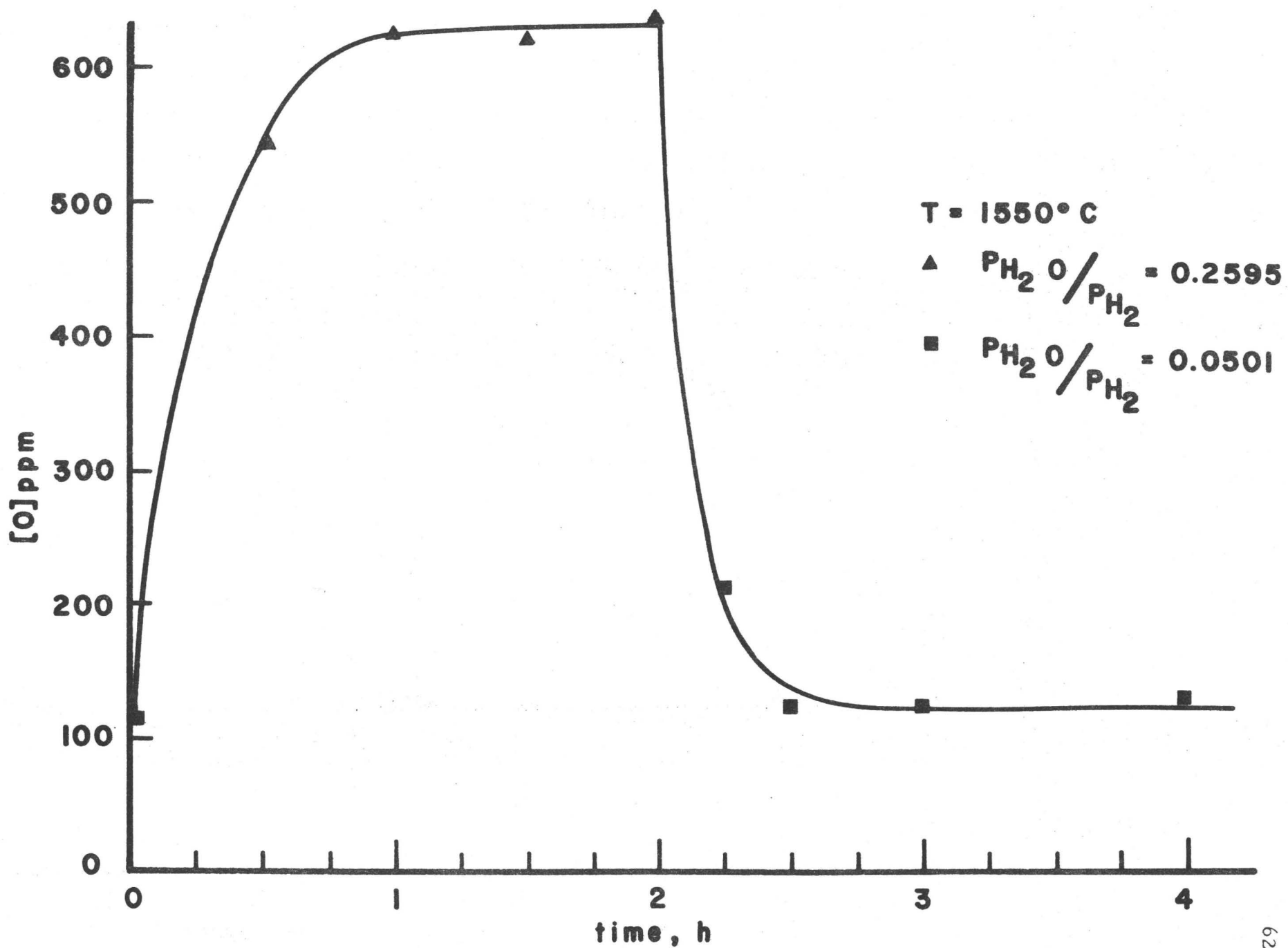
Fig. 5.1 Kinetic runs, Fe-O system

value of 123 ppm oxygen was reached within 30 min.

To ensure attainment of equilibrium, the experimental runs were held from 1 1/2 to 2 hr. at each experimental temperature. In many cases samples were taken from the melt at the end of the first hour, and then at the end of the second hour, and analyzed for oxygen. Both samples usually agreed within $\pm$ 5% of the oxygen value.

5.2.1.2 The Reaction $H_2(g) + \underline{O} = H_2O(g)$

The experimentally determined values for the apparent equilibrium constant

$$k_1' = \frac{P_{H_2O}}{P_{H_2}} \cdot \frac{1}{[\%O]} \tag{5.1}$$

for the reaction

$$H_2(g) + \underline{O} = H_2O(g) \tag{5.2}$$

are shown in Table 5.2.

In Fig. 5.2 log k_1' is plotted against the oxygen content of the melt. The equations representing the least square lines through the experimental points at each temperature are shown in Table 5.3.

The slope of those lines at a certain temperature is equal to the value of $e_o^{(o)}$ at that temperature:

$$\frac{\partial \log k_1'}{\partial [\%O]} = \frac{\partial \log (k_1 f_o)}{\partial [\%O]} = \frac{\partial \log f_o}{\partial [\%O]} = e_o^{(o)} \tag{5.3}$$

As seen from Table 5.3, the experimentally determined slope does not vary in a regular way with temperature. Therefore the value of $e_o^{(o)} = 0$ was adopted as being compatible with the accuracy and number of experimental runs performed at each temperature. When $e_o^{(o)} = 0$, the

TABLE 5.2

EXPERIMENTAL RESULTS FOR THE REACTION 1:

$$H_2(g) + \underline{O} = H_2O(g)$$
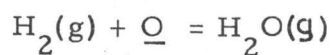
RUN	T, °C	P_{H_2O}/P_{H_2}	$\dot{O}$, ppm	k'_1	$\log k'_1$
11	1550	.0875	175	5.00	.699
121	1550	.0953	184	5.18	.714
41	1550	.0596	128	4.65	.668
42	1550	.0596	127	4.69	.671
51	1550	.0590	143	4.13	.616
61	1550	.3419	745	4.59	.662
71	1550	.3420	756	4.52	.656
81	1550	.3420	765	4.47	.650
82	1550	.2595	626	4.15	.618
85	1550	.0501	123	4.08	.610
31	1558	.0737	160	4.61	.663
32	1558	.0737	160	4.61	.664
21	1582	.1406	357	3.94	.595
35	1600	.0732	194	3.77	.577
43	1600	.0596	177	3.37	.527
52	1600	.0592	170	3.48	.542
62	1600	.3422	966	3.54	.549
92	1600	.2585	763	3.39	.530
102	1600	.1269	410	3.10	.491
132	1600	.3746	1065	3.52	.546
33	1608	.0737	219	3.37	.527
12	1610	.0877	259	3.39	.530
34	1643	.0732	262	2.79	.446
13	1650	.0877	309	2.84	.453
53	1650	.0609	214	2.84	.454
63	1650	.3424	1212	2.83	.451
73	1650	.3224	1104	2.92	.465
83	1650	.3766	1264	2.98	.474
113	1650	.2437	761	3.20	.506
123	1650	.1944	792	2.45	.390
44	1650	.0597	227	2.63	.420
45	1700	.0589	301	1.96	.291
54	1700	.0617	282	2.19	.340
64	1700	.3387	1437	2.36	.372
74	1700	.3427	1476	2.32	.366
144	1700	.0972	437	2.22	.347
154	1700	.3159	1482	2.13	.329
164	1700	.0929	391	2.37	.376
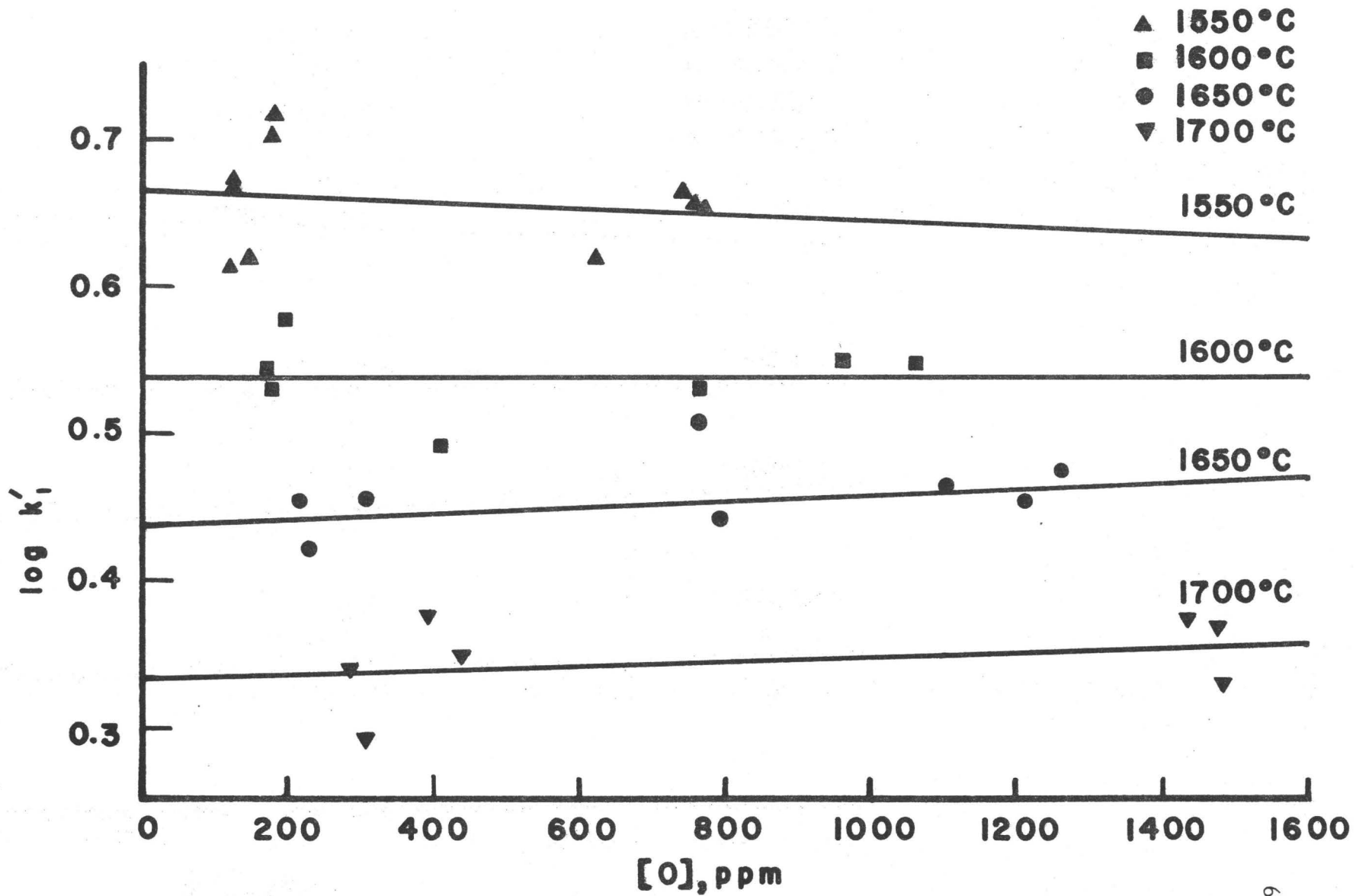
Fig. 5.2 Variation of $\log k_1'$ with the oxygen content in Fe-O melts

TABLE 5.3

VARIATION OF $\log k_1^!$ WITH THE OXYGEN CONTENT IN Fe-O MELTS

$T = 1550^{\circ}C$

$\log k_1^! = -0.191 \quad [\%O] \quad + 0.664$

$T = 1600^{\circ}C$

$\log k_1^! = \quad 0.029 \quad [\%O] \quad + 0.536$

$T = 1650^{\circ}C$

$\log k_1^! = + 0.211 \quad [\%O] \quad + 0.436$

$T = 1700^{\circ}C$

$\log k_1^! = 0.170 \quad [\%O] \quad + 0.332$

true equilibrium constant k_1 for the reaction (5.2) is equal to the apparent equilibrium constant k_1'.

In Fig. 5.3 $\log k_1$ is plotted against $1/T$. The least square line through the experimental points is represented by the equation

$$\log k_1 = \frac{7460 \ (\pm\ 500)}{T} - 3.43 \ (\pm\ 0.05) \tag{5.4}$$

with a correlation coefficient $r = 0.969$. The $\pm$ limits refer to the 95% confidence interval.

The standard free energy change for the reaction (5.2) can be calculated from (5.4):

$$\Delta G_1^o = - RT \ln k_1$$
$$= - 34000 \ (\pm\ 2000) + 15.70 \ (\pm\ 0.20) \ T \ (cal) \tag{5.5}$$

5.2.1.3 <u>The Reaction $\frac{1}{2} O_2(g) \rightarrow \underline{O}$</u>

The standard free energy change, ΔG_2^o, for the reaction

$$\frac{1}{2} O_2(g) = \underline{O} \tag{5.6}$$

can be obtained from (5.5) and the standard free energy change for the reaction

$$H_2(g) + \frac{1}{2} O_2(g) = H_2O(g) \tag{5.7}$$

which is taken as[40]

$$\Delta G_{5.7}^o = -59905 + 13.78T \ (cal) \tag{5.8}$$
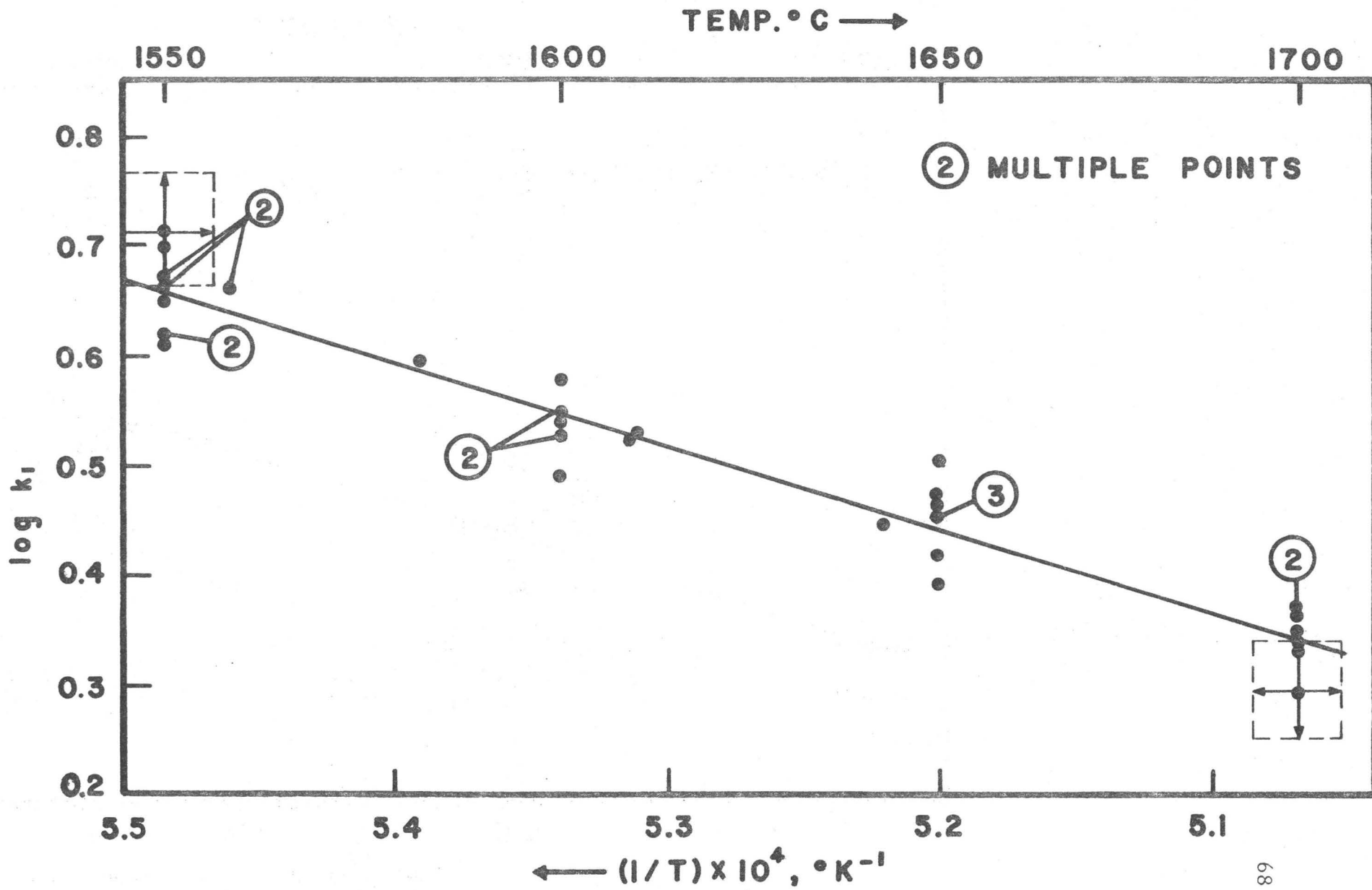
Fig. 5.3 Variation of log k_1 with temperature

By substracting (5.5) from (5.8) we obtain

$$\Delta G^o_2 = -25900 - 1.92T \quad \text{(cal)} \tag{5.9}$$

5.2.1.4 Solubility of Oxygen in Liquid Iron

In this work no attempt was made experimentally to determine the solubility limit of oxygen in liquid iron. However it can be derived indirectly by combining eqn. (5.4) with the following equation, given by Gokcen[22], for the reduction of liquid wustite with hydrogen:

$$H_2(g) + Fe_xO(l) = H_2O(g) + xFe(l) \tag{5.10}$$
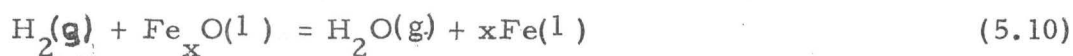
$$\log k_{5.10} = \frac{908}{T} - 0.615 \tag{5.11}$$

By substracting (5.2) from (5.10) we have:

$$Fe_xO(l) = xFe(l) + \underline{O} \tag{5.12}$$

$$\log k_{5.12} = - \frac{6550}{T} + 2.82 \tag{5.13}$$

When the solubility limit is reached, pure wustite of unit activity coexists with the melt and the mole fraction of iron is close to unity. Assuming Henrian behaviour for oxygen,

$$k_{5.12} = [\%O] \tag{5.14}$$

and

$$\log [\%O] = - \frac{6550}{T} + 2.82 \tag{5.15}$$

This equation represents the maximum solubility of oxygen in liquid iron

as a function of temperature, and is plotted on Fig. 5.4.
The solubility values calculated from this equation are:

T, $^{\circ}$C	%O
1550	0.17
1600	0.21
1650	0.26
1700	0.31

5.2.1.5 Experimental Errors

The main uncertainty in the experimentally determined value
of k_1 is the oxygen analysis. At least 3 and often up to 5 analyses were
performed on each sample. Usually all the values were within $\pm$ 5%
of the reported mean. Another $\pm$ 5% due to the uncertainty in the
reproducibility of the oxygen analyzer must be added, leading to a total
uncertainty of the reported value of $\pm$ 10%.

Other sources of error are the $\pm$ 2% uncertainty in the (P_{H_2O}/P_{H_2})
value and a $\pm$ 6°C error in temperature measurement and control.

To illustrate the effect of these errors, error bars have been
placed on two of the experimental points in Fig. 5.3. The vertical bars
represent the combined effect of the $\pm$ 10% uncertainty on the oxygen value
plus $\pm$ 2% uncertainty on the (P_{H_2O}/P_{H_2}) value. The horizontal bars
represent the $\pm$ 6°C uncertainty in the temperature.

It is seen that all the scatter of the experimental points can be
accounted for by these errors.

5.2.2 The System Fe-V-O

The results of experimental runs performed on the ternary Fe-V-O
system at 1550, 1600, 1650, and 1700°C are presented on tables 5.4, 5.5,
5.6, and 5.7 respectively. An asterisk denotes a run where equilibrium
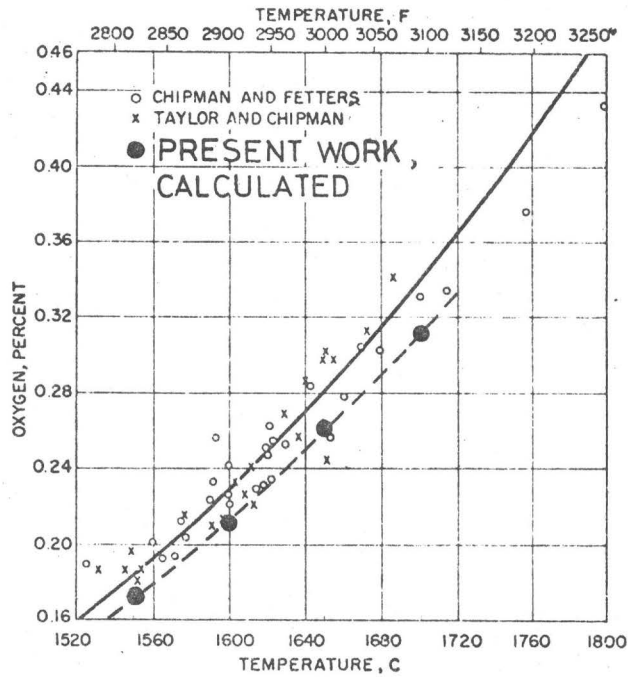
Fig. 5.4 Solubility of oxygen in liquid iron. Data calculated from the present work are compared with experimental data. (J. Chipman and K. L. Fetters: Trans. AIME, 1941, vol. 129, p. 953)
(C. R. Taylor and J. Chipman: Trans. AIME, 1943, vol. 154, p 228)

TABLE 5.4

EXPERIMENTAL RESULTS FOR THE SYSTEM Fe-V-O

H_2O/H_2 EQUILIBR. T = 1550°C

RUN	T, ^{o}C	P_{H_2O}/P_{H_2}	O , ppm	V , %	h_o	$f_o^{(v)}$	$\log f_o^{(v)}$
341	1550	.0592	159	.36	.0129	.814	-.089
351	1550	.0595	150	.55	.0130	.868	-.061
361*	1550	.0747	213	.44	.0163	.767	-.115
401	1550	.0490	171	.74	.0107	.627	-.203
411	1550	.0497	182	.92	.0109	.597	-.224
431*	1550	.0501	150	1.01	.0110	.731	-.136
451	1550	.2575	635	.07	.0563	.887	-.052
491	1550	.3407	927	.05	.0745	.804	-.095
531*	1550	.0950	235	.28	.0208	.884	-.053
541	1550	.1415	339	.17	.0310	.913	-.040
571*	1550	.0648	175	.53	.0142	.811	-.091
621*	1550	.1769	444	.10	.0387	.872	-.060
641*	1550	.0373	160	1.33	.0082	.509	-.293
651*	1550	.2444	544	.04	.0535	.983	-.007
661	1550	.1768	453	.09	.0387	.854	-.069
671*	1550	.1123	262	.19	.0246	.938	-.028
701*	1550	.2645	572	.04	.0579	1.012	.005

* Saturated Melts

TABLE 5.5

EXPERIMENTAL RESULTS FOR THE SYSTEM Fe-V-O. H_2O/H_2 EQUIL.
T = 1600°C

RUN	T, °C	P_{H_2O}/P_{H_2}	O, ppm	V, %	h_o	$f_o^{(v)}$	$\log f_o^{(v)}$
322	1600	.0594	215	.66	.0167	.777	-.109
332	1600	.0636	195	.17	.0179	.918	-.037
342	1600	.0592	201	.35	.0166	.828	-.082
352	1600	.0592	202	.58	.0167	.825	-.084
362	1600	.0752	240	.50	.0212	.882	-.055
402	1600	.0490	194	.75	.0138	.710	-.149
412	1600	.0496	222	.92	.0139	.628	-.202
422*	1600	.0496	254	1.52	.0140	.550	-.260
432	1600	.0495	220	1.04	.0139	.634	-.198
442	1600	.0501	234	1.00	.0141	.602	-.220
452	1600	.2585	807	.06	.0727	.901	-.045
472	1600	.2581	811	.08	.0726	.895	-.048
482	1600	.2577	780	.11	.0725	.930	-.032
492	1600	.3390	1061	.16	.0954	.899	-.046
512*	1600	.1490	433	.16	.0419	.968	-.014
522*	1600	.1283	425	.31	.0361	.849	-.071
532*	1600	.0954	293	.42	.0268	.916	-.038
542*	1600	.1422	437	.19	.0400	.915	-.038
552*	1600	.1444	413	.21	.0406	.983	-.007
572*	1600	.0648	233	.73	.0182	.783	-.106
562*	1600	.0514	216	1.03	.0145	.669	-.174
582*	1600	.0513	223	.98	.0144	.648	-.189
592	1600	.0368	129	.47	.0103	.802	-.096
602	1600	.0368	129	.48	.0103	.802	-.096
612	1600	.0368	159	1.01	.0103	.650	-.187
622	1600	.0368	156	1.03	.0104	.664	-.178
632*	1600	.2450	666	.06	.0689	1.035	.015
642*	1600	.0372	209	1.43	.0105	.500	-.301
652*	1600	.2481	662	.06	.0698	1.054	.023
662*	1600	.1771	539	.11	.0498	.924	-.034
672*	1600	.1122	351	.24	.0316	.899	-.046
682	1600	.0954	271	.22	.0268	.990	-.004
692	1600	.1918	540	.07	.0540	.999	-.000
702*	1600	.2646	727	.06	.0744	1.024	.010
712*	1600	.3753	1044	.03	.1056	1.011	.005
722*	1600	.0542	225	.95	.0153	.678	-.169
732	1600	.1918	538	.06	.0540	1.003	.001

* Saturated Melts

TABLE 5.6

EXPERIMENTAL RESULTS FOR THE SYSTEM Fe-V-O H_2O/H_2 EQUIL.

$T = 1650^{\circ}C$

RUN	T, $^{\circ}$C	P_{H_2O}/P_{H_2}	O , ppm	V, %	h_o	$f_o^{(v)}$	$\log f_o^{(v)}$
323	1650	.0594	280	.72	.0212	.758	-.120
333	1650	.0636	251	.17	.0227	.905	-.043
343	1650	.0592	265	.36	.0211	.797	-.099
353	1650	.0595	254	.58	.0213	.837	-.077
363	1650	.0753	340	.54	.0269	.791	-.102
403	1650	.0489	254	.74	.0174	.687	-.163
393	1650	.0489	250	.75	.0175	.699	-.156
413	1650	.0497	266	.93	.0177	.667	-.176
433	1650	.0501	297	1.08	.0179	.602	-.220
443*	1650	.1490	575	.28	.0532	.925	-.034
513*	1650	.1489	575	.28	.0532	.925	-.034
523*	1650	.1286	601	.51	.0459	.764	-.117
533*	1650	.0950	370	.55	.0339	.917	-.038
543*	1650	.1436	546	.28	.0513	.939	-.027
553*	1650	.1446	512	.32	.0516	1.009	.004
573*	1650	.0649	297	.93	.0232	.780	-.108
563*	1650	.0521	288	1.32	.0186	.646	-.190
583*	1650	.0516	272	1.25	.0184	.677	-.170
643	1650	.0371	262	1.45	.0132	.505	-.296
653*	1650	.2437	821	.07	.0870	1.060	.025
663*	1650	.1773	658	.15	.0633	.962	-.017
673*	1650	.1121	450	.34	.0400	.889	-.051
693*	1650	.1917	675	.12	.0685	1.014	.006
703*	1650	.2649	881	.07	.0946	1.073	.031
713*	1650	.3751	1273	.05	.1339	1.052	.022
723*	1650	.0550	314	1.32	.0196	.625	-.204

* Saturated Melts.

TABLE 5.7   75

EXPERIMENTAL RESULTS FOR THE SYSTEM Fe-V-O, H_2O/H_2 EQUIL.

T = 1700°C

RUN	T, $^\circ$C	P_{H_2O}/P_{H_2}	O , ppm	V , %	h_o	$f_o^{(v)}$	$\log f_o^{(v)}$
324	1700	.0595	363	.70	.0266	.734	-.134
334	1700	.0624	282	.17	.0279	.990	-.004
344	1700	.0592	329	.36	.0265	.805	-.094
354	1700	.0592	324	.59	.0265	.818	-.087
364	1700	.0754	415	.61	.0337	.813	-.090
404	1700	.0489	288	.74	.0219	.760	-.119
394	1700	.0487	286	.74	.0218	.762	-.118
434	1700	.0500	405	1.68	.0224	.552	-.258
494	1700	.3432	1476	.18	.1536	1.041	.017
534*	1700	.0956	472	.73	.0428	.907	-.042
554*	1700	.1449	695	.34	.0649	.933	-.030
574*	1700	.0649	375	1.10	.0291	.775	-.111
564*	1700	.0518	349	1.33	.0232	.664	-.178
584*	1700	.0368	293	1.96	.0165	.562	-.250
664*	1700	.1776	813	.17	.0795	.978	-.010
674*	1700	.1120	533	.48	.0501	.941	-.027
684	1700	.0954	461	.43	.0427	.926	-.033
694*	1700	.1917	809	.15	.0858	1.061	.026
704*	1700	.2637	1190	.11	.1181	.992	-.003
714	1700	.3748	1624	.03	.1678	1.033	.014
724*	1700	.0551	422	1.61	.0247	.584	-.233

* Saturated Melts.

with an oxide phase was achieved ("saturated" runs).

5.2.2.1 Effect of Vanadium on the Activity Coefficient of Oxygen in Liquid Iron

The activity coefficient of oxygen, f_o $(= f_o^{(v)})$, was calculated as outlined in § 3.2, using the values of k_1 and $e_o^{(o)}$ $(= 0)$ obtained from the binary Fe-O system.

A plot of $\log f_o^{(v)}$ versus wt.%V is presented in Fig. 5.5, 5.6, 5.7 and 5.8 for 1550, 1600, 1650, and 1700°C respectively. Both saturated and unsaturated runs are included. There is no indication of curvature, so a straight line is fitted through the experimental points passing through zero and minimizing the sum of the squares of the deviations of the experimental points. The slope of this line for a particular temperature is the first order free energy interaction parameter $e_o^{(v)} = (\partial \log f_o^{(v)} / \partial [\%V])_{\%V \to 0}$ for this temperature.

The resulting least square lines are represented by the following equations:

at 1550°C: $\qquad \log f_o^{(v)} = - 0.208 \ (\%V)$ $\qquad\qquad$ (5.16)

at 1600°C: $\qquad \log f_o^{(v)} = - 0.195 \ (\%V)$ $\qquad\qquad$ (5.17)

at 1650°C: $\qquad \log f_o^{(v)} = - 0.166 \ (\%V)$ $\qquad\qquad$ (5.18)

at 1700°C: $\qquad \log f_o^{(v)} = - 0.134 \ (\%V)$ $\qquad\qquad$ (5.19)

In Fig. 5.9 the effect of temperature on the interaction parameter is shown.

From the experimentally determined values of $e_o^{(v)}$, values of $e_o^{(v)}$ can be calculated using the relationships given in Table 2.3. Table 5.8 gives the values of $e_o^{(v)}$ and $\epsilon_o^{(v)}$ at the temperatures investigated.
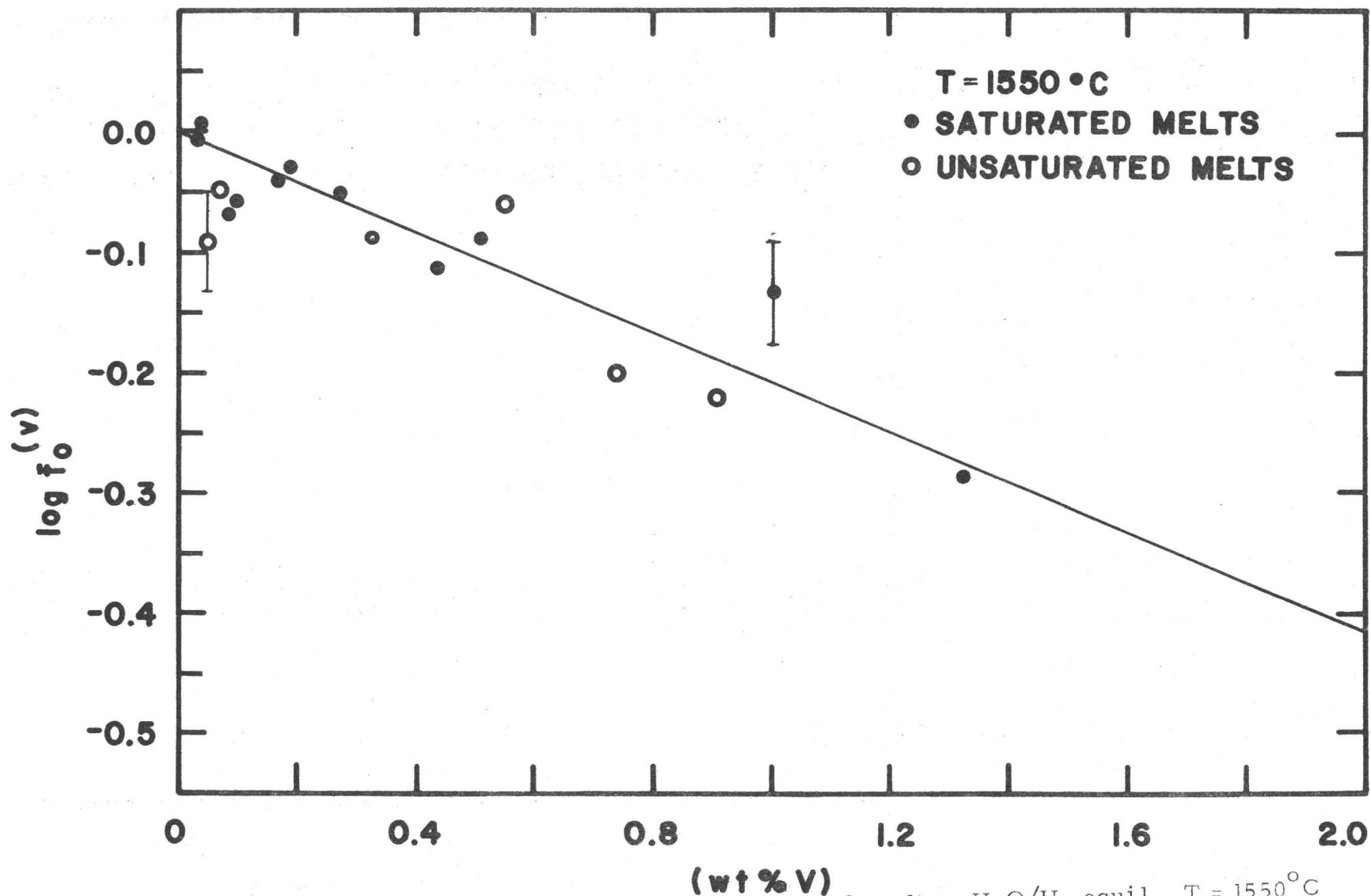
Fig. 5.5 Effect of V on the activity coefficient of O in Fe-V-O melts. H_2O/H_2 equil. $T = 1550^{\circ}C$
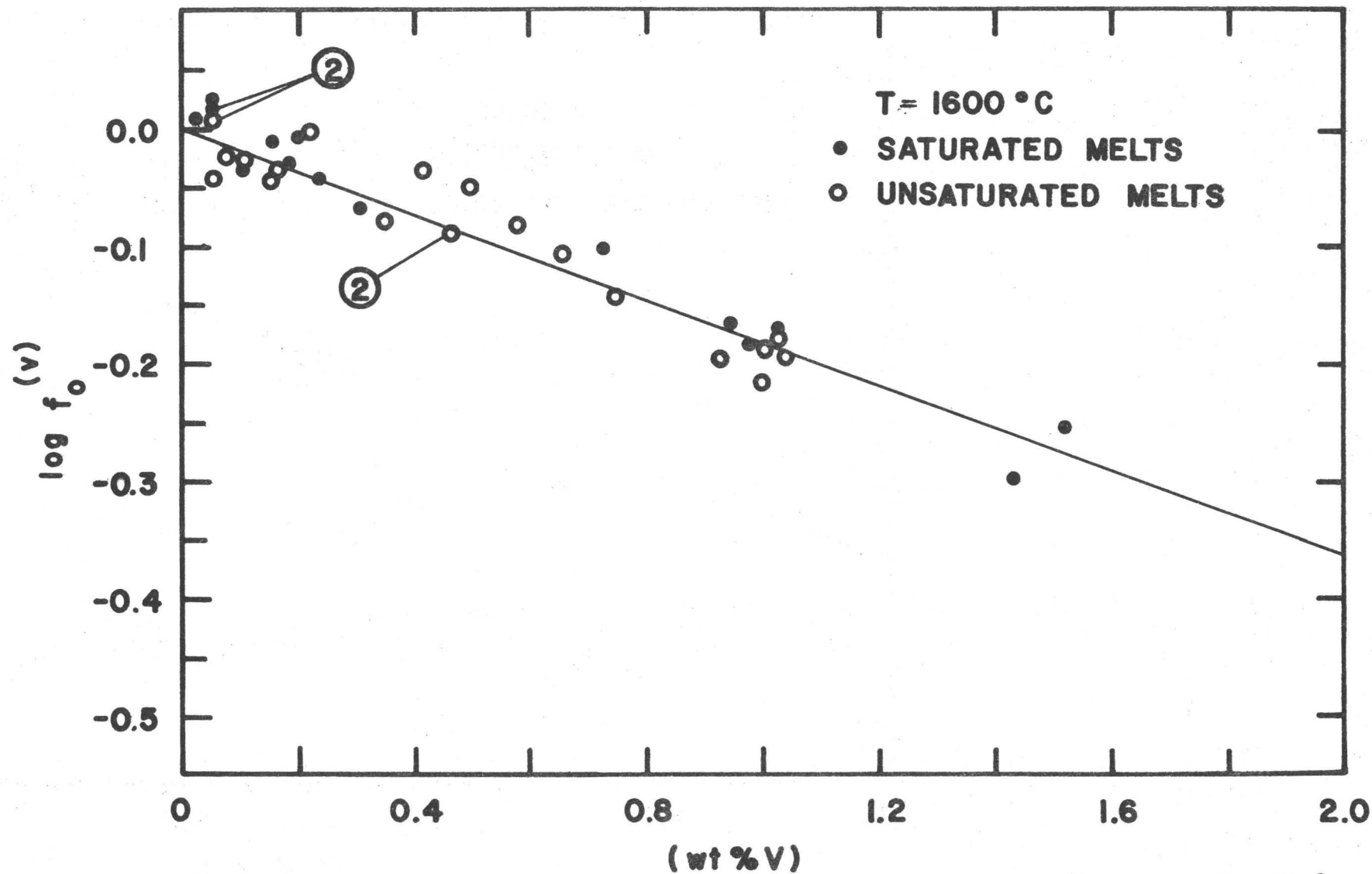
Fig. 5.6 Effect of V on the activity coefficient of O in Fe-V-O melts. H_2O/H_2 equil. $T = 1600^{\circ}C$

78
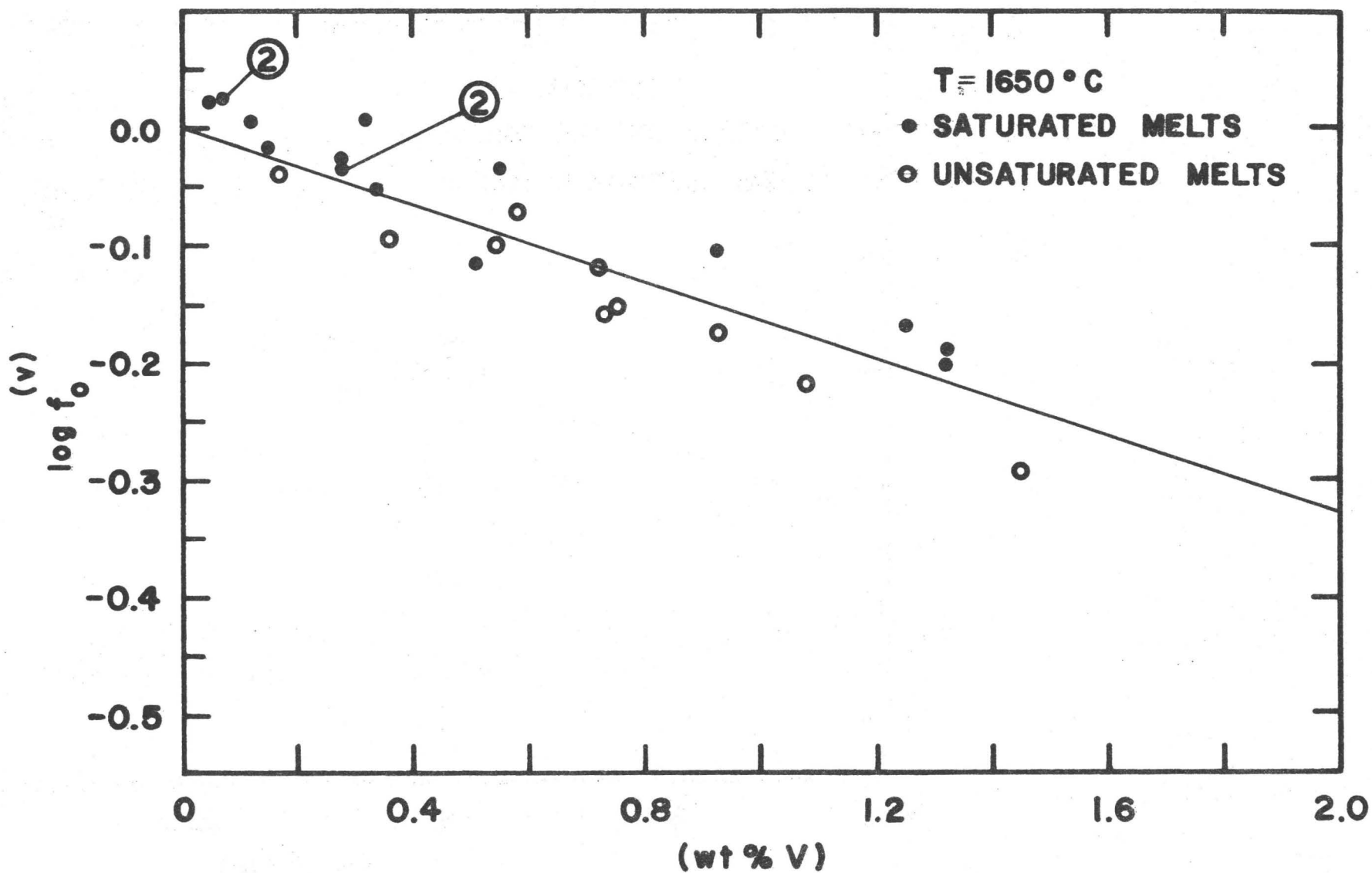
Fig. 5.7 Effect of V on the activity coefficient of O in Fe-V-O melts. H_2O/H_2 equil. $T = 1650^{\circ}C$
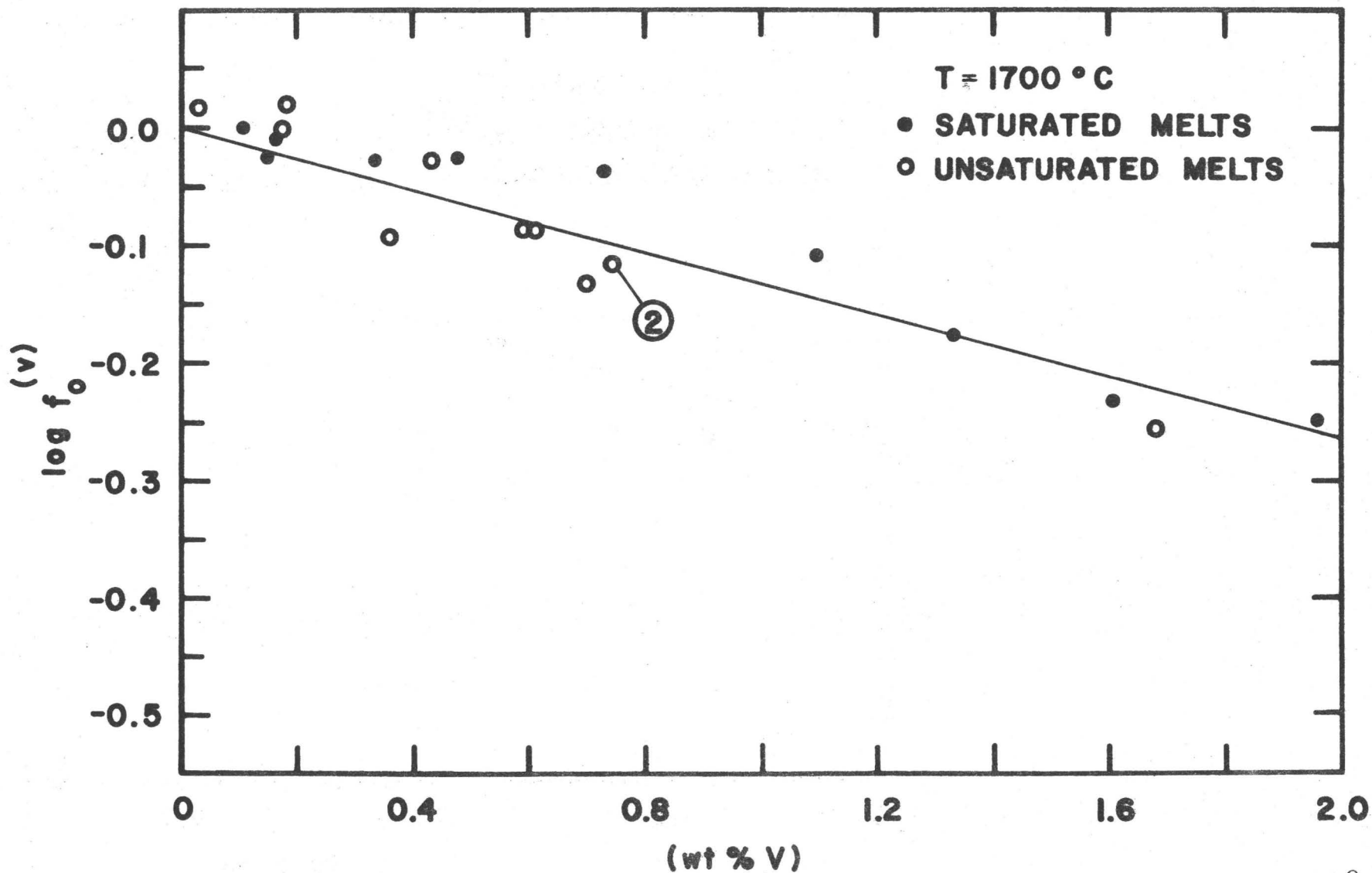
Fig. 5.8 Effect of V on the activity coefficient of O in Fe-V-O melts. H_2O/H_2 equil. $T = 1700^{\circ}C$
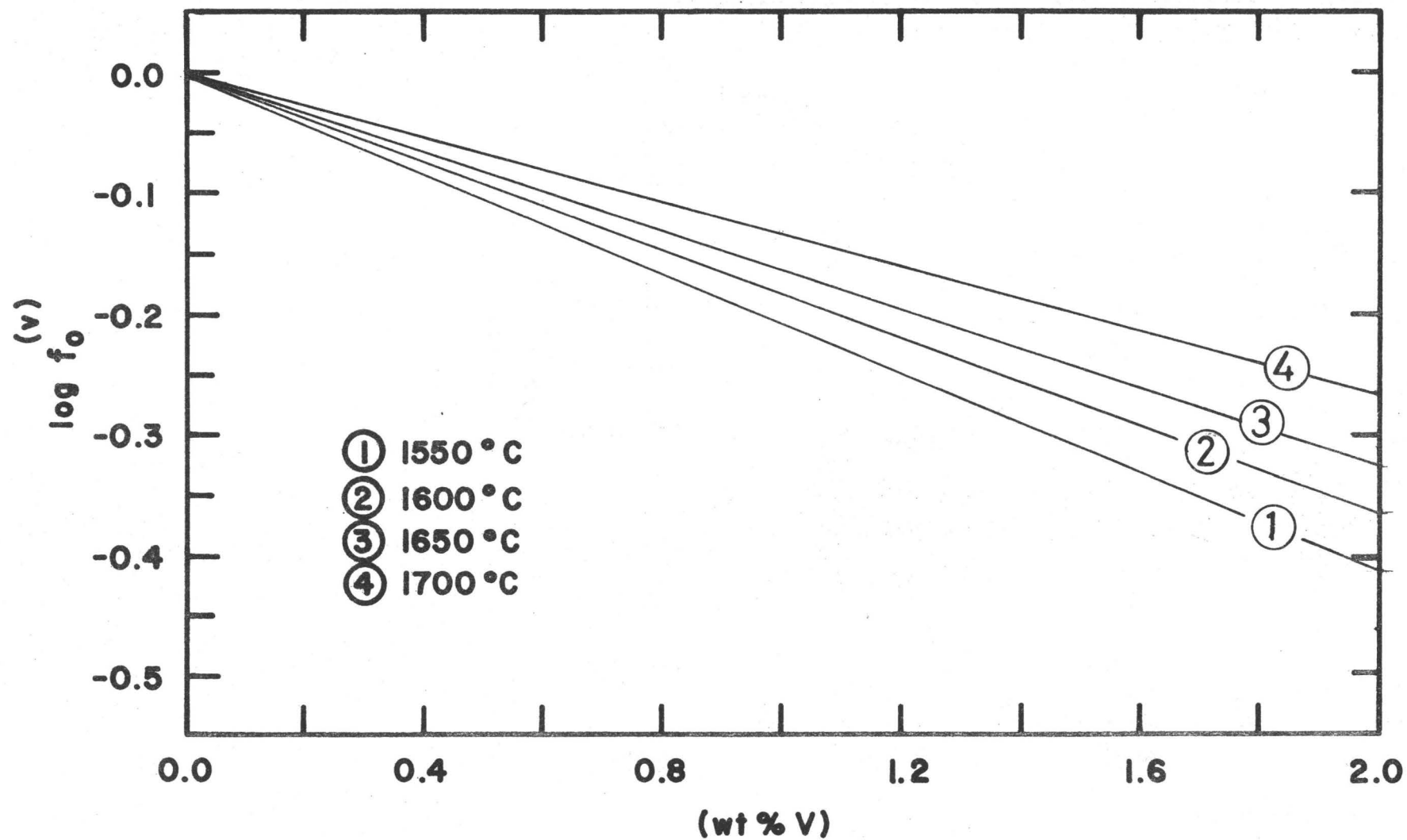
Fig.5.9 Effect of temperature on the activity coefficient of O in Fe-V-O melts. H_2O/H_2 determination.

TABLE 5.8

VANADIUM-OXYGEN 1st ORDER FREE ENERGY
INTERACTION PARAMETERS

T, $^{\circ}$C	$e_o^{(v)}$	$\epsilon_o^{(v)}$
1550	-0.208	-43.6
1600	-0.185	-38.6
1650	-0.166	-34.8
1700	-0.134	-28.1

In Fig. 5.10 the interaction parameters $e_o^{(v)}$ and $\epsilon_o^{(v)}$ are plotted against $1/T$. Least square lines fitted through the experimental points give the following equations:

$$e_o^{(v)} = - \frac{1730}{T} + 0.74 \qquad (5.20)$$

and

$$\epsilon_o^{(v)} = - \frac{361000}{T} + 154 \qquad (5.21)$$

The temperature dependence of the 1st order free energy interaction parameters in terms of 1st order enthalpy and entropy interaction parameters (eqn. 2.6) are:

$$e_o^{(v)} = \frac{h_o^{(v)}}{4.575T} - \frac{s_o^{(v)}}{4.575} \qquad (5.22)$$

and

$$\epsilon_o^{(v)} = \frac{\eta_o^{(v)}}{RT} - \frac{\sigma_o^{(v)}}{R} \qquad (5.23)$$

Comparing equation (5.20) with (5.22) and (5.21) with (5.23) the
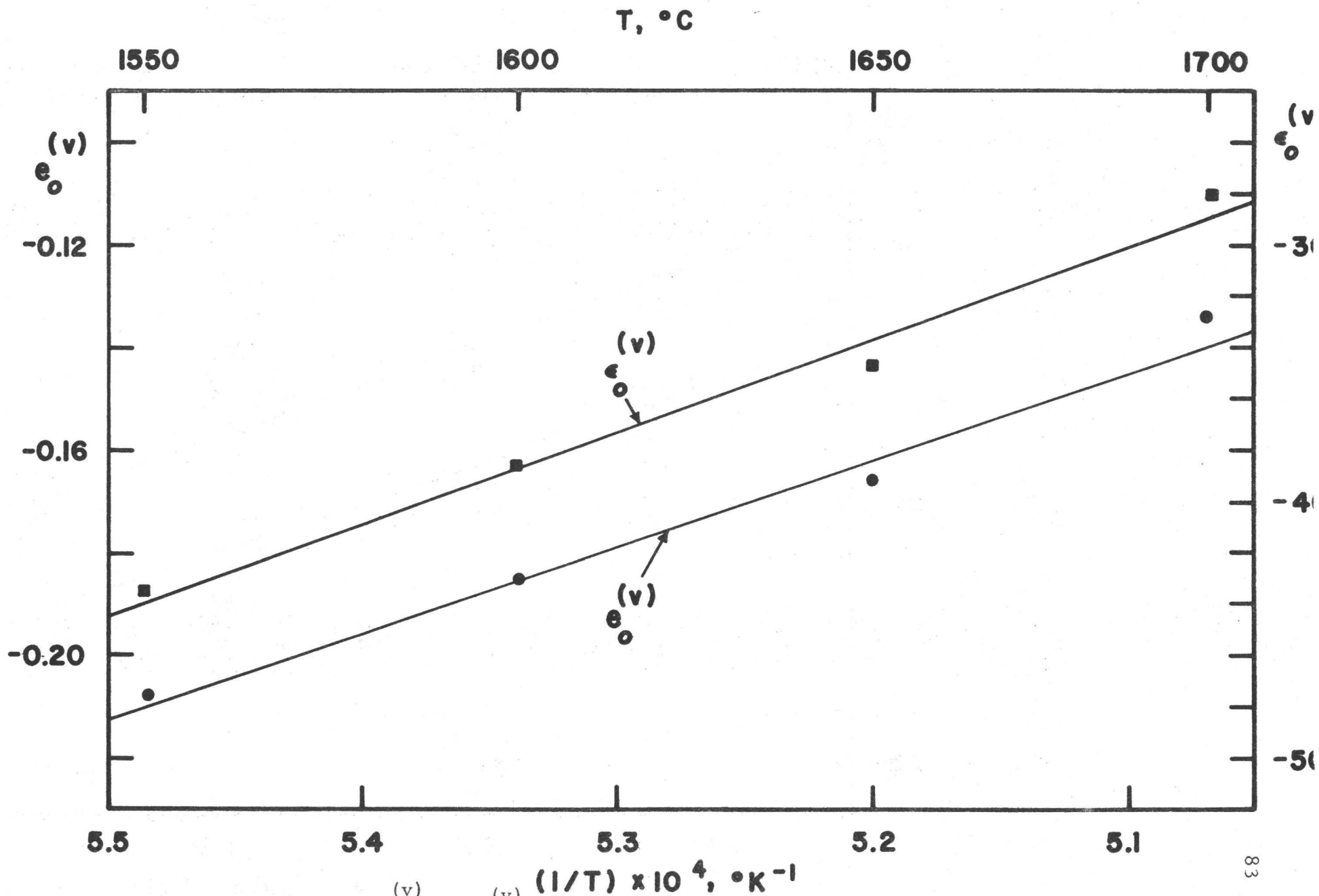
Fig. 5.10 Variation of $e_o^{(v)}$ and $\epsilon_o^{(v)}$ with temperature.

first order enthalpy and entropy interaction parameters can be calculated, and are presented in Table 5.9.

<div align="center">

TABLE 5.9

VANADIUM-OXYGEN 1st ORDER ENTHALPY

AND ENTROPY INTERACTION PARAMETERS

</div>

$$h_o^{(v)} = -7900$$

$$s_o^{(v)} = -3.39$$

$$\eta_o^{(v)} = -717400$$

$$\sigma_o^{(v)} = -306$$

Finally the Henrian activity coefficient of oxygen in liquid Fe-V alloys containing up to 2%V can be represented as a function of temperature by the following equation:

$$\log f_o^{(v)} = (- \frac{1730}{T} + 0.74) \times (\%V) \tag{5.24}$$

5.2.2.2 Experimental Errors

The same errors discussed in § 5.2.5. account for the scattering of the experimental points on Fig. 5.5-5.8. In addition, the uncertainty in the vanadium analysis is estimated to be $\pm$ 0.02%.

On the plot of $\log f_o^{(v)}$ vs wt.%V at 1550°C on Fig. 5.5 error bars have been placed on two points, corresponding to a $\pm$ 10% uncertainty on the oxygen analysis. It is seen that most of the scatter can be accounted for by the oxygen uncertainty alone.

5.3　EXPERIMENTS WITH THE OXYGEN PROBE

5.3.1　Experiments on Fe-O Melts

The performance of the oxygen probes was first checked in the binary Fe-O system at 1600°C, by comparing the analyzed oxygen with the oxygen calculated from the EMF measurement. All runs were done under an argon atmosphere. The oxygen content of the melt was increased by adding Fe_2O_3 and decreased by changing the furnace atmosphere to purified hydrogen.

In all of the reported experiments the probes were noted to be free of cracks after withdrawal from the melt. Some of the probes were checked and found to be still under reduced pressure.

Often, more than one probe was used at the same activity of oxygen in the melt. The EMF readings agreed to ± 3mV.

The experimental results for these tests are given in Table 5.10 and Fig. 5.11. The Henrian activity of oxygen was taken equal to its weight pct. in the Fe-O melts (§ 5.2.1.2), and was calculated from the experimental EMF using eqn. (3.32).

The agreement is good, inview of the uncertainty in the oxygen analysis ($\pm 10\%$ of the reported value). Similar scatter around the 45° line has been reported by Fruehan et al.[55] and by Gatellier et al[56].

5.3.2　Effect of Vanadium on the Activity Coefficient of Oxygen in Liquid Iron

The study on the effect of vanadium on the activity coefficient of oxygen in liquid iron was extended up to 12%V using the oxygen probe. All melts were saturated with oxygen. Experiments were carried out at 1550, 1600, 1650 and 1700°C; experimental points obtained at 1700°C are very few, because of probe failures at this temperature (§ 4.3.2.)

The experimental results are presented in Tables 5.11 - 5.14. In Figure 5.12 - 5.15 $\log f_O^{(v)}$ is plotted against the vanadium

TABLE 5.10

COMPARISON OF ANALYZED OXYGEN WITH OXYGEN DERIVED FROM
EMF MEASUREMENTS IN Fe-O MELTS.   T = 1600°C

RUN	T, $^{\circ}$C	E, mV	O, ppm from EMF	O, ppm analyzed
831	1600	94	84	57
823	1600	115	109	103
832	1600	149	166	132
821	1600	172	221	250
813	1600	185	260	271
837	1600	190	276	237
838	1600	209	350	337
833	1600	226	432	477
839	1600	240	514	465
811	1600	217	386	341
834	1600	259	650	549
835	1600	269	736	797
836	1600	273	773	727
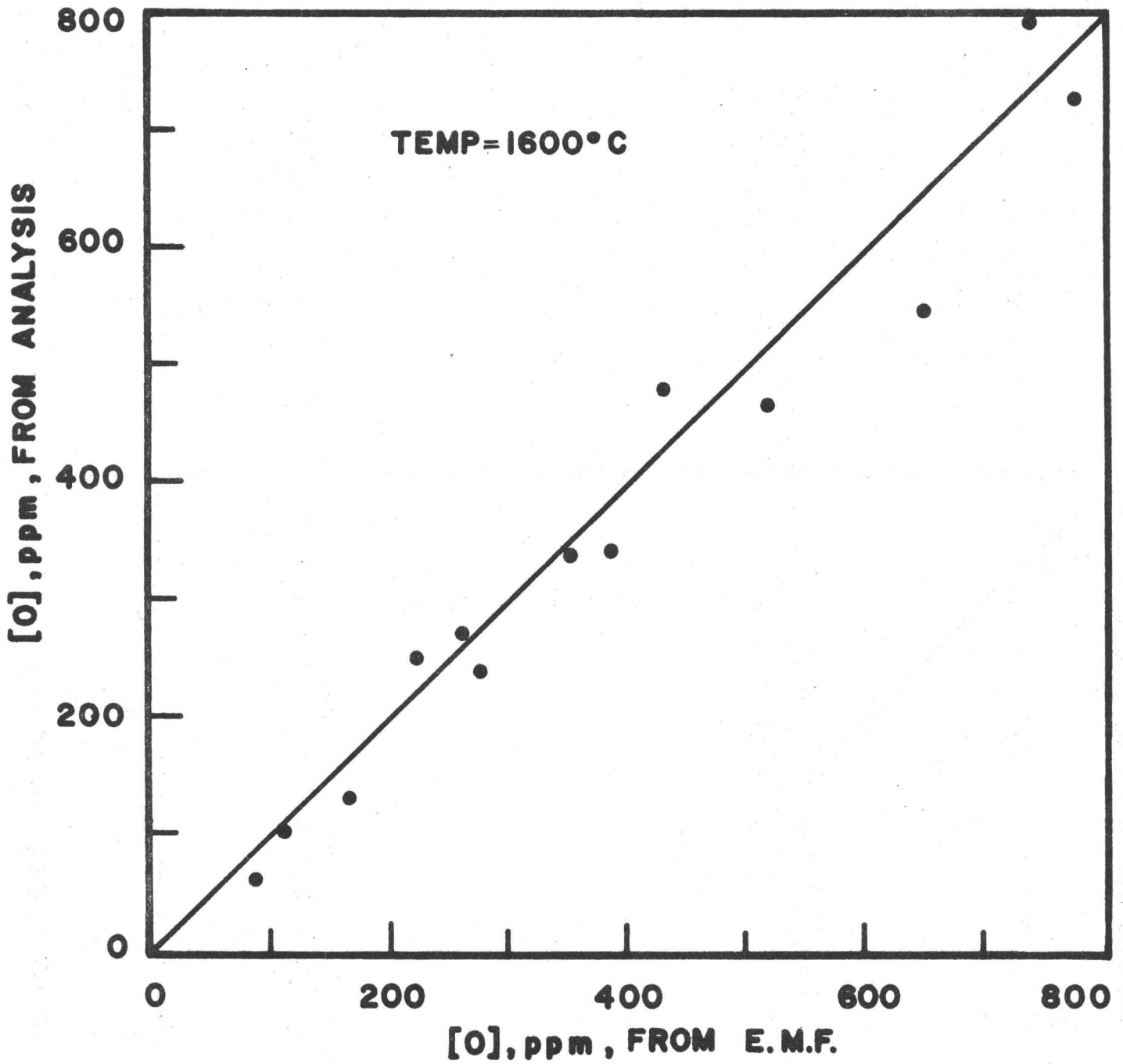
Fig. 5.11 Comparison of analyzed oxygen with oxygen derived from EMF
measurements in Fe-O melts at 1600°C.

TABLE 5.11

EXPERIMENTAL RESULTS - T = 1550°C
Fe-V-O SYSTEM WITH THE OXYGEN PROBE

Run	V wt. %	O, ppm	E, mV	h_o	$f_o^{(v)}$	$\log f_o^{(v)}$	N_V	a_V	γ_V
911	.57	177	172	150	.846	-.073	.0062	.00148	.237
912	.84	130	130	88	.675	-.171	.0092	.00330	.360
913	1.48	131	100	60	.457	-.340	.0162	.00585	.361
914	2.02	114	92	54	.474	-.324	.0221	.00682	.308
921	2.68	110	82	48	.433	-.364	.0293	.00825	.282
923	3.70	107	55	34	.316	-.501	.0404	.01382	.342
922	3.73	113	55	34	.299	-.525	.0407	.01382	.339
924	4.54	111	45	30	.268	-.572	.0495	.01674	.338
925	5.71	134	28	24	.179	-.748	.0622	.02316	.372
927	6.46	151	28	24	.159	-.800	.0704	.02316	.329
928	7.21	160	21	22	.137	-.864	.0785	.02648	.337
929	8.50	185	14	20	.108	-.965	.0924	.03027	.328
938	9.69	196	7	18	.093	-1.029	.1052	.03460	.329
939	10.91	260	-6	16	.060	-1.224	.1184	.04436	.375

TABLE 5.12

EXPERIMENTAL RESULTS T = 1600°C
Fe-V-O SYSTEM WITH THE OXYGEN PROBE

Run	V wt. %	O ppm	E mV	h_o	$f_o^{(v)}$	$\log f_o^{(v)}$	N_V	a_V	γ_V
881	.64	227	154	177	.780	-.108	.0070	.00237	.336
931	.92	210	135	140	.666	-.177	.0101	.00337	.335
883	1.20	182	130	131	.722	-.141	.0131	.00370	.282
884	1.77	155	105	96	.622	-.206	.0194	.00589	.304
885	1.79	167	110	103	.614	-.212	.0196	.00537	.274
886	2.72	160	95	85	.532	-.274	.0297	.00710	.239
932	2.74	169	74	66	.389	-.411	.0300	.01049	.350
933	3.51	161	54	51	.318	-.497	.0383	.01521	.397
892	3.66	158	63	57	.363	-.441	.0400	.01287	.322
934	3.89	170	57	53	.313	-.505	.0425	.01439	.339
935	5.09	178	48	48	.267	-.573	.0555	.01701	.306
893	6.02	191	35	40	.212	-.674	.0656	.02166	.330
936	7.05	237	27	37	.155	-.810	.0768	.02514	.327
938	8.94	280	20	34	.120	-.920	.0972	.02863	.295
896	9.20	259	11	30	.116	-.935	.1000	.03385	.339

TABLE 5.13

EXPERIMENTAL RESULTS. Fe-V-O SYSTEM WITH THE OXYGEN PROBE

T = 1650°C

Run	V wt. %	O, ppm	E, mV	h_o	$f_o^{(v)}$	$\log f_o^{(v)}$	N_V	a_V	γ_V
971	.67	342	163	287	.840	-.076	.0073	.00227	.309
941	1.15	303	140	218	.718	-.144	.0126	.00344	.273
972	1.87	260	113	157	.604	-.219	.0205	.00562	.274
943	2.50	248	97	129	.522	-.282	.0273	.00751	.275
942	2.62	265	82	108	.408	-.390	.0286	.00985	.344
945	3.89	242	64	87	.359	-.445	.0425	.01365	.321
965	5.16	303	62	85	.280	-.553	.0563	.01415	.251
946	5.46	270	51	74	.275	-.560	.0595	.01727	.290
951	5.62	276	42	67	.242	-.617	.0613	.02033	.332
968	5.79	261	34	61	.232	-.635	.0631	.02350	.372
952	6.75	340	45	69	.203	-.692	.0735	.01926	.262
954	7.99	355	35	61	.173	-.763	.0869	.02308	.266
969	8.71	415	28	56	.136	-.868	.0947	.02620	.277
974	9.41	399	20	51	.128	-.892	.1022	.03029	.296
975	9.49	407	22	52	.129	-.891	.1031	.02921	.283
976	11.54	534	12	46	.087	-1.061	.1251	.03501	.280
977	11.73	525	13	47	.089	-1.048	.1271	.03438	.270

TABLE 5.14

EXPERIMENTAL RESULTS - T = 1700°C
Fe-V-O SYSTEM WITH THE OXYGEN PROBE

Run	V wt. %	O, ppm	E, mV	h_o	$f_o^{(v)}$	$\log f_o^{(v)}$	N_V	a_V	γ_V
961	1.00	410	161	400	.974	-.011	.0109	.00260	.239
962	3.16	382	95	184	.481	-.318	.0345	.00835	.242
963	3.21	385	105	207	.537	-.270	.0351	.00700	.199
964	4.34	383	83	160	.417	-.380	.0474	.01032	.218
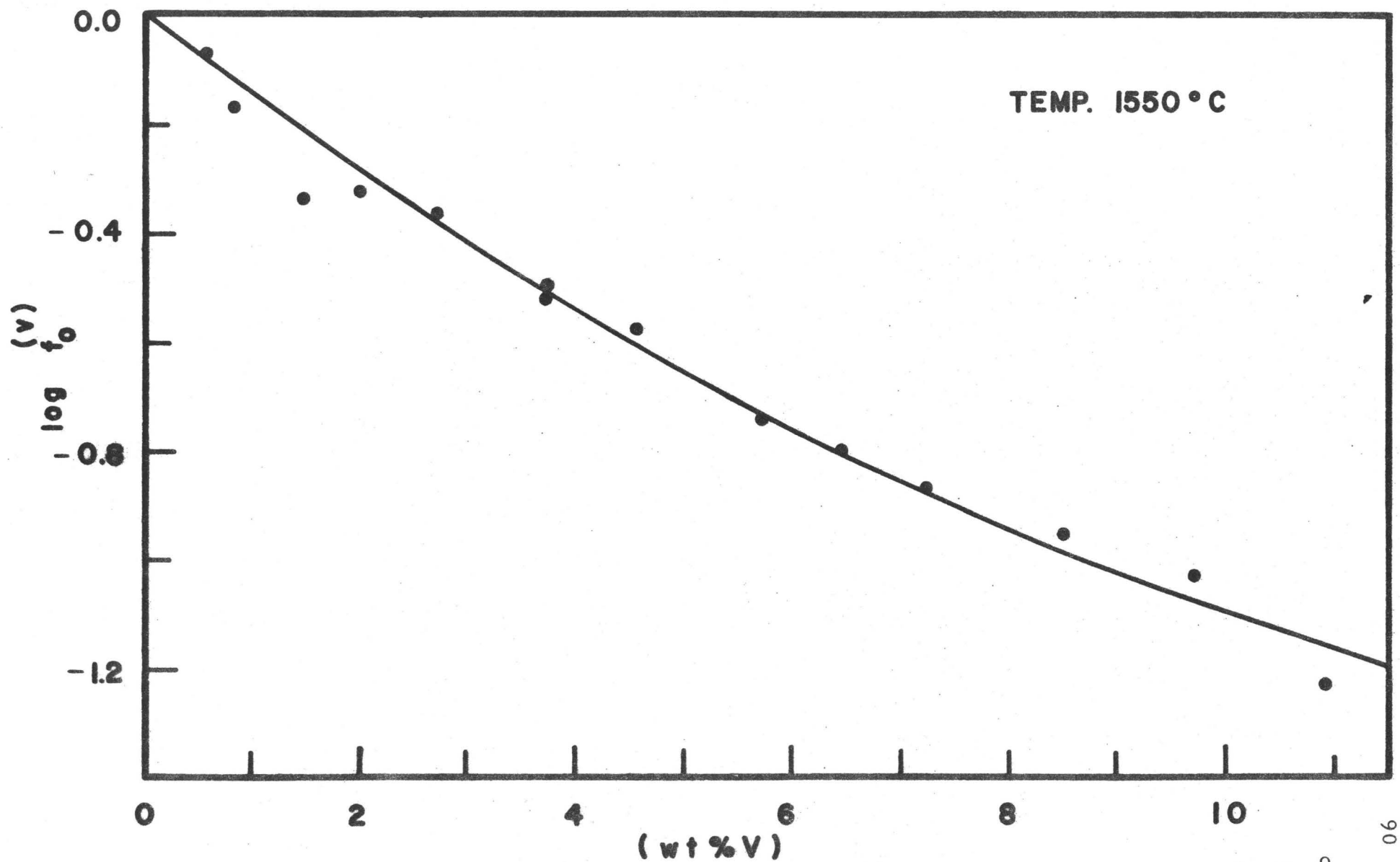
Fig. 5.12 Effect of V on the activity coefficient of O in Fe-V-O melts. Oxygen Probe data. T = 1550°C
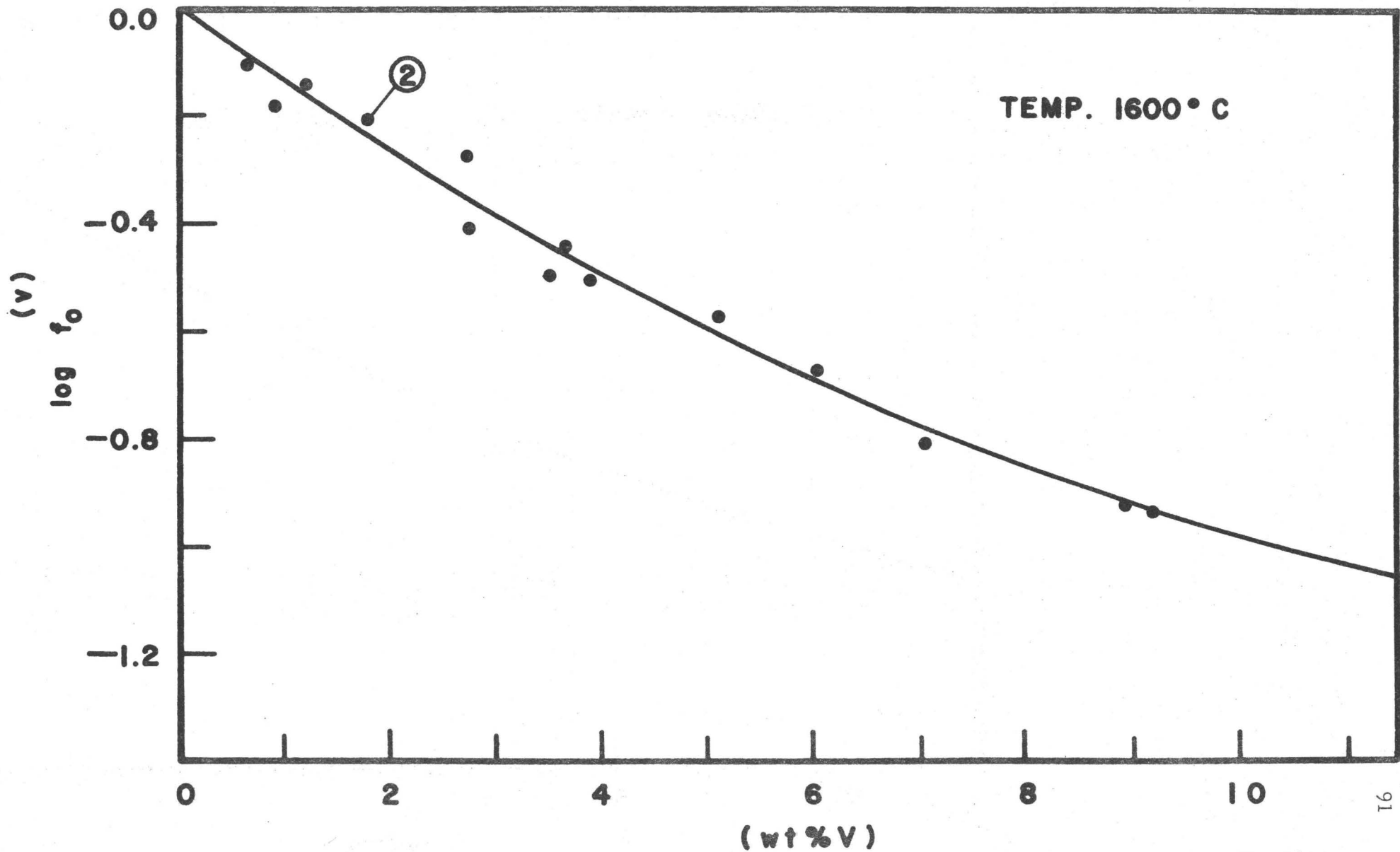
Fig. 5.13 Effect of V on the activity coefficient of O in Fe-V-O melts. Oxygen Probe data. T = 1600°C
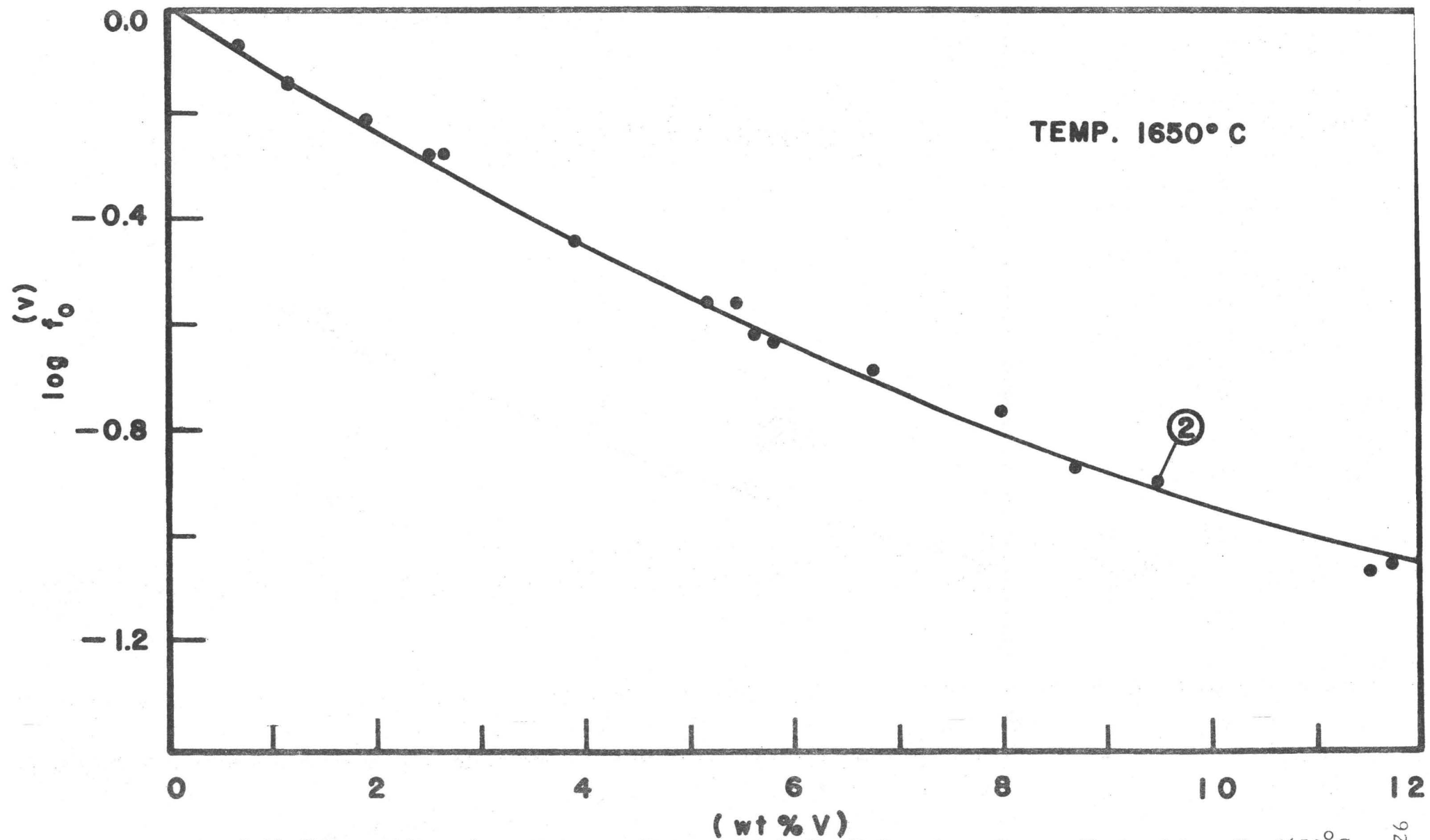
Fig. 5.14 Effect of V on the activity coefficient of O in Fe-V-O melts. Oxygen Probe data.   T = 1650°C
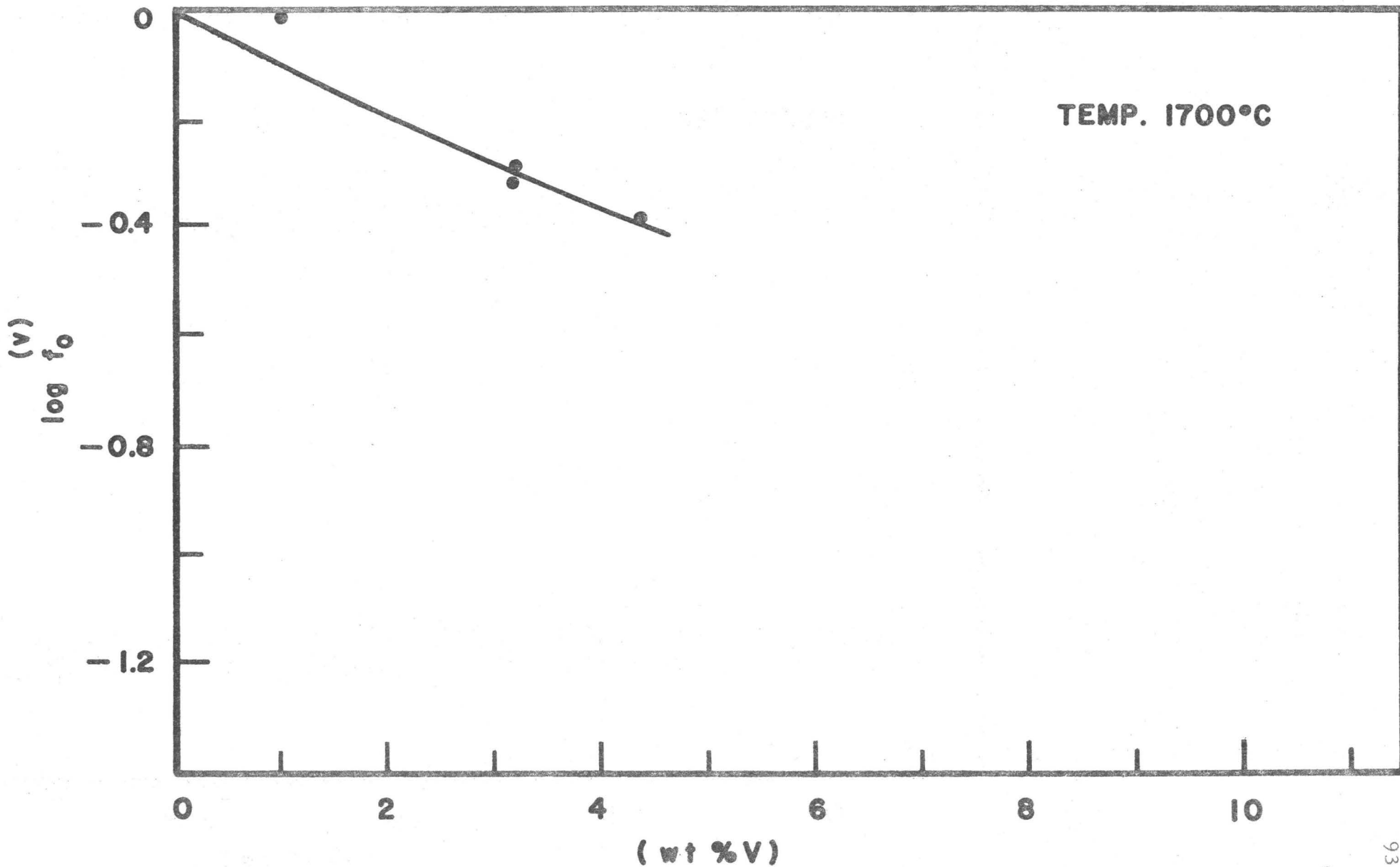
Fig. 5.15 Effect of V on the activity coefficient of O in Fe-V-O melts. Oxygen Probe data. T = 1700°C
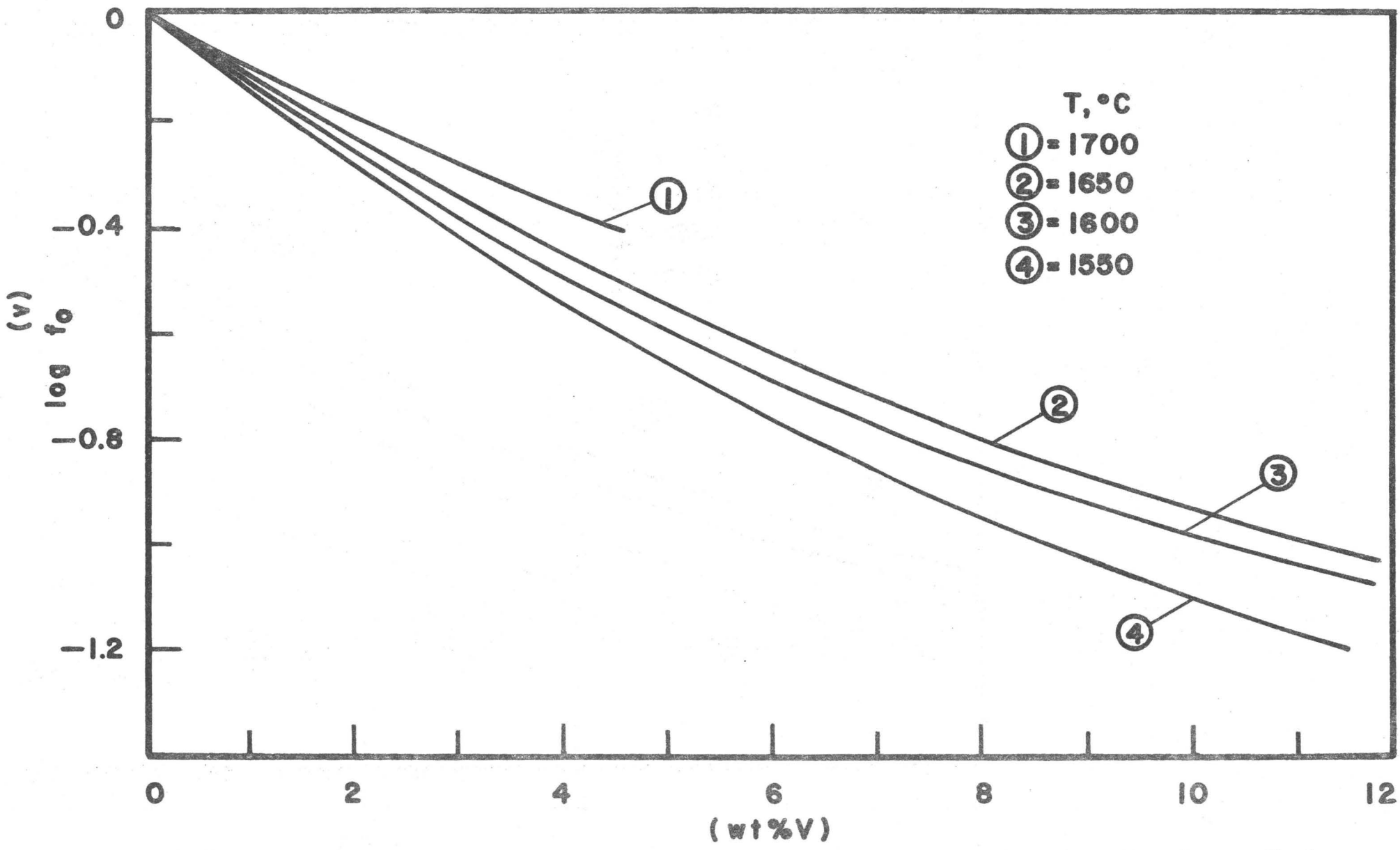
Fig. 5.17 Effect of temperature on the activity coefficient of oxygen in Fe-V-O melts. Oxygen Probe determination.

content of the melt. It is seen that the first order interaction parameter formalism is inadequate for describing the results over the range investigated. A second degree least square polynomial was therefore fitted through the experimental points, so that 2nd order free energy interaction parameter effects could be taken into consideration. The point $(0, 0)$ was included and weighted so that the fitted curves would pass through the origin.

The resulting equations are:

at 1550°C:
$$\log f_o^{(v)} = -0.15\,(\%V) + 4.0 \times 10^{-3}\,(\%V)^2 \quad (5.25)$$

at 1600°C:
$$\log f_o^{(v)} = -0.14\,(\%V) + 4.0 \times 10^{-3}\,(\%V)^2 \quad (5.26)$$

at 1650°C:
$$\log f_o^{(v)} = -0.12\,(\%V) + 2.9 \times 10^{-3}\,(\%V)^2 \quad (5.27)$$

No fit was attempted at 1700°C in view of the small number of experimental points.

In Fig. 5.17 the variation of the above curves with temperature is shown.

From eqns. (5.25) - (5.27) first and second order free energy interaction coefficients can be taken, and are presented in Table 5.15. In Fig. 5.18 they are plotted against $1/T$.

TABLE 5.15

VANADIUM-OXYGEN 1st AND 2nd ORDER

FREE ENERGY INTERACTION PARAMETERS

T, $^{\circ}$C	$e_o^{(v)}$	$r_o^{(v)} \times 10^3$	$\epsilon_o^{(v)}$	$\rho_o^{(v)}$
1550	-0.15	4.0	-31.4	73.8
1600	-0.14	4.0	-29.4	73.9
1650	-0.12	2.9	-25.2	53.3
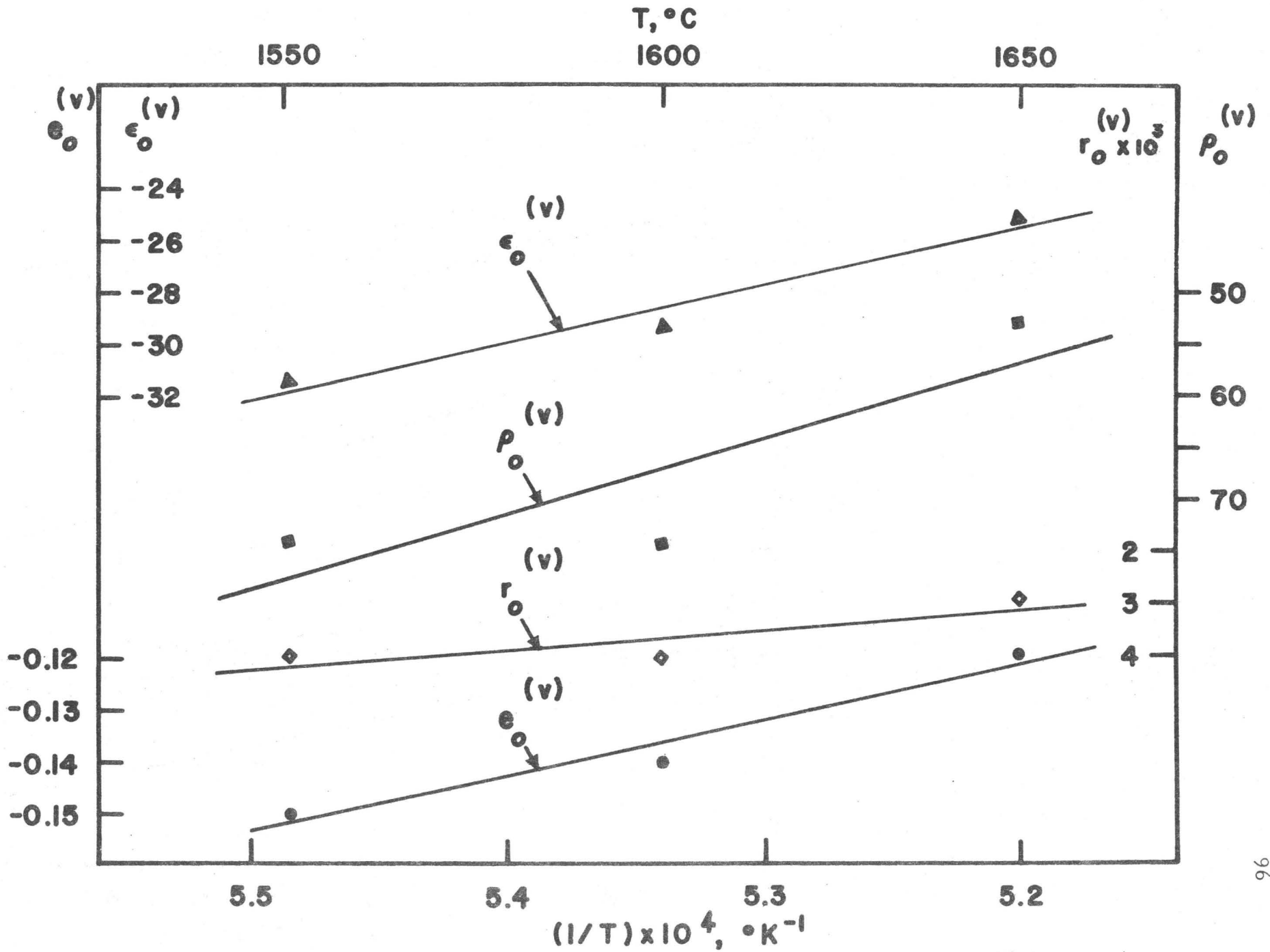
Fig. 5.18 Variations of lst and 2nd order free energy interaction parameters with temperature.

The least square lines through the experimental points in
Fig. 5.18 are represented by the following equations:

$$e_o^{(v)} = - \frac{1050}{T} + 0.42 \tag{5.28}$$

$$\epsilon_o^{(v)} = - \frac{216900}{T} + 87 \tag{5.29}$$

$$r_o^{(v)} = \frac{38.27}{T} - 0.017 \tag{5.30}$$

$$\rho_o^{(v)} = \frac{713160}{T} - 314 \tag{5.31}$$

From the above equations 1st and 2nd order enthalpy and entropy
interaction parameters can be calculated using equations (2.6) and (2.7)
and are presented in Table 5.16.

Finally, the Henrian activity of oxygen in liquid Fe-V alloys of
up to 12%V can be represented as a function of temperature by the following
equation:

$$\log f_o^{(v)} = (- \frac{1050}{T} + 0.42) \times (\%V) + (\frac{38.27}{T} - 0.017) \times (\%V)^2 \tag{5.32}$$

5.3.3. Activity of Vanadium in Iron-Vanadium Alloys

From the measured EMF of the oxygen probes the activity of
vanadium in the melts can be calculated, provided that the melts are in
equilibrium with an oxide phase. This oxide phase has been identified as
V_2O_3 throughout the range investigated (§ 5.4.1).

To determine the activity of V, the following cell reaction is
considered:

$$\underline{V} + \frac{1}{2} Cr_2O_3(s) = \frac{1}{2} V_2O_3(s) + Cr(s) \tag{5.33}$$
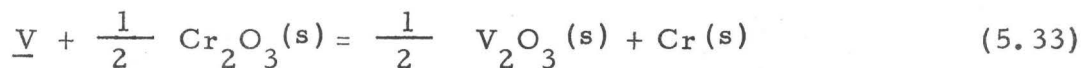
TABLE 5.16

VANADIUM-OXYGEN 1st and 2nd ORDER ENTHALPY AND ENTROPY INTERAC-

TION PARAMETERS

$$h_o^{(v)} = -4800$$

$$s_o^{(v)} = -1.92$$

$$\eta_o^{(v)} = -431000$$

$$\sigma_o^{(v)} = -173$$

$$l_o^{(v)} = 175$$

$$p_o^{(v)} = 0.078$$

$$\lambda_o^{(v)} = 1417000$$

$$\pi_o^{(v)} = 624$$

the standard state for vanadium in the left hand side of this equation being pure solid vanadium.

The free energy change for reaction (5.33) is

$$\Delta G_{(5.33)} = \Delta G^o_{(5.33)} + RT \ln k_{(5.33)}$$

$$= \Delta G^o_{(5.33)} - RT \ln a_v \qquad (5.34)$$

$\Delta G^o_{(5.33)}$ being the standard free energy change for reaction (5.33) and a_v being the Raoultian activity of V. $\Delta G_{(5.33)}$ is related to the measured EMF, E (in V), by the following equation:

$$\Delta G_{(5.33)} = -3EF \qquad (5.35)$$

$\Delta G^o_{(5.33)}$ can be calculated from the known free energies of formation of Cr_2O_3[62] and V_2O_3. Values for the latter were taken from the second part of this work (§ 12.5) and were extrapolated using existing high temperature calorimetric data[63, 64]. The $\Delta G^o_{(5.33)}$ is related to a standard EMF, E^o, by the equation

$$\Delta G^o_{(5.33)} = -3E^oF \qquad (5.36)$$

From eqns. (5.34), (5.35) and (5.36) the Raoultain activity of V can be written as

$$\log a_v = 3F (E^o - E)/2.303RT \qquad (5.37)$$

The value of E^o is calculated as -0.169 , -0.171 , -0.173 and -0.176V at 1550, 1600, 1650 and 1700°C respectively.

The experimental results are given in Tables 5.11 - 5.14. In Fig. 5.19 - 5.22 the Raoultain activity of V is plotted against its mole
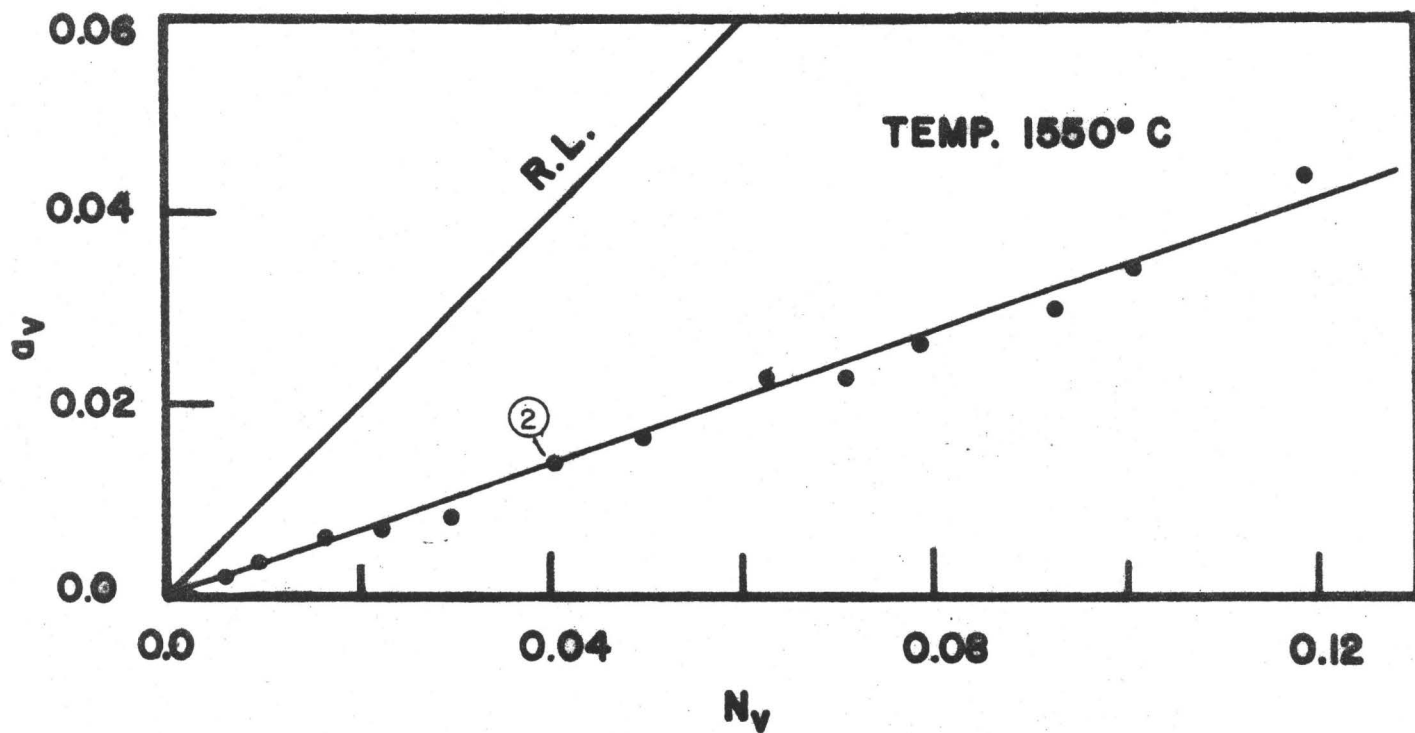
Fig. 5.19 Activity of V in Fe-V melts. T = 1550°C
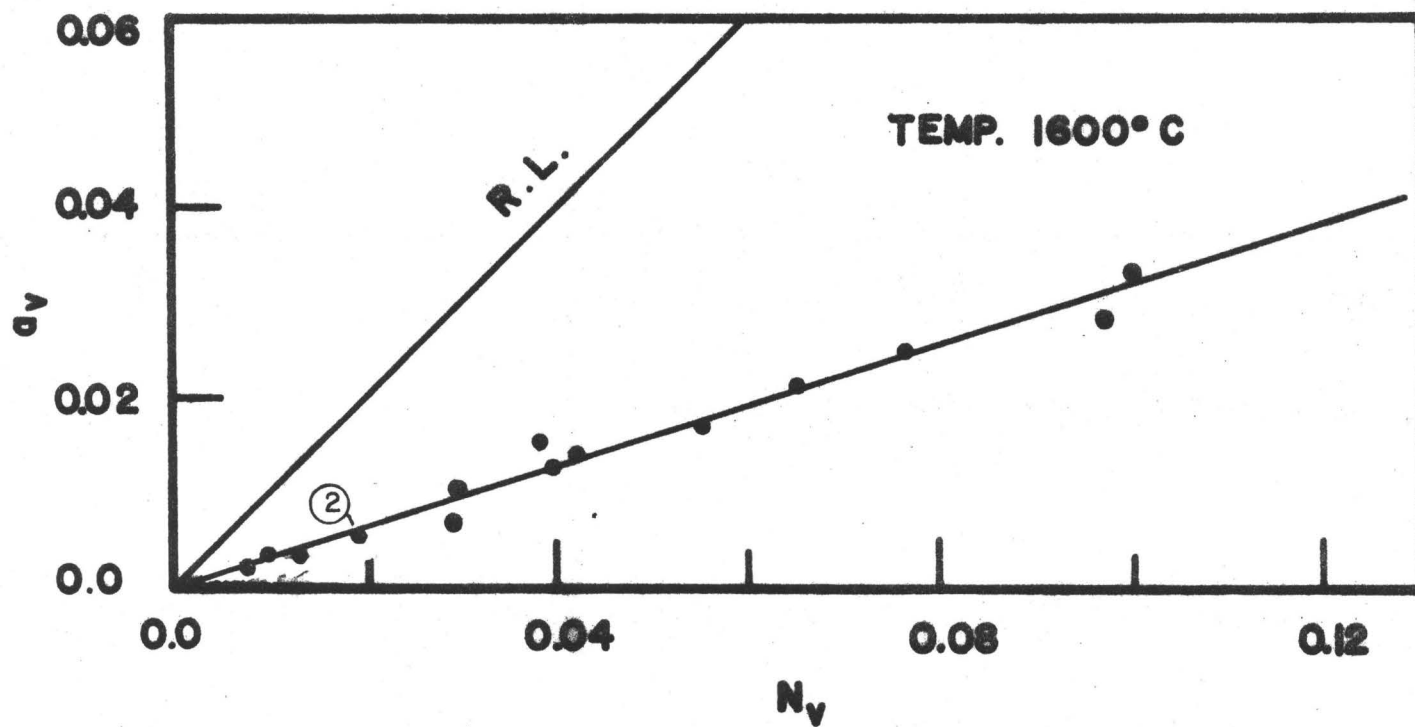
Fig. 5.20 Activity of V in Fe-V melts. T = 1600°C
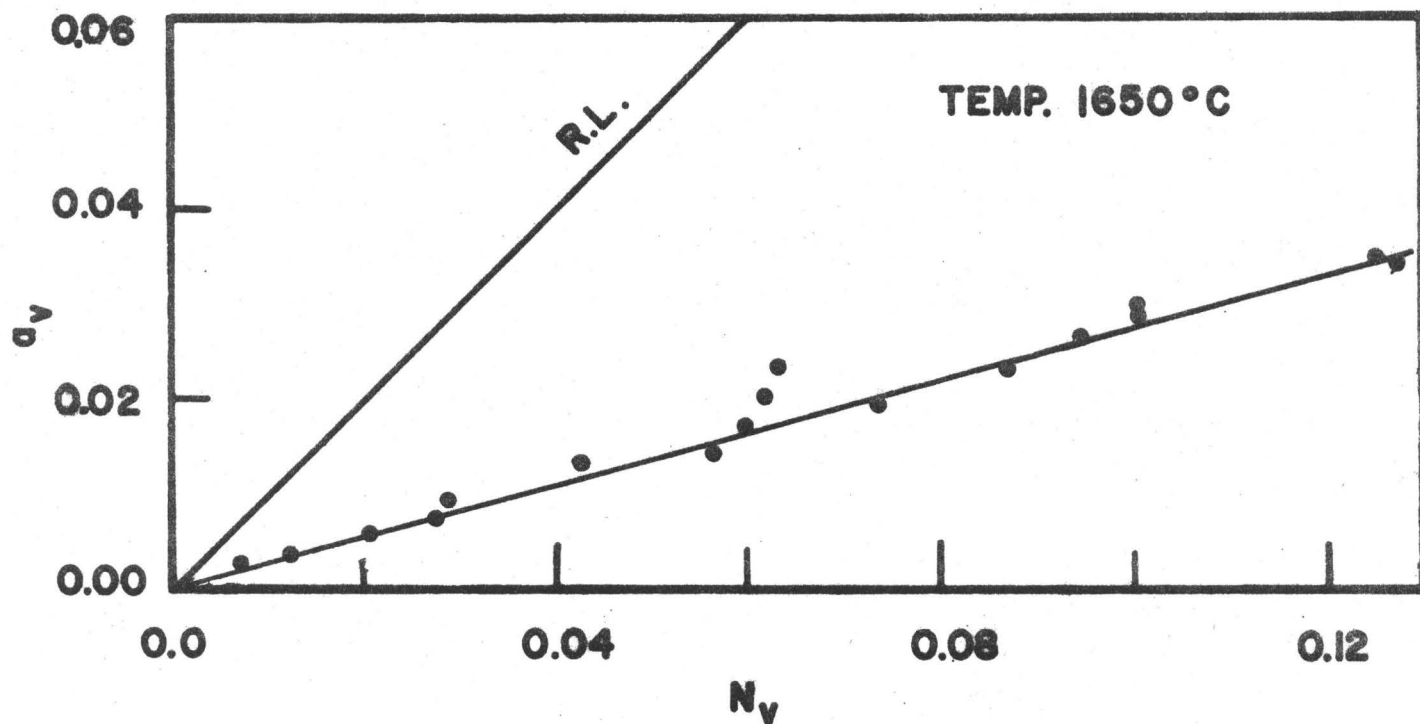
Fig. 5.21 Activity of V in Fe-V melts. T = 1650°C
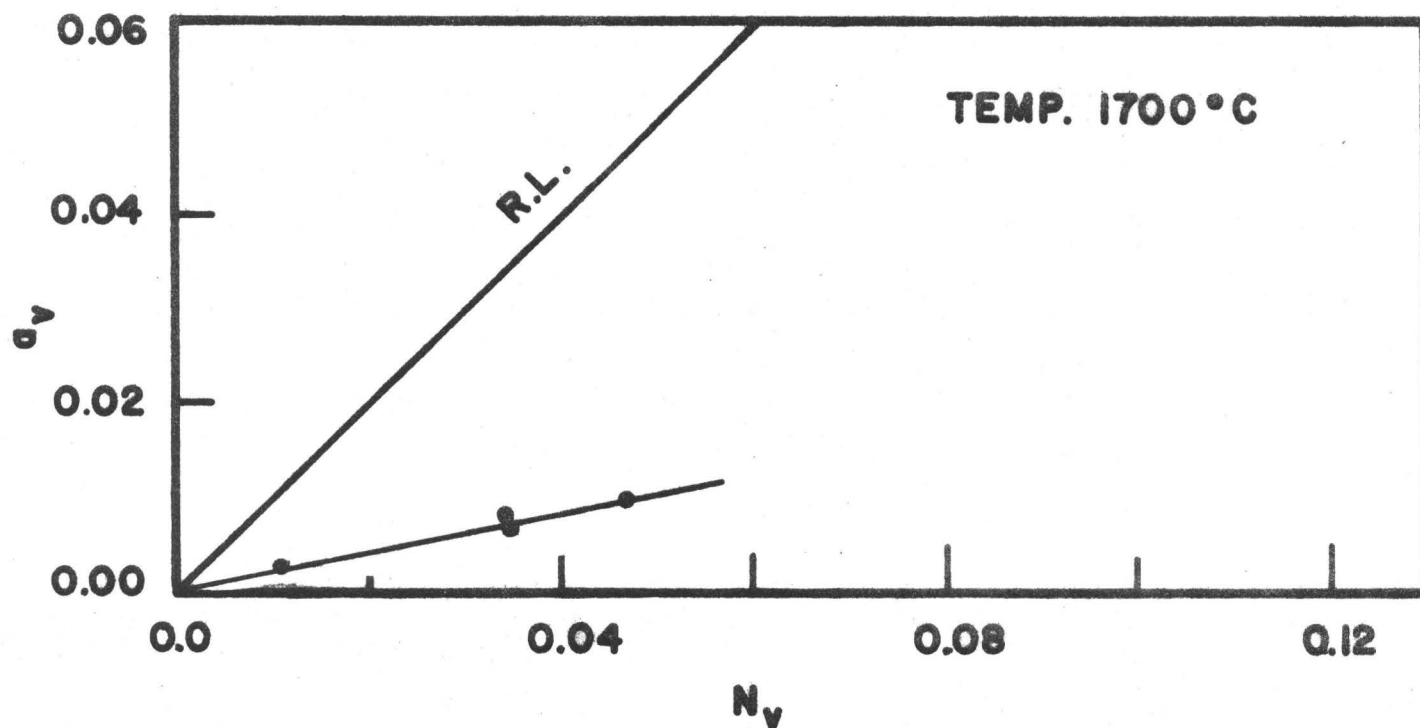
Fig. 5.22 Activity of V in Fe-V melts. T = 1700°C

fraction at the experimental temperatures studied. It is seen that solutions of V in liquid Fe exhibit a rather strong negative deviation from Raoult's Law, and that they obey Henry's Law throughout the range investigated.

A least square line was fitted through the experimental points at each temperature. The slope of these lines, representing the activity coefficient of vanadium at infinite dilution, γ_V^o, is given in Table 5.17A at the temperatures investigated.

TABLE 5.17A
VALUES OF γ_V^o AT THE EXPERIMENTAL TEMPERATURES

T, ^{o}C	γ_V^o
1550	0.35 $\pm$ 0.017*
1600	0.32 $\pm$ 0.020*
1650	0.27 $\pm$ 0.019*

No fit was attempted at 1700°C in view of the small number of experimental points.

It is seen from Table 5.17A that γ_V^o decreases as the temperature increases, which is not what one would expect. This should be attributed to the experimental uncertainty in the slope, and the value of γ_V^o can be considered as 0.31 $\pm$ 0.04 throughout the temperature range investigated.

5.3.4 Experimental Errors

The experimental errors associated with the oxygen probe work are the usual $\pm$ 6°C uncertainty in the temperature measurement and control, $\pm$ 10% in the oxygen analysis, and, in addition, $\pm$ 2mV in the reproducibility of the EMF of the oxygen probe. These errors account for the scatter of the experimental points.

---

* 95% confidence interval

Another error is the uncertainty in the free energy of formation of Cr_2O_3. As already stated, use of the equation (3.32) results in a 12% higher value for the activity of oxygen than the equation derived and used by Fruehan et al[55].

5.4   DEOXIDATION OF LIQUID IRON WITH VANADIUM

A study of the deoxidation reactions with vandium in liquid iron was made using data from the H_2O/H_2 equilibration melts which were saturated with oxygen, and all the data from the oxygen probe runs. The data are given in tables 5.17, 5.18, 5.19 and 5.20 for 1550, 1600, 1650 and 1700°C respectively.

Solutions of vanadium were found to obey Henry's law at all concentrations examined (§ 5.3.3) and the Henrian activity of vanadium in liquid iron (based on the 1 wt.% standard state) is taken to be equal to its weight % in the melt in all the oxygen probe runs. A slight correction for the influence of oxygen on the activity coefficient of vanadium ($e_V^{(o)}$) has been applied to the melts from the H_2O/H_2 equilibrations. This correction is within the uncertainty on V analysis for runs with the probe, so it was not applied in this case.

5.4.1   Identification of the Products of the Deoxidation Reactions

It is essential that the products of the deoxidation reactions be identified, so that the reactions can be formulated. The identification was done mainly with X-ray diffraction techniques and confirmed with electron microprobe analysis.

The oxide product was filed carefully from the top of the ingots with a clean sharp file and ground in a porcelain mortar. It was then mixed with transparent household cement, rolled to a cylinder of about 0.5mm in diameter and 1 cm long, and mounted on a Debye-Scherrer camera (114.6 mm diameter). Its diffraction pattern was taken using Co

TABLE 5.17

Fe-V-O MELTS SATURATED WITH OXYGEN T = 1550°C

Run	T, °C	O , ppm	%V	log h_o	log h_v
361	1550	213	.44	-1.787	-.372
431	1550	150	1.01	-1.960	-.007
531	1550	235	.28	-1.682	-.565
541	1550	339	.17	-1.509	-.805
571	1550	175	.53	-1.848	-.285
621	1550	444	.10	-1.412	-1.038
641	1550	160	1.33	-2.089	.113
651	1550	544	.04	-1.272	-1.423
661	1550	453	.09	-1.412	-1.081
671	1550	262	.19	-1.610	-.730
701	1550	572	.04	-1.238	-1.415
911	1550	177	.57	-1.825	-.244
912	1550	139	.84	-2.057	-.078
913	1550	131	1.48	-2.223	.170
914	1550	114	2.02	-2.267	.305
921	1550	110	2.68	-2.322	.428
923	1550	107	3.70	-2.472	.568
922	1550	113	3.73	-2.472	.572
924	1550	111	4.54	-2.527	.657
925	1550	134	5.71	-2.621	.757
927	1550	151	6.46	-2.621	.810
928	1550	160	7.21	-2.660	.858
929	1550	185	8.50	-2.698	.929
938	1550	196	9.69	-2.737	.986
939	1550	260	10.91	-2.809	1.038

TABLE 5.18

Fe-V-O MELTS SATURATED WITH OXYGEN T = 1600°C

Run	T, °C	O, ppm	%V	log h_o	log h_v
422	1600	254	1.52	-1.855	.168
512	1600	433	.16	-1.378	-.816
522	1600	425	.31	-1.443	-.532
532	1600	293	.42	-1.571	-.390
542	1600	437	.19	-1.398	-.745
552	1600	413	.21	-1.391	-.696
572	1600	233	.73	-1.739	-.149
562	1600	216	1.03	-1.840	.001
582	1600	223	.98	-1.840	-.024
632	1600	666	.06	-1.162	-1.226
642	1600	209	1.43	-1.981	.142
652	1600	662	.06	-1.156	-1.261
662	1600	539	.11	-1.303	-.986
672	1600	351	.24	-1.501	-.635
702	1600	727	.06	-1.128	-1.287
712	1600	1044	.03	-.976	-1.570
722	1600	225	.95	-1.817	-.037
881	1600	227	.64	-1.752	-.192
931	1600	210	.92	-1.854	-.037
883	1600	182	1.20	-1.881	.079
884	1600	155	1.77	-2.016	.248
885	1600	167	1.79	-1.989	.253
886	1600	160	2.72	-2.070	.435
932	1600	169	2.74	-2.183	.438
933	1600	161	3.51	-2.290	.545
892	1600	158	3.66	-2.242	.563
934	1600	170	3.89	-2.274	.590
935	1600	178	5.09	-2.323	.707
893	1600	191	6.02	-2.393	.780
936	1600	237	7.05	-2.436	.848
938	1600	280	8.94	-2.473	.951
896	1600	259	9.20	-2.522	.964

TABLE 5.19

Fe-V-O MELTS SATURATED WITH OXYGEN   T = 1650°C

Run	T, °C	O, ppm	%V	log h_o	log h_v
443	1650	575	.28	−1.274	−.578
513	1650	575	.28	−1.274	−.585
523	1650	601	.31	−1.338	−.323
533	1650	370	.55	−1.470	−.277
543	1650	546	.28	−1.290	−.582
553	1650	512	.32	−1.287	−.515
573	1650	297	.93	−1.635	−.045
563	1650	288	1.32	−1.730	.105
583	1650	272	1.25	−1.735	.083
653	1650	821	.07	−1.060	−1.180
663	1650	658	.15	−1.198	−.853
673	1650	450	.34	−1.398	−.499
693	1650	675	.12	−1.165	−.942
703	1650	881	.07	−1.024	−1.201
713	1650	1273	.05	−.873	−1.395
723	1650	314	1.32	−1.707	.103
971	1650	342	.67	−1.542	−.174
941	1650	303	1.15	−1.662	.061
972	1650	260	1.87	−1.804	.272
943	1650	248	2.50	−1.888	.398
942	1650	265	2.62	−1.966	.418
945	1650	242	3.89	−2.061	.590
965	1650	303	5.16	−2.071	.713
946	1650	270	5.46	−2.129	.737
951	1650	276	5.62	−2.176	.750
968	1650	261	5.79	−2.218	.763
952	1650	340	6.75	−2.160	.829
954	1650	355	7.99	−2.213	.903
969	1650	415	8.71	−2.250	.940
974	1650	399	9.41	−2.291	.974
975	1650	407	9.49	−2.281	.977
976	1650	534	11.54	−2.333	1.062
977	1650	525	11.73	−2.328	1.069

TABLE 5.20

Fe-V-O MELTS SATURATED WITH OXYGEN   T = 1700°C

Run	T, °C	O , ppm	%V	log h_o	log h_v
534	1700	472	.73	-1.368	-.154
554	1700	695	.34	-1.188	-.503
574	1700	375	1.10	-1.537	.026
564	1700	349	1.33	-1.635	.109
584	1700	293	1.96	-1.783	.280
664	1700	813	.17	-1.100	-.794
674	1700	533	.48	-1.300	-.344
694	1700	809	.15	-1.066	-.858
704	1700	1190	.11	-.928	-1.009
724	1700	422	1.61	-1.608	.190
961	1700	410	1.00	-1.398	-.002
962	1700	382	3.16	-1.736	.500
963	1700	385	3.21	-1.685	.507
964	1700	383	4.34	-1.797	.637

radiation filtered through an Fe window.

Two oxide products were identified: the iron-vanadium spinel, FeV_2O_4, and the vandium trioxide, V_2O_3. Both are solid at steelmaking temperatures. No interaction was observed between the alumina crucibles and any of the above oxides.

Typical X-ray diffraction patterns are given in tables 5.21 and 5.22 for FeV_2O_4 and V_2O_3 respectively.

FeV_2O_4 was found on ingots containing less than 0.2%V, while V_2O_3 was identified in all of the ingots examined, containing more than 0.75%V. In runs made at 1550°C, V_2O_3 was identified in ingots containing around 0.25%V. In runs made at higher temperatures a mixture of the two oxides was found sometimes for V contents between 0.3 and 0.7%, indicating that FeV_2O_4 was the product at that particular temperature and V content, and on cooling (which was done rather slowly in the resistance furnace) V_2O_3 was formed. The boundary between FeV_2O_4 and V_2O_3 formation can safely be placed around 0.2%V at 1550°C, but is less well defined at higher temperatures.

Many ingots were sectioned and examined metallographically. Ingots in which FeV_2O_4 was the product contained numerous inclusions. On the other hand, inclusions were small and scarce in ingots where V_2O_3 was the product.

This phenomenon has been discussed by McLean[66] in the case of aluminate inclusions in steel. It is known that as the interfacial tension between the steel and a nonmetallic phase decreases, the tendency of the nonmetallic phase to separate also decreases[67, 68]. Since the interfacial tension between molten iron and a solid oxide is always decreased when the solid phase contains iron oxide[69], this would mean that the iron-vanadium spinel is more likely to remain within the steel than vanadium trioxide.

Some micrographs of inclusions are given in Fig. 5.23-5.24.

TABLE 5.21

X-RAY DIFFRACTION PATTERN OF OXIDE ON INGOT 512 (0.16%V)

Line	Pat	d obs	d due to FeV_2O_4*	d due to FeV_2O_4+	d due to Fe**	Choice
1	w	2.98	2.99	2.93		FeV_2O_4
2	m	2.54	2.55	2.50		FeV_2O_4
3	w	2.11	2.12	2.07		FeV_2O_4
4	vs	2.02			2.03	Fe
5	vw	1.72	1.73	1.69		FeV_2O_4
6	mw	1.62		1.60		FeV_2O_4
7	mw	1.49	1.50	1.47		FeV_2O_4
8	m	1.43			1.43	Fe
9	vw	1.29		1.27		FeV_2O_4
10	s	1.17		1.25	1.17	Fe
11	w	1.10	1.10		1.13	FeV_2O_4
12	vw	1.06	1.06			FeV_2O_4
13	vw	1.01	1.00			FeV_2O_4
14	vw	0.98	0.97			FeV_2O_4
15	vw	0.94				-

* From C.H. Mathewson, E. Spire and C. Samans: Trans. A.S.S.T., 1932, vol. 20, pp 357-384.

+ ASTM Powder File Card No. 15-122.

** ASTM Powder File Card No. 6-0696.

TABLE 5.22

X-RAY DIFFRACTION PATTERN OF THE OXIDE ON INGOT 641 (1.33%V)

Line	Pat.	d obs	d due to V_2O_3*	d due to Fe+	Choice
1	s	3.66	3.65		V_2O_3
2	vs	2.68	2.70		V_2O_3
3	s	2.50	2.47		V_2O_3
4	w	2.20	2.18		V_2O_3
5	s	2.03		2.027	Fe
6	s	1.84	1.83		V_2O_3
7	s	1.69	1.69		V_2O_3
8	vw	1.61			-
9	vw	1.60	1.597		V_2O_3
10	w	1.48	1.47		V_2O_3
11	s	1.45	1.43	1.43	Fe / V_2O_3
12	vw	1.35	1.33		V_2O_3
13	vw	1.31			-
14	w	1.26	1.24		V_2O_3
15	vw	1.21	1.22		V_2O_3
16	vw	1.19	1.19		V_2O_3
17	vw	1.16	1.17	1.17	Fe/V_2O_3
18	vw	1.14	1.13		V_2O_3
19	vw	1.04		1.01	Fe

* ASTM Powder Index Card No. 1-1293

+ ASTM Powder Index Card No. 6-0696

The nonmetallic inclusions from several ingots were studied using an ACTON electron microprobe. They were scanned for elements such as Al, Mn, Si, with negative results. It was not possible to analyze for oxygen with this microprobe.

X-ray images of several inclusions are shown in Fig. 5.25 - 5.28.

Quantitative analysis for V and Fe with pure metals as standards gave results consistent with the presence of V_2O_3 and FeV_2O_4 inclusions.

The morphology of the oxide layer on top of several ingots was also examined under a scanning electron microscope (Cambridge Stereo-Scan). On ingots where FeV_2O_4 was the oxide product, well-shaped octahedral patterns could be recognized (Fig. 5.29 - 5.30), in agreement with the cubic crystal structure of the spinel. On ingots where V_2O_3 was the oxide product, the surface was dull, and no crystalline patterns could be observed.

5.4.2 The Deoxidation Reactions

Having identified the deoxidation products, the deoxidation reactions are written as

$$Fe(1) + 2\underline{V} + 4\underline{O} = FeV_2O_4(s) \tag{5.38}$$
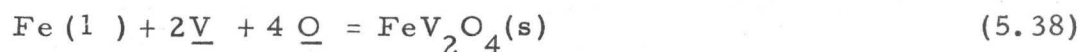
$$k_3 = 1/h_v^2 \ h_o^4 \tag{5.39}$$

for the vanadium levels for which the spinel is the product, and

$$2\underline{V} + 3\underline{O} = V_2O_3(s) \tag{5.40}$$

$$k_4 = 1/h_v^2 \ h_o^3$$

for the vanadium levels for which the trioxide is the product.

112
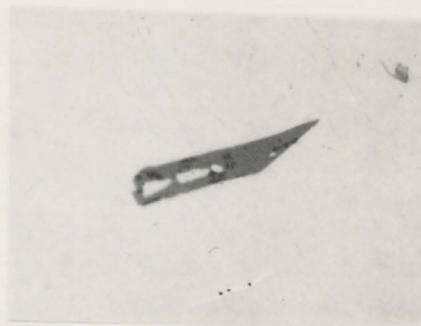
Fig. 5.23   Micrograph of V_2O_3 inclusions.
Ingot No. 422 (1.52%V)
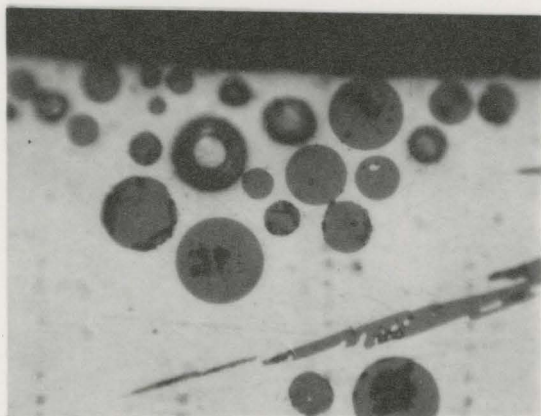
Fig. 5.24a   Micrograph of FeV_2O_4 inclusions.
Ingot No. 661 (0.09%V)
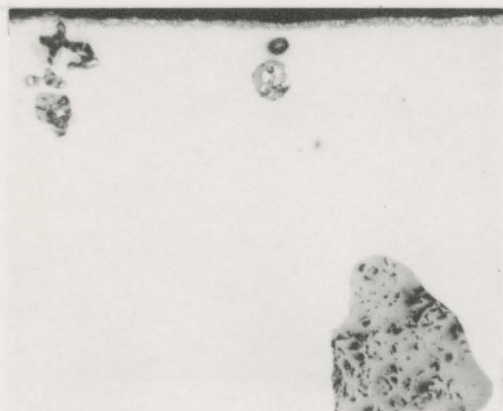
Fig. 5.24b   Micrograph of FeV_2O_4 inclusions.
Ingot No. 712 (0.03%V)

50 μ

Optical Micrograph   Electron Image
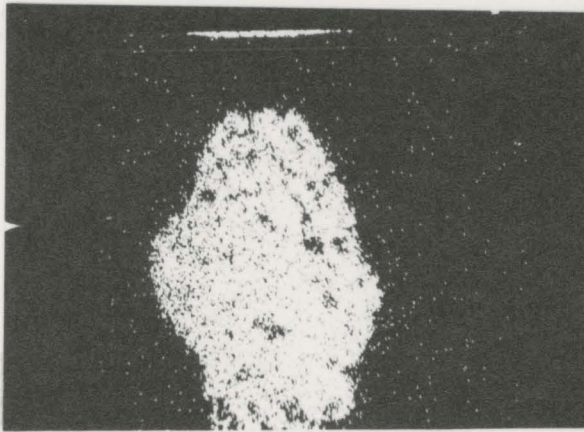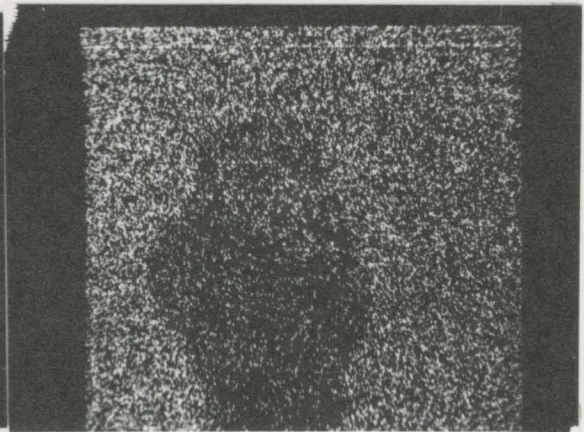
V K_α Fe K_α

Fig. 5.25   Electron microprobe pictures of
              FeV_2O_4 inclusions.
              Ingot 512 (0.16%V)

50 μ

Optical Micrograph   Electron Image

V K$_a$ Fe K$_a$
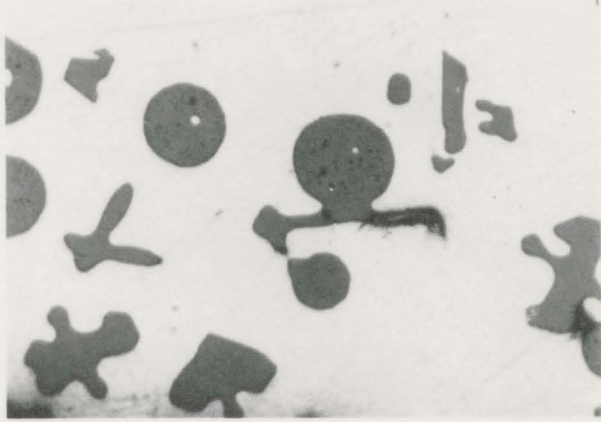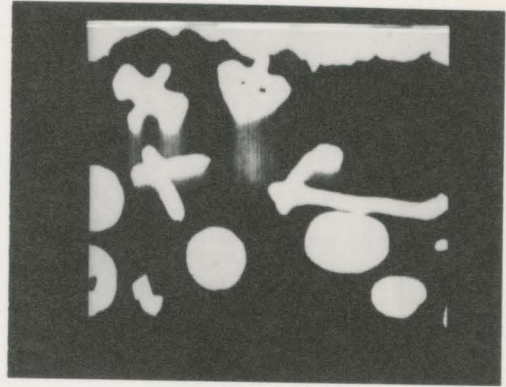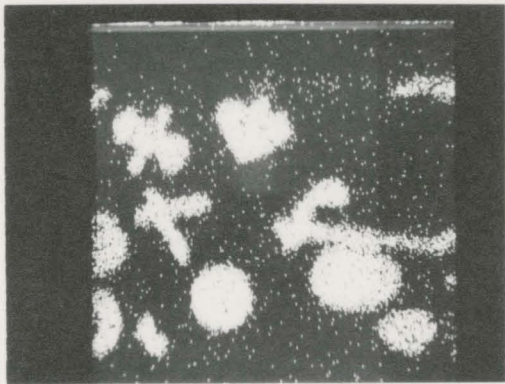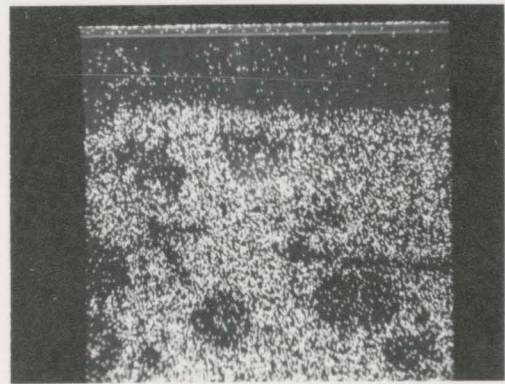
Fig. 5.26a   Electron microprobe pictures of
                      FeV$_2$O$_4$ inclusions.
                      Ingot 662 (0.11%V)
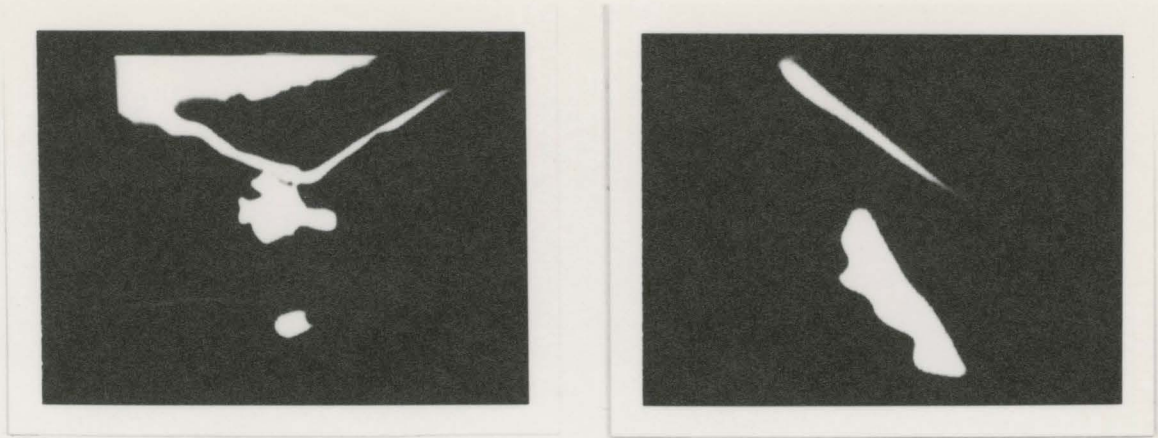
20μ   10μ

Electron Image

V K$_a$

Fe K$_a$
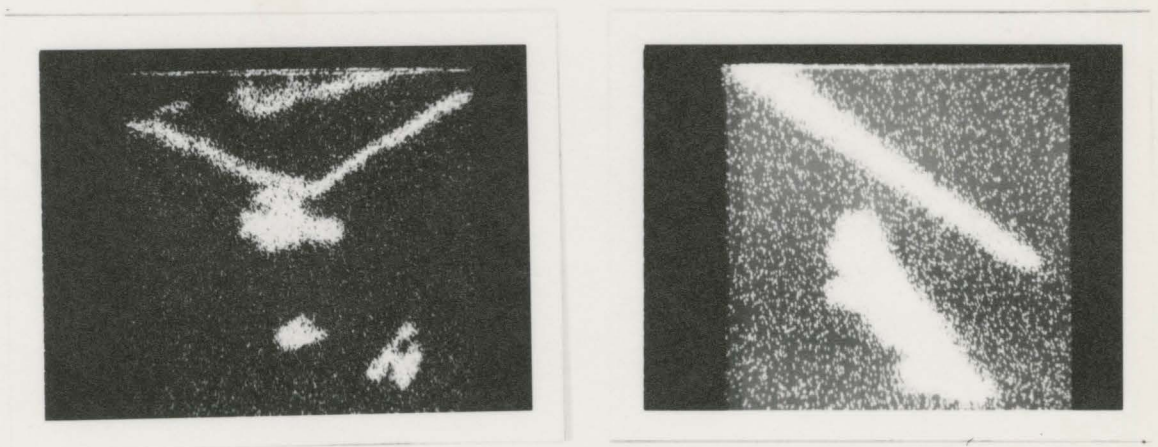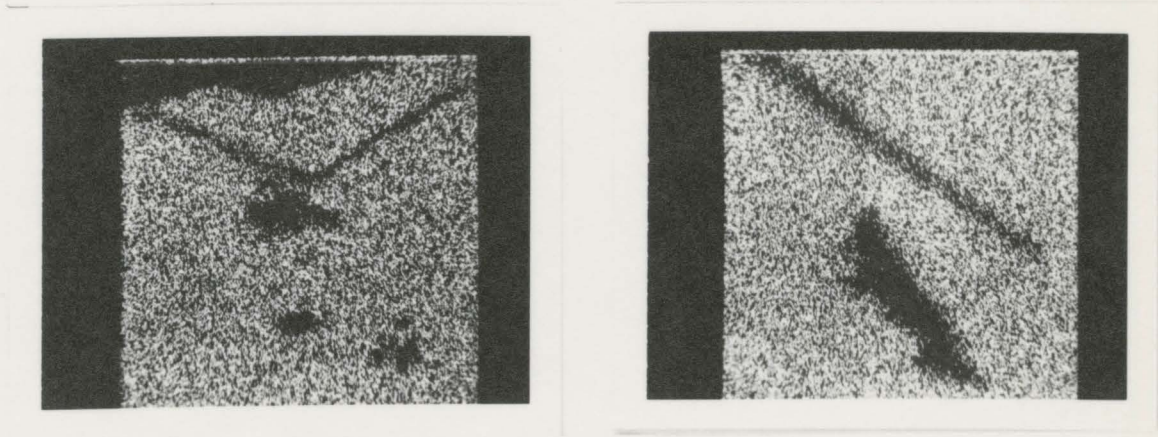
Fig. 5.27-   Electron microprobe pictures of V$_2$O$_3$
5.28   inclusions. Ingot 422 (1.52%V)

20μ

2μ
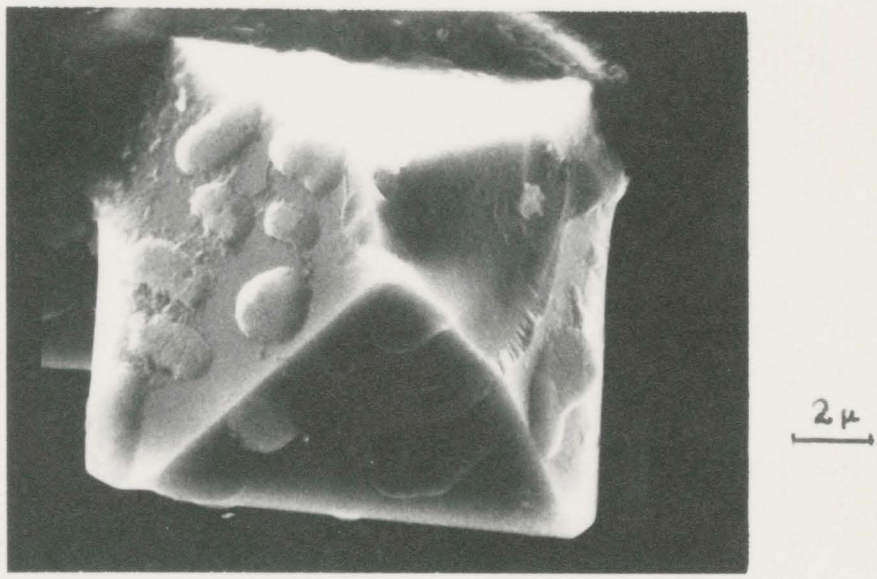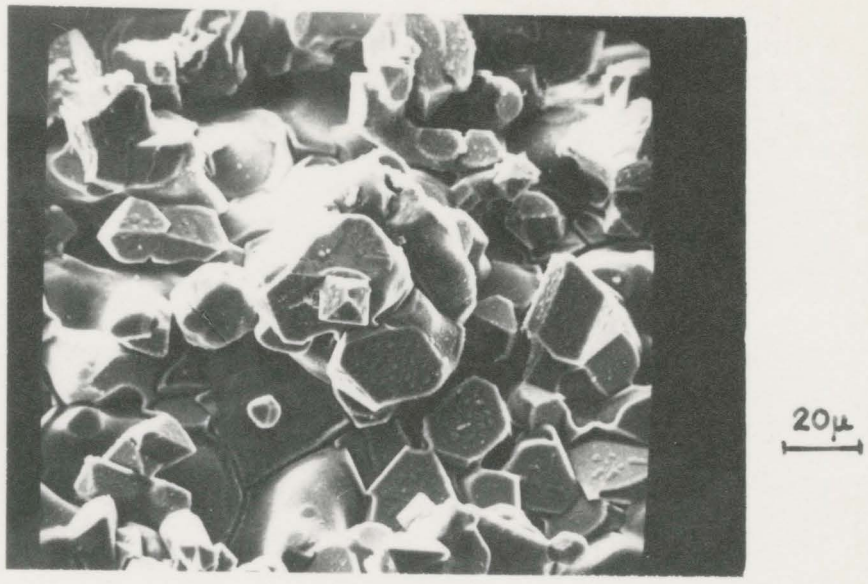
Fig. 5.29   SEM pictures of oxide on surface of ingot
512 (0.16%V)
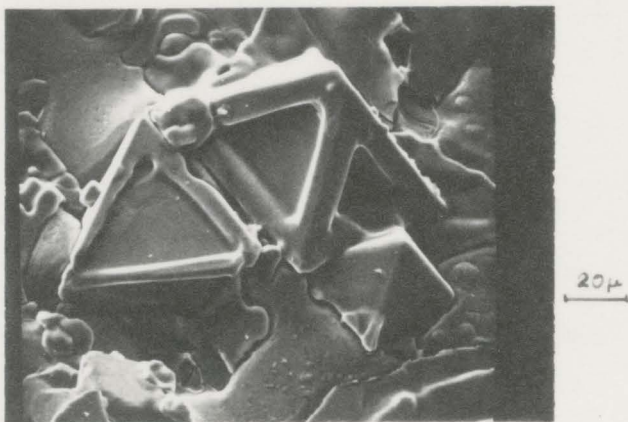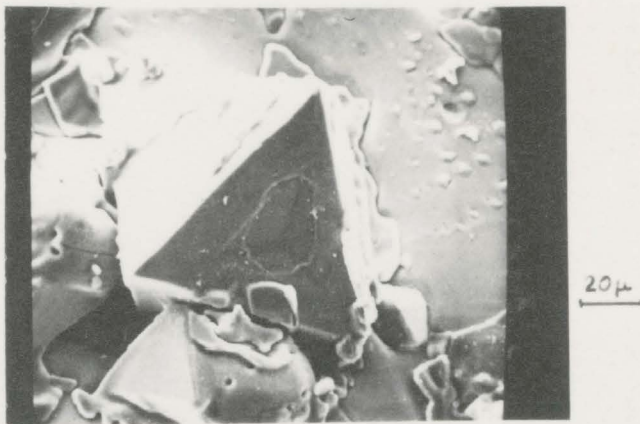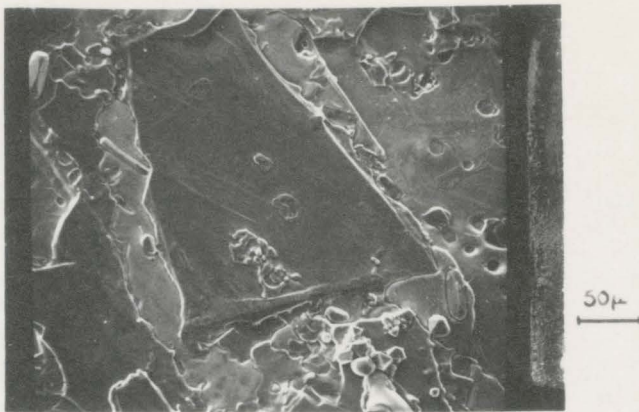
Fig. 5.30   SEM pictures of oxide on surface of
ingot 621 (0.10%V)

Data for these reactions, taken from tables 5.17 - 5.20, are plotted as $\log h_o$ against $\log h_v$ in Fig. 5.31 - 5.35.

Least square lines with slopes $-\frac{1}{2}$ and $-\frac{2}{3}$ were fitted through the experimental points for which FeV_2O_4 and V_2O_3 are the reaction products respectively. These lines are represented by the following equations:

(a) $T = 1550^{\circ}C$

$$FeV_2O_4: \log h_o = -1.949 - \frac{1}{2} \log h_v \qquad (5.41)$$

$$V_2O_3: \quad \log h_o = -2.067 - \frac{2}{3} \log h_v \qquad (5.42)$$

(b) $T = 1600^{\circ}C$

$$FeV_2O_4: \log h_o = -1.770 - \frac{1}{2} \log h_v \qquad (5.43)$$

$$V_2O_3: \quad \log h_o = -1.853 - \frac{2}{3} \log h_v \qquad (5.44)$$

(c) $T = 1650^{\circ}C$

$$FeV_2O_4: \log h_o = -1.590 - \frac{1}{2} \log h_v \qquad (5.45)$$

$$V_2O_3: \quad \log h_o = -1.643 - \frac{2}{3} \log h_v \qquad (5.46)$$

(d) $T = 1700^{\circ}C$

$$FeV_2O_4: \log h_o = -1.450 - \frac{1}{2} \log h_v \qquad (5.47)$$

$$V_2O_3: \quad \log h_o = -1.467 - \frac{2}{3} \log h_v \qquad (5.48)$$

The point where these lines intersect at each temperature is the point where FeV_2O_4 and V_2O_3 coexist in equilibrium with the melt.
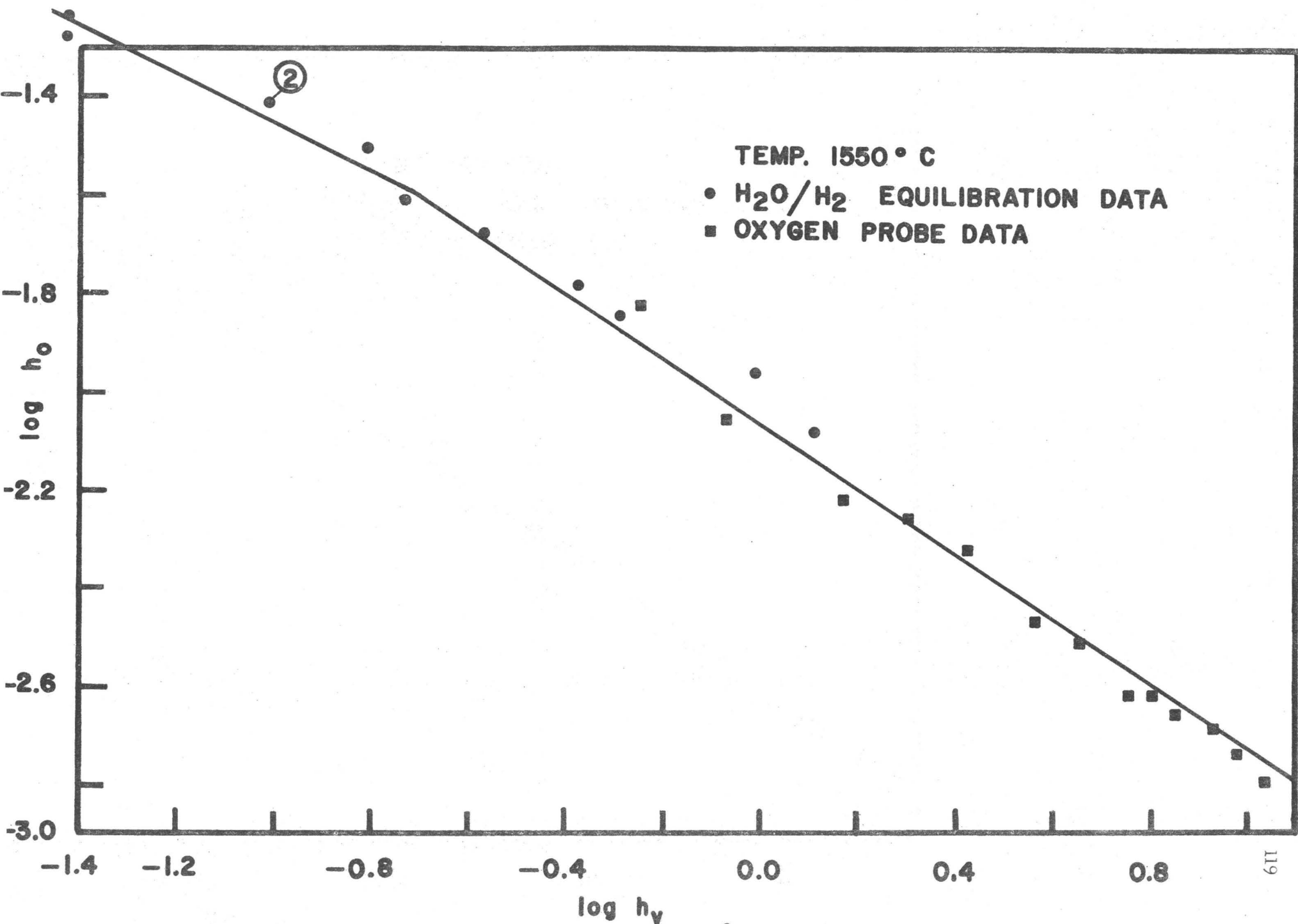
Fig. 5.31 Variation of $\log h_o$ with $\log h_v$. T = 1550°C
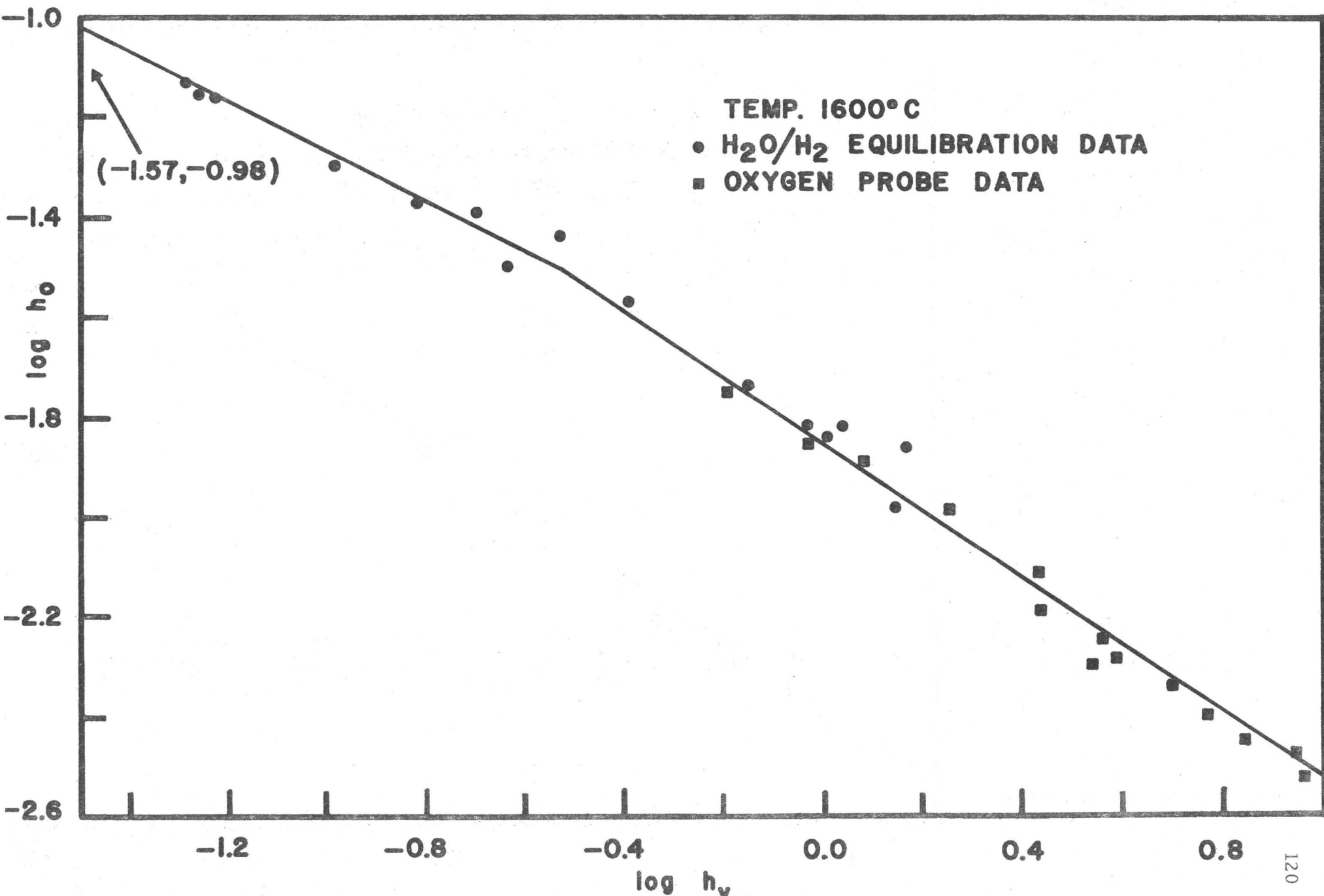
Fig. 5.32 Variation of $\log h_O$ with $\log h_V$. T = 1600°C
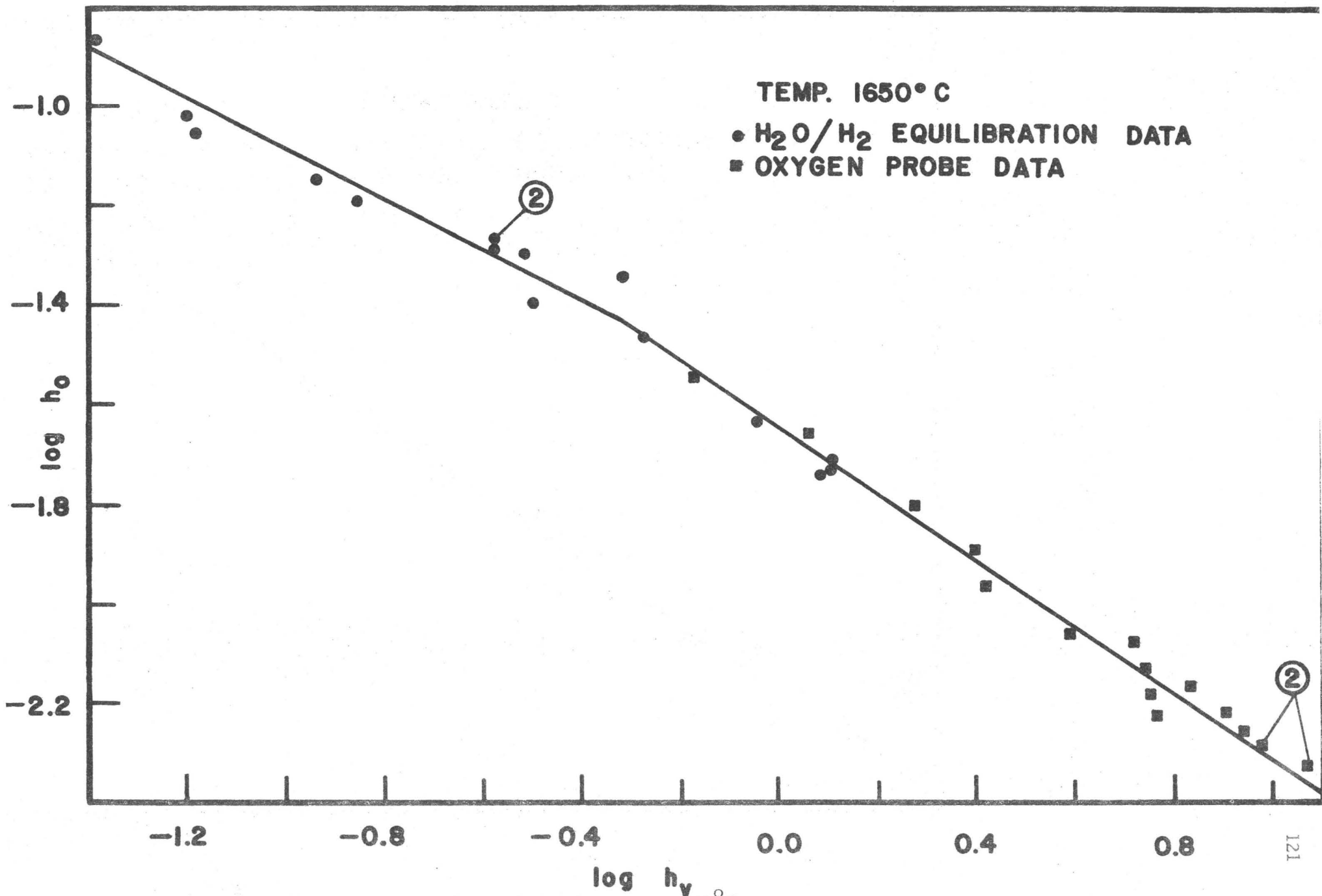
Fig. 5.33 Variation of $\log h_o$ with $\log h_v$. $T = 1650^{\circ}C$
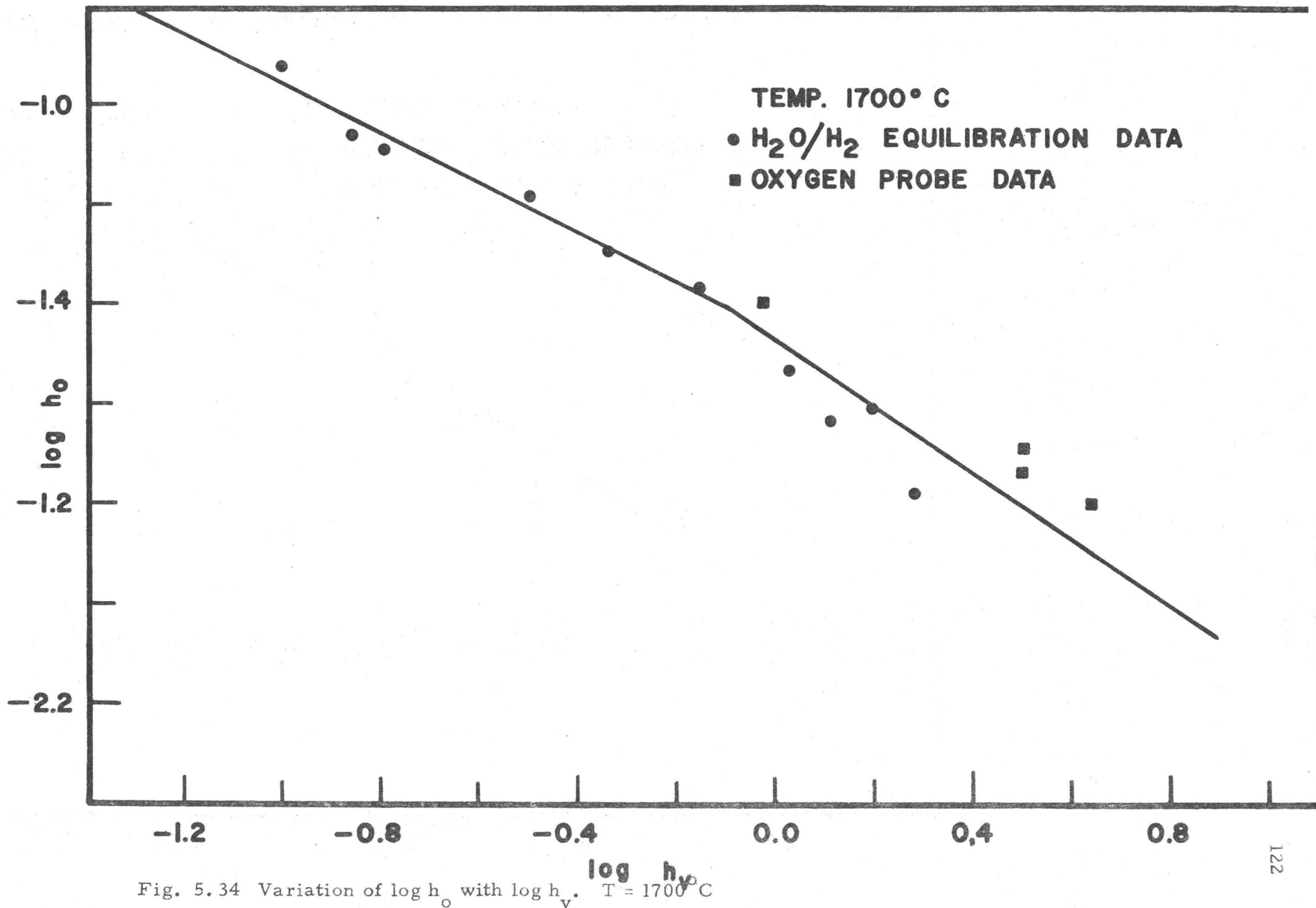
Fig. 5.34 Variation of $\log h_o$ with $\log h_v$.   T = 1700° C
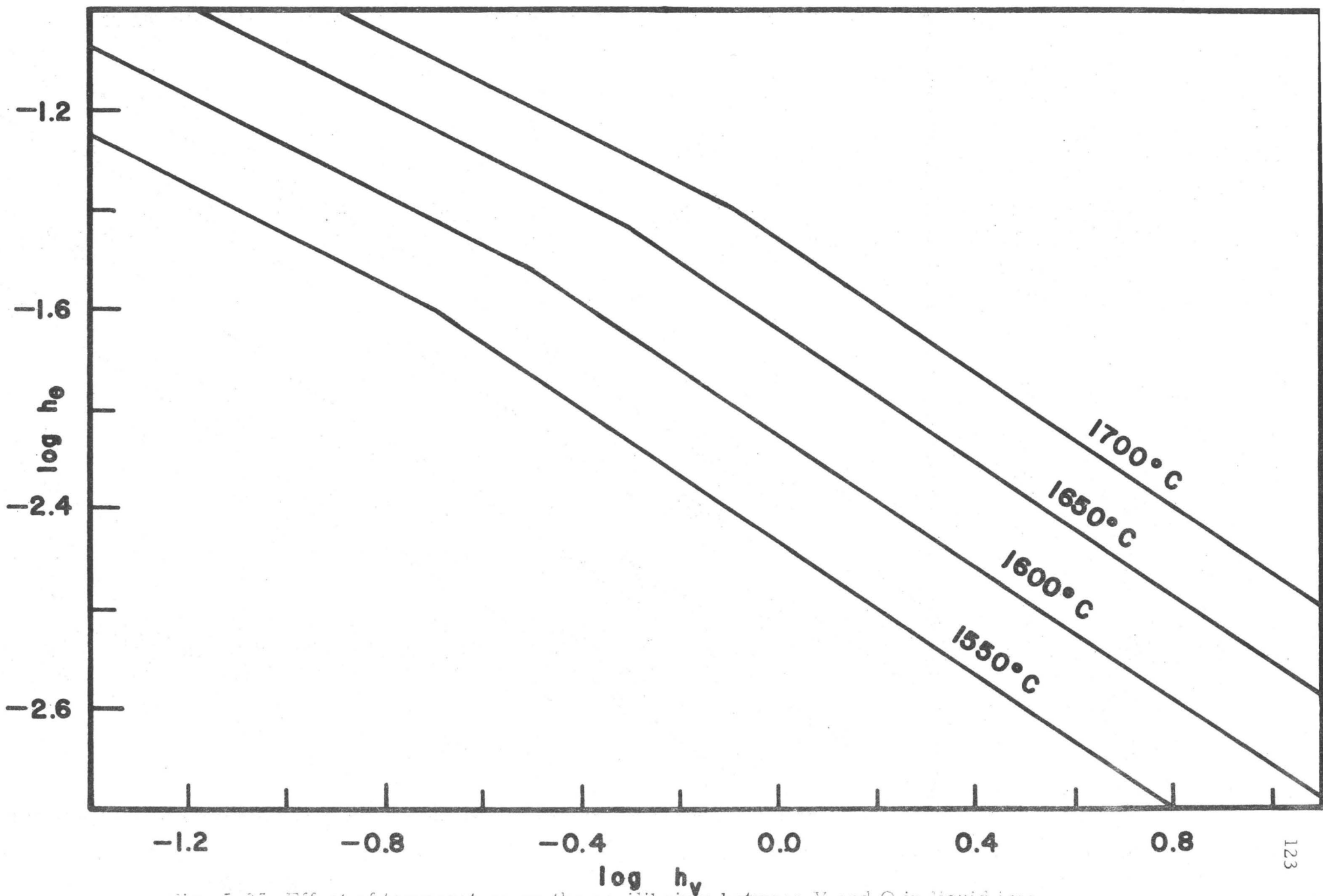
Fig. 5.35 Effect of temperature on the equilibrium between V and O in liquid iron.

123

As mentioned before, this point is rather well defined at 1550°C, at 0.2%V. At higher temperatures the experimental slope of the points was used in conjunction with the X-ray data to determine this point.

The points of intersection lie at 0.20, 0.30, 0.47, and 0.75%V at 1550, 1600, 1650 and 1700°C respectively.

From equations (5.41) - (5.48) the equilibrium constants k_3 and k_4 for the reactions (5.38) and (5.40) can be calculated, and are plotted in Fig. 5.36 against $1/T$. The least square lines through the points in this figure give the temperature dependence of k_3 and k_4:

$$\log k_3 = \frac{48300}{T} - 18.70 \tag{5.49}$$

$$\log k_4 = \frac{43400}{T} - 17.61 \tag{5.50}$$

From the above equations the free energy changes for the reactions (5.38) and (5.40) are calculated as

$$\Delta G_3^\circ = -220900 + 85.55\,T \text{ (cal)} \tag{5.51}$$

$$\Delta G_4^\circ = -198550 + 80.57\,T \text{ (cal)} \tag{5.52}$$

Based on the data presented in Tables 5.17 - 5.20 the deoxidation diagrams can be constructed and are presented in Fig. 5.37, 5.38, 5.39 and 5.40 for 1550, 1600, 1650 and 1700°C respectively. It is seen that the solubility of oxygen decreases to a minimum with increasing V content, and then it starts increasing. This increase is due to the decreasing activity coefficient of oxygen. The variation of the deoxidation diagrams with temperature is shown in Fig. 5.41.

5.4.3   Thermodynamics of Iron-Vanadium Spinel Formation

By subtracting eqn. (5.40) from (5.38) the thermodynamics of
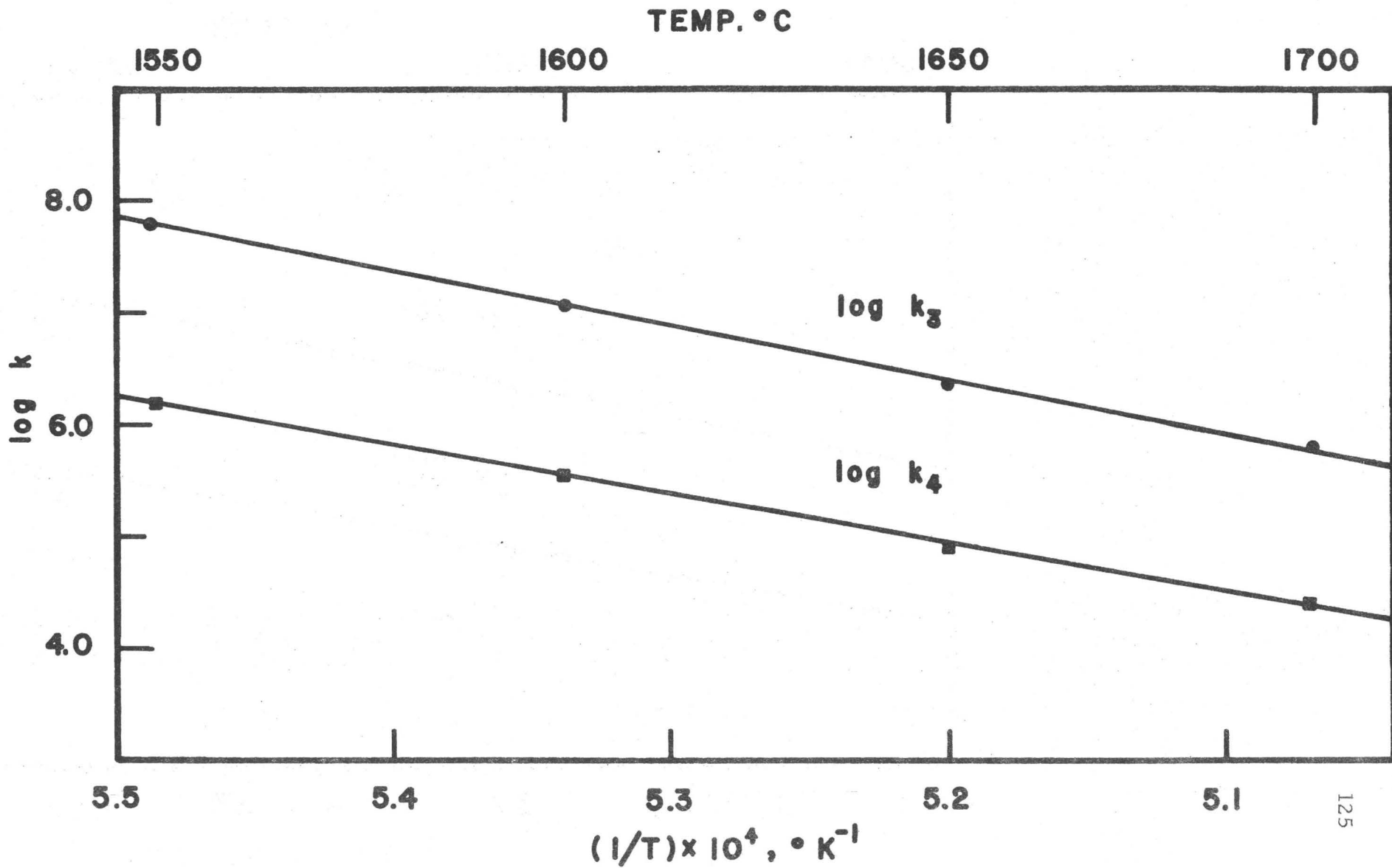
Fig. 5.36 Variation of $\log k_3$ and $\log k_4$ with temperature.
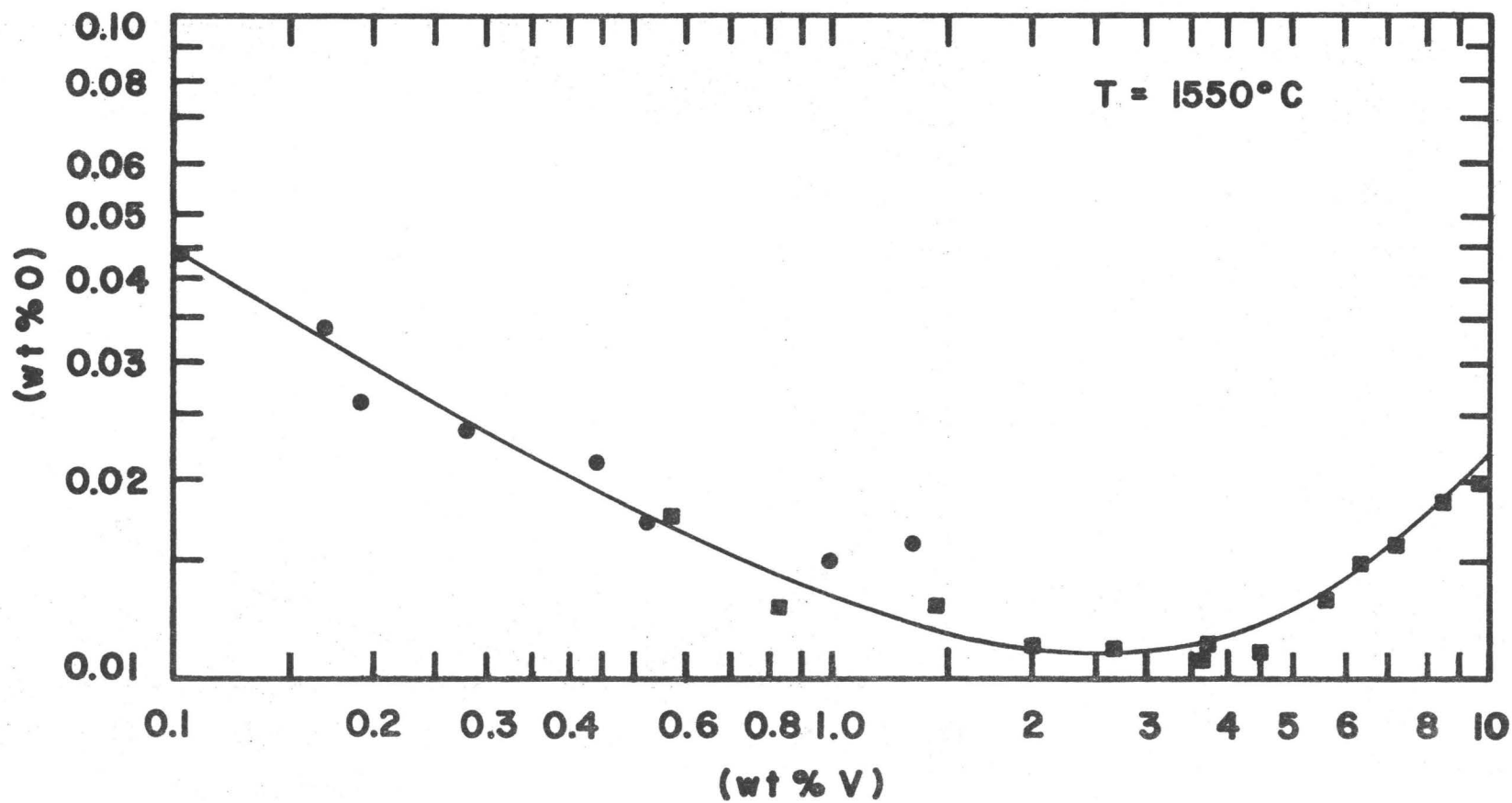
Fig. 5.37 Solubility of oxygen in the Fe-V-O melts. T = 1550°C
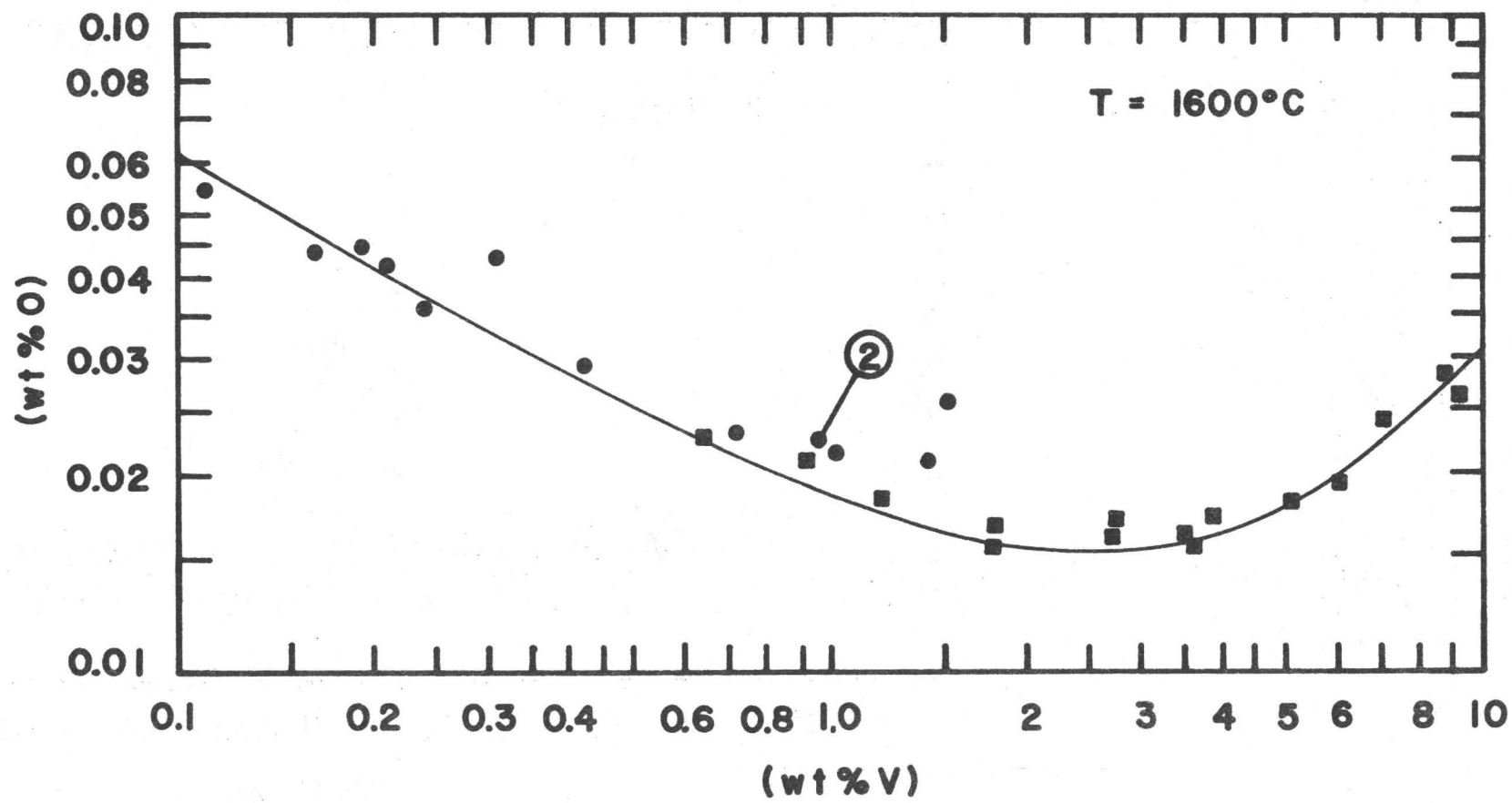
Fig. 5.38 Solubility of oxygen in the Fe-V-O melts. T = 1600°C
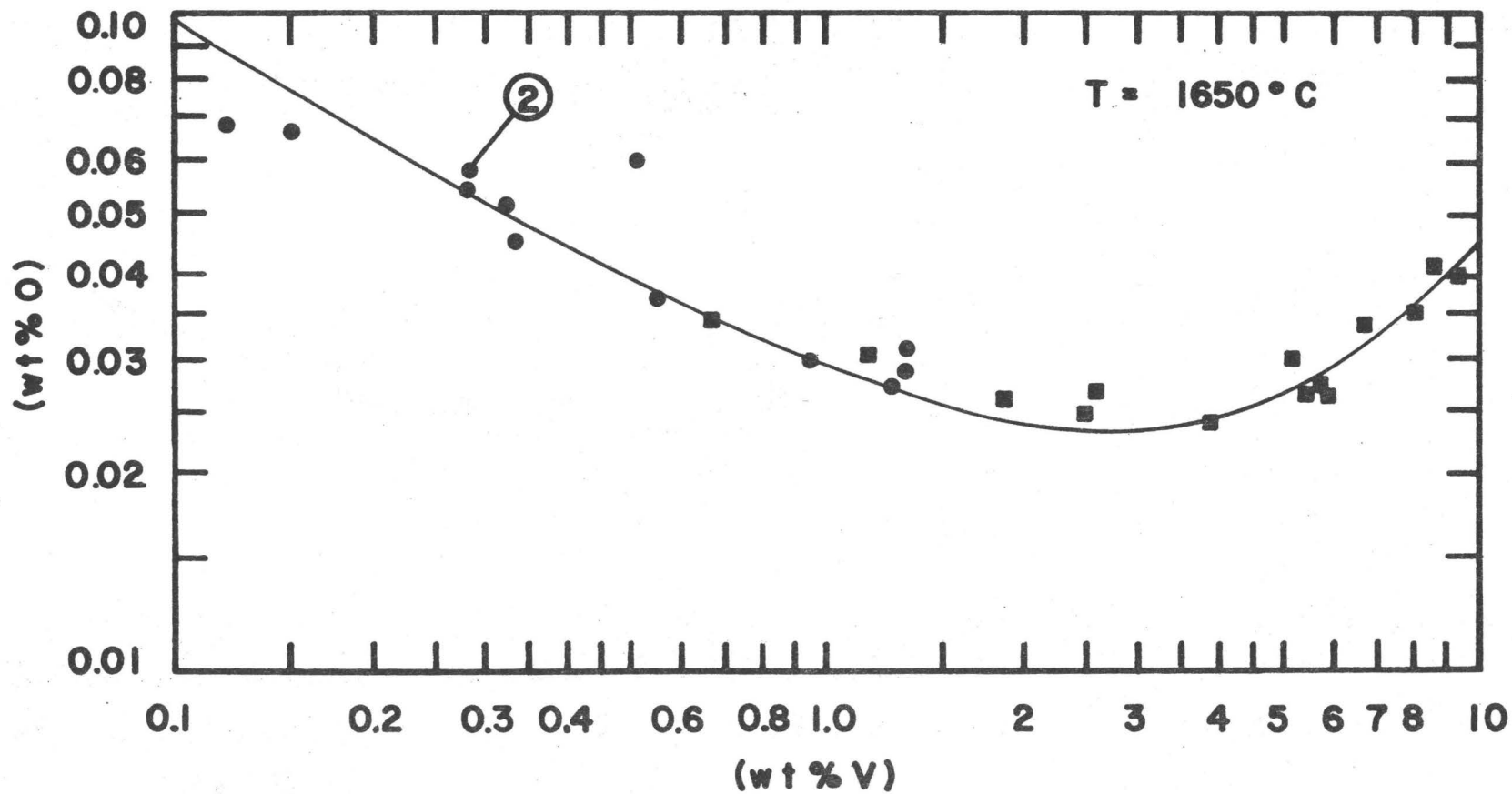
Fig. 5.39 Solubility of oxygen in the Fe-V-O melts. T = 1650°C
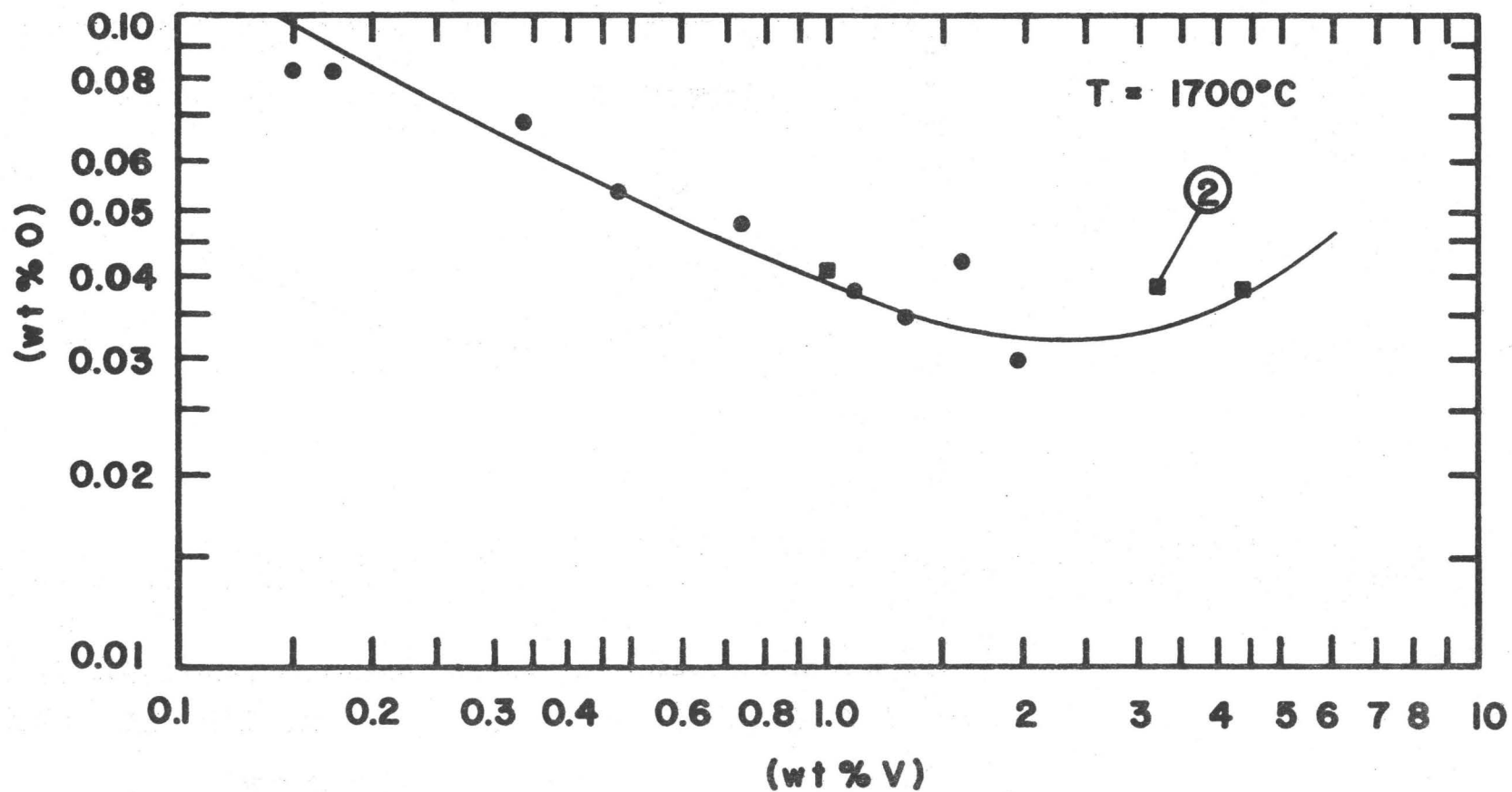
Fig. 5.40 Solubility of oxygen in the Fe-V-O melts. T = 1700°C
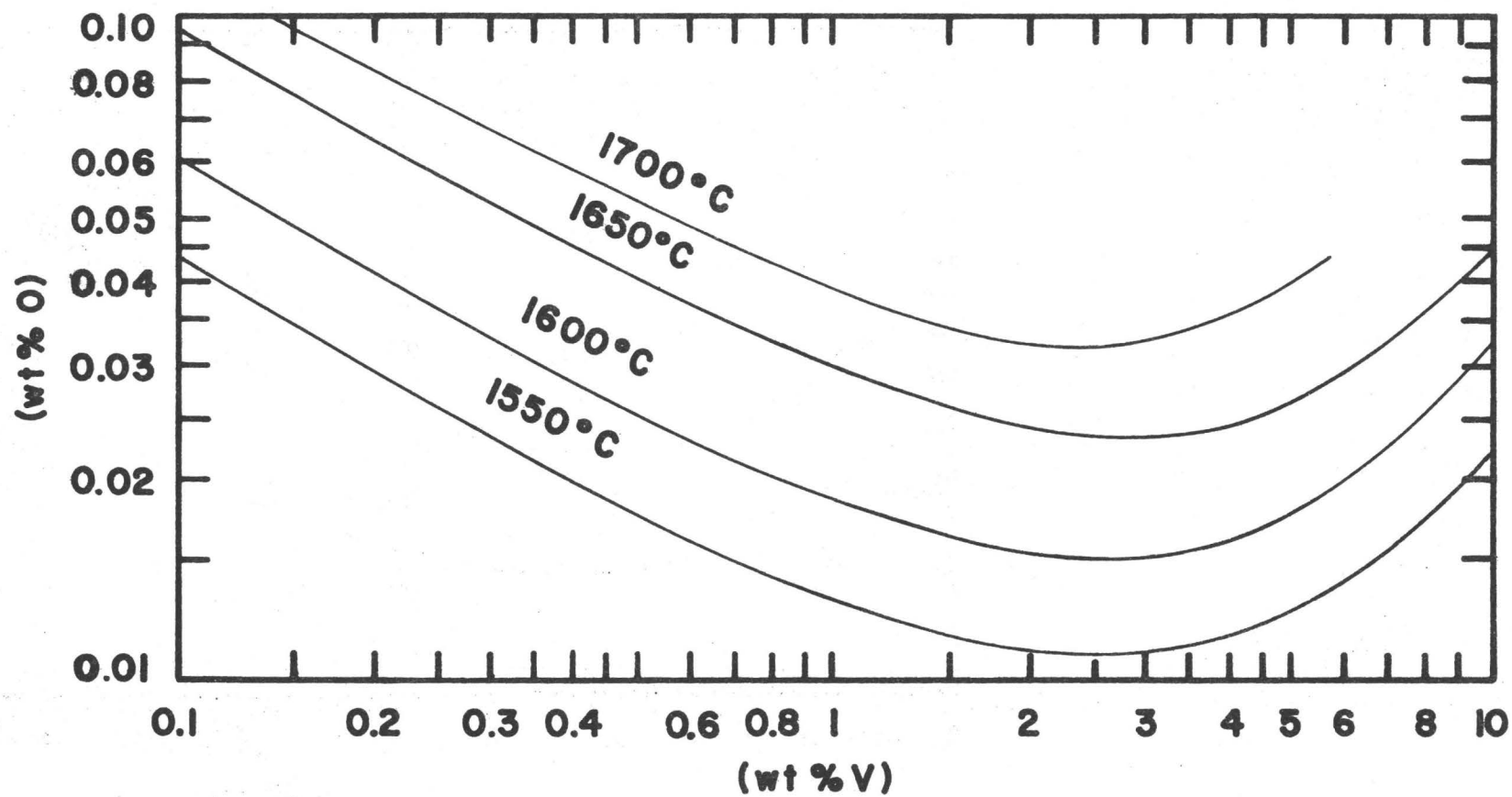
Fig. 5.41 Effect of temperature on the solubility of oxygen in Fe-V-O melts.

the formation of the iron-vanadium spinel can be derived:

$$Fe\,(l\,) + V_2O_3(s) + \underline{O} = FeV_2O_4(s) \tag{5.53}$$
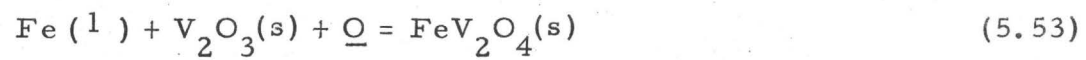
$$\Delta G^{\circ}_{5.53} = -21400 + 4.98\,T \text{ (cal)} \tag{5.54}$$

CHAPTER 6

DISCUSSION

6.1   THE SYSTEM Fe-O

There is quite a controversy in the literature about the behaviour of oxygen in liquid iron. Many investigators[21, 23, 25, 26] report that the self interaction parameter $e_o^{(o)}$ is negative, with values ranging from -0.20[23] to -0.47[25] at 1600°C. Other investigators on the other hand report that solutions of oxygen in liquid iron obey Henry's law, i.e. $e_o^{(o)} = 0$ [24, 42].

Schenck and Steinmetz[26] have calculated $\epsilon_o^{(o)}$ as -24.7 at 1600°C from the iron-oxygen phase diagram[41]. This value of $\epsilon_o^{(o)}$ corresponds to $e_o^{(o)} = -0.38$. They tried to verify this experimentally, but their results gave $e_o^{(o)} = -0.13$ at 1600°C and -0.32 at 1625°C. These two values are internally inconsistent, as the $e_o^{(o)}$ should decrease in absolute value with increasing temperature, approaching zero as the system comes closer to ideality. They attributed this inconsistency to experimental uncertainty, and accepted the value of $e_o^{(o)} = -0.20$[23] at 1600°C.

The largest deviation from Henry's law has been reported by Matoba and Kuwana[25], who give the temperature dependence of $e_o^{(o)}$ as

$$e_o^{(o)} = \frac{-10130}{T} + 4.94 \qquad (6.1)$$

This equation yields the following values for $e_o^{(o)}$:

$T, {}^{\circ}C$	$e_O^{(o)}$
1550	-0.62
1600	-0.47
1650	-0.33
1700	-0.19

The generally accepted and widely used value for $e_O^{(o)}$ is -0.20 at $1600^{\circ}C$, given by Floridis and Chipman[23].

On the other hand, Tankins, Gokcen and Belton[24] have extensively investigated the activity of oxygen in liquid iron, nickel and cobalt, and have found that solutions of oxygen in these metals obey Henry's law, i.e. that $e_O^{(o)} = 0$. The same has been reported by Larché[42].

The present study also failed to reveal a deviation from Henry's law, so it was assumed that $e_O^{(o)} = 0$. In order to investigate the effect of a value of $e_O^{(o)} = -0.20^{(23)}$ at $1600^{\circ}C$ on the equilibrium constant k_1 for the reaction

$$H_2(g) + \underline{O} = H_2O(g) \tag{6.2}$$
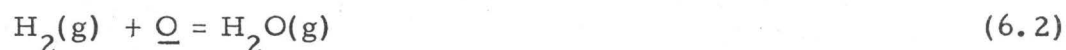
the data for $\log K_1$ at $1600^{\circ}C$ presented in Table 5.2 have been recalculated assuming $e_O^{(o)} = -0.20$ and are presented in Table 6.1.

TABLE 6.1

EFFECT OF A VALUE OF $e_o^{(o)} = -0.20$ ON THE
$\log k_1$ at $1600^\circ C$

| RUN | $e_o^{(o)} = 0$ | | $e_o^{(o)} = -0.20$ | |
	$h_o \times 10^4$	$\log k_1$	$h_o \times 10^4$	$\log k_1$
35	194	0.577	192	0.581
43	177	0.527	176	0.530
52	170	0.542	169	0.544
62	966	0.549	924	0.569
92	763	0.530	737	0.545
102	410	0.491	402	0.499
132	1065	0.546	1014	0.568
		Ave: 0.537		Ave: 0.548
		s = 0.026		s = 0.028

It is seen that the difference in the average value of $\log k_1$ at $1600^\circ C$ is small and it should be even smaller at higher temperatures.

In Fig. 6.1 the results of the present investigation for the reaction (6.2) are plotted as $\log k_1$ vs. $1/T$ together with the results of previous investigations. It is seen that the agreement is excellent with most previous workers.

6.2 EFFECT OF VANADIUM ON THE ACTIVITY COEFFICIENT OF OXYGEN IN LIQUID IRON

The effect of vanadium on the activity coefficient of oxygen in liquid iron has been studied by H_2O/H_2 equilibrium (§ 5.2.2.1) for V levels up to 2%, and with an oxygen probe (§ 5.3.2) for V levels up to
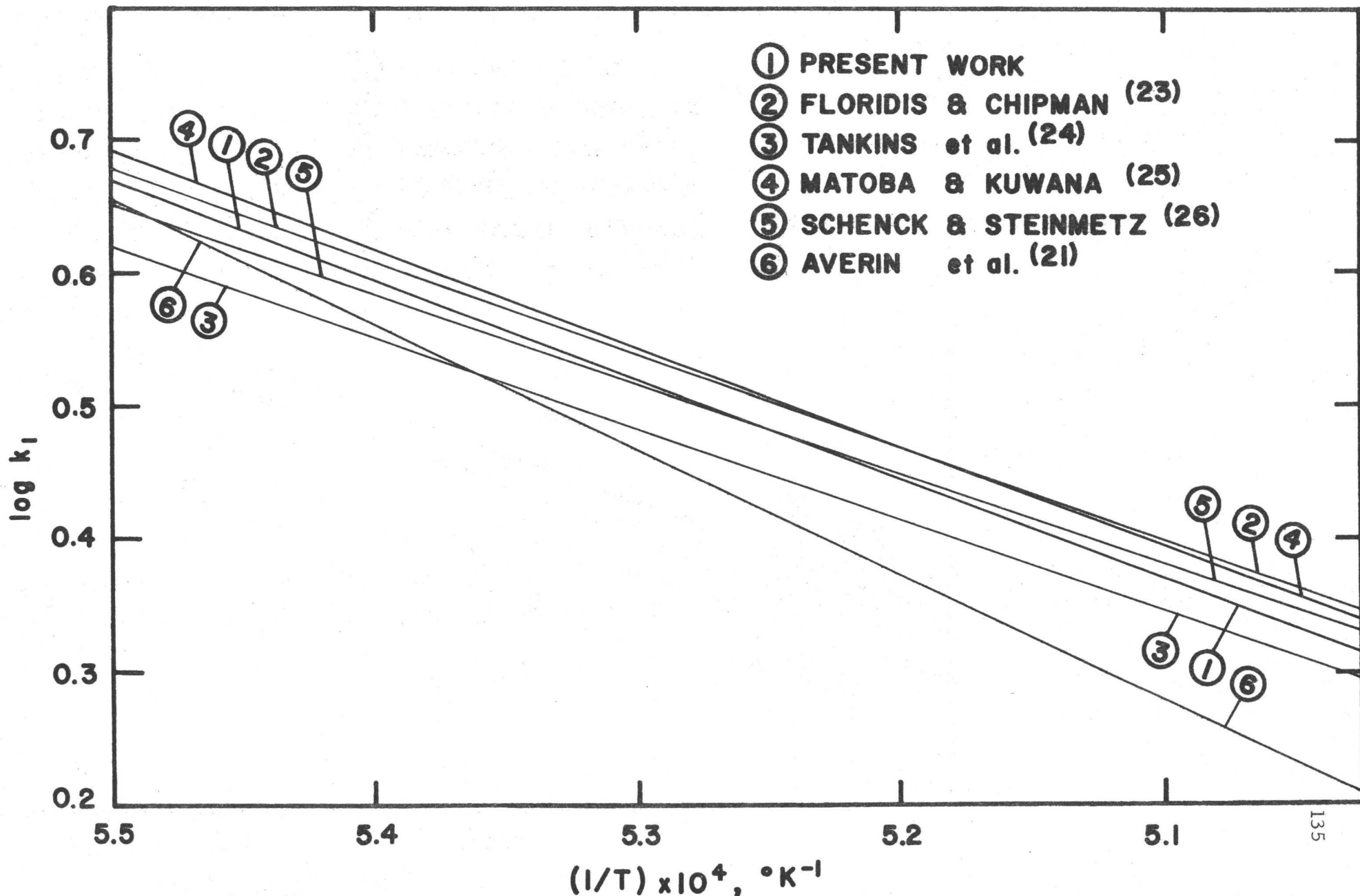
Fig. 6.1 Variation of log k_1 with temperature from various investigations.

12%. The 1st order free energy interaction parameters obtained by these methods are compared in Table 6.2.

<div align="center">

TABLE 6.2

COMPARISON OF THE 1st ORDER F.E. INTERACTION PARAMETERS
OBTAINED IN THE PRESENT WORK

</div>

T, $^{\circ}$C	$e_o^{(v)}$	
	H$_2$O/H$_2$ equil. 0 - 2% V	Oxygen Probe 0-12%V
1550	-0.208	-0.15
1600	-0.185	-0.14
1650	-0.166	-0.12
1700	-0.134	-

The agreement is judged good, in view of the different ranges investigated with the two methods; only 2 to 4 experimental points obtained with the oxygen probe are in the range investigated with H$_2$O/H$_2$. Another factor which may contribute to the difference is the uncertainty of the activity of oxygen in the reference electrode of the oxygen probe. As mentioned before, eqn. (3.32) used here gives activities of oxygen 12% higher than the equation used by Fruehan et al[55]. A lower activity of oxygen would lead to lower activity coefficient, and therefore a more negative value for the $e_o^{(v)}$.

The first order interaction parameters obtained with H$_2$O/H$_2$ equilibration in the range 0-2%V (Tables 5.8, 5.9) are considered to be more reliable, as they are based on a large number of experimental points within the above range. It is these values, or equation (5.24), that we recommend for use for vanadium contents less than 2%, which covers most commercial steels.

For V contents higher than 2%V, 1st and 2nd order interaction parameters should be used, as derived from the oxygen probe work (Tables 5.15 or eqn. (5.32)).

The first order free energy interaction parameters, based on a wt.% scale, obtained from the H_2O/H_2 equilibration are compared with previous investigators in Table 3.2.

It is difficult to comment on the large differences that exist between the various investigators.

The smallest values have been reported by Narita[29]. All his melts were saturated, i.e. equilibrium with an oxide was achieved. It is possible that oxides were present in his samples; analysis of these samples would give a higher oxygen content, resulting in a smaller activity coefficient, and therefore a more negative value for $e_o^{(v)}$. Also he quenched the samples in water, a fact that might have caused oxidation on the surface of the samples, which again would give rise to higher oxygen values if the samples were not cleaned carefully.

The value reported by Schenck and Steinmetz[32] is the result of a small number of experimental points.

No weight can be placed on Pargeter's[33] value in view of the tremendous scatter of his experimental points. He disregarded about half of them, and derived the value of $e_o^{(v)}$ from the rest.

Kershaw's[34] values were obtained using a levitation melting technique to equilibrate droplets of Fe or Fe-V with H_2O/H_2 gas mixtures. This technique is subject to heavy thermal diffusion errors, especially when used with gas mixtures of very different molecular weight[37] such as H_2O and H_2. Because of this error, his experimental values of $\log k_1$ for reaction (6.2) are approximately 30% higher than the generally accepted values[23]. He derived the interaction parameter $e_o^{(v)}$ by comparing results from the ternary Fe-V-O with results from the binary Fe-O, obtained under identical experimental conditions. It is claimed that thermal diffusion effects are cancelled in this way, and that correct

values of $e_o^{(v)}$ can be obtained. His results are in fair agreement with the present work.

The value reported by Chipman and Dastur[28] is the result of an expert determination. It should be noted however that Chipman himself has found earlier values of the interaction parameters determined in his laboratory to be in error. Such is the case with the parameter $e_o^{(Al)}$, determined in 1953 as -12 (Gokcen and Chipman[43]) and again in 1963 (d'Entremont, Guernsey and Chipman[44]) as -1.0, i.e. smaller by a factor of 10.

Fischer and Haussmann[31] used one of the early oxygen probes[46] with air as the reference electrode to determine the $e_o^{(v)}$. The optimum flow rate for the air in the reference electrode was sometimes too high, resulting in the inside wall of the electrolyte tube being cooler than the melt, therefore giving rise to a thermal EMF across the electrolyte, for which they applied a correction.

Fruehan[25] used an oxygen probe with Cr, Cr_2O_3 as the reference electrode, and determined the activity of oxygen at $1600^o C$ in Fe-V-O melts of up to 36%V. His results are in very good agreement with the probe results of the present work.

In Appendix I a theoretical calculation for the $\epsilon_o^{(v)}$ is presented according to various solution models. The results are compared with the experimental values in Table Al. All models predict smaller interaction parameters than the experimental values, as expected. (§ 2.4)

6.3 ACTIVITY OF VANADIUM IN LIQUID IRON

The only experimental determination of the activity of vanadium in liquid iron is the one by Fruehan[35] at $1600^o C$, who used a technique

identical with the one of the present investigation. He reported a value of γ_V^o = 0.10 at 1600°C relative to solid vanadium, as compared with γ_V^o = 0.31 obtained from the present work. It should be noted that Fruehan's experimental results are in very good agreement with ours; the difference in γ_V^o arises from the different values used for the standard free energy change for the reaction (5.33).

Myles and Aldred[70] determined the activity of Fe in solid Fe-V alloys at 1327°C using a torsion-effusion technique. From the activity of Fe they calculated the activity of V using the Gibbs-Duhem equation. They found the activity of V to exhibit a negative deviation from Raoult's law. The activity of vanadium (at 1327°C) determined by them at N_V = 0.1 is a_V = 0.0138, as compared with a_V = 0.034 determined by the present work at 1600°C.

6.4 DEOXIDATION OF LIQUID IRON WITH VANADIUM

According to the present investigation there are two deoxidation reactions occurring with vandium, depending on the vandium content of the melt. The products are FeV_2O_4 and V_2O_3 respectively. The same products have been identified by Chipman and Dastur[28] and Narita[29, 30]. Karasev et al.[36] in addition to the above mentioned products reported V_2O_2 at vanadium levels higher than 0.3%. As mentioned in § 3.3 they did not identify the V_2O_2 by X-ray techniques. They assumed that it forms because on plotting their experimental results as $\log (P_{H_2O}/P_{H_2})$ vs. $\log (\%V)$ they observed that at vanadium concentrations higher than 0.3% the experimental slope was very close to -1, which would require VO or V_2O_2 to be the reaction product.

In the present work the V_2O_2 (or VO) was not identified in any melt, and the slope of the lines for vanadium concentrations higher than the ones for which FeV_2O_4 is the reaction product in Fig. 5.31 — 5.34 lies very close to -2/3. It can safely be concluded therefore that V_2O_3

is the only deoxidation product, apart from FeV_2O_4, for V concentrations up to 12%.

In Table 3.3 the previous investigations are compared with the present work. Our results are in good agreement with Chipman and Dastur[28] and Narita[29], and in poor agreement with Karasev et al[36].

The concentration of vandium for which the change from one deoxidation product to another takes place are compared in Table 6.3.

TABLE 6.3

CONCENTRATIONS OF V(wt. %) CORRESPONDING TO A CHANGE IN THE DEOXIDATION PRODUCT

T, °C	$FeV_2O_4 \rightarrow V_2O_3$				$V_2O_3 \rightarrow V_2O_2$
	Chipman and Dastur[28]	Karasev et al[36]	Narita (29, (30)	Present Work	Karasev et al[36]
1550		0.2		0.20	0.3
1600	0.17	0.2	0.15	0.30	0.3
1650		0.2	0.35	0.48	0.3
1700		0.2	0.55	0.75	0.3

In the deoxidation diagrams presented in Fig. 5.37 - 5.40 it is seen that a minimumof the oxygen content of the melt occurs at a certain vanadium content. This minimum at 1600°C is around 160 ppm oxygen for vanadium content betwen 2 and 3%. This is in excellent agreement with Fruehan[35] who observed a minimum of 170-180 ppm oxygen around 3%V.

St. Pierre and Blackburn[71] have discussed the relationship between first order interactions and oxide solubilities in liquid iron. Assuming that the activity coefficients are adequately described by first

order interaction parameters, they derived an equation to predict the atom fraction N_x^* of a deoxidizing element X in liquid Fe-O-X alloys for which a minimum in the oxygen content occurs. If $\epsilon_o^{(x)} \ll o$, which is the case for the present system, they have shown that

$$N_x^* = - \frac{r}{\epsilon_o^{(x)}} \tag{6.3}$$

where r is the ratio of metal to oxygen in the oxide $X_a O_b$ and $\epsilon_o^{(x)}$ is the first order free energy interaction parameter.

In the case of V_2O_3, using the value of $\epsilon_o^{(v)} = -38.6$ at $1600^{\circ}C$ (Table 5.8) and $r = 2/3$, eqn. (6.3) gives $N_v^* = 0.0173$ which corresponds to 1.6%V, in good agreement with the experimental value.

CHAPTER 7

CONCLUDING REMARKS

The thermodynamics of iron-oxygen and iron-vanadium-oxygen alloys have been studied in the temperature range 1550-1700°C, using H_2O/H_2 equilibration or an oxygen probe.

The effect of vanadium on the activity coefficient of oxygen is described by the equation

$$\log f_O^{(v)} = (- \frac{1730}{T} + 0.74) \text{ x } (\%V) \tag{7.1}$$

for vanadium concentrations of up to 2%, and by the equation

$$\log f_O^{(v)} = (- \frac{1050}{T} + 0.42) \text{ x } (\%V) + (\frac{38.27}{T} - 0.017) \text{ x } (\%V)^2 \tag{7.2}$$

for vanadium concentrations between 2-12%.

Solutions of vanadium in liquid iron were found to obey Henry's law for concentrations up to 12%. The Raoultian activity coefficient of vanadium at infinite dilution, γ_V^o, was found to be 0.31 in the temperature range investigated.

The deoxidation reactions occurring in the Fe-V-O system are described by the following equations:

$$\text{Fe (1)} + 2 \underline{V} + 4 \underline{O} = \text{Fe } V_2O_4(s) \tag{7.3}$$

and

$$2 \underline{V} + 3 \underline{O} = V_2O_3(s) \tag{7.4}$$

142

The free energy changes for the above reactions are:

$$\Delta G^o_{7.3} = -220900 + 85.55\,T \text{ (cal)} \qquad (7.5)$$

and

$$\Delta G^o_{7.4} = -198550 + 80.57\,T \text{ (cal)} \qquad (7.6)$$

Deoxidation diagrams are presented at 1550, 1600, 1650 and 1700°C. The solubility of oxygen in Fe-V-O melts decreases with increasing vanadium content to a minimum (110, 160, 250 and 320 ppm oxygen at 1550, 1600, 1650 and 1700°C respectively) at around 2.5%V and then increases.

PART II

THERMODYNAMIC EQUILIBRIUM IN THE SYSTEMS $V-VO_{0.2\pm x}$,
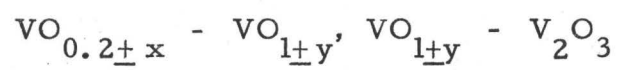
$$VO_{0.2\pm x} - VO_{1\pm y}, \quad VO_{1\pm y} - V_2O_3$$

INTRODUCTION

This part is dealing with the thermodynamic equilibrium in the systems $V-VO_{0.2\pm x}$, $VO_{0.2\pm x} - VO_{1\pm y}$, and $VO_{1\pm y} - V_2O_3$.

A literature survey of the V-O system is presented. The solid state EMF method for measuring thermodynamic equilibria is reviewed. The experimental apparatus and technique are described and the experimental results presented and discussed. The free energies of formation of $VO_{0.2}$, VO and V_2O_3 are derived and compared with existing calorimetric data.

CHAPTER 8

REVIEW OF THE VANADIUM-OXYGEN SYSTEM

8.1   INTRODUCTION

The vanadium-oxygen system is a very complicated one in that a large number of oxides, most of them with a wide range of nonstoichiometry, have been reported.   There are many discrepancies in the literature on the existence, nonstoichiometric ranges and thermodynamic properties of the oxides, and on the phase diagram of the system.

An incomplete phase diagram has been presented by Rostoker and Yamamoto[72].   Stringer[73] published a critical literature review and presented a more or less correct phase diagram based on this review.   He also proposed a nomenclature for the phases, which we will be using here.

In the following, a review of the phase diagram from metallic vandium up to the V_2O_3 will be presented, and of the thermodynamic properties of the oxides involved.

8.2   STABILITY RANGES AND STRUCTURE OF THE OXIDE PHASES
8.2.1   The Primary Vanadium-Oxygen Solid Solution (α-Phase)

Oxygen is soluble to some extent in vandium.   Allen, Kubaschewski and von Goldbeck[74] reported a solubility of approximately 0.8 at. % (0.25 wt. %) at 1000°C.   Seybolt and Sumsion[75] reported a solubility limit of 3.2 at. % (1 wt. %) of oxygen at 1400°C.   Rostoker and Yamamoto[72] report that the solubility diminishes from about 3.2 at. % (1 wt. %) at 1600°C to less than 0.8 at. % (0.25 wt. %) at 900°C, in good agreement with the previous determinations.

Oxygen enters the BCC vanadium lattice interstitially, producing

a slight lattice expansion. The lattice parameter of the α-phase as a function of the oxygen content is given in Fig. 8.1.

8.2.2   The β-Phase $(VO_{0.2 + x})$

Seybolt and Sumsion[75] reported that when the concentration of oxygen exceeds 3 at. % a new phase appears, which is a BC tetragonal deformation of the BCC vanadium. According to them the stability range of this phase is from 14 at. % (5 wt. %) to 25 at. % (9. 5 wt. %) at 1100°C, and the variation with temperature is not great. However, Rostoker and Yamamoto[72] reported that the lattice parameters varied smoothly throughout the range 6.1 at. % (2 wt. %) to 26. 6 at. % (10. 3 wt. %), suggesting that the homogeneity range is much larger.

The lattice parameter data as reported in these two investigations are presented in Fig. 8.2. Fig. 8.3 shows the structure of the β-phase according to Seybolt and Sumsion[75].

8.2.3   The γ-Phase

Rostoker and Yamamoto[72] reported that alloys containing close to 35 at. % (15 wt. %) oxygen consist of β + VO above 1200°C, but below 1100°C they give microstructural evidence of a peritectoid reaction, producing a new phase. They did not consider the evidence sufficient to attach the formula V_2O to the compound. Its structure was not determined, but the powder pattern, as obtained after substracting the lines corresponding to the β and VO, was tentatively indexed as hexagonal. Westman and Nordmark[76] reported a phase of composition $VO_{0.53}$ and suggested that it has an extremely narrow homogeneity range.

The γ-phase is apparently formed by a sluggish peritectoid reaction below 1100°C[72] and it is very easy to miss.

Fig. 8.1
Lattice parameters in the
α-phase (from[73])

Fig. 8.2
Lattice parameters in the
β-phase (from[73])

Fig. 8.3
The structure of the β-phase
(from[75])
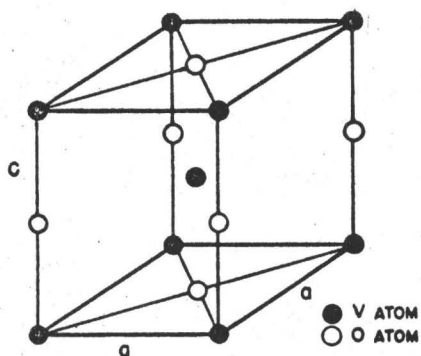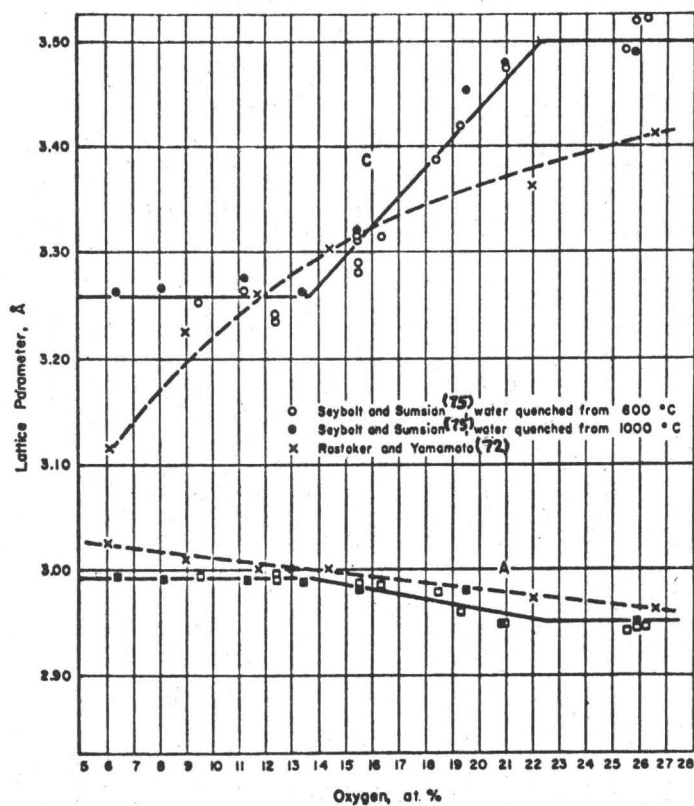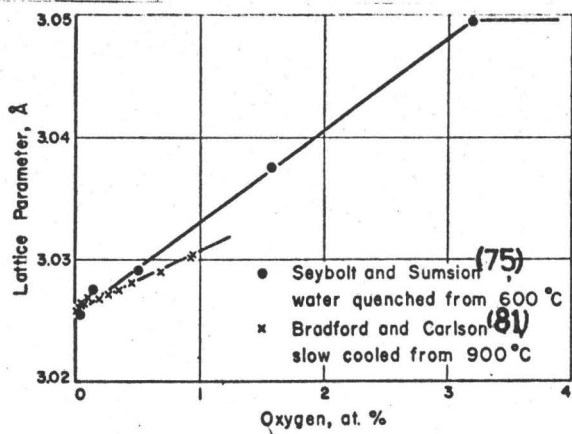
8.2.4   Vanadium Monoxide (δ-Phase)

Vanadium monoxide (VO) has a sodium chloride structure, and is stable over a wide range of compositions. Departures from stoichiometry are accommodated by defects on either the anion or the cation lattice.

Schonberg[77] and Andersson[78] reported that VO is stable between the limits $VO_{0.80}$ to $VO_{1.30}$ at high temperatures, breaking down to the β-phase and an unknown phase (x-phase) at lower temperature. Vol'f et al[79] also reported two low temperature oxides:

       Oxide I $VO_{0.86}$ - $VO_{1.047}$ $4.024 \leq a \leq 4.071 \,\overset{\circ}{A}$

       Oxide II $VO_{1.057}$ - $VO_{1.27}$ $4.082 \leq a \leq 4.134 \,\overset{\circ}{A}$
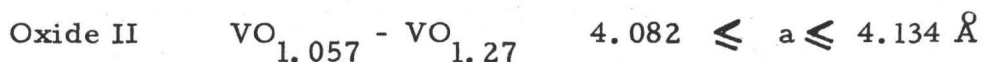
Gel'd et al[80] re-examined this field and reported only one oxide, VO, between $VO_{0.85}$ and $VO_{1.23}$.

According to Westman and Nordmark[76] the limits of the δ phase are $VO_{0.87}$ to $VO_{1.20}$.

The lattice parameter relationships for the δ phase from the various investigators are given in Fig. 8.4.

8.2.5   The ϵ-Phase

Westman and Nordmark[76] found a low temperature phase with body-centered tetragonal structure with a very narrow homogeneity range at $VO_{1.27}$. This is probably the x-phase reported by Schonberg[77] and Andersson[78].

8.2.6   Vanadium Trioxide (ζ - Phase)

Vanadium trioxide has a rhombohedral structure similar to that of corundum, a-Al_2O_3. Gel'd et al[80] suggested that it has a narrow homogeneity range, since second phases were detected in alloys of compositions $VO_{1.44}$ and $VO_{1.65}$.
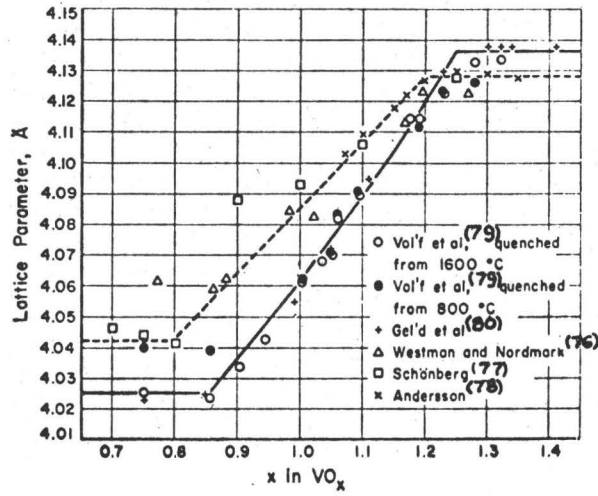
Fig. 8.4 Lattice parameters in the δ phase ('VO') (from[73]).
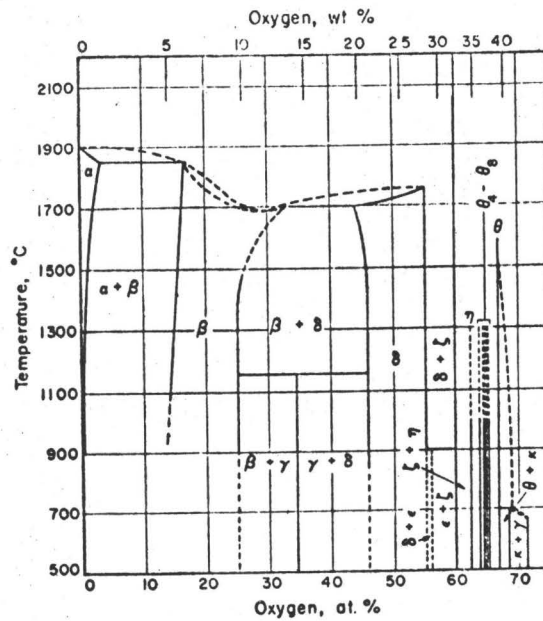
Fig. 8.5 The vanadium-oxygen phase diagram (from[73]).

TABLE 8.1

LOWER OXIDE PHASES IN THE SYSTEM V-O

Oxide Phase	Stability Range	Structure	Lattice Parameters $\overset{\circ}{A}$	Ref.
α	$VO_{0.00} - VO_{0.01}$	b.c.c	a = 3.025 to a = 3.049 $\overset{\circ}{A}$	75
β	$VO_{0.17} - VO_{0.35}$	b.c. tet.	a = 2.992, c = 3.263 to a = 2.943, c = 3.523	75
γ	$VO_{0.53}$	hexagonal ?	-	
δ	$VO_{0.85} - VO_{1.25}$	NaCl	a = 4.024 to a = 4.138	80
ϵ	$VO_{1.27}$	b.c. tet.	a = 16.623, c = 16.515	76
ζ	V_2O_3	$a-Al_2O_3$ (rombohedral)	a = 4.952, c = 14.002	82

8.2.7　The V-O Phase Diagram

Table 8.1 presents the oxide phases whose existence seem likely on the basis of the literature, together with their stability ranges, structures, and lattice parameters.　The reference quoted refers to the lattice parameter values.

Fig. 8.5 presents the most probable phase diagram for the system.　This diagram is essentially that of Rostoker and Yamamoto[72], slightly modified to take account of more recent data.

8.3　THERMODYNAMIC PROPERTIES OF VANADIUM OXIDES

Heats of formation of VO and V_2O_3 have been reported by Brewer[83], Allen et al[74], Rossini et al[84], Vol'f and Ariya[85] and Mah and Kelley[86].　The results of these investigations are summarized in Table 8.2.

TABLE 8.2

HEATS OF FORMATION OF V OXIDES AT 298.15°K

kcal/mole

Oxide	Brewer[83]	Allen et al[74]	Rossini et al[84]	Vol'f et al[85]	Mah et al[86]
VO	-98 $\pm$ 5	-105.5 $\pm$ 5	-100	-102 $\pm$ 1	-103.2 $\pm$ 0.3
V_2O_3	-296.1 $\pm$ 6	-299.4 $\pm$ 7	-290	-300 $\pm$ 4	-291.3 $\pm$ 0.4
VO_2	-171.0 $\pm$ 2	-175.0 $\pm$ 4	-172	-	-170.6 $\pm$ 0.2
V_2O_5	-372.5 $\pm$ 5	-380.6 $\pm$ 8.5	-373	-376 $\pm$ 2	-370.6 $\pm$ 0.5

Mah and Kelley[86] have combined the heats of formation obtained from their work with existing entropy[63] and high temperature heat content[64] data to obtain heats and free energies of formation at temperatures to 2000°K, which they tabulated.

Allen et al.[74] have determined the free energy relationships in the primary solid solution (a-phase).　They report that the partial molar free

energy of oxygen at 1000°C decreases from an extrapolated value of 330 kcal/mole O_2 for pure V to 160 kcal/mole O_2 at the solubility limit.

There appears to be no information in the literature on the thermodynamic properties of the β-phase, $VO_{0.2 \pm x}$.

Kobayashi[87] in 1933 made the only direct high temperature measurements involving the lower oxides of vanadium, VO and V_2O_3, by equilibrating a solid phase consisting initially of pure V (97% V) with H_2-H_2O atmospheres, and observing the changes in colour of the solid. The changes from "metallic" (V) to "gray" (VO) to "black" (V_2O_3) and vice versa were ascribed to the two reactions:

$$V_2O_3(s) + H_2(g) = 2VO(s) + H_2O(g) \tag{8.1}$$

$$VO(s) + H_2(g) = V(s) + H_2O(g) \tag{8.2}$$
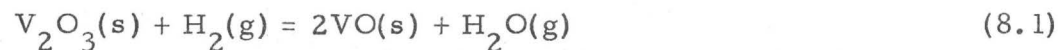
although he did not confirm this by chemical or x-ray analysis.

Kobayashi's results give the free energies of the above reactions as:

$$\Delta G^\circ_{8.1} = 29600 - 8.0\,T \quad 823 - 1385^\circ K \tag{8.3}$$

and

$$\Delta G_{8.2} = 56400 - 14.38T \quad 1325 - 1670^\circ K \tag{8.4}$$

Allen et al[74] slightly corrected eqns. (8.3) and (8.4), combined them with the free energy of formation of H_2O and gave the following free energy changes for the corresponding reactions:

$$2\,V_2O_3(s) = 4VO(s) + O_2(g) \tag{8.5}$$

$$\Delta G^\circ_{8.5} = 175,300 - 40.5T; \quad 823 - 1385^\circ K \tag{8.6}$$

and

$$2VO(s) = 2V(s) + O_2(g) \tag{8.7}$$

$$\Delta G^\circ_{8.7} = 205,900 - 35.9T; \quad 900 - 1800^\circ K \tag{8.8}$$

CHAPTER 9

THEORETICAL AND EXPERIMENTAL CONSIDERATIONS

9.1   INTRODUCTION

The method chosen to study the thermodynamic equilibrium between the lower oxides of vanadium is a high temperature EMF technique.

It has long been recognized that galvanic cells incorporation solid electrolytes possess many advantages for the measurement of high temperature thermodynamic properties. During the past decade advances in solid state EMF techniques have been primarily based on solid oxide electrolytes, introduced by Kiukkola and Wagner[88, 89] in 1957. Many papers appeared in the literature describing successful applications of oxygen concentration cells to measure thermodynamic properties of oxide systems.

In the following, the principle and limitations of the oxygen concentration cells will be described.

9.2   THE OXYGEN CONCENTRATION CELL

The oxygen concentration electrochemical cell consists of two electrodes I and II with oxygen chemical potentials μ_I and μ_{II} respectively, separated by a solid oxide electrolyte which conducts essentially via oxygen ions:

$$\text{Pt} \left| \mu_I(O_2) \right| \text{Solid oxide electrolyte} \left| \mu_{II}(O_2) \right| \text{Pt} \qquad (9.1)$$

At elevated temperatures ($>500^\circ$C) this cell is the source of an electromotive force E which is given by the expression[88]

$$E = \frac{1}{4F} \int_{\mu_{I}(O_2)}^{\mu_{II}(O_2)} t_i \; d\mu_{O_2} \tag{9.2}$$

where:

   E   the EMF in Volts

   F   the Faraday constant (23066 cal. volt^{-1} equiv^{-1})

   t_i the ionic transport number of the electrolyte:

$$t_i = \frac{\sigma_i}{\sigma_T} \tag{9.3}$$

σ_i and σ_T being the ionic and the total conductivity respectively.

The total conductivity of the electrolyte can be represented as the sum of the ionic and electronic conductivity, the latter being the sum of the conductivity due to electrons (or n-semiconductivity, σ_-) and to electron holes (or p-semiconductivity, σ_+):

$$\sigma_T = \sigma_i + \sigma_e = \sigma_i + \sigma_- + \sigma_+ \tag{9.4}$$

Following Mitoff[90] we can represent the oxygen concentration cell (9.1) with an electrical equivalent, as shown on Fig. 9.1.
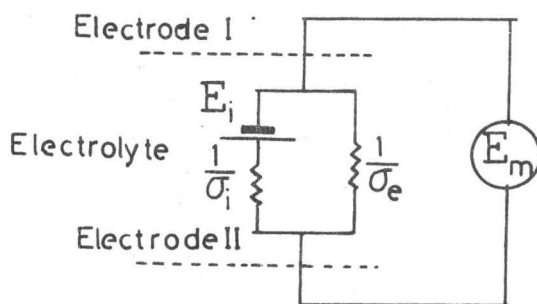
Fig. 9.1 Electrical Equivalent of the Oxygen Concentration Cell.

In this figure E_m is the measured EMF, E_i is the potential of purely ionic origin, and σ_i, σ_e represent the ionic and electronic conductivity of the electrolyte.

Application of the Kirchoff's equation leads to the following equations:

$$E_m = \frac{E_i \, \sigma_i}{\sigma_i + \sigma_e} \tag{9.4}$$

$$t_i = \frac{E_m}{E_i} \tag{9.5}$$

If the electrolyte conducts mainly with ions ($\sigma_e \ll \sigma_i$), $E_m = E_i$ and $t_i = 1$.

If the electrolyte conducts mainly with electrons ($\sigma_i \ll \sigma_e$), $E_m = 0$.

If there is a large concentration of ionic vacancies in the electrolyte, fixed by the composition, then the ionic contribution to the total conductivity of the electrolyte will not be a function of the partial pressure of oxygen around the electrolyte. On the other hand, the electronic contribution to the conductivity depends on the P_{O_2}: in general, the electron conduction will increase with decreasing P_{O_2} and the electron hole conduction will increase with increasing P_{O_2}[88]. It follows that the total conductivity is related to the oxygen partial pressure by the equation[57]

$$\sigma_T = \sigma_i + k_1 \, P_{O_2}^{1/n} + k_2 \, P_{O_2}^{-1/m} \tag{9.6}$$

The variation of the total conductivity with P_{O_2} is shown schematically in Fig. 9.2. At high P_{O_2} (section AB) positive hole conduction predominates, while at low P_{O_2} (section CD) electronic conduction predominates. The horizontal region BC is the range of P_{O_2} for which t_i is virtually unity.
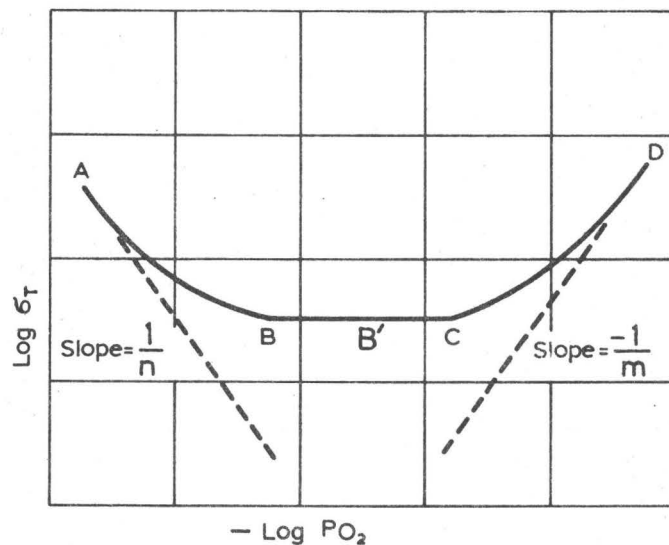
Fig. 9.2 Variation of electrical conductivity of oxides with oxygen partial pressure, at constant temperature .

Fig. 9.3 Estimates by Steele and Alcock[57] of range of oxygen partial pressure over which t_{ion} = 0.99 at $1000^{o}C$ for a number of oxide solid solutions.

Variations of this plot occur with many systems:[57]

(a) MgO, CaO, SrO_2, Al_2O_3, ZrO_2, HfO_2, ThO_2 show only a minimum without the horizontal portion BC.

(b) Solid solutions based on zirconia show only the portion B'CD, i.e. ionic conduction with increasing n-type conduction at low P_{O_2}.

(c) Thoria based solid solutions show a behaviour described by the section ABB', i.e. positive hole conduction at high P_{O_2}, followed by a range over which t_i is virtually unity.

It is evident that in order to measure thermodynamic properties of oxides, the solid electrolyte used must be essentially anionic conductor ($t_i = 1$). Then eqn. (9.2) gives

$$E = \frac{RT}{4F} \ln\left[\frac{P_{O_2}^{I}}{P_{O_2}^{II}}\right] \qquad (9.7)$$

$P_{O_2}^{I}$ and $P_{O_2}^{II}$ being the partial pressures of oxygen of electrodes I and II. Steele and Alcock[57] have estimated the ranges of P_{O_2} for which the ionic transport number is greater than 0.99 at $1000^{\circ}C$ for many solid oxide electrolytes. Their estimate is given in Fig. 9.3. As mentioned in § 3.4.1 some investigators [58, 59] have successfully used $ZrO_2(CaO)$ electrolytes down to a P_{O_2} of 10^{-22} atm at $1000^{\circ}C$, implying that ZrO_2 based electrolytes are essentially anionic conductors at partial pressures of oxygen lower than the ones shown in Fig. 9.3.

9.3 CRITERIA FOR APPLICABILITY OF OXYGEN CONC.CELLS

From consideration of previous experimental work and difficulties encountered, one can establish the necessary criteria for the successful operation of a high temperature galvanic cell using solid electrolytes:

(a) The galvanic cell must be reversible in establishing local equilibrium of the electrode-electrolyte interface.

(b)   There must be no difference in composition between the electrode interface and the bulk of the electrode material.

(c)   No reaction other than the one described by the cell reaction should take place: there must be no reaction between electrolyte and electrodes, or electrodes and cell atmosphere.

(d)   The electronic transport number of the electrolyte must be very small. It is impossible to assign a realistic upper limit to t_e which can be tolerated. A value of $t_e = 0.01$ would not have a great effect in lowering the EMF of the cell, according to eqn. 9.2 but could cause "polarization" problems in some systems, as discussed in § 9.4.

(e)   Thermal emf and contact potentials must be negligible.

9.4   THE POLARISATION PROBLEM

The polarisation problem is probably the major source of error in experimental work with solid electrolytes, and has been adequately discussed by Steele[92]. It is caused by internal 'short circuiting' of the cell due to the small electronic conductivity of the electrolyte, which allows oxygen to be transferred within the electrolyte from one electrode to the other in the direction imposed by the oxygen chemical potential gradient i.e. from the cathode (positive terminal) to the anode (negative terminal). This flux of oxygen may disturb the oxygen chemical potential established at the anode-electrolyte interface, unless the relevant chemical reactions are sufficiently rapid. If the equilibrium is disturbed the electrode system may readjust to a different steady state condition corresponding to an undefined higher oxygen chemical potential and the cell EMF will be reduced accordingly[57].

9.5   LOCAL THERMODYNAMIC EQUILIBRIUM

The relationships derived between the EMF and the associated

oxygen potentials of the electrodes require local thermodynamic equilibrium to be maintained at the relevant phase boundaries. It is therefore necessary to ensure that the galvanic cell is behaving reversibly[92]; this is done by passing a small current through the cell in either direction and noting whether the observed voltage returns to the original value recorded before the cell equilibrium was disturbed.

Steele[92] has discussed the reversibility of several electrode systems. As far as metal-metal oxide systems are concerned, the reversibility properties are variable. The Fe-FeO system exhibits a high degree of reversibility, while Nb-NbO and Cr-Cr$_2$O$_3$ electrodes often display irreversible behaviour in the absence of any special precautions such as using electrolyte materials of high resistance.

9.6   APPARATUS AND CELL ASSEMBLY

The cell can be operated either under vacuum or under an inert gas atmosphere. It is particularly important of course that the gas must be adequately purified. "Getters", consisting of Ti or Zr foil should be placed around the galvanic cell to remove adsorbed gases released at high temperatures and to react with gases permeating through the furnace tube.

The simple cell assembly used by Kiukkola and Wagner[89] was found to be adequate for investigations involving electrode systems whose difference in oxygen chemical potential is not large. It has been suggested[57, 92] that when the two metal-metal oxide electrodes have very different oxygen potentials, separate compartments should be employed for the two electrodes to prevent the gas surrounding one electrode to come into contact with the other electrode, and to promote local equilibrium with the gaseous environment.

Typical developments in cell designs are illustrated in Fig. 9.4-9.5.

(a)

Electrode(1)
Pt
Electrolyte(2)
Pt
oxide electrolyte

INITIAL CELL ARRANGEMENT
(cf. Kiukkola and Wagner)

(b)

Electrode(1)
Electrode(2)
oxide electrolyte

SCHMALZRIED

Electrode(1)
Electrode(2)
oxide electrolyte

Benz and Schmalzried
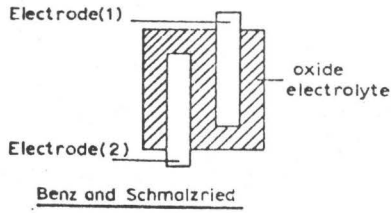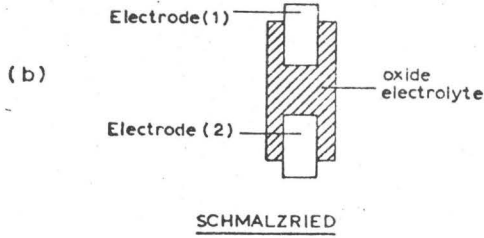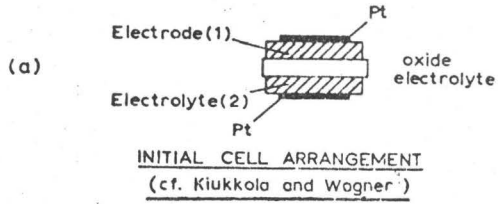
Fig.9.4 Cells without separate electrode compartments (From[92])

alumina
Electrode(1)
Thoria based electrolyte
Stabilised zirconia tube
Electrode(2)

Pt foil
Zirconium or Titanium strip

(a)　　　(b)

alumina
Electrode(1)
Protective collar electrode 1 material
Oxide electrolyte
Electrode(2)
small pieces of electrode 2 material
alumina
Pt foil
Zirconium or Titanium strip

(c)　　　(d)
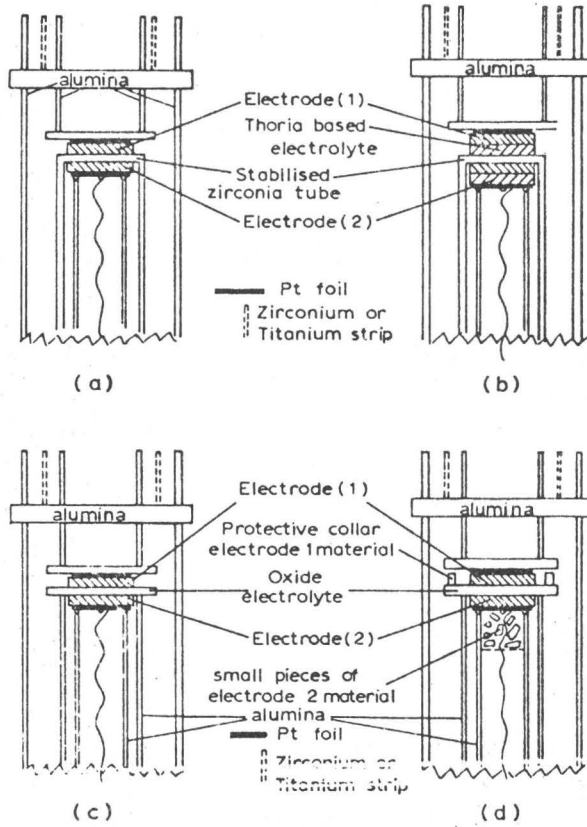
Fig.9.5 Cells with separate electrode compartments (From[92])

CHAPTER 10

EXPERIMENTAL

10.1   INTRODUCTION

The systems to be investigated were anticipated to have an equilibrium P_{O_2} lower than 10^{-25} atm at $1000^{\circ}C$. No measurements have been reported at such low partial pressures of oxygen. It was hoped that thoria-yttria solid solutions would exhibit mainly anionic conductivity under these conditions.

In the following, the preparation of the electrolytes and electrodes will be described, as well as the experimental set up and procedure followed.

10.2   PREPARATION OF THE ELECTROLYTES

The ThO_2-Y_2O_3 solid solutions used as electrolytes were prepared as described by Zador[93]. Two compositions were employed: ThO_2 + 5 mole pct Y_2O_3 and ThO_2 + 10 mole pct Y_2O_3.

The starting materials were thorium nitrate ($Th(NO_3)_4 \cdot 4H_2O$) and yttrium nitrate ($Y(NO_3)_3 \cdot 6H_2O$), supplied from Alfa Inorganics. In a preliminary investigation the H_2O content of these materials was measured by decomposing them to the corresponding oxides by slow heating up to $900^{\circ}C$.

An aqueous solution of thorium and yttrium nitrates of the appropriate mole ratio was prepared to contain 11 wt.% of their oxides, and the pH of this solution was adjusted to 1.7 - 1.8 by adding dil. NH_4OH. A 5 wt.% ammonium oxalate solution in water was also prepared, and its pH adjusted to 3.0 by adding dil. HNO_3. The nitrate solution was added to the oxalate

at room temperature with vigourous stirring, and the pH was then re-adjusted to 2.0. The thorium and yttrium oxalate precipitate thus formed was allowed to settle overnight. It was then filtered, dried, and ignited to $900^{\circ}C$ in air in a Pt crucible to give the oxide solid solution. The oxide was ground, fired again in air at $1200^{\circ}C$, and ground again. It was then pressed into pellets 3/8" dia and 1/8" thick, in a hardened tool steel die by applying a pressure of 30 t/sq. inch.

Any trace of contamination was carefully removed from the pellets by scraping them with a sharp blade. The pellets were then sintered at $2000^{\circ}C$ in argon for 3 h. This treatment produced oxygen deficient ThO_2-Y_2O_3 pellets. Stoichiometry was restored by heating overnight at $1000^{\circ}C$ in air, followed by equilibration for a few hours in a gas stream having a $P_{H_2O}/P_{H_2} = 1$ at $1000^{\circ}C$.

The prepared electrolytes were dense, white and translucent.

X-ray diffraction patterns of the $ThO_2 + Y_2O_3$ (90/10 mole pct) solid solution gave a lattice parameter a = 5.57 Å, in good agreement with the work of Hund and Mezger[94]. Based on this, the X-ray density of this solid solution is calculated as 9.16 g/cm^3. The measured density of the pellets ranged from 8.6 to 8.9 g/cm^3, i.e. 94 to 97% of the theoretical. These figures are slightly better than those obtained by Wimmer et al[95].

10.3   PREPARATION OF THE REFERENCE ELECTRODES

Fe, FeO and Cr, Cr_2O_3 mixtures were used as reference electrodes in this study.

The Fe, FeO electrode was prepared by mixing electrolytic iron powder and analytical purity Fe_2O_3 in quantities to give a ratio of Fe:FeO of 1:1 by weight. The mixture was then pressed in a hardened tool steel die, and the pellets were sealed under vacuum in a silica capsule and heated at $1200^{\circ}C$ for 12 h.

The Cr, Cr_2O_3 electrode was prepared by mixing powdered Cr with Cr_2O_3 in the ratio of 90:10 by weight. The mixture was pressed, and heated to $1400^{\circ}C$ for 24 h in a silica capsule which had been evacuated and backfilled with Ar so that the pressure in the capsule would be approximately 1 atm at $1400^{\circ}C$.

The metal powders were supplied from Alfa Inorganics. Typical analysis is shown on Table 10.1.

The oxides were supplied either from Fischer Scientific or from Alfa Inorganics. No analysis is available, but they were of "reagent grade" purity.

10.4   PREPARATION OF THE ELECTRODES

The desired electrodes were the following binary mixtures:

I $V + VO_{0.2-x}$

II $VO_{0.2+x} + VO_{1-y}$

III $VO_{1+y} + V_2O_3$.
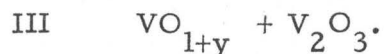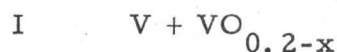
They were prepared by mixing the appropriate amounts of V metal powder and V_2O_3. Both were supplied from Alfa Inorganics. Typical analysis of V is given in Table 10.1. The mixture was compressed into pellets in a hardened tool steel die, and the pellets were fused in an argon arc furnace with a water-cooled copper mold. They were then annealed at $1300^{\circ}C$ for 24 h into a silica capsule which had been evacuated and backfilled with Ar at reduced pressure. After the annealing they were quenched in water and polished to a flat surface on one side.

The phases present were checked by X-ray analysis, using a Debye-Scherrer camera (114.6 mm diameter) and copper radiation filtered through a nickel window. Typical diffraction patterns of the above mixtures are given in Tables 10.2 - 10.4.

TABLE 10.1

ANALYSIS OF MATERIALS USED

MATERIAL	TYPICAL IMPURITY LEVELS (in ppm)
IRON	C $<$ 1000, O $<$ 3000, N $<$ 1000, metals $\leqslant$ 100
CHROMIUM	Fe:150, O:800, N:30, others $<$ 10
VANADIUM	Fe:1000, Si:800, Al:200, C:900, Cr:600, others $<$ 100

TABLE 10.2

X-RAY DIFFRACTION PATTERN FOR THE MIXTURE
$V + VO_{0.2}$

Line No.	Pat.	$d_{obs.}$	d due to V a = 3.030	d due to $VO_{0.2}$ a = 3.000 c = 3.220	Choice
1	vs	2.186		2.195	$VO_{0.2}$
2	w	2.144	2.143		V
3	s	2.111		2.121	$VO_{0.2}$
4	mw	1.498	1.517	1.500	$V/VO_{0.2}$
5	w	1.286		1.282	$VO_{0.2}$
6	mw	1.238	1.237	1.238	$V/VO_{0.2}$
7	w	1.099		1.097	$VO_{0.2}$
8	w	1.062		1.061	$VO_{0.2}$
9	w	0.956	0.958	0.955	$V/VO_{0.2}$
10	w	0.947			-
11	vw	0.886		0.886	$VO_{0.2}$
12	vvw	0.817	0.810		V
13	vvw	0.807		0.806	$VO_{0.2}$
14	vvw	0.804		0.805	$VO_{0.2}$

TABLE 10.3

X-RAY DIFFRACTION PATTERN FOR MIXTURE

$VO_{0.2}$ + VO
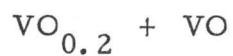
Line No.	Pat.	d_{obs}	due to $VO_{0.2}$ a = 2.930 c = 3.570	due to VO a = 4.020	Choice
1	mw	2.301		2.320	VO
2	mw	2.254			$VO_{0.2}$
3	m	2.058	2.072		$VO_{0.2}$
4	mw	2.006		2.010	VO
5	f	1.885			-
6	f	1.791	1.785		$VO_{0.2}$
7	f	1.461	1.465		$VO_{0.2}$
8	w	1.418		1.421	VO
9	f	1.361	1.352		$VO_{0.2}$
10	f	1.230	1.230		$VO_{0.2}$
11	f	1.034	1.036	1.005	$VO_{0.2}$/VO
12	f	1.927		0.922	VO
13	f	0.902	0.896	0.899	$VO_{0.2}$/VO
14	f	0.833			-
15	f	0.823		0.821	VO

TABLE 10.4

X-RAY DIFFRACTION PATTERN FOR THE MIXTURE VO + V$_2$O$_3$

Line No.	Pat.	d$_{obs}$	d due to VO a = 4.110	d due to V$_2$O$_3$ ASTM power file Card No. 1-1293	Choice
1	w	3.572		3.65	V$_2$O$_3$
2	mw	2.673		2.70	V$_2$O$_3$
3	w	2.441		2.47	V$_2$O$_3$
4	vw	2.360	2.373		VO
5	vvw	2.170		2.18	V$_2$O$_3$
6	w	2.052	2.055		VO
7	vvw	1.813		1.83	V$_2$O$_3$
8	mw	1.689		1.69	V$_2$O$_3$
9	w	1.457	1.453		VO
10	vvw	1.425		1.43	V$_2$O$_3$
11	f	1.329		1.33	V$_2$O$_3$
12	f	1.244		1.24	V$_2$O$_3$
13	vvw	1.235	1.239		VO
14	f	1.214		1.22	V$_2$O$_3$
15	f	1.189	1.186	1.19	VO/V$_2$O$_3$
16	f	1.172		1.17	V$_2$O$_3$
17	f	1.123		1.13	V$_2$O$_3$
18	f	1.092		1.09	V$_2$O$_3$
19	f	1.058		1.06	V$_2$O$_3$
20	f	1.036	1.027		VO
21	f	0.946	0.943		VO
22	f	0.935			-
23	f	0.924	0.919		VO

TABLE 10.5   169

X-RAY DIFFRACTION PATTERN OF MIXTURE $VO_{0.2}$ + VO ANNEALED AT $1000^{\circ}C$ FOR 2 WEEKS

Line No.	Pat.	d_{obs}	d due to $VO_{0.2}$ a =2.930 c=3.570	d due to VO a=4.02	d due to phase $\gamma*$	Choice
1	w	2.318		2.32		VO
2	mw	2.260	2.265			$VO_{0.2}$
3	f	2.191				γ ?
4	f	2.099				γ ?
5	s	2.063	2.072			$VO_{0.2}$
6	f	2.028				γ ?
7	s	2.010		2.010		VO
8	f	1.877			1.886	γ ?
9	vvw	1.791	1.785		1.786	$VO_{0.2}$
10	w	1.626			1.589	γ ?
11	mw	1.425		1.421	1.456	VO
12	w	1.358	1.352		1.355	$VO_{0.2}$
13	vw	1.258				γ ?
14	vw	1.233	1.230			$VO_{0.2}$
15	f	1.215			1.219	γ ?
16	f	1.179				γ ?
17	f	1.164			1.168	γ ?
18	f	0.926		0.922		VO
19	f	0.901	0.896	0.899		VO
20	f	0.825		0.821		VO

* As reported by Rostoker and Yamamoto[72]

To check for the existence of the γ-phase, one pellet of composition in the phase field $VO_{0.2}$-VO was annealed for 2 weeks at $1000^{\circ}C$ and then quenched in water. Its X-ray diffraction pattern is given in Table 10.5. A comparison with Table 10.3 shows that many extra lines appear in Table 10.5, all of them faint. Some agreement exists between these extra lines and the ones reported by Rostoker and Yamamoto[72] and attributed to the γ phase. It should therefore be concluded that the γ phase does exist, but forms via a very sluggish reaction, since after two weeks of annealing the alloy is still a mixture of three phases, and the amount of γ phase formed must be small, as all the lines attributed to the γ phase are faint.

From Tables 10.2-10.4 is seen that the lattice parameters of the various phases from this investigation are in good agreement with previous investigations (Fig. 8.1, 8.2, 8.4).

10.5   CELL DESIGN

Two different cell designs were used in this investigation:

(a) The first was similar to the original open cell assembly used by Kiukkola and Wagner[89] and is pictured in Fig. 10.1. It is made out of fused quartz and consists of a finger-like cell holder against the closed end of which the cell is pressed with the pushing rod F. The pressure is applied with the screw-type metallic fitting shown at the right. Contact with the electrodes is made with two platinum wires.

The cell holder fits into a furnace tube, made out of fused quartz, where it seals through the ground cone joint (B).

A Ti foil is placed around the cell to act as a "getter" for oxygen.

The temperature of the cell was measured with a Pt-Pt 13% Rh thermocouple which was inserted from the left end of the furnace tube and was extending up to the galvanic cell.

The furnace tube was flushed with purified Ar.

GAS INLET

GAS OUTLET

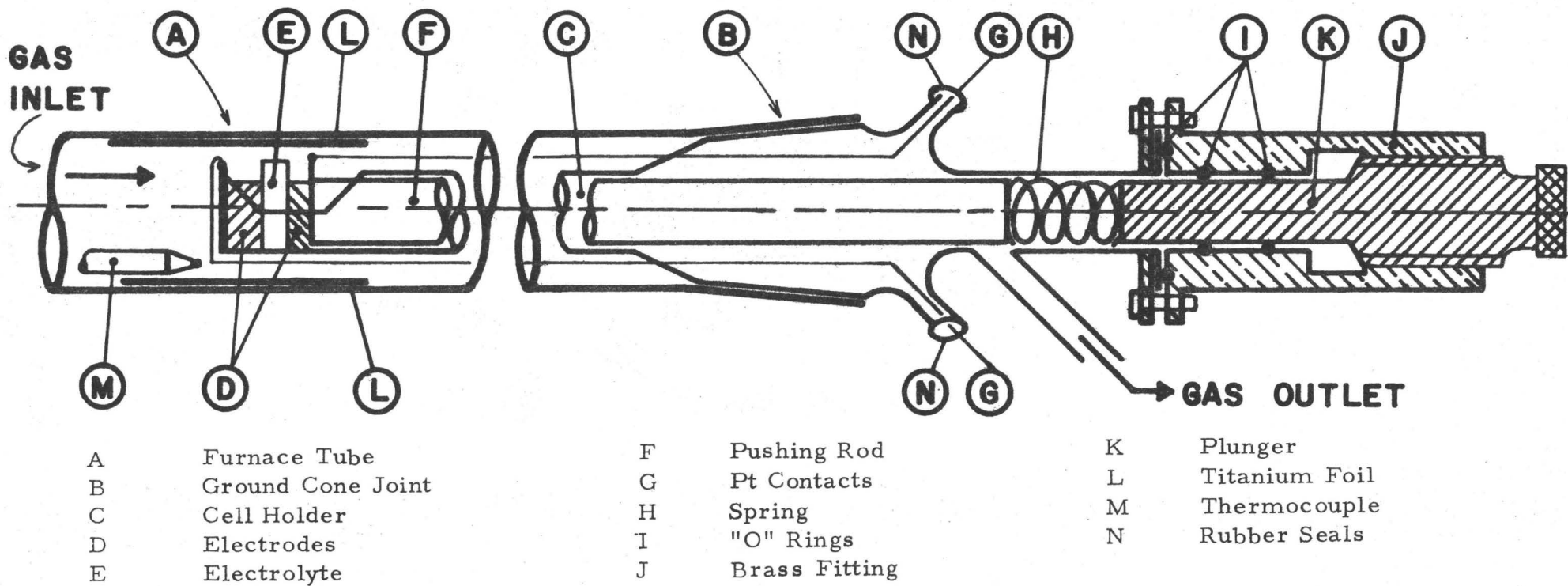| A	Furnace Tube	F	Pushing Rod	K	Plunger
B	Ground Cone Joint	G	Pt Contacts	L	Titanium Foil
C	Cell Holder	H	Spring	M	Thermocouple
D	Electrodes	I	"O" Rings	N	Rubber Seals
E	Electrolyte	J	Brass Fitting		

Fig. 10.1   Cell design for EMF measurements.

This simple cell design was found to produce quite stable and reproducible results with all the cells employed.

(b) The second design was a modification of the first to give separate electrode compartments. A calcia stabilized zirconia tube (1/2" OD, 18" long) with a flat closed end was placed into the cell holder (Fig. 10.1) in the place of the pushing rod F. The electrode with the higher oxygen potential was placed inside the tube. On the outside a thoria-yttria pellet was placed in contact with the tube, and the second electrode was placed in contact with the thria-yttria pellet. The electrode inside the tube was flushed with a separate stream of argon.

This cell assembly produced results which were indistinguishable from the ones produced for cells of type (a).

10.6   THE GAS CLEANING TRAIN

Vanadium has a great affinity for oxygen, so great care was taken to ensure complete cleaning of the Ar used to flush the system. High purity Ar was passed over ascarite to remove CO_2, magnesium perchlorate to remove H_2O, and then over Zr sponge held at $700^{\circ}C$ to remove traces of O_2, and it was then admitted to the furnace.

The oxygen potential in the purified Ar was measured by means of a ZrO_2 (CaO) tube carrying internal and external Pt leads and utilizing air as the reference electrode. A separate small furnace was used for this purpose, held at $650^{\circ}C$.

10.7   FURNACE AND FURNACE CONTROL

A tubular horizontal SiC resistance furnace was used in this work. The temperature was controlled by a proportional "on"-"off" controller to $\pm 1^{\circ}C$, and measured with a Pt-Pt 13% Rh thermocouple.

10.8   EMF MEASUREMENT

The cell EMF was measured with a Croydon potentiometer equipped with a reflecting mirror galvanometer.

A resistance ranging from 10^4 to 10^7 Ω could be introduced in series to the measuring circuit. When taking an EMF reading, the highest resistance was introduced and gradually removed until the final EMF reading was obtained with no resistance in the circuit. In this way the equilibrium potential of the cell was not disturbed.

The potentiometer readings were checked with a Keithley Electrometer (model 610) with an input impedance of 10^{14} Ω. The readings agreed very well, although the electrometer scale could not be read very accurately in some ranges.

10.9   EXPERIMENTAL PROCEDURE

To start an experiment, the cell was set up from the electrolyte and the appropriate electrodes, and placed into the furnace. The furnace chamber was flushed with purified Ar for 2 h at room temperature, and then the flow of Ar was adjusted to 0.1 l/min and the furnace was turned on. When the desired temperature was reached, the EMF measurements were taken, after allowing sufficient time for equilibrium to be reached. The cell was allowed to stand at temperature from 2 to 12 hours, during which EMF readings were taken at intervals, to ensure stability of the reading. Then the temperature was changed and the same procedure followed.

The temperature was cycled over the range investigated, and EMF readings were taken during the heating and cooling cycles. Total time for an experiment was from 36 to 48 h.

Each cell was tested at least twice for reversibility (§ 9.5). This was accomplished by passing a small current through the cell in either direction and noting whether the observed voltage returned to the original value recorded before the cell equilibrium was disturbed.

The current was passed either by setting the potentiometer dials to a reading 200-300 mV higher or lower than the equilibrium EMF and closing the circuit from 10 to 20 sec, or by applying 1.5V directly from a battery to the cell for 10-60 sec.

EMF readings were taken with the furnace power "on" and "off". No difference was observed between the two, showing that the furnace current had no effect on the EMF reading.

CHAPTER 11

EXPERIMENTAL RESULTS

11.1   INTRODUCTION

Before starting the work on the vanadium oxides the experimental set up was checked by measuring the potentials of cells which had been used by other investigators.

The equilibrium partial pressure of oxygen was then measured over the following metal-oxide or oxide-oxide mixtures:

Mixture I:	$V + VO_{0.2-x}$	$(700-1220^{\circ}C)$
Mixture II:	$VO_{0.2+x} + VO_{1-y}$	$(1200-1450^{\circ}C)$
Mixture III:	$VO_{1+y} + V_2O_3$	$(900-1200^{\circ}C)$

using oxygen concentration cells with $ThO_2(Y_2O_3)$ electrolytes.

The temperature ranges were such as to ensure stability of the oxide mixtures (Fig. 8.5).

Fe-FeO was initially chosen as reference electrode but it was found to penetrate the electrolyte heavily at temperatures higher than $1050^{\circ}C$ and was substituted with $Cr-Cr_2O_3$.

Cell assemblies with and without separate electrode compartments were used (§ 10.5) with no noticeable difference in the results.

The Ar atmosphere was purified so as not to oxidize the Cr in the reference electrode. After prolonged experiments, electrode mixtures (I) and (II) were slightly oxidized, although the interface in contact with the electrolyte was not.

The compositions of electrolyte used were $ThO_2 + Y_2O_3$ (90:10 and

95:5) no difference being observed in the results. The first composition was used for most of the experiments.

11.2   THE CELL Cu, Cu_2O | $ThO_2 + Y_2O_3$ | Fe, FeO
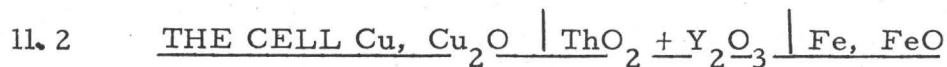
This cell was investigated with cell design (a) (§ 10.5) in the temperature range 670-950°C. The results are presented in Table 11.1 and Fig. 11.1, where they are compared with a previous investigation[57]. The agreement is very good.

11.3   CELL I: Fe, FeO | $ThO_2 + Y_2O_3$ | V, $VO_{0.2-x}$

This cell was investigated between 720-960°C with cell design (a) (§ 10.5).

The experimental results are shown in Table 11.2 and Fig. 11.2.
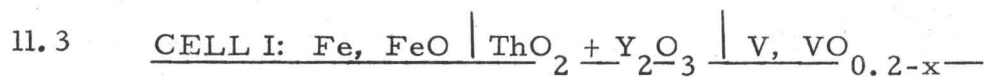
The least square line through the experimental points is represented by the equation

$$E_I = 0.8285 - 0.1145 \times 10^{-3}T \ (V) \tag{11.1}$$

11.4   CELL II: Fe, FeO | $ZrO_2 + CaO$ | $ThO_2 + Y_2O_3$ | V, $VO_{0.2-x}$
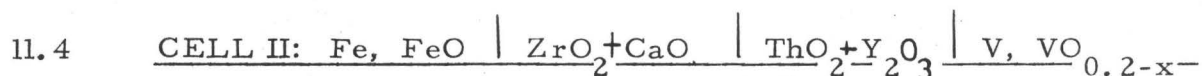
This cell was investigated in the same range as cell I with cell design (b) (§ 10.5) (separate electrode compartments). The results, shown in Table 11.3 and Fig. 11.3, are in excellent agreement with the ones from cell I. The least square line through the experimental points in Fig. 11.3 is

$$E_{II} = 0.846 - 0.113 \times 10^{-3}T \ (V) \tag{11.2}$$

TABLE 11.1

EMF MEASUREMENTS FOR THE CELL
$$Cu, \ Cu_2O \ \big| \ ThO_2(Y_2O_3) \ \big| \ Fe, \ FeO$$
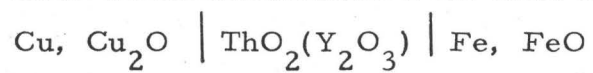
T, $^{\circ}$C	EMF, mV
948	544
849	541
764	539
672	536
770	539
858	542
900	543
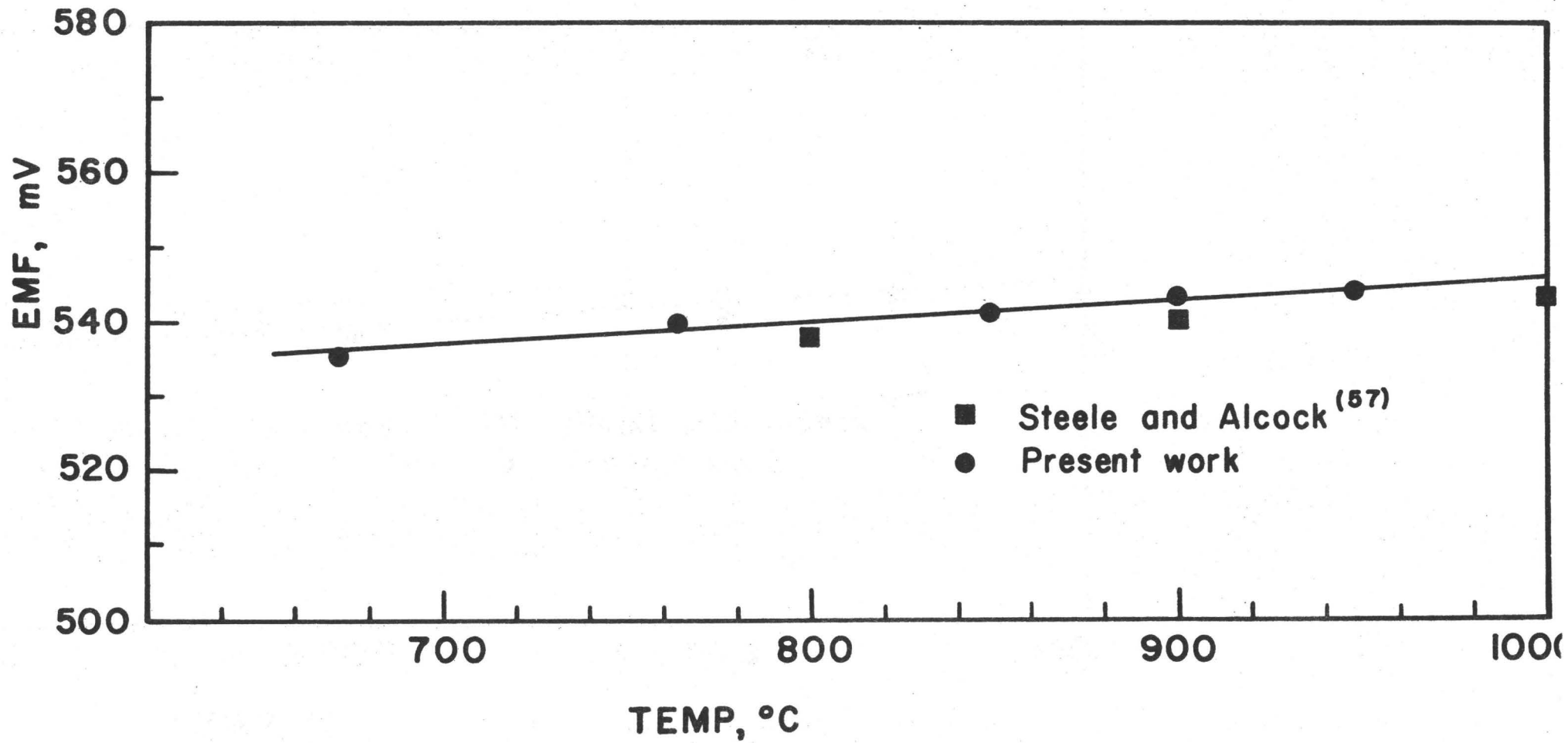
Fig. 11.1 EMF measurements for the cell Cu, $Cu_2O/ThO_2(Y_2O_3)/Fe$, FeO.

TABLE 11.2

EMF MEASUREMENTS FOR THE CELL
Fe, FeO $\mid$ ThO$_2$ + Y$_2$O$_3$ $\mid$ V, VO$_{0.2-x}$
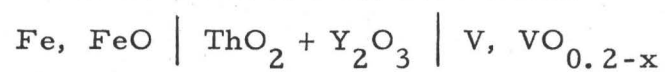
T, °C	EMF, mV
790	707
853	700
898	695
962	687
919	693
881	697
829	702
786	706
748	712
711	716
874	696
909	694
941	688
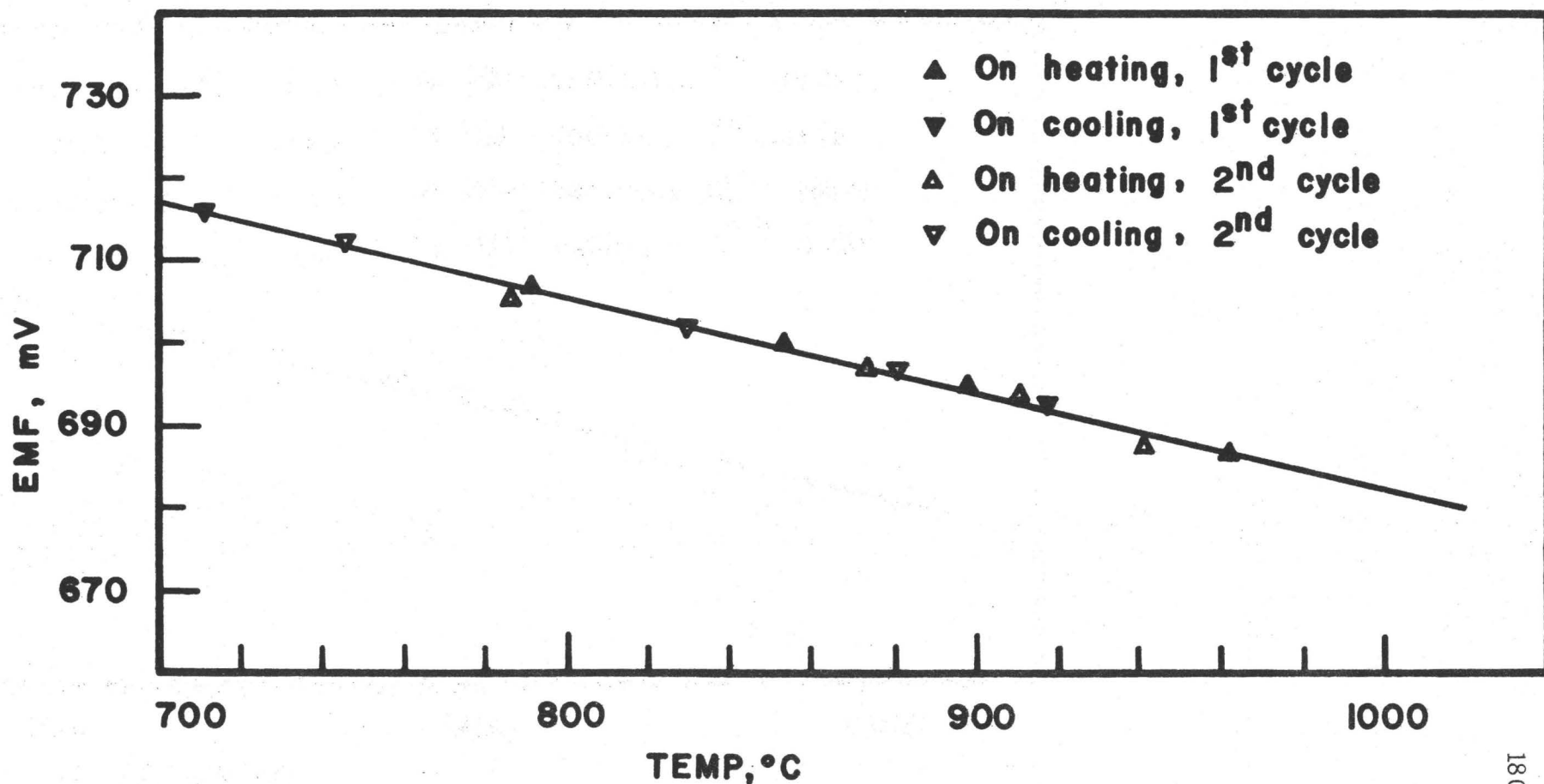
Fig. 11.2 EMF measurements for the cell Fe, FeO $\mid$ ThO$_2$ + Y$_2$O$_3$ $\mid$ V, VO$_{0.2-x}$

TABLE 11.3

EMF MEASUREMENTS FOR THE CELL
Fe, FeO | ZrO_2 + CaO | $ThO_2 + Y_2O_3$ | V, $VO_{0.2-x}$
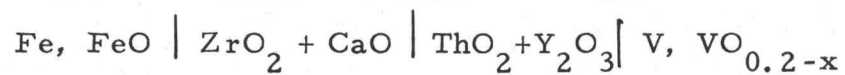
T, $^{\circ}$C	EMF, V
744	0.717
767	0.711
803	0.706
851	0.700
889	0.697
955	0.687
917	0.692
858	0.700
821	0.702
760	0.711
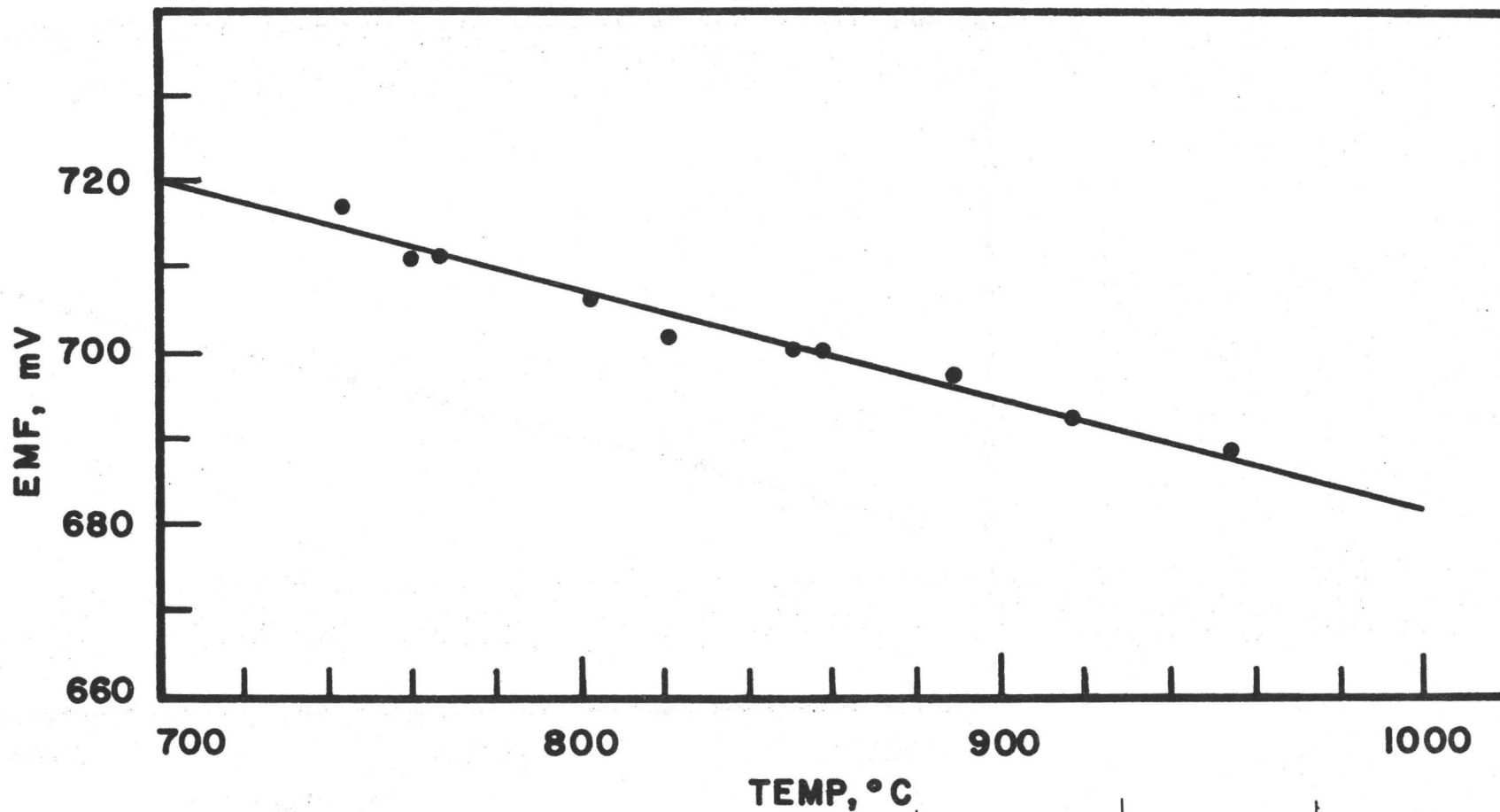
Fig. 11.3 EMF measurements for the cell Fe, FeO | ZrO_2 + CaO | ThO_2+Y_2O_3 | V, $VO_{0.2-x}$

11.5 <u>CELL III: Cr, Cr$_2$O$_3$</u> | ELECTROLYTE | V, VO$_{0.2-x}$
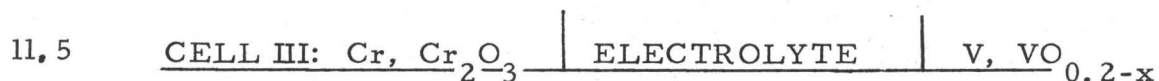
This cell was investigated between 1000-1220°C with the open cell design (a), and also with cell design (b). The results again are undistinguishable, and are shown on Table 11.4 and Fig. 11.4.

The least square line through the points is

$$E_{III} = 0.2789 - 2.73 \times 10^{-5} T \quad (V) \tag{11.3}$$

11.6 <u>CELL IV: Cr, Cr$_2$O$_3$</u> | ELECTROLYTE | VO$_{0.2+x'}$ VO$_{1-y}$
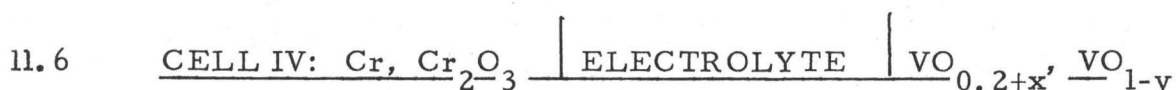
This cell was investigated between 1200-1450°C with the open cell design (a). The experimental results are presented in Table 11.5 and Fig. 11.5. As reported earlier (§ 8.2.3) the right hand electrode is decomposing slowly below approximately 1200°C to a new phase, and for this reason only the results above 1200°C are reported here. It should be noted however that results taken in the range 1000-1200°C fit very well the extrapolated line of Fig. 11.5. Also this cell was investigated in the range 700-1000°C with Fe, FeO as reference electrode, and gave results in very good agreement with the extrapolated values reported here.

The least square line through the points in Fig. 11.5 is

$$E_{IV} = 0.0265 + 0.998 \times 10^{-4} T \quad (V) \tag{11.4}$$

11.7 <u>CELL V: Cr, Cr$_2$O$_3$</u> | ELECTROLYTE | VO$_{1.25'}$ VO$_{1.5}$
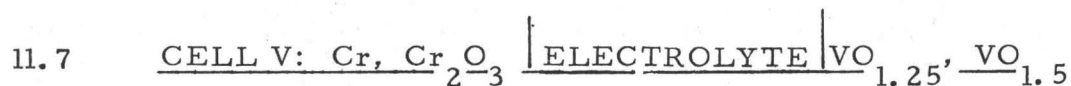
Experimental points for this cell, taken again with cell design (a) and (b) in the temperature range 900-1200°C, are presented in Table 11.6 and Fig. 11.6.

The least square line through the points is

$$E_V = -0.0565 + 8.604 \times 10^{-5} T \quad (V) \tag{11.5}$$

TABLE 11.4

EMF MEASUREMENTS FOR THE CELL
$$\text{Cr, } Cr_2O_3 \mid \text{electrolyte} \mid \text{V, } VO_{0.2-x}$$
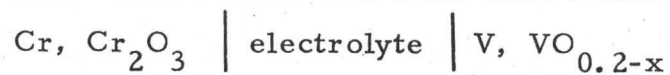
T, $^{\circ}$C	EMF, mV
1093	240
1100	242
1134	239
1224	238
1191	238
1167	240
1071	242
1009	245
1020	243
1045	242
1076	243
1190	239
1208	237
1029*	243
1092*	242
1126*	242
1183*	241
1206*	239
1092*	243
1026*	243

* Cell design (b) (Separate electrode compartments). All others with cell design (a).
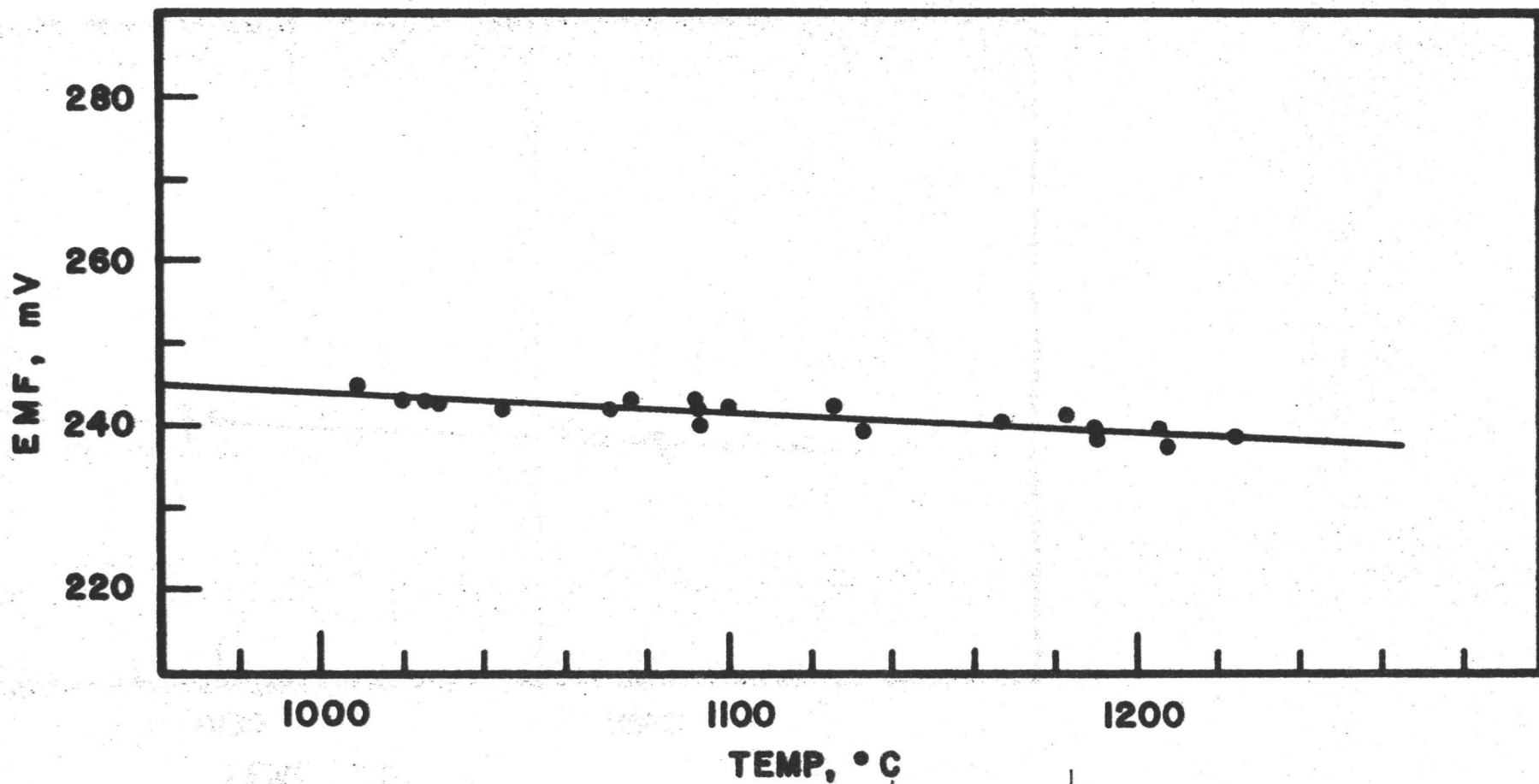
Fig. 11.4 EMF measurements for the cell Cr, Cr_2O_3 | electrolyte | V, $VO_{0.2-x}$

TABLE 11.5

EMF MEASUREMENTS FOR THE CELL

$$Cr, \ Cr_2O_3 \ \left| \ ThO_2 \ (Y_2O_3) \ \right| \ VO_{0.2+x}, \ VO_{1-y}$$
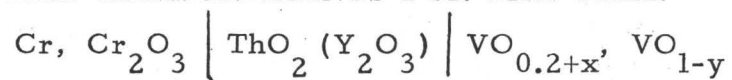
T, $^{\circ}$C	EMF, mV
1224	175
1282	183
1327	186
1375	191
1408	195
1448	197
1432	197
1385	193
1317	185
1280	182
1298	183
1348	188
1411	194
1309	185
1262	179

(all with cell design (a))
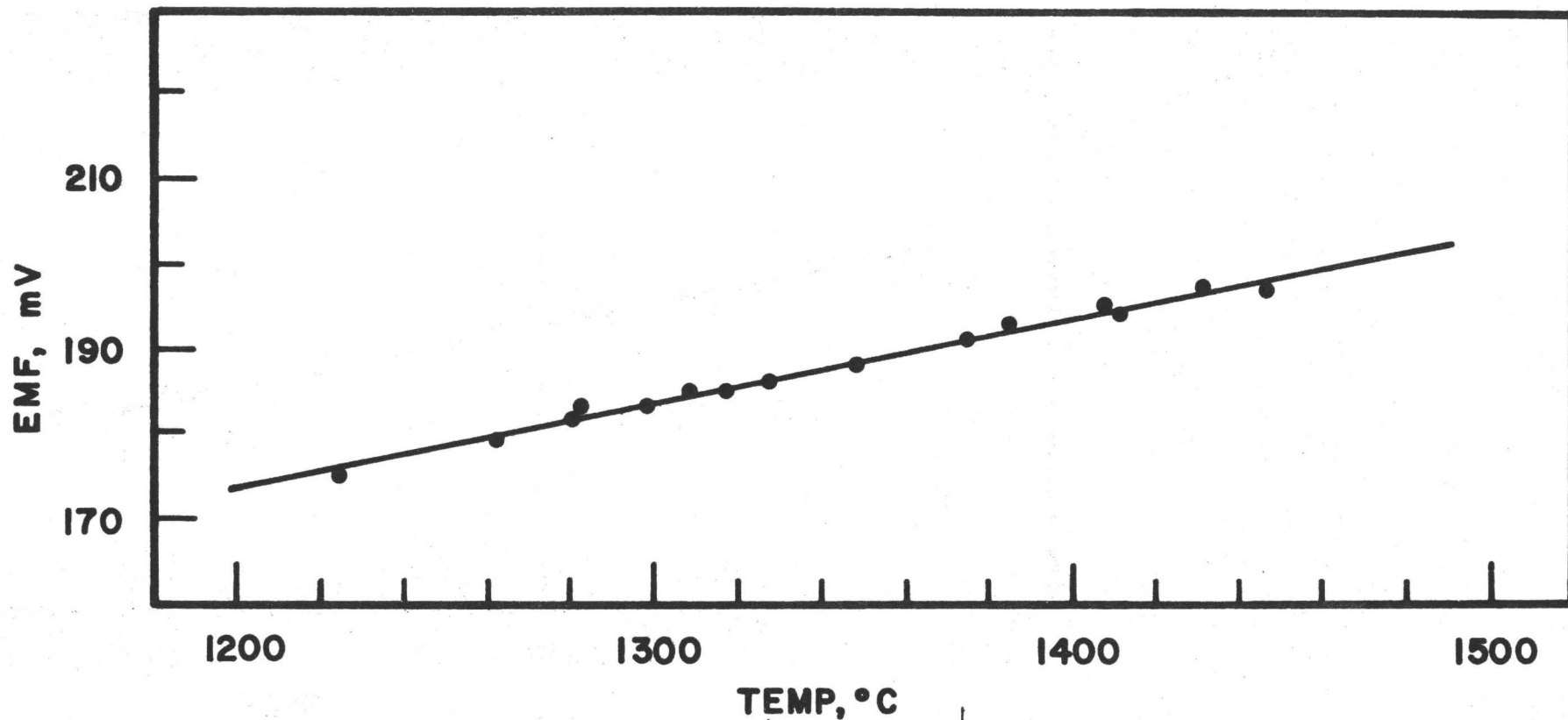
Fig. 11.5 EMF measurements for the cell Cr, $Cr_2O_3 \mid ThO_2(Y_2O_3) \mid VO_{0.2+x}$, VO_{1-y}

TABLE 11.6

EMF MEASUREMENTS FOR THE CELL
Cr, Cr_2O_3 | electrolyte | VO_{1+y}, V_2O_3
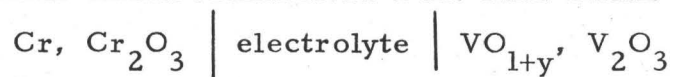
T, $^\circ$C	EMF, mV
973	49
1033	53.5
1086	60
1189	70
1167	67
1053	59
1025	57
990	54
954	50
922	47
895	44.5
1001*	53
1033*	56
1053*	56
1065*	57
1075*	60
1108*	62
1143*	66
1119*	65
1095*	62
1065*	59
1059*	57
1038*	55

* Cell design (b) (closed cell assembly). All others with cell assembly(a).
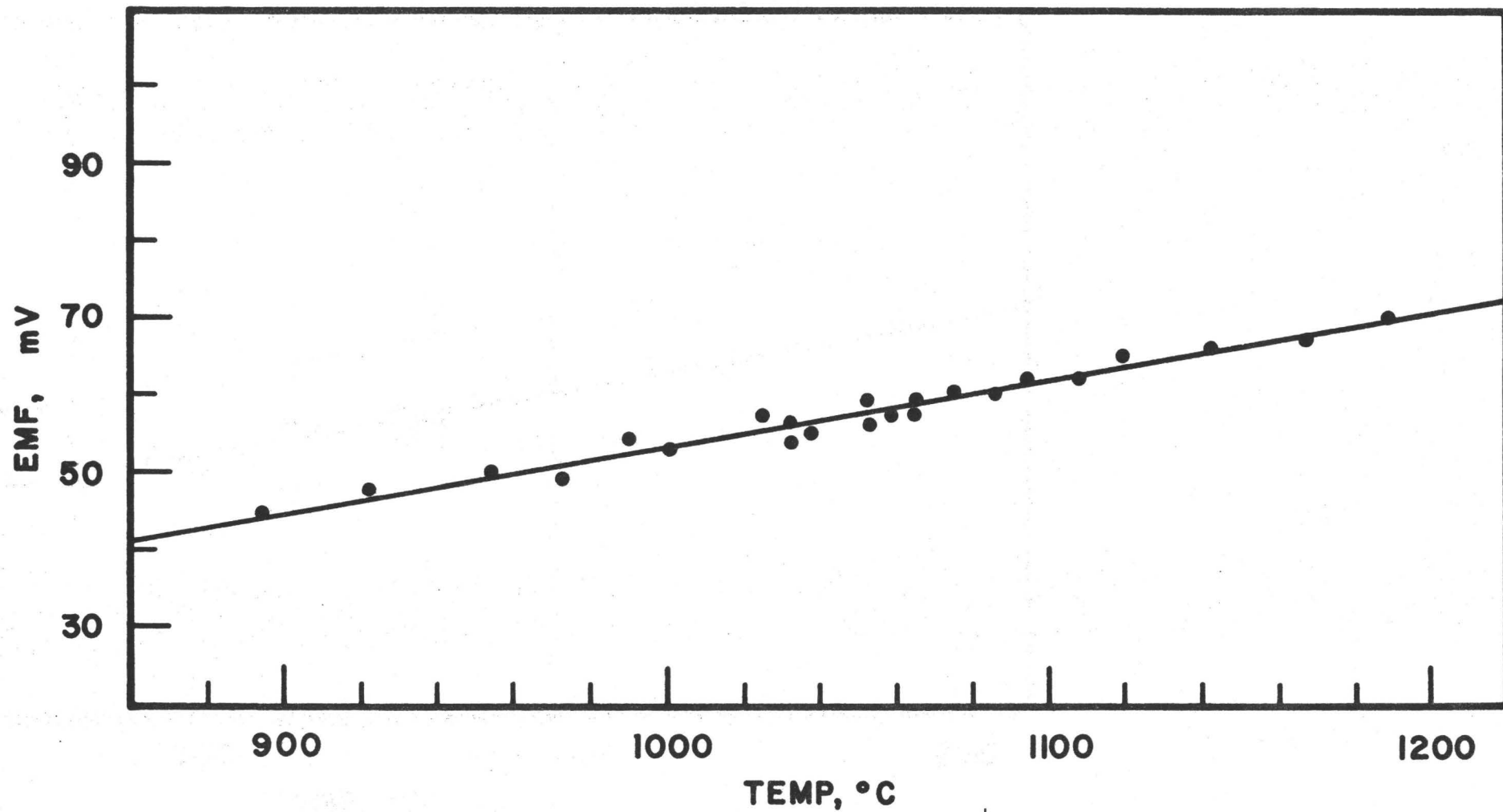
Fig. 11.6 EMF measurements for the cell Cr, Cr_2O_3|electrolyte |VO_{1+y}, V_2O_3

(In the experiments with this cell high purity helium was used to flush the furnace.)

CHAPTER 12

DISCUSSION

12.1   INTRODUCTION

Based on the EMF measurements, the activity of oxygen in equilibrium with the oxide mixtures investigated is calculated, and the free energy of formation of the lower oxides of vanadium are estimated, using a method proposed by Smiltens[98].

12.2 THE Fe, FeO REFERENCE ELECTRODE

The Fe, FeO is the best choice as reference electrode in solid state EMF measurements, because it has been found to exhibit a high degree of reversibility[92] and also the thermodynamic properties of FeO are among the most accurately known. The free energy change for the reaction

$$1.9 \ Fe(s) + O_2(g) = 2 \ Fe_{0.95}O \qquad (12.1)$$

has been assessed[92] as

$$\Delta G^o_{12.1} = - \ 126470 + 31.26 \ T \ (\pm 250)(cal) \qquad (12.2)$$

in the temperature range 873-1600°K.

From eqn. (12.2) the P_{O_2} in equilibrium with Fe, and FeO is calculated as

$$\log P_{O_2} (Fe, FeO) = - \ \frac{27650}{T} + 6.83 \qquad (12.3)$$

In the present work the Fe, FeO electrode performed very well up to 1050°C. Above this temperature it was found to penetrate the electrolyte pellets; at high enough temperatures (around 1300°C) it completely penetrated a 1/8 in. thick electrolyte after 12 hours. For this reason Cr, Cr_2O_3 was used as reference electrode, and the Fe, FeO was only used with cells I and II to check the results obtained with Cr, Cr_2O_3.

12.3 THE Cr, Cr_2O_3 REFERENCE ELECTRODE

There are several disadvantages associated with the use of a Cr, Cr_2O_3 mixture as reference electrode:

(a) it has often been found to display irreversible behaviour[92]

(b) its thermodynamic properties are not as accurately known as those for the Fe, FeO mixtures.

The value for the free energy change for the reaction

$$2 \, Cr \, (s) + \frac{3}{2} \, O_2(g) = Cr_2O_3(s) \tag{12.4}$$
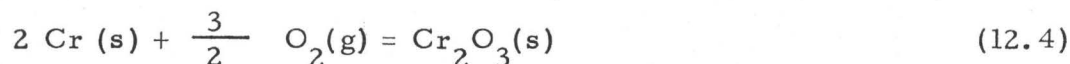
used here is the one given by Jeannin, Mannerskantz and Richardson[62]:

$$\Delta G^{o}_{12.4} = -266700 + 59.95T \, (\pm 300) \, (cal) \tag{12.5}$$

for the temperature range 1300-1600 ^{o}K. This equation gives values in the above temperature range approximately 2000 cal higher than the values for the free energy of formation of Cr_2O_3 tabulated by Elliott and Gleiser[96], based on Coughlin's data[97].

From eqn. (12.5) the partial pressure of oxygen in equilibrium with Cr, Cr_2O_3 is calculated as

$$\log P_{O_2} \, (Cr, \, Cr_2O_3) = - \frac{38900}{T} + 8.74 \tag{12.6}$$

Tretjakow and Schmalzried[58] measured the free energy of formation of Cr_2O_3 using the following cell:

$$Pt \, \bigg| \, air \, \bigg| \, ZrO_2 \, (CaO) \, \bigg| \, Cr, \, Cr_2O_3 \, \bigg| \, Pt \tag{12.6.1}$$
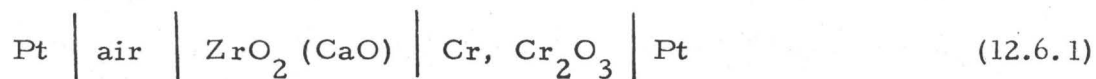
The electrolyte, in the form of tubes, was supplied by Degussa (Frankfurt) or Podolsker (USSR). From the EMF of the cell in the range 1000-1500°K the free energy of formation of Cr_2O_3 was calculated as

$$\Delta G^{o} = -258600 + 55.2T \, (\pm 300 \, cal) \tag{12.6.2}$$
$$(1000 - 1500 \, ^{o}K)$$

Pugliese and Fitterer[59], measured the EMF of the same cell with electrolyte tubes supplied by the Zirconium Corp. of America. They reported results in good agreement with Tredjakow and Schmalzried, and gave the free energy of formation of Cr_2O_3 as

$$\Delta G^O = -263590 + 59.6\,T \qquad (12.6.3)$$
$$(1000 - 1500^O K)$$

utilizing both their results and the results of Tredjakow and Schmalzried.

A comparison of the above values is shown on Table 12.1.

An attempt was made in the present work to measure the free energy of formation of Cr_2O_3 by using the following cell:

$$Fe, FeO \,\Big|\, ZrO_2\,(CaO) \,\Big|\, Cr,\ Cr_2O_3 \qquad (12.7)$$
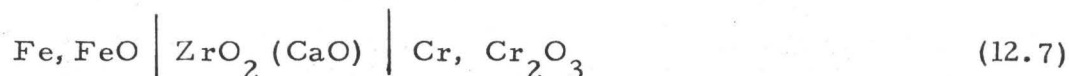
in the temperature range 800-1100°C.

The electrolyte was in the form of tube, supplied by Zirconium Corp. of America. The EMF of this cell was erratic and drifted heavily towards lower values, indicating that the electrolyte had an increased electronic conductivity at this P_{O_2} range.

In view of this fact we are unable to comment on the successful application of ZrO_2 (CaO) electrolytes by the previously mentioned investigators[58, 59].

The above cell with ThO_2 (Y_2O_3) (90/10) pellets as electrolyte gave results within the expected range, but the reproducibility was poor at temperatures below 1050°C. At higher temperatures the FeO penetrated the electrolytes, so no successful results can be reported for this cell.

However by comparing the results from cells I and III (§11.3, 11.5) an indirect check was made. The EMF for the cell 12.7, $E_{12.7}$, can be obtained as the difference between the EMF of the cells I and III, E_I and E_{III}:

TABLE 12.1

FREE ENERGY OF FORMATION

of Cr_2O_3

T, ^{o}K	$\Delta G^{o} (Cr_2O_3)$, cal			
	Jeannin et al[62]	Tretjakow and Schmalzried[58]	Pugliese and Fitterer[59]	Elliot and Gleiser[96]
1000	-206700	-203400	-204000	-209150
1100	-200800	-197900	-198000	-203000
1200	-194800	-192400	-192100	-196900
1300	-188800	-186800	-186100	-190800
1400	-182800	-181300	-180100	-184700
1500	-176800	-175800	-174200	-178600

$$E_{12.7} = E_I = E_{III} = 0.550 - 0.872 \times 10^{-4}\,T \tag{12.10}$$

From eqn. (12.10) the free energy of formation of Cr_2O_3 is calculated as

$$\Delta G^o = -265700 + 58.96T \tag{12.11}$$
$$(1100\text{-}1500^o K)$$

using eqn. (12.2) for the free energy of formation of FeO. Eqn. (12.11) is in very good agreement with eqn. (12.5), their values at $1200^o K$ differing by 100 cal.

12.4 ACTIVITIES OF OXYGEN IN EQUILIBRIUM WITH VANADIUM OXIDES

From the EMF measurements on cells III, IV, and V the partial pressures of oxygen in equilibrium with the mixtures:

I: $V + VO_{0.2-x}$

II: $VO_{0.2+x} + VO_{1-y}$ and

III: $VO_{1+y} + V_2O_3$
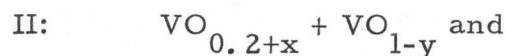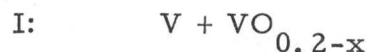
are calculated using eqn. (9.7) and eqn. (12.6) for the partial pressure of oxygen over Cr, Cr_2O_3:

$$\log P_{O_2}(I) = -\frac{44500}{T} + 9.29 \ (1000\text{-}1220^o C) \tag{12.12}$$

$$\log P_{O_2}(II) = -\frac{39400}{T} + 6.72 \ (1200\text{-}1460^o C) \tag{12.13}$$

$$\log P_{O_2}(III) = -\frac{37700}{T} + 7.00 \ (900 - 1200^o C) \tag{12.14}$$

These equations are plotted in Fig. 12.1.

Using the stability ranges of the oxides presented in Table 8.1, the free energy changes (per mole O_2) for the following reactions are calculated as follows:

$$\frac{2}{0.17} \ V \ (s) + O_2(g) = \frac{2}{0.17} \ VO_{0.17} \tag{12.15}$$

$$\Delta G^o_{12.15} = -203500 + 42.49T \tag{12.16}$$
$$(1000 - 1220^oC)$$

$$4VO_{0.35}(s) + O_2(g) = 4 \ VO_{0.85} \ (s) \tag{12.17}$$
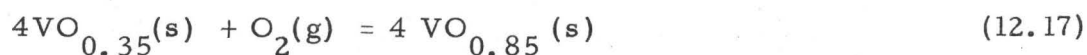
$$\Delta G^o_{12.17} = -180200 + 30.74T \tag{12.18}$$
$$(1200 - 1460^oC)$$

$$8 \ VO_{1.25} \ (s) + O_2(g) = 8 \ VO_{1.50} \ (s) \tag{12.19}$$
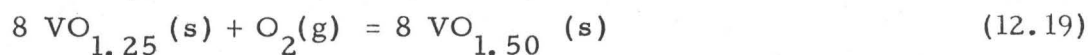
$$\Delta G^o_{12.19} = -172400 + 32.02T \tag{12.20}$$
$$(900 - 1200^oC)$$

Eqns. (12.18) and (12.20) agree rather poorly with eqns. (8.6) and (8.8) derived by Allen et al[74] based on Kobayashi's[87] results. A comparison is given in Table 12.2.
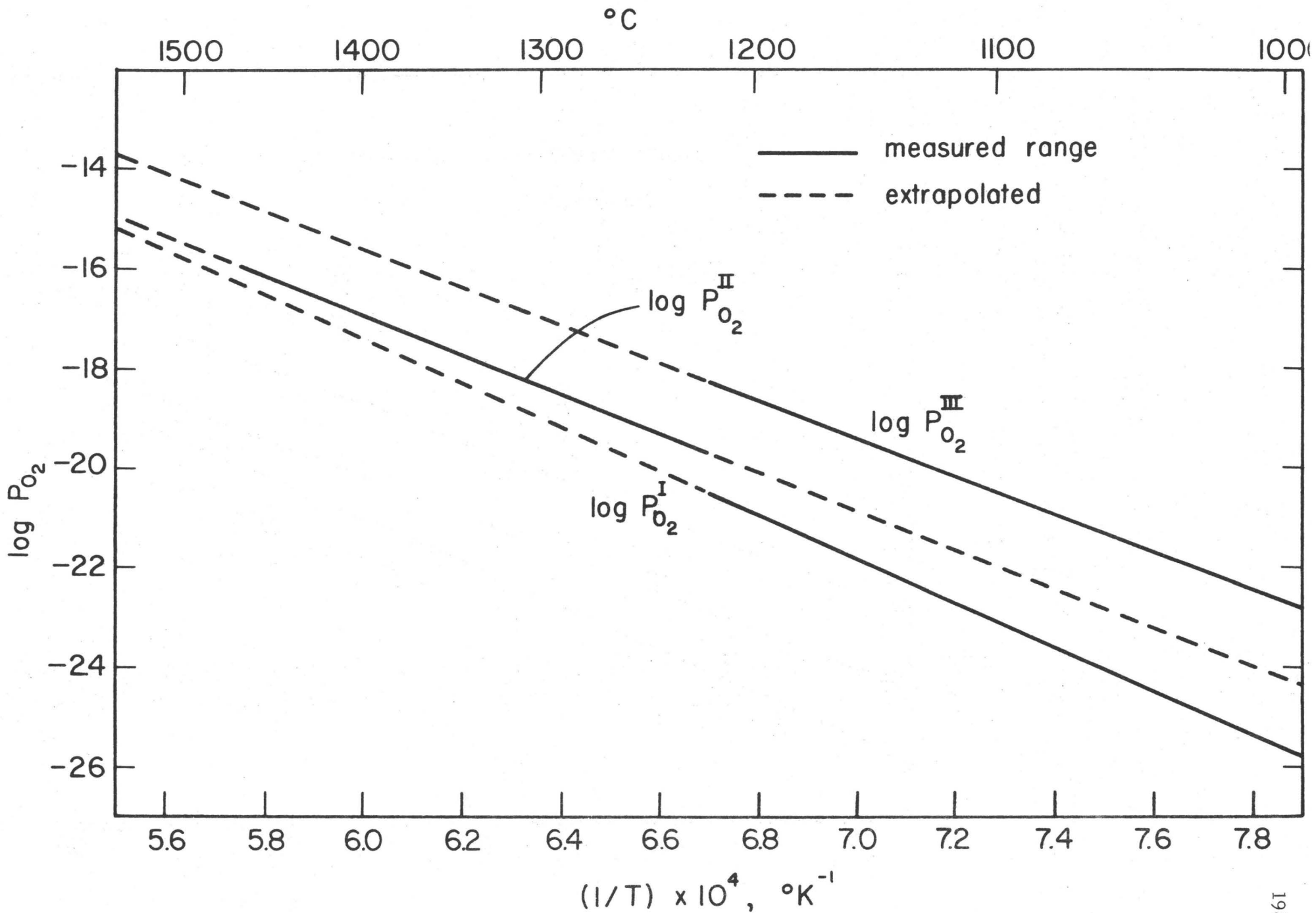
Fig. 12.1 Variational $\log P_{O_2}$ (I), $\log P_{O_2}$ (II), $\log P_{O_2}$ (III) with temperature.

TABLE 12.2

FREE ENERGY CHANGE FOR THE REACTIONS

(12.17 and (12.19)

T, °C	$\Delta G^o_{12.17}$, cal		$\Delta G^o_{12.19}$, cal	
	Present Work	Allen et al[74]	Present Work	Allen et al[74]
1100	-138000	-156600	-128400	-119700
1200	-134900	-153000	-125200	-115600
1300	-131800	-149400	-122000	-111600
1400	-128800	-145800	-118800	-107500

12.5   FREE ENERGIES OF FORMATION OF THE LOWER OXIDES OF

VANADIUM

From our data the free energy of formation of the lower oxides
of vanadium can be obtained, using the method described by Smiltens[98].

The general reaction for the oxidation of a nonstoichiometric oxide
$MeO_{x'}$ to another nonstoichiometric oxide $MeO_{x''}$ is

$$MeO_{x'} + \frac{1}{2} \quad (x'' - x') \, O_2 = MeO_{x''} \tag{12.21}$$
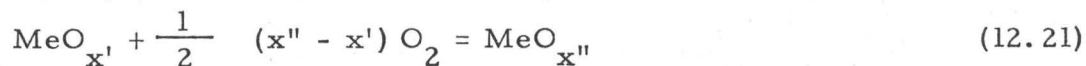
where x' and x" are any possible values of x within the phase fields ' and "
respectively (Fig. 12.2) In this figure ln P' and ln P" are the natural logarithms
of the oxygen pressures for the two phase equilibrium (phase ', oxygen)
and (phase ", oxygen) and ln P_b is that for the three phase equilibrium
(phase ', phase ", oxygen).   When the oxides are stoichiometric, the widths
of the fields $(x'_{br} - x'_{bl})$ and $(x''_{br} - x'_{bl})$ are zero; then x' = x'_{br} and
x" = x''_{bl} and the standard free energy change for the reaction 12.21 can be
found by the familiar van't Hoff equation:
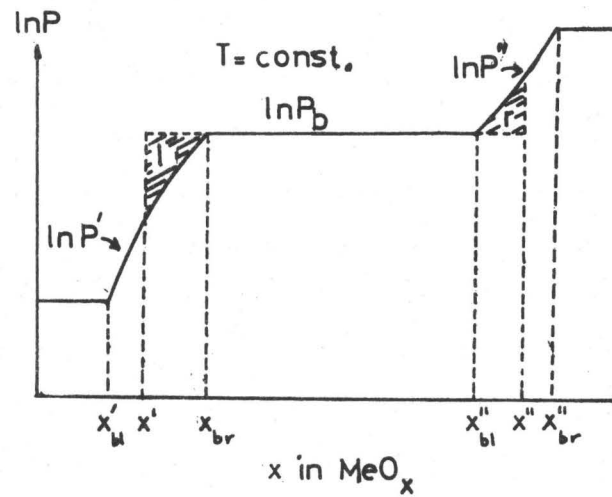
Fig. 12.2 Schematic isotherm for deriving the correction term C.
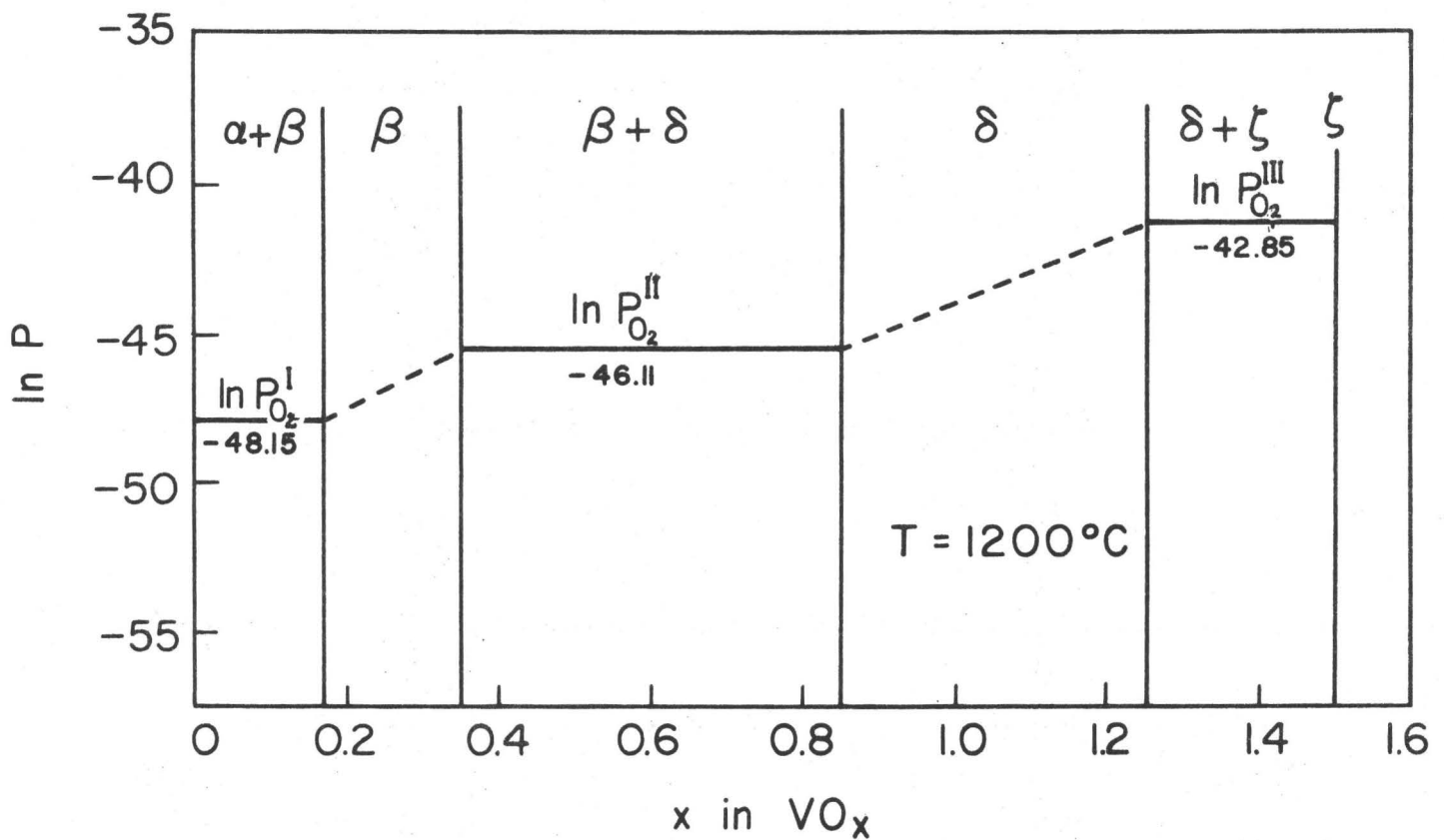
Fig. 12.3 The 1200°C isotherm for the V-O system.

$$\Delta G^{o}_{12.21} = \frac{1}{2} \; (x'' - x') \; RT \; \ln P_b \qquad (12.22)$$

With nonstoichiometric oxides the standard free energy change obtained from eqn. (12.22) would be incorrect. Smiltens[98] derived a correction term C to be added to eqn. (12.29) in the case of nonstoichiometric oxides. This correction term C is

$$C = \frac{1}{2} \; RT \left(\int_{x'}^{x'_{br}} \ln \frac{P'}{P_b} \; dx + \int_{x''_{bl}}^{x''} \ln \frac{P''}{P_b} \; dx \right) \qquad (12.23)$$

Since $P' < P_b$ the first integral in eqn. 12.23, which equals the area l, is always negative, and since $P'' < P_b$, the second integral, which equals the area r, is always positive. Therefore in order to calculate the sum of integrals in eqn. 12.23 one has to measure the areas l and r, and, taking them both as signless quantities, subtract the area l from the area r:

$$C = \frac{1}{2} \; RT \left(\left| area \; r \right| - \left| area \; l \right| \right) \qquad (12.24)$$

The corrected free energy change for the reaction (12.21) therefore is

$$\Delta G^{o}_{12.21} = \frac{1}{2} \; (x'' - x') \; RT \; \ln P_b + \frac{1}{2} \; RT \left(\left| area \; r \right| - \left| area \; l \right| \right) \quad (12.25)$$

Application of equations of this type in the present work requires knowledge of the homogeneity ranges of the oxides and of the shape of the curve for ln P', ln P''. The homogeneity ranges for the vanadium oxides were taken from the literature (Table 8.1). The range for VO is well defined ($VO_{0.85}$ - $VO_{1.25}$) for temperatures above $1000^{o}C$, and $VO_{1.50}$ will be considered as stoichiometric, although it probably has a narrow range of nonstoichiometry. The greatest uncertainty lies in the $VO_{0.2+x}$ field.

For the calculations this field was considered as $VO_{0.17}$ - $VO_{0.35}$.

The $1200^{\circ}C$ isotherm for the present systems is given in Fig. 12.3. The variation of the oxygen activity within the homogeneity ranges is approximated by a straight line.

The following equations were formulated:

$$V(s) + \frac{1}{2} \; 0.17 \; O_2(g) = VO_{0.17}(s) \tag{12.26}$$

$$VO_{0.17}(s) + \frac{1}{2} \; 0.18 \; O_2(g) = VO_{0.35}(s) \tag{12.27}$$

$$VO_{0.35}(s) + \frac{1}{2} \; 0.50 \; O_2(g) = VO_{0.85}(s) \tag{12.28}$$

$$VO_{0.85}(s) + \frac{1}{2} \; 0.40 \; O_2(g) = VO_{1.25}(s) \tag{12.29}$$

$$VO_{1.25}(s) + \frac{1}{2} \; 0.25 \; O_2(g) = VO_{1.50}(s) \tag{12.30}$$
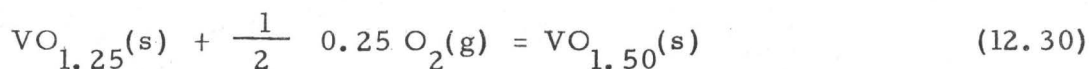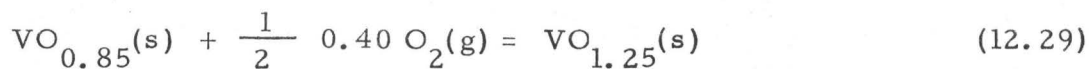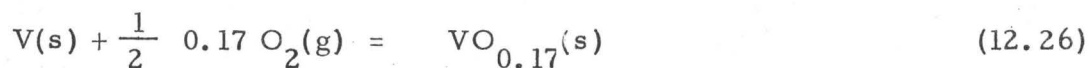
with the corresponding free energy changes being, according to eqn. 12.25,

$$\Delta G^{o}_{12.26} = \frac{1}{2} \; 0.17 \; RT \ln P_{I} \tag{12.31}$$

$$\Delta G_{12.27} = \frac{1}{2} \; 0.18 \; RT \ln P_{I} + \frac{1}{2} \; RT \frac{1}{2} \; 0.18 \left| \ln P_{II} - \ln P_{I} \right| \tag{12.32}$$

$$\Delta G_{12.28} = \frac{1}{2} \; 0.50 \; RT \ln P_{II} \tag{12.33}$$

$$\Delta G_{12.29} = \frac{1}{2} \; 0.40 \; RT \ln P_{II} + \frac{1}{2} RT \frac{1}{2} 0.40 \left| \ln P_{III} - \ln P_{II} \right| \tag{12.34}$$

$$\Delta G_{12.30} = \frac{1}{2} \; 0.25 \; RT \ln P_{III} \tag{12.35}$$

The free energies of formation, per gram formula weight, of the oxides of V are calculated as follows:

$$\Delta G^{\circ} (VO_{0.17}) = \Delta G^{\circ}_{12.26} \tag{12.36}$$

$$\Delta G^{\circ} (VO_{0.35}) = \Delta G^{\circ} (VO_{0.17}) + \Delta G^{\circ}_{12.27} \tag{12.37}$$

$$\Delta G^{\circ} (VO_{0.85}) = \Delta G^{\circ} (VO_{0.35}) + \Delta G^{\circ}_{12.28} \tag{12.38}$$

$$\Delta G^{\circ} (VO_{1.25}) = \Delta G^{\circ}_{VO_{0.85}} + \Delta G^{\circ}_{12.29} \tag{12.39}$$

$$\Delta G^{\circ} (VO_{1.50}) = \Delta G^{\circ}_{VO_{1.25}} + \Delta G^{\circ}_{12.30} \tag{12.40}$$

A computer calculation of the above led to the free energy values tabulated in Table 12.3.

The free energy of formation per mole of oxygen was also computed, and presented in Table 12.4.

In Fig. 12.4 the free energy of formation of the lower oxides of vanadium are plotted against the temperature together with Mah and Kelley's[86] data. According to our data the $\frac{2}{3}$ V_2O_3 and the 2VO lines run nearly parallel to each other. The $\frac{2}{0.17}$ $VO_{0.17}$ line, extrapolated over a wide temperature range, intersects the 2VO line around $2000^{\circ}K$, indicating that at high enough temperature, probably around the melting point of vanadium, $VO_{0.17}$ decomposes to V and VO.

Table 12.5 compares the free energies of formation of the lower oxides of vanadium obtained from this investigation with Mah and Kelley's[86] data and with Elliott and Gleiser's[96] compilation.

TABLE 12.3

FREE ENERGY OF FORMATION OF THE LOWER OXIDES OF VANADIUM

kcal/gram formula weight

T, °K	$VO_{0.17}$	$VO_{0.35}$	$VO_{0.85}$	$VO_{1.25}$	$VO_{1.50}$
1100	-13.3	-27.0	-63.6	-91.9	-109.1
1150	-13.1	-26.6	-62.8	-90.9	-107.9
1200	-13.0	-26.3	-62.1	-89.9	-106.6
1250	-12.8	-25.9	-61.4	-88.8	-105.4
1300	-12.6	-25.6	-60.7	-87.8	-104.1
1350	-12.4	-25.2	-59.9	-86.7	-102.9
1400	-12.2	-24.9	-59.2	-85.7	-101.7
1450	-12.1	-24.6	-58.5	-84.6	-100.4
1500	-11.9	-24.2	-57.7	-83.6	-99.2
1550	-11.7	-23.9	-57.0	-82.6	-97.9
1600	-11.5	-23.5	-56.3	-81.5	-96.7
1650	-11.3	-23.2	-55.5	-80.5	-95.4
1700	-11.2	-22.8	-54.8	-79.4	-94.2

TABLE 12.4

FREE ENERGY OF FORMATION OF THE LOWER OXIDES OF VANADIUM,

kcal/mole O_2

T, °K	$VO_{0.17}$	$VO_{0.35}$	$VO_{0.85}$	$VO_{1.25}$	$VO_{1.50}$
1100	-156.8	-154.1	-149.6	-147.1	-145.5
1150	-154.7	-152.1	-147.9	-145.4	-143.8
1200	-152.5	-150.2	-146.1	-143.8	-142.2
1250	-150.4	-148.2	-144.4	-142.1	-140.5
1300	-148.3	-146.2	-142.7	-140.4	-138.9
1350	-146.2	-144.2	-141.0	-138.8	-137.2
1400	-144.0	-142.3	-139.3	-137.1	-135.5
1450	-141.9	-140.3	-137.6	-135.4	-133.9
1500	-139.8	-138.3	-135.8	-133.8	-132.2
1550	-137.7	-136.3	-134.1	-132.1	-130.6
1600	-135.5	-134.4	-132.4	-130.4	-128.9
1650	-133.4	-132.4	-130.7	-128.7	-127.2
1700	-131.3	-130.4	-129.0	-127.1	-125.6
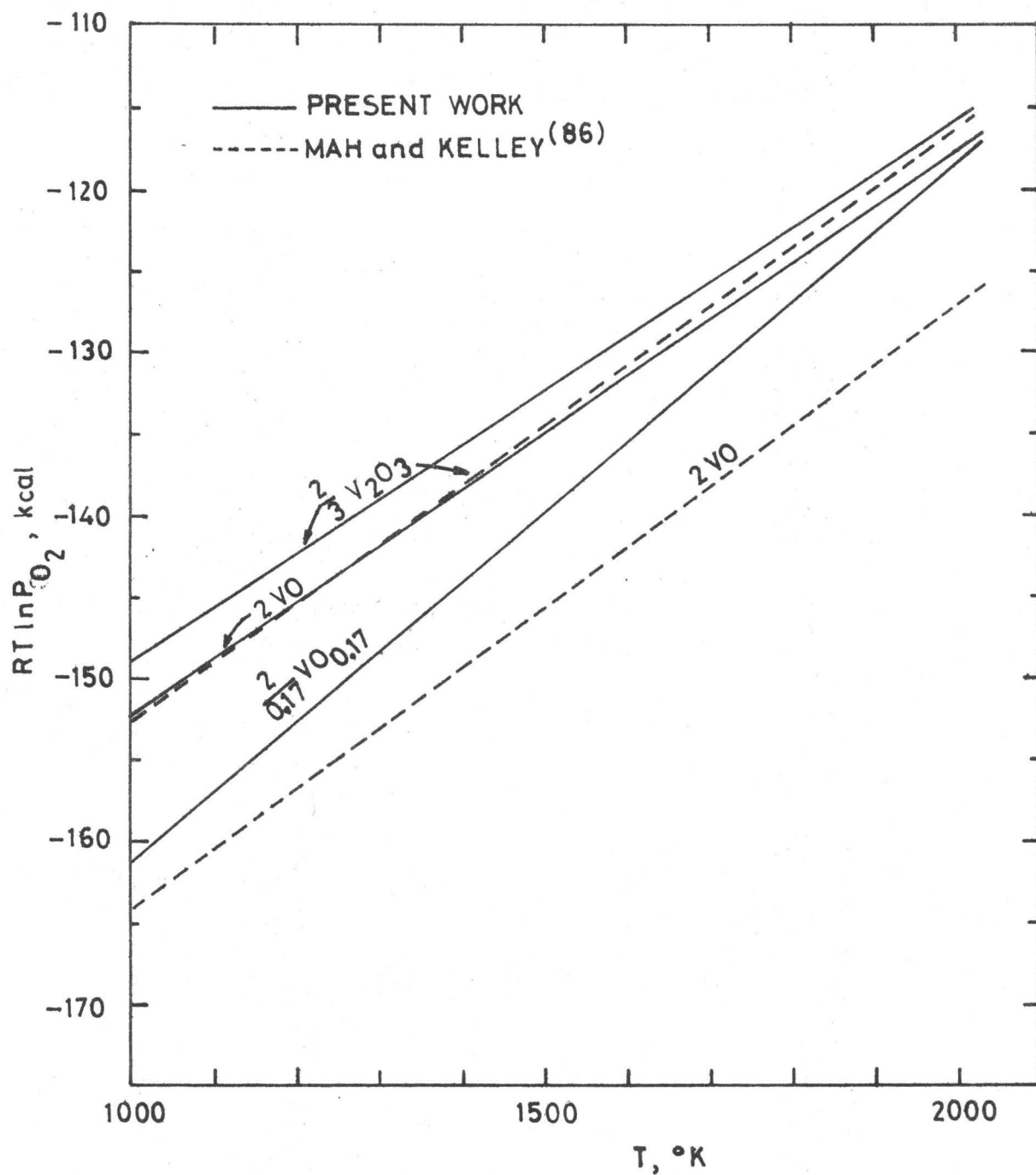
Fig. 12.4 Free energy of formation of the lower oxides of vanadium.

TABLE 12.5

COMPARISON OF THE FREE ENERGY OF FORMATION
OF VO AND V_2O_3

T, $^\circ$K	$-\Delta G_f^o$ (VO), kcal			$-\Delta G_f^o$ (V_2O_3), kcal		
	Present Work	Mah and Kelley[86]	Elliott and Gleiser(96)	Present Work	Mah and Kelley[86]	Elliott and Gleiser(96)
1200	72.5	78.3	75.0	213.3	218.4	223.0
1300	70.7	76.4	73.0	208.3	212.7	217.5
1400	69.0	74.5	71.5	203.2	207.1	211.5
1500	67.4	72.7	69.5	198.3	201.6	206.0
1600	65.7	70.9	67.5	193.3	196.1	200.5
1700	64.0	69.1	66.0	188.4	190.6	195.0

Both Mah and Kelley's[86] and Elliott and Gleiser's[96] data are calorimetric; Mah and Kelley's are considered as the most reliable from the literature.

The agreement of the above data with the present work is fair, our values for the free energy of formation of VO and V_2O_3 being approximately 2-5 kcal higher than Mah and Kelley's. From Fig. 12.4 it is seen that the free energy of formation, per mole O_2, for VO according to Mah and Kelley's work is more negative than our value, per mole O_2, for the $VO_{0.17}$. This latter value is not subject to errors due to uncertainties of the homogeneity field or of the variation of P_{O_2} within the homogeneity field (§ 12.6). The only uncertainty arises from the activity of oxygen in the reference electrode; both Fe, FeO and Cr, Cr_2O_3 were used as reference electrodes, and the results obtained agreed very well. Therefore our value for the free energy of formation of $VO_{0.17}$, per mole O_2, should be accurate. The free energy of formation of VO as given by Mah and Kelley[86] is therefore

incompatible with the present work.

12.6   UNCERTAINTIES

The uncertainties in the present work arise from experimental errors and from uncertainties in the activity of oxygen in the reference electrode.

The experimental errors are: $\pm 2^{\circ}C$ in the temperature measurement and control, and ± 2 mV in the reproducibility of the cell EMF. The latter is slightly worse than the errors generally reported for EMF measurements in systems of high oxygen potentials, and about the same as the one reported in a study on the Nb, NbO system[99]. This $\pm 2mV$ uncertainty in the EMF has a small effect on the free energy change of the relevant reaction (± 180 cal per mole O_2).

The uncertainty on the values of Jeannin et al.[62] for the free energy of formation of Cr_2O_3 has been estimated as ± 300 cal/mole Cr_2O_3 or ± 200 cal/mole O_2.

The combined uncertainty   then for the free energy changes given by the equations (12.16), (12.18), and (12.20) is of the order of ± 500 cal per mole O_2.

The uncertainties involved in determining the free energy of formation of the lower vanadium oxides (Tables 12.3, 12.4) depend, in addition, on the knowledge of the homogeneity ranges and of the variation of oxygen potential with composition within the homogeneity ranges. The error introduced by assuming the variation of the latter to be linear within the homogeneity range is small, as the correction term C is small. For example, the correction term in the β range at $1200^{\circ}C$ (Fig. 12.4) is 270 cal and for the δ range 950 cal. The error introduced by our assumptions on the correction term is estimated to be at most plus or minus one half of the above values, i.e. ± 140 cal for the β range and

$\pm$ 500 cal for the δ range.

The errors in the homogeneity ranges would also introduce an uncertainty. In order to illustrate the magnitude of this uncertainty the free energies of formation of the oxides were recalculated assuming the homogeneity range for the phase β to be $VO_{0.10}$ - $VO_{0.40}$ and are presented in Tables 12.6 - 12.7 per gram formula weight and per mole O_2. It is seen that the differences are of the order of 0.5 - 2 kcal per mole O_2 for both VO and V_2O_3.

In view of the above factors we cannot assign a realistic error limit for the free energy of formation of VO and V_2O_3. Probably the values reported in Table 12.14 are accurate to $\pm$ 2 kcal per mole O_2 for VO and V_2O_3. For $VO_{0.17}$ the error can be realistically estimated at $\pm$ 500 cal per mole O_2.

12.7   CONCLUDING REMARKS

The thermodynamic equilibria in the systems

I: $V - VO_{0.2-x}$

II: $VO_{0.2+x} - VO_{1-y}$

III: $VO_{1+y} - VO_{1.5}$

were determined with an EMF technique using $ThO_2(Y_2O_3)$ electrolytes and Cr, Cr_2O_3 as the reference electrode.

The partial pressure of oxygen in equilibrium with the above systems is given by the following equations:

$$\log P_{O_2} (I) = (-44500/T) + 9.29 \quad (1000\text{-}1220^{\circ}C) \tag{12.41}$$

$$\log P_{O_2} (II) = (-39400/T) + 6.72 \quad (1200\text{-}1460^{\circ}C) \tag{12.42}$$

$$\log P_{O_2} (III) = (-37700/T) + 7.00 \quad (900 - 1200^{\circ}C) \tag{12.43}$$

TABLE 12.6

FREE ENERGIES OF FORMATION OF THE LOWER OXIDES OF VANADIUM

kcal/gram formula weight

T, °K	$VO_{0.1}$	$VO_{0.4}$	$VO_{0.85}$	$VO_{1.25}$	$VO_{1.50}$
1100	-7.8	-32.1	-65.1	-93.5	-110.6
1150	-7.7	-31.7	-64.3	-92.3	-109.3
1200	-7.6	-31.2	-63.4	-91.2	-108.0
1250	-7.5	-30.7	-62.6	-90.1	-106.6
1300	-7.4	-30.3	-61.8	-88.9	-105.3
1350	-7.3	-29.8	-61.0	-87.8	-104.0
1400	-7.2	-29.3	-60.2	-86.7	-102.6
1450	-7.1	-28.9	-59.4	-85.5	-101.3
1500	-7.0	-28.4	-58.6	-84.4	-100.0
1550	-6.9	-27.9	-57.7	-83.3	-98.7
1600	-6.8	-27.4	-56.9	-82.2	-97.3
1650	-6.7	-27.0	-56.1	-81.0	-96.0
1700	-6.6	-26.5	-55.3	-79.9	-94.7

TABLE 12.7

FREE ENERGIES OF FORMATION OF THE LOWER OXIDES OF VANADIUM

kcal/mole O_2

T, °K	$VO_{0.1}$	$VO_{0.4}$	$VO_{0.85}$	$VO_{1.25}$	$VO_{1.50}$
1100	-156.8	-160.7	-153.1	-149.5	-147.5
1150	-154.7	-158.3	-151.2	-147.7	-145.7
1200	-152.5	-156.0	-149.3	-145.9	-144.0
1250	-150.4	-153.6	-147.4	-144.1	-142.2
1300	-148.3	-151.3	-145.4	-142.3	-140.4
1350	-146.2	-148.9	-143.5	-140.5	-138.6
1400	-144.0	-146.6	-141.6	-138.7	-136.9
1450	-141.9	-144.3	-139.7	-136.9	-135.1
1500	-139.8	-141.9	-137.8	-135.1	-133.3
1550	-137.7	-139.6	-135.9	-133.3	-131.5
1600	-135.5	-137.2	-133.9	-131.5	-129.8
1650	-133.4	-134.9	-132.0	-129.7	-128.0
1700	-131.3	-132.5	-130.1	-127.8	-126.2

From the above equations the free energy changes for the following reactions were deduced:

$$\frac{2}{0.17}\ V\ (s)\ +\ O_2(g)\ =\ \frac{2}{0.17}\ VO_{0.17}$$
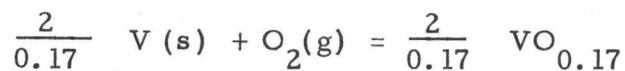
$$\Delta G^{o} = -203500 + 42.49T\ (\pm 500\ cal)\ (1000 - 1220^{o}C)$$

$$4\ VO_{0.35}\ (s) + O_2(g) = 4VO_{0.85}(s)$$
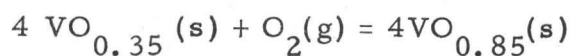
$$\Delta G^{o} = -180200 + 30.74\ (\pm 500\ cal)\ (1200 - 1460^{o}C)$$

$$8\ VO_{1.25}\ (s) + O_2(g) = 8\ VO_{1.50}\ (s)$$
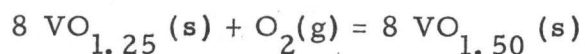
$$\Delta G^{o} = -172400 + 32.02T\ (\pm 500\ cal)$$

$$900 - 1200^{o}C$$

The free energies for formation of $VO_{0.2+x}$, VO_{1+y}, $VO_{1.5}$ were estimated and presented in tabular form.

APPENDIX I

PREDICTION OF $e_o^{(v)}$ USING PHYSICAL MODELS

As mentioned on § 2.4 many physical models of solutions have been presented, but none of them can be satisfactorily applied to every solution. Furthermore, no one predicts with any degree of accuracy the behaviour of electronegative solutes, such as oxygen or sulfur, in metallic solvents.

In the following section, two calculations are presented, based on Alcock and Richardson's regular and quasichemical solution models (§ 2.4). They are for 1600°C.

(a) The value of $e_o^{(v)}$ according to Alcock and Richardson's regular solution model can be calculated from eqn. (2-26), which, with oxygen and vanadium as solutes in iron, can be rewritten as

$$\left[\frac{\partial \ln\gamma_{o(Fe+V)}}{\partial N_v}\right]_{N_v \to 0} = \epsilon_o^{(v)} = \ln\gamma_{o(v)} - \ln\gamma_{o(Fe)} - \ln\gamma_{v(Fe)} = $$

$$= \frac{\Delta\bar{H}_{o(v)} - \Delta\bar{H}_{o(Fe)} - \Delta\bar{H}_{v(Fe)}}{RT} \qquad (A-1)$$

From the determination of the activity of V in Fe-V melts (§ 5.3.3) γ_v^o has been determined as

$$\gamma_v^o = 0.31 \qquad (A-2)$$

From this, $\Delta\bar{H}_{v(Fe)}$ can be calculated at 1600°C:

$$\Delta \overline{H}_{v(Fe)} = RT \ln \gamma_{v(Fe)}$$

$$= 4.574T \log \gamma_{v(Fe)}$$

$$= -4400 \text{ cal} \tag{A-3}$$

There are no data available for the partial molar heat of solution of oxygen in vanadium, $\Delta \overline{H}_{o(v)}$. However, the value of $\Delta \overline{H}_{o(v)} - \Delta \overline{H}_{o(Fe)}$ is not likely to differ greatly from -26 kcal, which is the difference between the chemical potentials of oxygen, per gram atom, in equilibrium with Fe + FeO and V + VO at 1600°C.

With these values, eqn (A-1) gives at 1600°C:

$$\epsilon_o^{(v)} = -5.8 \tag{A-4}$$

as compared with the experimental value of -38.6.

(b) The value of $\epsilon_o^{(v)}$ according to Alcock and Richardson's quasichemical solution model can be calculated from eqns. (2-27) and (2.28) which are rewritten for the case of Fe-V-O solutions as:

$$\left[\frac{\partial \ln \gamma_{o(Fe+v)}}{\partial N_v} \right]_{N_v \to 0} = \epsilon_o^{(v)} = \frac{-z(K-1)}{N_{Fe} + KN_v} \tag{A-5}$$

where

$$K = \left(\frac{\gamma_{o(Fe)} \; \gamma_{v(Fe+v)}}{\gamma_{o(v)} \; \gamma_{Fe(Fe+v)}} \right)^{\frac{1}{z}} \tag{A-6}$$

For $N_v \to 0$, $\gamma_{v(Fe+v)} = 0.31$ (eqn. A-2), and $\gamma_{Fe(Fe+v)} = 1$. Eqn. (A-6) can be rewritten as

$$\log K = \frac{1}{z} \left[\log \gamma_{o(Fe)} - \log \gamma_{o(v)} - 0.51 \right] \tag{A-7}$$

As in the previous calculation, it will be assumed that

$$\Delta \bar{H}_{o(v)} - \Delta \bar{H}_{o(Fe)} = -26000 \text{ cal} \qquad (A-8)$$

Hence,

$$4.574T \left(\log \gamma_{o(v)} - \log \gamma_{o(Fe)} \right) = -26000 \text{ cal} \qquad (A-9)$$

and

$$\log \gamma_{o(Fe)} - \log \gamma_{o(v)} = 3.03 \qquad (A-10)$$

Assuming that $z = 8$, eqn. (A-7) gives a value of $K = 2$, and eqn. (A-5) gives $\epsilon_o^{(v)} = -8$ at 1600^oC. It should be noted that the quasichemical value of $\epsilon_o^{(v)}$ is markedly influenced by the choice of the coordination number z: if z were taken as 6 or 4, $\epsilon_o^{(v)}$ would become -9.8 or -13.0 respectively, with the same values for the partial molar heats. It is evident that although the quasichemical model looks a better proposition than the regular, it falls far short of accounting for the experimental value of $\epsilon_o^{(v)}$.

The calculated values for the $\epsilon_o^{(v)}$ according to the regular and quasichemical solution models are compared with the experimental value in Table Al.

TABLE Al

COMPARISON OF THE EXPERIMENTAL VALUE OF ϵ_o^v WITH THE VALUES DERIVED BY THEORETICAL MODELS. $T = 1600^o$C

Experimental Value of $\epsilon_o^{(v)}$	Regular Solution Model[14]	Quasichemical Solution Model[15]		
		$z = 8$	$z = 6$	$z = 4$
-38.6	-5.8	-8	-9.8	-13.0

REFERENCES

1. C. Wagner: Thermodynamics of Alloys. pp51-52, Addison-Wesley, Cambridge, Mass. 1952.

2. C.H.P. Lupis and J.F. Elliott: Trans. TMS-AIME, 1965, vol. 233, pp. 829-830.

3. C.H.P. Lupis and J.F. Elliott: Trans. TMS-AIME, 1966, vol. 236, p 130.

4. C.H.P. Lupis and J.F. Elliott: Acta Met., 1966, vol. 14, pp 529-538.

5. H. Schenck, M.G. Frohberg and E. Steinmetz: Arch. Eisenhüttenwes., 1960, vol. 31, pp 671-76.

6. L.S. Darken: Trans. TMS-AIME, 1967, vol. 239, pp 80-89.

7. L.S. Darken: Trans. TMS-AIME, 1967, vol. 239, pp 90-96.

8. K. Denbigh: The Principles of Chemical Equilibrium, Ch. 8. Cambridge University Press, Second Ed., 1966.

9. J.H. Hildebrand: Proc. Nat. Acad. Sci, 1927, vol. 13, pp. 267-72.

10. J.H. Hildebrand and R.L. Scott: The Solubility of Non-Electrolytes, Reinhold Publishing Corp., NY 1950.

11. J.H. Hildebrand and R.L. Scott: Regular Solutions. Prentiss-Hall, Englewood Cliffs, N.J. 1962.

12. K. Denbigh: The Principles of Chemical Equilibrium; ch 14, 2nd Ed., Cambridge University Press 1966.

13. E.A. Guggenheim: Mixtures. Oxford Clarendon Press, 1952.

14. C.B. Alcock and F.D. Richardson: Acta Met., 1958, vol. 6, pp 385-395.

15. C.B. Alcock and F.D. Richardson: Acta Met., 1960, vol. 8, pp. 882-887.

16. G.R. Belton and E.S. Tankins: Trans. TMS-AIME, 1965, vol. 233, pp 1892-98.

17. J. Chipman: J. Am. Chem. Soc., 1933, vol. 55, pp 3131-3136.

18. M.G. Fontana and J. Chipman: Trans. ASM, 1936, vol. 24, pp 313-336.

19. J. Chipman and A.M. Samarin: Trans. AIME, 1937, vol. 125, pp 331-337.

20. M.N. Dastur and J. Chipman: Trans. AIME, 1949, vol 185, pp 441-445.

21. V.V. Averin, A.Y. Polyakov, and A.M. Samarin: Izv. Akad. Nauk. SSSR, Otd. Techn. Nauk. (Metally), 1955, vol. 8, pp 90-95.

22. N.A. Gokcen: Trans. AIME, 1956, vol. 206, pp 1558-1567.

23. T.P. Floridis and J. Chipman: Trans. TMS-AIME, 1958, vol 212, pp 549 - 553.

24. E.S. Tankins, N.A. Gokcen and G.R. Belton: Trans. TMS-AIME, 1964, vol. 203, pp 820-827.

25. S. Matoba and T. Kuwana: Tetsu-to-Hagane Overseas, 1965, vol 5, pp 187-195.

26. H. Schenck and E. Steinmets: Arch. Eisenhüttenwes, 1967, vol 38, pp 813-819.

27. J.C. d'Entremont: Trans. TMS-AIME, 1963, vol 227, pp 482-485.

28. J. Chipman and M.N. Dastur: Trans. AIME, 1951, vol 191, pp 111-115.

29. K. Narita: Nippon Kagaku Zasshi, 1958, vol. 79, pp 866-872.

30. K. Narita and S. Koyama: Trans. ISIJ, 1969, vol 9, pp 53-58.

31. W.A. Fischer and M. Haussmann: Arch. Eisenhüttenwes., 1966, vol 37, pp 959-961.

32. H. Schenck and E. Steinmetz: Arch. Eisenhüttenwes, 1967, vol 38, pp 871-873.

33. J.K. Pargeter: Can. Met. Quarterly, 1967, vol 6, pp 21-37.

34. P. Kershaw: Ph.D. Thesis, McMaster University, 1968.

35. R.J. Fruehan: Met. Trans., 1970, vol 1, pp 2083-2088.

36. R.A. Karasev, A. Yu Polyakov, A.M. Samarin: Doklady Akad.
    Nauk. SSSR, 1952, vol 85, pp 1313-1316.
    Isvest. Acad. Nauk. SSSR, Otdel. Tekh. Nauk., 1952, No 12,
    pp 1794-1800.

37. M.N. Dastur and J. Chipman: The Faraday Soc. Symposium on the
    Physical Chemistry of Process Metallurgy (1948). pp 100-108

38. NBS Misc. Publ. 260-14: Determination of Oxygen in Ferrous
    Materials SRM 1090, 1091 and 1092. U.S. Department of Commerce,
    National Bureau of Standards, 1966.

39. S. Spauszus: Methoden der Chemischen Stahl-und Eisenanalyse,
    p 106-107, Deutscher Verlag fur Grundstoffindustrie, Leipzig 1967.

40. JANAP Thermochemical Tables. The Dow Chemical Co., Midland,
    Mich., 1961.

41. M. Hansen: Constitution of Binary Alloys. McGraw-Hill, NY,
    London 1958.

42. F. Larché: M.Sc. Thesis, McMaster University, 1968.

43. N.A. Gokcen and J. Chipman: Trans. AIME, 1953, vol. 197,
    pp 173-178.

44. J.C. d'Entremont, D.L. Guernsey and J. Chipman: Trans. TMS-AIME,
    1963, vol 227, pp 14-17.

45. Y. Matsushita and K. Goto: Trans. I.S.I.J., 1966, vol 6, pp 21-28.

46. W.A. Fischer and W. Ackermann: Arch. Eisenhüttenwes., 1965, vol 36,
    pp 643-648.

47. W.A. Fischer and W. Ackermann: Arch. Eisenhüttenwes., 1966,
    vol 37, pp 43-47.

48. R. Baker and J.M. West: J.I.S.I., 1966, vol 204, pp 212-216.

49.   K. Schwerdtfeger: Trans. TMS-AIME, 1967, vol 239, pp 1276-1281.

50.   G. R. Fitterer: J. of Metals, 1966, vol 18, pp 961-966, J. of Metals,
      1967, vol 19, pp 92-96.

51.   D. K. Faurschou and J. C. Pope: Internal Report PM-I-69-11,
      Mines Branch, Dept. of Energy, Mines and Resources,
      Ottawa 1969.

52.   D. K. Faurschou and M. Price: Internal Report PM-I-69-12
      Mines Branch, Dept. of Energy, Mines and Resources, Ottawa 1969.

53.   S. L. Gertsman, D. K. Faurschou and J. C. Pope: Internal Report
      PM-M-70-7 Mines Branch, Dept. of Energy, Mines and
      Resources, Ottawa 1970.

54.   E. T. Turkdogan and R. J. Fruehan: AISI Year Book, 1968, pp 279-301.

55.   R. J. Fruehan, L. J. Martonik and E. T. Turkdogan: Trans. TMS-
      AIME, 1969, vol 245, pp 1501-1509.

56.   C. Gatellier et al: Rev. de Mét., 1969, vol   , pp 673-693.

57.   B. C. H. Steele and C. B. Alcock: Trans. TMS-AIME, 1965, vol 233,
      pp 1359-1367.

58.   J. D. Tretjakow and H. Schmalzried: Ber. Buntesgesellschaft fur
      Phys. Chem., 1965, vol 69, pp 396-402.

59.   L. A. Pugliese and G. R. Fitterer: Met. Trans., 1970, vol. 1,
      pp 1997-2002.

60.   W. A. Fischer and D. Janke: Arch. Eisenhüttenw., 1968, vol 39,
      pp 89-99.

61.   R. J. Fruehan: Met. Trans., 1970, vol. 1, pp 865-870.

62.   Y. Jeannin , C. Mannerskantz and F. D. Richardson: Trans.
      TMS-AIME, 1963, vol 227, pp 300-305.

63.   K. K. Kelley and E. G. King: Contributions to the Data on Theoretical
      Metallurgy. XIV. Entropies of the Elements and Inorganic
      Compounds. US Bureau of Mines Bull. 592, 1961.

64. K.K. Kelley: Contributions to the Data on Theoretical Metallurgy. XIII. High Temperature Heat Content, Heat Capacity, and Entropy Data for the Elements and Inorganic Compounds: U.S. Bureau of Mines Bull. 584, 1960.

65. J.F. Elliott, M. Gleiser and V. Ramakrishna: Thermochemistry for Steelmaking, vol. II. Addison-Wesley; Reading, Mass., 1963.

66. A. McLean: J. of Metals, March 1968, vol. 20, pp 96-100.

67. O. Repetylo, M. Olette and P. Kozakevitch: J. of Metals, May 1967, vol 19, pp 45-49.

68. P. Kozakevitch and L.D. Lukas: Revue de Mét., 1968, vol. 65, pp 589-598.

69. P. Kozakevitch and G. Urbain: Mem. Sci. Rev. Mét., 1961, vol 58, pp 517-534.

70. K. Myles and A.T. Aldred: J. Phys. Chem., 1964, vol 68, pp 64-69.

71. G.R. St. Pierre and R.D. Blackburn: Trans. TMS-AIME, 1968, vol 242, pp 2-4.

72. W. Rostoker and A.S. Yamamoto: Trans. ASM, 1955, vol. 47, pp 1002-1017.

73. J. Stringer: J. of the Less-Common Metals, 1965, vol 8, pp 1-14.

74. N.P. Allen, O. Kubaschewski and O. von Goldbeck: J. Electrochem. Soc., 1951, vol 98, pp 417-424.

75. A.U. Seybolt and H.T. Sumsion: Trans. AIME, 1953, vol 197, pp 292-299.

76. S. Westman and C. Nordmark: Acta Chem. Schand., 1960, vol 14, p 465.

77. N. Schonberg: Acta Chem. Scand., 1954, vol 8, p 221.

78. G. Anderson: Acta Chem. Scand., 1954, vol 8, pp 1599

79. E. Vol'F, S.S. Tolkachev and I.I. Kozhina: Vestn. Leningr. Univ., Ser. Fiz i Khim., 1959, vol 10, pp 87-90.

80. P. V. Gel'd, S. I. Alyamovskii, and I. I. Matvennko: Zhurnal Struktumoi Khimii, 1961, vol. 2, pp 301-307.

81. S. A. Bradford and D. N. Carlson: Trans. ASM, 1962, vol. 55, pp 169-178.

82. R. E. Newnham and Y. M. de Haan: Z. Krist., 1962, vol. 117, pp 235-243.

83. L. Brewer: Chem Rev., 1953, vol 52, pp 1

84. R. D. Rossini, D. D. Wagman, W. H. Evans, S. Levine and I. Jaffe: Selected Values of Chemical Thermodynamic Properties, NBS (US) Circ. 500, 1952, p 1268.

85. E. Vol'f and S. M. Ariya: Zh. Obshch. Khim., 1959, vol 29, pp 2470.

86. A. D. Mah and K. K. Kelley: Heats and Free Energies of Formation of Oxides of Vanadium. U. S. Bureau of Mines Rept. Invest. 5858, 1961.

87. M. Kobayashi: Sci. Repts. Tohoku Imp Univ., 1933, vol. 22, pp 1240-1255.

88. K. Kiukkola and C. Wagner: J. Electrochem. Soc., 1957, vol 104, p 308-316.

89. K. Kiukkola and C. Wagner: J. Electrochem. Soc., 1957, vol 104, pp 379-387.

90. S. P. Mitoff: J. Chem. Phys., 1962, vol 36, pp 1383-1389.

91. P. C. Lidster and H. B. Bell: Trans. TMS-AIME, vol 245, pp 2273-2277.

92. B. C. H. Steele: in "Electromotive Force Measurements in High Temperature Systems." Ed. by C. B. Alcock. American Elsevier Co., 1968, pp 3-27.

93. S. Zador: Ph. D. Thesis, University of London, 1967.

94. F. Hund and R. Mezger: Z. Physik. Chem. (Leipzig), 1952, vol 201, pp 268-77.

95. J. M. Wimmer, L. R. Bidwell and N. M. Tallan: J. Am. Ceramic Soc., 1967, vol 50, pp 198-201.

96. J. F. Elliott and M. Gleiser: Thermochemistry for Steelmaking,
     vol I., Addison-Wesley, Reading, Mass., 1960.

97. J. P. Coughlin: U.S. Bureau of Mines Bull. No. 542.

98. J. Smiltens: J. Am. Chem. Soc., 1957, vol 79, pp 4877-4880.

99. C. B. Alcock and B. C. H. Steele: In Science of Ceramics, vol 2,
     pp 397-406. Ed. G. H. Stewart. Academic Press, London and
     NY, 1965.